The University of Nottingham

Control Methodology and Modelling of Active Fixtures

Otto Jan BAKKER

Werktuigbouwkundig Ingenieur, Technische Universiteit Delft

De werken van de Heere zijn groot,

zij worden onderzocht door allen die er vreugde in vinden.

Great are the works of the Lord;

They are studied by all who delight in them.

Psalm 111: 2

Abstract

Fixtures are used to fixate, position and support workpieces, and are critical elements in manufacturing processes. Machining is one of these manufacturing processes, and this is often done by computer numerical control (CNC) machines. A major trend observed in production industry is that manufacturing is increasingly done in small batches in combination with a quick changeover from one product to another, in combination with a surge in automation. Several novel fixture concepts have been developed that allow for a reconfiguration of the fixture layout, such that different types of workpieces can be fixtured using the same fixture components. However, the initial novel fixturing concepts lacked accuracy, and, in addition, required long set-up times. Recently, a new fixturing concept has been developed, the so-called intelligent fixturing system. Sensors and actuators are integrated in an intelligent fixturing system, which allows for an automatic and precise reconfiguration of the fixturing elements. Additionally, the actuated fixture elements can be used to exert optimal clamping forces to minimise the workpiece deflection during the machining process, this is called active fixturing.

A literature survey has been carried out, in which it has been established that the main process variables to control in active fixturing, are the reaction forces at the contacts where the workpiece is fixated and supported by the fixture (the locating points), and/or the part or fixture displacements. Furthermore, four knowledge gaps were identified: (1) a lack of computationally efficient models of workpiece response during machining; (2) a lack of methodic structural analysis approach of part-fixture interaction; (3) a lack of model-based control design, which can potentially speed up the fixture design process; and (4) a lack of control design methodology for active fixturing systems.

An active fixturing system can be divided into the following subsystems: the part,

the part-fixture contact interface, passive fixture elements, the actuated clamp, sensors and the controller(s). In the thesis, a methodical research approach has been applied to address the knowledge gaps by analysing the active fixturing subsystems. In addition, a model-based control design methodology has been proposed. The research has aimed to establish mathematical models, or the necessary tools and methodology to build the subsystem models, and methods to connect the subsystem models into an overall model of the active fixturing system. On basis of the subsystem analyses, two simple, yet complete, active fixturing systems have been modelled. Parameter studies have been held to assess the performance of the control design. In addition, an industrial case study has been analysed, using the developed control design methodology.

The study of the subsystems resulted in the comprehensive structural dynamic analysis of workpieces: a finite element model of the workpiece is built. Typically, finite element models contain too many degrees of freedom for real-time control applications. It was found that model reduction techniques can be used to reduce significantly the number of degrees of freedom. Methodologies for the selection of the degrees of freedom and for ensuring that the model reduction is accurate enough for practical use have been established. Mathematical models for hydraulically and electromechanically actuated clamps have been established. Compensators for closed-loop servo-control of the clamps have been investigated and control strategies to maintain workholding stability are found. Finally, a methodology to establish the overall model of an active fixturing system has been implemented. The control design methodology, and the mathematical tools established in the thesis have been verified against case studies of simple active fixturing systems. Furthermore, from the industrial case study it is concluded that the control design methodology can be successfully applied on complex fixturing systems. Additionally, a mathematical model for a piezoelectrically actuated clamp was derived, which also demonstrates the general applicability of the control design methodology derived here, as a new established actuator model is integrated in the control design. The overall conclusion, is hence that a good methodology for the model-based control design of active part-fixturing systems has been developed, which enables the engineer to speed up the design process of active fixturing systems.

Acknowledgements

Although this thesis has only one named author, it could not have been written without the contribution of many others, directly or indirectly by collaboration, or just by showing their interest in the work. Here, I would like to thank all who have contributed to the creating of this thesis. Special thanks are due to the following:

First, I am grateful to the Engineering and Physical Sciences Research Council of the United Kingdom, and the European Commission through the AFFIX project for funding this research.

I would like to thank my supervisor, Dr Atanas Popov. Atanas, thank you for the efforts you have invested in me, and for the discussions, both personal and academic, that were always motivating. Thank you for the flexibility and for knowing that the door was always open, despite your increasingly busy agenda. You have often inspired me to continue investigating and to dig that extra bit deeper. Thanks for your thorough and precise correction work in the writing process. My sincerest gratitude goes to my other supervisor, Prof Svetan Ratchev for his timely and critical questions that were always spot on and kept me focussed on the practice.

Thanks to my colleagues from Innovative Technology Research Centre Building, room C32 and to all the people from the Precision Manufacturing Centre. Thank you guys, for being there and for the fun times. Especially, Thomas Papastathis and Marco Ryll, thanks for being such good friends, for our discussions on fixturing systems and for making our travel to the AFFIX meetings an enjoyable experience.

Thanks to all the people involved in the AFFIX project and especially to Edoardo Salvi and Angelo Merlo of Centro Studi Industriali, Milan, for involving me in the AFFIX Demonstrator 3C and inviting me over for the tests in Milan. Edoardo, thank you for

arranging my stay in Milan and for our helpful discussions on the fixturing system.

At this place, I would like to thank my parents and my brother, who have always encouraged, supported and loved me. Finally, all honours and thanks to our God and Father in Christ, the great Creator of all things, Who upholds, directs, disposes, and governs all creatures, actions, and things. Let Your Name be exalted in heaven and on earth.

Contents

List of Tables

List of Figures

List of Abbreviations

AC   Alternating Current

ADFB   Actuator Displacement FeedBack

BIW   Body In White

CMM   Coordinate Measurement Machine

CNC   Computer Numerical Control

DC   Direct Current

DOF   Degree Of Freedom

DfM   Design for Manufacturing

DfX   Design for 'X'

EMA   Electromechanically Actuated

FE   Finite Element

FEA   Finite Element Analysis

FEM   Finite Element Method

FFB   Force FeedBack

FIM   Fixed Interface Mode

HA   Hydraulically Actuated

HIL   Hardware In the Loop

IC   Integrated Circuit

IFS   Intelligent Fixturing System

LMS   Least Mean Squares

LQG   Linear-Quadratic-Gaussian

LaF   Lag Filter

LeF   Lead Filter

MEMS	MicroElectroMechanical System
MIMO	Multi-Input Multi-Output
MIT	Massachusetts Institute of Technology
NGV	Nozzle Guiding Vane
P	Proportional
PEA	Piezoelectric Actuator
PDFB	Part Displacement FeedBack
PKM	Parallel Kinematic Mechanism
PMDC	Permanent Magnet DC motor
PMSM	Permanent Magnet Synchronous Motor
PI	Proportional Integral
PID	Proportional Integral Derivative
NGV	Nozzle Guiding Vane
SISO	Single-Input Single-Output
TVD	Tuned Viscoelastic Damper
emf	electromotive force
rpm	revolutions per minute

Notation

Latin Symbols

A	piston surface area	[m^2]
$\boldsymbol{A}$	state matrix	
$\mathcal{B}$	set of boundary coordinates	
$\boldsymbol{B}$	input matrix	
B_2	gain in charge feedback scheme	[-]
C	capacitance piezoelectric actuator	[f]
$\boldsymbol{C}$	output matrix	
$C(s)$	transfer function controller	[-]
C_d	Von Mises discharge coefficient	[-]
C_e	capacitance charge feedback scheme	[F]
$\boldsymbol{D}$	feed-through matrix	
E	bulk modulus of oil / Young's Modulus	[N/m^2]
F_act	force output actuator	[N]
$F_{\mathrm{c},i}$	reaction force at clamp i	[N]
F_e	external force	[N]
F_m	machining force	[N]
F_p	piezoelectric force	[N]
$F_{\mathrm{loc},i}$	reaction force at locator i	[N]
F_μ	Coulomb friction force	[N]
H	transfer function	
I	inertia moment (indices omitted)	[m^4]

$\mathcal{I}$	set of internal coordinates	
$\boldsymbol{K}$	(reduced) stiffness matrix	[N/m]
K_{fb}	feedback gain	[-]
K_{m}	velocity gain	[s^{-1}]
K_{p}	proportional gain	[-]
K_{v}	gain motor servo-valve	[s^{-1}]
L	inductance	[H]
$\boldsymbol{M}$	(reduced) mass matrix	[kg]
M_0	piston mass	[kg]
$\boldsymbol{P}$	modal load	[N]
P_{L}	pressure due to load	[Pa]
P_{c}	pressure in cylinder	[Pa]
P_{s}	supply pressure of oil	[Pa]
$\Re$	real part complex eigenvalue	
R	electric resistance	[Ω]
$\mathcal{R}$	set of redundant coordinates	
$\boldsymbol{R}_{bb}$	reaction force on $\mathcal{R}$	[N]
$\boldsymbol{R}_{ib}$	reaction force on $\mathcal{I}$	[N]
$\mathcal{T}$	kinetic energy	[J]
T_{e}	external torque	[Nm]
T_{em}	transformer coefficient	[N/V]
T_{D}	time constant PID-controller	[s]
T_{I}	time constant PID-controller	[s]
$\mathcal{V}$	potential energy	[J]
V_0	volume of effective cylinder compartment	[m^3]
V_{C}	control voltage	[V]
V_{CC}	control voltage Danaher controller	[V]
$V(s)$	transfer function valve dynamics	[-]
V_{pea}	steering voltage piezoelectric actuator	[V]
a_1, a_2	port coefficients of valve	[-]
b	port-width coefficient valve	[-]

c	damping coefficients dashpots	[Ns/m]
c_{h}	hydraulic stiffness of valve	[N/m]
c_{o}	stiffness of oil cylinder	[N/m]
d	grinding wheel diameter	[m]
d_1/d_2	inner / outer diameter diaphragm	[m]
$\boldsymbol{f}$	external force vector	[N]
f_r	viscous friction coefficient electric motor	[m]
k	spring stiffness	[N/m]
k_{T}	torque coefficient	[Nm/A]
k_{bemf}	back-emf coefficient	[Vs/rad]
m	mass	[kg]
p	ball screw pitch	[m/rad]
$\boldsymbol{p}$	generalised displacement coordinates	
r	reference value valve displacement	
r_1/r_2	inner / outer radius diaphragm	[m]
s	complex eigenvalue Laplace form	[s^{-1}]
t	thickness diaphragm	[m]
t	time	[s]
v_{w}	grinding wheel speed	[m/s]
w	viscous friction coefficient	[Ns/m]
x	displacement	[m]
y	displacement	[m]
z	displacement	[m]

Greek Symbols

$\boldsymbol{\Lambda}_{nn}$	modal stiffness matrix	[N/m]
$\boldsymbol{\Phi}$	modal matrix	[-]
$\boldsymbol{\Psi}$	transformation matrix	
α	proportional damping coefficient	[-]
α_{LF}	coefficient lag/lead filter	[-]

β	proportional damping coefficient	[-]
β	relative damping coefficient	[-]
β_{v}	damping coefficient PMSM controller / hydraulic servo valve	[-]
δ	difference matrix	
η	modal displacement	[m]
θ	angular displacement	[rad]
$\lambda\,(\lambda_n)$	(n^{th}) eigenvalue	
ν	Poisson's coefficient	[-]
ρ	density	[kg/m^3]
τ_{v}	servo-valve actuator time constant	[s]
ϕ	modal vector	
φ	phase change	[rad]
ω	input frequency	[rad/s]
ω_0	undamped natural frequency cylinder	[rad/s]
ω_{LF}	corner frequency lag/lead filter	[rad/s]
ω_{v}	bandwidth frequency PMSM controller / hydraulic servo valve	[rad/s]

Introduction

1.1 Background and Motivation

The advancement of jet aircraft since the Second World War increased the demand for complex-shaped parts (especially in jet engines). These complex parts are hard to manufacture and in order to tackle problems regarding the manufacturability of complex parts, in 1952 the first numerically controlled milling machine was developed at Massachusetts Institute of Technology (MIT) [74].

This not only enabled industry to make complex parts, but also improved designs of components optimised with respect to strength and weight requirements. The increase of prosperity in the Western World, the rise of new manufacturing powerhouses such as Japan, South Korea and Taiwan, and the strong increase of interest on loans, demanded a response from the industry in the Western World. The answer was found in reducing the stockpiles and further automation to save out on interest and labour costs respectively.

The advance of microelectronics saw the coming of easy programmable Computer Numerical Control (CNC) machine tools, and in other technology sectors the development of mechatronics (sometimes called smart or advanced technology). Thanks to the programmability of CNC machines, they proved to be an essential tool in automation. Figure 1.1 illustrates a (dated) decision strategy for the automation of machine tools. In this Figure, one can see that it is economically viable to make simple parts in low volume on manually controlled machines. When the risk of production failure increases, e.g. due to the complexity of the part, CNC machines should be applied for the manufac-

turing of the component. In the case of simple parts, made in high volumes, mechanical automation of the machine tools is advisable.

Further globalisation and the rise of new low-cost manufacturing countries, such as Brazil, China and India in the last two decades, meant that design and production became more dispersed around the world [35, 89]. Which meant that, the mass production of simple parts (high-volume low-value) has been moved away to countries with lower labour costs, such as China and the Czech Republic [35, 84]. Components that are deemed strategic to the enterprise/country and have great added-value to the final product, typically the low-volume high-value products, are manufactured in-house in Western Countries. This especially concerns the areas of precision and micro-manufacturing [35, 84].

In order to remain competitive and make new products for new markets, the industry in the Western World needs to remain or become technology leader. There is a need for innovative solutions to enable faster and more reliable production to reduce the through-put times [15, 35, 84]. Furthermore, the automation and programmability of CNC machine tools enabled a flexibility in production that allowed for the (increasingly) fast turnover of product generations, characterising today's mass consumer markets; a trend clearly observable in the markets for consumer microelectronics and cars.

In manufacturing, fixtures, or workpiece holders are used to fixate, position and support workpieces during the production process. Fixtures play a crucial role in the whole process [74, 84], as their performance determines the result of the whole manufacturing (and assembly) process of a product. Traditionally, fixturing has been done by means of machine vices, dovetail slots and V-blocks or dedicated fixtures (fixture design suited for the workholding of only one kind of parts). However, the requirements for (con)current fixture design are for fixturing capabilities that fulfil the demands for the flexibility needed in manufacturing in the Western World as described above [84]. For this reason, fixturing concepts have been contrived that are able to fixture complex and compliant parts but that can also be reconfigured such that different workpieces can be fixtured. An example of one of these concepts is the so-called modular fixture, an example of such a fixture is shown in Figure 1.2, where a workpiece is fixtured on a standard baseplate by, mainly black, standard components. However, there are some

problems surrounding these fixturing concepts, as they suffer generally from the following drawbacks: long setup times, low accuracy, and repeatability. For example, compared to dedicated fixtures it takes a long to set up the modular fixture shown in Figure 1.2, not to mention the time it costs to assemble the fixture (a series of) another kind of part. Additionally, due to the tolerance stack-up of the modular components and tolerances introduced during the assembly of fixture, the accuracy of the fixture is lower. Furthermore, over time, the fixture components will get dislocated, deteriorating the accuracy of the fixture over time.

In order to overcome these problems, fixturing concepts with automatic reconfiguration capabilities have been developed. In this concept, fixture elements are equipped with sensors and actuators. These fixtures have robotic capabilities and can automatically (re)position the fixture components. Furthermore, the actuated elements of these fixtures can be utilised to generate active control forces to minimise the deformation of the part during the machining operation. Thus, more accuracy would be obtained when comparing these fixtures with the traditional passive fixture designs. The concept is called 'active fixturing'. In the AFFIX research project [5], automatical reconfigurability and active fixturing have been studied by a consortium of universities, industrial companies, and research institutes. This thesis has been written on basis of the research the author has done in the AFFIX project.

1.2 Research Aims and Objectives

One of the main issues is, that "[there] is almost a complete absence of intelligence and control in current fixturing systems. Components are still commonly held using a series of structural hard-points on the fixturing system throughout the manufacturing process" [5]. This work seeks to establish a systematic approach of simulation-based control design for active fixturing systems. This primary research aim is supported by achieving the following research objectives which represent the key steps in the establishing of a control design methodology for active fixturing systems:

- Identify the key process parameters that can be used for the control of active fixturing systems during machining processes.

- Establish dynamic models that describe the dynamic behaviour of the subsystems of the active fixturing system.

- Develop tools to keep the size of the models relatively small, yet accurate enough for real-time simulation-based control.

- Establish tools to connect subsystems and combine them into one overall model.

- Formulate a structured methodology that enables a systematic approach of the control design.

- Conduct parameter studies with the goal to assess the performance of the control system(s).

The introduction of active control in fixturing will increase the accuracy of the fixture, and as the control strategy is model-based, the methodology allows for the control design to be established during the design of the fixturing system, thus contributing to a reduction in the time needed for fixture development.

1.3   Thesis Outline

An overview of the structure of the thesis is shown in Figure 1.3. Three horizontal blocks are drawn with dashed lines. Firstly, there is the block of Chapters 1, 2 and 3, where the framework of the study is outlined. Secondly, in Figure 1.3, there is the block of Chapters 4 and 5. In this block, the methodology is worked out in detail. The third block contains Chapters 6 and 7, in these chapters, an industrial case study is worked out as illustration of the applicability of the developed methodology. Two vertical blocks are drawn in Figure 1.3 with dashed lines. In Chapters 4 and 6, active fixturing systems are modelled and in Chapters 5 and 7 the control design of active fixturing systems is studied. In more detail, the contents per chapter are as follows:

Chapter 1 Introduction

Background, motivation, research aims and objectives of the work are given.

Chapter 2 Literature Review

General fixturing background information and fixture design principles are introduced. The chapter provides a review of the current state of the art in the field of fixturing techniques for reconfigurable fixtures. Based on the review of the design principles and the fixturing concepts, fixture performance is discussed and process variables for the control of active fixtures are established. A review is held on the active control of variables in several fixturing concepts that are presented in the literature. Furthermore, the elements of control for the active control of related systems are briefly investigated by looking at the field of structural control and identification of the subsystems of an active fixture system.

Chapter 3 Methodology

In Chapter 3, the research approach taken is explained and key assumptions made are presented. On basis of the research approach, an active control design methodology for actuated part-fixture systems is established.

From Chapter 3, research methodology is worked out in detail in Chapters 4 and 5, which form the backbone of the thesis. An industrial case study has been carried out within the framework of the AFFIX project. The complexity and unique features of the industrial case study, considered in Chapter 6 and 7, requires an extensive analysis. This allows the reader, who has little or no interest in knowing the minutious details of the tools for the analysis of fixture systems established in Chapters 4 and 5, and little time to spare, to move directly to Chapters 6 and 7, and see how the control design methodology established in Chapter 3 can be applied.

Chapter 4 Analysis of Active Fixture Subsystems

An active fixturing system generally can be divided into several subsystems: a part, the part-fixture contact interface, passive fixture elements, the actuated clamp, controller etc.. Mathematical models, and the necessary tools to build subsystems models are established and methods for the connection of the mathematical models of the subsystems are derived subsequently.

Chapter 5 Analysis of Simple Fixture Systems

On basis of the models for the subsystems established in Chapter 4, simple active fixturing systems are analysed. The control design methodology as set out in Chapter 3, the mathematical tools developed in Chapter 4, and the control design itself, in terms of absolute stability and chatter suppression in the frequency domain, are verified against these simple systems by means of parametric studies.

Chapter 6 Industrial Case Study: Modelling

Chapters 6 and 7 form the application and, hence, the verification of the control design methodology. The design of an advanced fixturing system is analysed, and the subsystems of the fixturing system are identified. Based on the tools established in Chapter 4, the active fixture subsystems are modelled. It is shown that the methodology is expandable for new actuator models and an overall model of the active fixturing system is built.

Chapter 7 Industrial Case Study: Results

The performance of the control design for the industrial case study is investigated in detail on basis of the overall model established in Chapter 6. Parametric studies are used to verify the control in terms of absolute stability, workholding stability, and chatter suppression in the time and frequency domain by means of parametric studies.

Chapter 8 Conclusions and Further Work

The main conclusions are given, the research contribution is identified, and areas for further work are suggested.

1.4 Figures
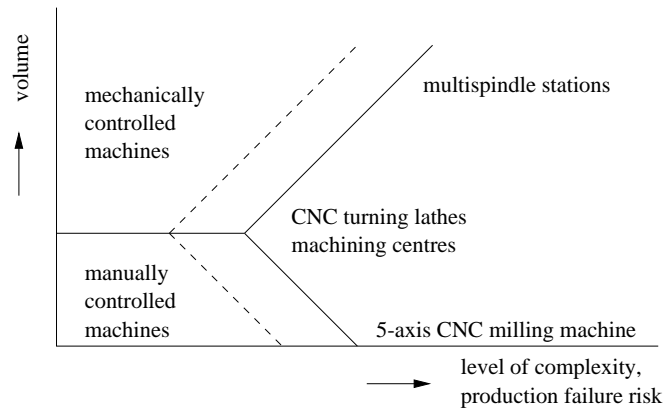
Figure 1.1: K-graph for automation strategy, translation of [74, Fig. 11.16].
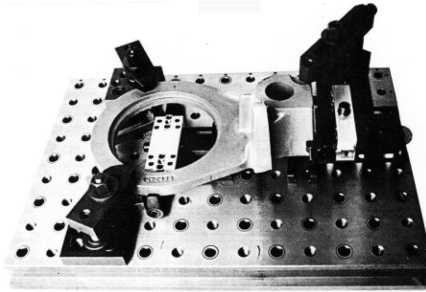
Figure 1.2: Example of a modular fixture. Source: Ref. [84, Fig. 19].
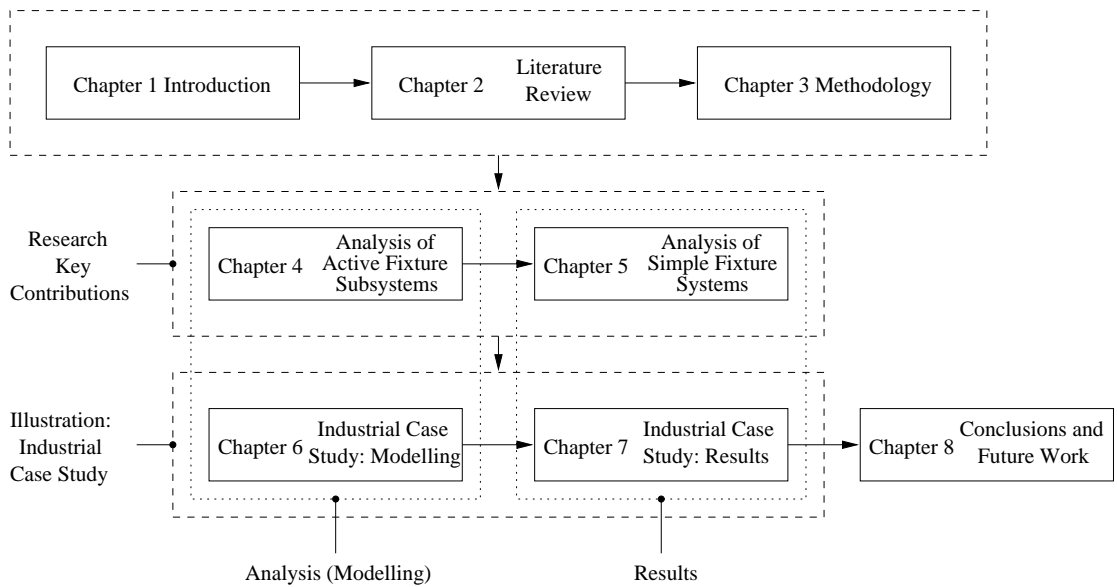
Figure 1.3: Thesis structure.

Literature Review

2.1 Introduction

In Chapter 1 it was observed that the development of computers has lead to an approach of "smart" or "advanced" technologies. Drawing on the same source, the application of computer numerical control has lead to the development of machine centres and multi-spindle stations, which can handle as many different jobs as time and dimensions allow. As a result, a paradigm shift occurred in manufacturing as one machine or a cell can do many different jobs, with a minimal required effort in time and money for transformation. This flexible utilisation of manufacturing equipment, however, requires a production architecture, among which novel fixturing technology, with a high degree of reconfigurability. Meanwhile, the performance of the new fixtures should be equal to that of the so-called dedicated fixtures, with the added benefit of flexibility. Several factors influencing fixture performance are reviewed in this chapter on basis of the fixture design process.

The functioning of a fixture during machining is dominated by its mechanical performance, but its functionality and design can only be understood after careful examination of the rationale behind the design and its interaction with the manufacturing environment [65]. This review will therefore focus on the mechanical aspects of fixture design to identify the relevant parameters that govern the fixture performance and how these can be adapted to improve the workholding capabilities of the new generation of fixtures. This survey is organised as follows. To familiarise the reader with fixturing,

firstly, the basics of fixturing are explained in Section 2.2. The initial stages of fixture design for a workpiece that lead to a fixture layout are considered in Section 2.3. Different design concepts for the reconfiguration of the fixture layout exist, and these strategies are discussed in Section 2.4. The aspects of fixture performance and their verification, forming the next link in the fixture design cycle, are studied in Section 2.5. When applying a mechatronic design approach, smart or intelligent technologies can be utilised to improve the fixture performance. The relevant elements of the integration of mechatronics and fixturing technology are studied in Section 2.6. A summary of the whole survey and the identification of the knowledge gaps can be found in Section 2.7.

2.2 On the Basics of Fixturing

This section seeks to give a brief introduction into fixturing to familiarise the reader with the area. Firstly, the basic requirements for fixture design are considered in Section 2.2.1 and subsequently some of the basic fixture elements, which are discussed in this and the following chapters, are introduced in Section 2.2.2.

2.2.1 Basic Requirements for Fixture Design

During machining and assembly operations workpieces need to be fastened to a holder. This is called fixturing and the devices used for holding a part are called fixtures or workpiece holders. Therefore, fixtures have to fulfil the following three main functions [74, 115, 116, 142]:

- **locating** (positioning of the part),

- **holding** (fixation of a part by clamping the part),

- **supporting** (prevention of elastic and plastic deformation).

Hence, fixtures have to locate the workpiece accurately, unambiguously and do so quickly and reliable; supply sufficient clamping force for rigid and stable workholding; prevent against the occurrence of damage of its locating reference points or planes, and provide strong, rigid and stable support against deformation; enable a quick and easy loading and unloading of the part; allow for easy disposal of coolant and chips; provide

easy and safe handling for the fixture machinist; be durable and maintainable at low cost; be as "flexible" as possible with respect to number of different parts it can handle (universality), and to the slight variation in part dimensions which it should be able to accommodate for (adjustability).

Rong *et al.* [142], see Figure 2.1(a), have categorised fixture design in four stages: setup planning, fixture planning, fixture configuration design and fixture design verification. Note that other authors, such as [115], distinguish two separate stages within the "fixture configuration design". As mentioned in Section 2.1, the first part of this literature review will be devoted to a discussion of the specifics regarding fixture designs. As Rong *et al.* [142] discuss the design of fixtures from a computer-aided design perspective, and this research has a different outlook, not all the bullet points shown in Figure 2.1 will be discussed here in detail.

2.2.2 Basic Fixture Elements

Traditionally, parts are fixtured by simple means such as vices, dovetail slots and V-blocks. Such instruments have the advantage, that they are quite universal, quick to load and unload. Moreover, machine vices can be equipped with so-called "soft jaws". Material can be removed from these soft jaws such that they have the same shape as the part. However, these solutions do not offer much support against deflection, which is crucial when machining more compliant parts.

In order to provide more support, most fixtures are actually more complex constructions and consist of multiple fixture elements or 'fixels'. These fixture elements can be formally distinguished into four categories [115, 116]:

- **locators**, which are used to position the workpiece with respect to the coordinate frame of the machine tool. Additionally, locators also provide support for the workpiece;

- **clamps**, which are applied to exert clamping forces which hold the part securely in the fixture by pushing the part against the locators;

- additionally, extra **supports** can be placed, these supports are not used to establish the position of the part, but only to suppress excess deformation due to clamping

and machining forces;

- the locators, clamps and supports are fastened onto a **fixture body** or a **chuck**[1], that is mounted onto the machine.

Sometimes, especially for drilling and boring operations, an additional feature for tool guidance is added to the fixture design. Strictly speaking, this is called a **jig** and not a fixture although often these two terms are confused [74, 115]. The term jig is also used to refer to an external device to position a workpiece in a fixture.

Several basic design solutions are contrived for (the configuration of) the fixture elements. It is readily understood that different parts each require individual unique fixturing solutions, as different parts come in different shapes and dimensions. The uniqueness of the fixture layout means that the fixture becomes less universal.

When large series of the same part are manufactured it becomes economically viable - and therefore common practice - to design **dedicated fixtures**. The design of a dedicated fixture is such that the fixture element forms one integrated part and the layout cannot be altered. As fixture elements have a fixed position, parts can be positioned reliably and repeatably. These sorts of fixtures typically have high stiffness and relatively low setup times, but it can only be used for one particular workpiece. When series are smaller, because of low demand for and/or short life-cycle of the product, a more flexible use of the fixture is desirable. Several design approaches exist to construct **reconfigurable fixtures**.

2.3 Initial Fixture Design

2.3.1 Setup Planning

One of the major complicating factors in fixture design in general is that the fixturing is strongly a workpiece and a process dependent part of the manufacturing chain. Already during product/part design the design engineer needs to address the issues regarding the manufacturability of the workpiece. Several guidelines for best practice during design

---

[1]A chuck would be a self-holding fixture body, whereas fastening on a fixture body requires additional means, such as bolt and nuts.

have been set up under names such as Design for Manufacturing (DfM), Design for 'X' (DfX) and "concurrent engineering" [74]. As seen in Figure 2.1(a), during this stage of the fixture design the following questions need to be addressed: (1), in which orientation of the workpiece (surfaces) can most machining processes be executed? (2), in what order will the machining take place? Forming processes often require allowances, which result in poor locating of the part with respect to the fixture's reference frame and therefore cannot be used as geometrical reference points. This leads to the third question: (3) are any specially designed reference points required? Furthermore, at this stage a fundamental choice has to be made, based on the stiffness of the workpiece relative to the machining forces. In order to avoid a stack-up of tolerances, it is paramount that manufacturing operations are carried out in the same part-fixture setup [74, 142].

If the workpiece is relatively compliant, like e.g. turbine blades, it may be necessary to use non-conventional fixturing technologies, such as concepts based on phase-change materials or pin-type array fixtures [116]. A further discussion of fixture technology can be found in Section 2.4.

2.3.2 Fixture Layout Synthesis

The next stage in fixturing design is the fixture planning, as can be observed in Figure 2.1(a). The order in which the fixture layout synthesis is executed is also shown in Figure 2.1. Firstly, locating points are to be selected during the fixture planning from the reference points and surfaces assigned for location during the setup planning. The validity of the locating scheme is verified with a kinematic restraint analysis on basis of the screw theory. The rigid body motion of the workpiece can be mapped onto a so-called screw, which means that the motion is decomposed into a rotation about an axis followed by a translation along that axis. In the screw theory, the twist represents the velocity of workpiece. Hence, if the all six degrees of freedom of the rigid part are properly constrained, the twist is zero [115, 116, 142, 170, 172].

Regarding the locator layout synthesis, the engineer can utilise the accumulated knowledge gained from previous fixture designs. For example, in case the position for the locating points is not restricted, it is best to place to locators far apart, as this minimises the reaction forces against applied machining moments. Or, fixture designs

for parts from the same part family can be reused with only small changes. This sort of knowledge based design has been the incentive of extensive research into the computer aided approaches of automatisation and optimisation of locator layouts using rule-based, expert systems and case-based methods [23, 66, 75, 115, 116, 142].

Additional supports are placed on the basis of a deformation analysis. An overwhelming majority of research publications only consider static forces acting on the part, notable exceptions can be found in the papers by Daimon *et al.* [32] and Deiab [37], who take the *dynamic mode shapes* into account in a structural modification strategy to establish a support layout design. In certain cases, it can be very hard or impossible to place additional supports. In order to address this problem, Ceglarek and coworkers, e.g. [24], studied methods to achieve finite element analysis-based locator layout synthesis for sheet metal part handling or assembly fixtures.

Further down in fixture layout synthesis, suitable clamping locations are determined. Together, clamps and locators should provide form as well as force closure. Force closure is obtained when a given clamping force results in reaction forces at the locators that are pointed inward into the part. To fulfil the conditions for stable workholding, contact(s) between part and locators is required at all times, and the clamping force must be large enough to maintain force closure under any external loading of bounded magnitude. It is perceived that workpiece contact with locators:

- prevents the workpiece from moving (macro-slip) inside the fixture,

- minimises the vibrational workpiece displacement.

Force closure and, of course, force and moment equilibrium are generally verified with (a modified version of) the screw theory, where the part is considered to be rigid, by calculating the "wrench". The wrench relates the force and torque acting on the workpiece in a similar way as the twist does for the motion. This is what is called the total restraint analysis in Figure 2.1(b). Only few examples can be found of studies where a flexible part is considered in the clamping force analysis. Force closure does not necessarily coincide with form closure, as force closure is a stricter condition than form closure [115, 172]. This is illustrated in Figure 2.2, where a simple triangular rigid part is fixtured; the system is considered to be frictionless. In the fixture layout on the lefthand

side in the Figure, form closure, but no force closure exists, since the reaction force in L3 points outward the part. Since locator L1 basically acts as a pivot, force closure may be obtained when locator L1 is moved up above the dotted line, shown on the righthand side of Figure 2.2.

Another observation can be made from Figure 2.2. When the clamp is moved farther away from locator L1, the moment arm is increasing. When the clamping force is kept at the same value, an increase in the length of the moment arm means an increase of the reaction forces at locators L2 and L3. Then for certain external loading conditions, the clamping force may be minimised by placing the clamp at a certain position. Minimal clamping forces have a major advantage, being that the workpiece deformation due to the clamping forces is minimal as well. Additionally, as the forces in the fixture are lower, comparatively less material (money) is needed to construct a system with desired stiffness. Generally speaking, clamping forces can be minimised by an optimal placement of a clamp. During the machining process this optimal placement and the clamping intensity (exerted clamping force) can actually change. For this reason, much research effort has been placed in methods to find the optimal places for the clamps [75, 89, 115]. Additional clamps can also be placed.

2.3.3 Conclusion

A good fixture design yields a fixture that fulfils its three main functions in the sense that it accurately locates, fixates and supports a part in sufficient manner. Fixture elements should allow for some adjustability for properly locating the part in the fixture. It has been observed that stable workholding (fixation) requires that "lift off" from the locators should not occur, i.e. the part-locator contact is required at all times. This should prevent excessive vibrations and dislocation of the part during the machining or assembly process. In order to achieve this, approximate calculations can be made, using the screw theory to verify the existence of force closure. It is the strong belief of the author of this thesis, that as the demands for small tolerances become ever stringent, and hence modelling becomes ever more important [15], static *and* dynamic finite element analyses will increasingly become an important tool in fixture layout design, to study the deflection of the proposed fixture layout design aforehand. Additionally, the external

load may be minimised by establishing the optimal positions for the clamps and by adjusting the clamping intensity during the machining process.

Furthermore, appropriate placement of locators and support will minimise the deflection of the part due to external loads.

2.4 Fixturing Concepts for Flexible Manufacturing

Serious scientific research effort has been undertaken to establish the underpinning science for the development of new fixturing technology for flexible manufacturing. This resulted in myriad of publications and patents of fixturing strategies and design concepts for workholding, regarding the fixture configuration design. Kleinwinkel *et al.* [84], Nee *et al.* [116] and Shirinzadeh [147] have undertaken the effort to categorise the concepts and the latter two References have summarised their findings in useful diagrams. These diagrams have been combined and the resulting diagram is shown in Figure 2.3. The names for some of the strategies have been updated and some emerging concepts have been added. Furthermore, the concepts based on phase-change base technology have been classified on basis of fixturing concept, rather than on basis of the physics behind phase-change. This is actually already suggested in the taxonomy given in Ref. [116]. As can be seen in Figure 2.3, seven basic fixturing concepts (and the generic category "other fixturing concepts") have been identified in Refs [116, 147], which can then be further categorised. These basic fixturing concepts are studied in more detail in the following sections.

2.4.1 Modular Fixtures

Modular fixtures are constructed with standard elements and modular fixture elements. An example of a modular fixture is shown in Figure 1.2. The fixture elements are easily connected by means of universal connection methods. There are two main concepts for universal connection methods: 'T-slots' and 'holes'. For this reason, the modular elements can best be described as adult versions of construction toys such as fishertechnik®, Lego® or Meccano®. Many approaches for computer-aided-design automatisation have been reported in the literature [18, 75, 116, 142, 147]. The perceived drawbacks of the

modular fixturing concept are: the kits for modular fixture elements are expensive, and locating accuracy in some cases is sub-standard, due to poor accuracy obtained during the assembly of the fixture, tolerances of the fixture elements and small relative displacements of the fixture elements during machining, deterioration of the locating accuracy of time.

2.4.2 Flexible Pallet Systems

Assembled from the same elements as modular fixtures, flexible pallet systems are fixtures that are applied in big machines or multi-spindle stations and can handle multiple parts at a time. The design for flexible pallet systems allows for individual loading and unloading of the workpiece.

2.4.3 Sensor-Based Fixture Design

Sensor-based fixture design is a fixturing strategy where vision and sensor systems are utilised to ensure that the part is located correctly in the fixture (foolproofing). This is an important step towards the automatic loading into fixtures [16, 142]. Shirinzadeh [147] proposed to apply sensors and vision systems to establish the location and orientation of a part and to use this information to control the tooling operations in an assembly fixture. An example of this fixturing concept that is produced on commercial basis is the DELFOi Flexapod [38, 73].

2.4.4 Phase-Change Based Concepts

Phase-change based concepts rely on immobilising a workpiece by, apart from its machining areas, immersing it in a phase-change substance. After positioning the workpiece with an additional jig, the substance is solidified around the workpiece. The actual physics behind solidification depend on the substance that is used: pseudo-phase change material, low-melt alloy, bi-phase liquid, electro- and magneto-rheostatic liquids, etc..

Complex, fragile and flexible parts are encased into highly fixturable (easy-to-fixture) brick-shaped parts and protected against possible damage caused by the fixture contacts. Nee *et al.* [116] distinguish between three different approaches. **Fluidised bed**: the container with phase-change liquid is the fixture itself. **Encapsulation**, in

this strategy the part and the solidified liquid are taken out of the container and fixtured in an additional fixture. **Phase-change baseplate**, a concept where not the part, but the fixture elements are immersed in the phase-change liquid and the solidified fluid holds the fixture elements together. The phase-change based concepts are highly flexible, but some specific drawbacks are associated with this technology. Typically, these special liquids are toxic, the retrieval of the workpiece from the solidified liquid may be a slow process, the energy demand for this technique is considerable and coolants and cutting fluids may diffuse into the solid, deteriorating the performance capacity of the special liquid [122].

2.4.5 Chuck-Based Concepts

In case the machining forces are low and one of the sides of the workpiece is flat, it can be sufficient to fixture only the flat side with a chuck, whose self-holding capability relies on **magnetic** forces [35, 74, 84, 147], or **vacuum** forces [74, 84, 104], or on the workpiece being **frozen** onto the chuck [84]. De Meter [36] developed another principle to fasten a part onto a chuck. This fixturing technology relies on the application of an **UV-light activated adhesive layer** on a chuck that fixates the part.

2.4.6 Pin-Type Array Fixtures

Pin-type array fixtures together with related concepts for reconfigurable tools and dies are based on a bed of pins. A mechanism inside the bed allows the tip of the individual pins to be positioned in axial direction, such that the surface of the tool is enveloped by the tips of the pins. **Actuated and passive designs** of this mechanism can be found in the literature [113, 165]. In some designs the pins are only used to **support-and-locate** a workpiece, see e.g. Figure 2.4(a), a discussion of this type of designs is given in Refs [116, 165], whilst in other designs the pins are used to **clamp** the workpiece, see e.g. Figure 2.4(b). Closer attention to the actuation of clamps (in general) will be paid in Section 2.6.4.2. Typically, an external jig is required to locate the part on the bed of pins. As seen in Figure 2.4, pin spacing and dimensions can vary per application. This concept has not only been applied to the fixturing of turbine blades and sheet metal parts, but also to other (large) parts, such as engine blocks fixtured with pin-type

arrays [35].

2.4.7   Automatically Reconfigurable Fixtures

Five basic design strategies for automatically reconfigurable fixtures can be identified in literature. All these concepts rely on robots. Fixture modules can be assembled and **reconfigured by means of robot systems**, where a robot places the fixture elements in the holes of a base plate [16] or on magnetic chucks [18, 35, 116, 147]. The lack of positional accuracy reported for modular fixtures is also reported for this concept, as it relies on the positional accuracy of the robot.

Other strategies rely on the robot-as-fixture paradigm. The first of these concepts are the **actuated pin-type array fixtures** as described above. Secondly, concepts based on **grippers** that grasp objects are discussed in Ref. [116]. Often these designs are used in micro-machining and come under the name of "micro-manipulator" or "tweezers". The positional accuracy and load bearing capacity of dexterous grippers for larger object is generally lower than that of fixtures. For this reason, other gripping strategies have been proposed, e.g. the designs presented in Refs [25, 152] where a part can be grasped, positioned and orientated. The remaining two fixturing concepts are robots in the form of **parallel kinematic mechanisms** (PMKs) and **Cartesian coordinate robots**. PKMs are mainly applied in assembly fixtures [85]. See e.g. Refs [7, 88, 164] for early applications of PKMs in fixturing, while more recent approaches can be found in Refs [17, 35, 38, 73]. Molfino *et al.* [112] propose the use of many PKMs (a swarm) to be able to relocate support points during the machining process. An illustration of this concept is shown in Figure 2.5(a), where a group of PKM-based fixture elements provides extra support at the tool location. PKMs can be positioned more accurately than Cartesian robots and have a proven capability to provide large stiffness, and they are often applied in modern machining centres [17, 47]. Cartesian robots, however, are easier to control and more compact than PKM-based robots. Design proposals involving Cartesian robots can be found in Tol [160] and Madden [96]. At The University of Nottingham, a more advanced version of Chan and Lin's multifinger modules [25] has been designed by the authors of Refs [120, 143]; their concept is shown in Figure 2.5(b). More advanced 3D concepts of Cartesian robot based concepts have been developed for the assembly of

cars at the body in white[2] lines, e.g. [2, 6]. Related to the Cartesian coordinate design approach is the design of Du and Lin [42]. A short discussion on the working of the concept is given in Section 2.6.3.3.

2.4.8 Conclusion

Many solutions for the fixturing problem are reported in the literature. As fixture design is highly dependent on the manufacturing process and the part (compliance, machining area, reference or datum points, part dimensions), some concepts will prove to be invalid fixturing strategies under certain circumstances. Furthermore, pin-type array fixtures and phase-change fixtures yield a design with an entire different fixture layout, when compared to strategies that seek to fixture a part based on statically determined fixture layouts. External jigs are needed to locate the workpiece, and subsequently load it in these non-conventional workpiece holders. Another important observation to make is that most fixturing solutions for flexible manufacturing, shown in Figure 2.3, can be classified as prior art. More recently, concepts were developed for automatically reconfigurable fixtures. Self-reconfigurable fixtures based on PKMs and Cartesian robots have been developed. Furthermore, a new fixturing capability is emerging from these self-reconfigurable fixturing techniques: in process reconfigurability [112] for the optimal placement of clamps and supports during the whole process time.

2.5 Fixture Design Verification

Fixture design verification, see Figure 2.1, is traditionally the stage in which the fixture performance is analysed [89, 116, 142].

2.5.1 Fixture Performance

The fixture performance is determined by the surface quality and dimensional errors the workpiece has, after all the machining processes planned for that specific part-fixture

---

[2]Body in White (BIW) refers to the stage in the production of cars in which the car body sheet metal (including doors, hoods, and deck lids) is assembled, but before the chassis, engine and trim (windshields, seats, upholstery, electronics, etc.) have been added to the assembly, or to the design of these sheet metal components.

setup are carried out. Fixture-related sources contributing to poor surface quality and tolerances can be sorted into the following categories: workpiece and fixture deformation due to clamping and machining forces, locating errors due to tolerances in the workpiece dimensions, locator placement and locator dimensions, poor workpiece positioning [84, 94, 131, 134, 168]. Workpiece error and the associated fixture-related sources can be analysed with the diagram presented in Figure 2.6.

When a part has poor tolerances at the datum points, in some occasions, one is able to optimise the position and orientation of the workpiece by allowing for some adjustability of the locators, thus compensating for the workpiece-tolerance-induced locating errors. This compensation process can actually be automatised using sensor-based and automatically reconfigurable fixturing concepts, see Section 2.4 for a discussion of these concepts. Workpiece deformation due to external forces, which can originate from machining, gravitational or clamping, can be minimised by placing the locators such that the reaction forces, against an applied machining moment at the locators, are minimal. Additional supports can be placed to prevent excessive deflection. Furthermore, the applied clamping force should be as low as possible, as discussed in Section 2.3.

2.5.2 Verification Analyses

The verification of the fixture design is an important step in the design cycle, Rong *et al.* [142] and Nee *et al.* [116] devote the second half of their books on this issue, and Leopold [89] stresses its importance quite early in the introduction of his review paper. Fixture design verification usually consists of the following analyses:

- A **tolerance sensitivity analysis** - the designed position of the locators and their actual location differs due to tolerances. This can have a profound influence on the position and orientation of the part in the fixture. With a tolerance sensitivity analysis, one can determine this influence of the misplacement of the locators and calculate the allowable tolerances in the locator placement [76, 98, 141]. Automatically reconfigurable fixtures holding integrated position transducers should offer sufficient resolution. Wang [166] describes a procedure to measure fixturing error using CMMs (coordinate measurement machines). The recent strong advance of optical CMM (photogrammetry) [31, 57] will probably further the use of CMMs

for fixturing.

- an **accessibility analysis** - studies the accessibility of the part for the machine tools, usually done by calculating the working envelope of the machine tools [142, 167], or by means of virtual reality [92].

- A **stability analysis** - a more thorough analysis of the workholding stability, that verifies the existence of force closure as specified during the fixture layout synthesis. Analyses focus on friction force, minimum clamping forces, clamping sequences, workpiece and fixture deformation [89, 142]. In the next sections some relevant research of the modelling of the mechanics at the part-fixture interface and of static and dynamic analysis of deformable part-fixture systems will be briefly considered.

2.6   Design Approach for Intelligent Fixturing System

The design cycle for fixtures for flexible manufacturing has been studied in the previous sections. On this basis, requirements for the new generation of fixtures can be specified. Additionally, the process variables for the control of part-fixture systems during machining can be established. Subsequently, some state-of-the-art examples of controlled machining fixtures will be considered. A brief survey will be made in the field of structural control where the design of controllers for similar systems is studied.

2.6.1   Requirements for an Intelligent Fixturing System

From the study of the design process one can establish the desired specifications for a fixturing system that can meet the demands for flexible use of manufacturing facilities. Such a fixturing system is often referred to as an intelligent fixturing system (IFS) [89, 115]. In general, fixtures will have to supply accurate location (locating), stiffness for support, sufficient clamping force and stable workholding. The main IFS requirements can be listed as follows[3]:

---

[3]Note that not all these requirements may be needed at the same time due to financial and/or part-specific constraints.

- Low reconfiguration times, for this reason IFS will be automatically reconfigurable. Such designs, described in Section 2.4, are PKM, Cartesian based systems, pin-type array, or certain gripper designs.

- Accurate locating, the two major problems in current design are the tolerances in the placement and in the dimension of the locators. For this reason IFS is equipped with position sensors and (optical[4]) CMM to achieve an accurately positioned and oriented fixture layout.

- Automatic adjustability of the IFS aided by CMM systems, to realise optimal locating for parts with poor, but still acceptable, tolerances.

- Capabilities for realigning and manipulation of the workpiece aided by CMM and other sensory systems to compensate for badly loaded workpieces, as proposed in [120, 143], see also Figure 2.5(b).

- Reconfigurability of clamps and supports during the manufacturing process, this part of the fixture layout can be re-optimised during the process.

- Active control of clamping forces, to minimise the deformation in the part-fixture system due to the clamping forces. As a result, a minimisation of the forces in the system during machining will also lead to a decrease in workpiece slippage in the fixture and improve the part's dimensional errors.

2.6.2 Key Process Variables for Active Control of Fixtures During Machining

From the review held on fixture design, it may be observed that in fixture design the clamping force, clamp position and support positions are the candidates for controlled inputs throughout the machining process in order to minimise the deflection.

---

[4]In a recent paper, Cuypers *et al.* [31] quote an accuracy of order 10-100 μm when measuring relatively large objects, which is of lower accuracy than traditional CMMs or other displacement sensors [31], the quoted accuracy is in agreement with the worked-out maximum accuracy of the GOM TRITOP system [57] in terms of resolution, which is dependent on the size of the measured part and the number of pixels.

The relevant variables for control are the reaction forces at the locators. In certain cases one can compensate the part displacement, but this gives conflicts with the requirement for the workpiece to have contact with the locators at all time whilst fixtured.

At the same time, sensing other variables than the reaction forces at the locators, supports and clamps, may prove to difficult. Firstly, the part and fixture are continuous systems, and as such have an infinite number of degrees of freedom. Although, a combination of relatively stiff and flexible elements often allows a lumped-parameter model. Secondly, requirements for accessibility put hefty constraints on sensor placements. For example, the part displacement at the machining area determines the final dimensional accuracy and surface quality, yet probes cannot touch the surface during machining and chips, cutting fluid and the cutter obstruct vision and other contactless sensory systems. Another strategy to measure part displacements is presented by de Meter and Hockenberger [106], who measure the displacement near the locators with eddy current sensors. Thirdly, sparks, noise, vibrations, cutting fluid, etc., create a harsh environment, requiring the application of robust equipment. Finally, the application of many sensors is not economically viable.

2.6.3 Related Work

Three approaches, regarding the active control of part-fixture deformation, can be identified in the literature. Firstly, direct compensation for part displacement (position control), secondly, controlling the reaction forces at the locators, and, thirdly, suppressing machine chatter. These approaches will be discussed in the following sections. The (proposed) control strategies of each of these concepts are summarised in Table 2.1. The majority of the applied strategies are adaptive control or compensators that require online tuning.

2.6.3.1 Chatter Suppression

2.6.3.1.1 Fixture-Based Concepts

Vibrations originating from workpiece-machine interaction have an adverse effect on the machining quality. One of the strategies taken to improve tool-life and surface finish is to suppress one or more of the dominant modes of vibration by following the vibrations

of the tool. An early approach is made by Tansel *et al.* [154], who designed a fixture for micro-manufacturing, for improved tool-life by suppressing chatter. Rashid and Nicolescu developed a grinding table (or chuck, or pallet) to cancel vibrations in milling [135]. Recently, this approach has started to receive much attention in Germany: [3, 20]. A similar approach is found in the designs for fixtures that are developed for vibration-assisted grinding in micro-manufacturing, see e.g. [181].

2.6.3.1.2 Structural Control-Based Approaches

This strategy is different from the fixture-based concepts discussed above in Section 2.6.3.1.1 in the sense that chatter is not suppressed by means of fixture elements, but by external (extraneous) elements that are directly attached onto the workpiece as is done in structural control [29, 71]. Rashid and Nicolescu [136] developed a concept with *passive* damping elements, called tuned viscoelastic dampers (TVDs). The viscoelastic properties of the damper give that the stiffness of the element *also* depends on the local velocity of material. Zhang and Sims [179] attached a piezoelectric element to the workpiece for *active* vibration damping.

2.6.3.2 Compensation of Part Displacement

Related to the chatter suppression fixture designs are the micro-positioning tables for grinding that can compensate for workpiece deformation due to machining forces [53, 176]. Another approach has been taken by Culpepper *et al.* [30], who developed an eccentric ball-shaft-based positioning table fixture concept, where the balls are actuated by ball-screw actuators to increase the accuracy of part positioning. In another paper Varadarajan and Culpepper [161], improved the design by now positioning the balls by means of piezoelectric actuation and flexure bearings. Yamaguchi *et al.* [173] describe an active assembly fixture consisting of 4 two-segment arms of which the first segment is actuated along its axis. The fixture can position parts onto a certain location, making use of vision, force sensors and inverse kinematics. Within the AFFIX research consortium [5], clamp modules have been developed that can be used for force control, aligning and position of parts, and compensation of error in part dimensions. Zhang *et al.* [177] proposed a device to be applied in a modular welding fixture that can compensate for

variation in part dimensions. Furthermore, Park and Mills developed a robot arm with an active gripper able to damp-out vibrations and to compensate for static deformation due to gravitational forces in metal sheet assemblies [121].

2.6.3.3 Force-Controlled Fixtures

Wiens and coworkers from the University of Florida [171], developed a concept for a force-controlled fixture for meso-scale manufacturing, which is shown in Figure 2.7(a). Similar to the concept by Yamaguchi *et al.* [173], the fixture consists of four fixels that can be used to position and orientate the workpiece. The fixel consists of a monolithic four-bar PKM mechanism utilised for active force control and part manipulation.

Velíšek *et al.* [162] developed an intelligent pneumatic clamping device that is aware of both the presence of a part (loaded condition) and the clamp location. The clamps work simultaneous and in opposite directions, an external jig is needed to load and hold the part.

Du and Lin [42] developed a prototype of an automatically reconfigurable fixture for planar objects, consisting of three pins that can be repositioned. One pin can be repositioned with a Cartesian coordinate based mechanism and the two other pins can be repositioned with a rotary table based mechanism as is shown in Figure 2.7(b). The pin on the moveable module, see Figure 2.7(b), is used to clamp the part onto the two locators. In Ref. [43], Du *et al.* applied an online measurement of the workpiece stiffness in the fixture during machining to control the clamping forces.

The concept described by Tol [160] is based on that of Du and Lin [42], but uses 4 pins and is based on the Cartesian robot concept instead of two rotating disc elements. Furthermore, the concept developed by the authors of Ref. [120, 143] can also be used for control of the reaction forces.

The best documented and well-known approach to a force-controlled fixture is probably the 'Intelligent Fixturing System' developed at the National University of Singapore by Nee and coworkers [114, 115]. The schematic design is shown in Figure 2.8(a). The design of the IFS starts after determining the optimal placement and clamping order [156] and the optimal clamping forces [155]. Wang *et al.* [169] propose to calculate the optimal clamping forces for the IFS off-line, i.e. aforehand, and then use these calcu-

lated forces in the real world. Additionally, a proposal for a simple model-based online control of the clamping forces was made [168]. The clamping force in the Singapore IFS is generated by a ball screw driven by a permanent magnet DC motor [97]. For extra accuracy the ball screw is controlled by a cascaded controller that compares the clamping force with the actuator displacement multiplied by a constant stiffness gain. Not explicitly drawn in Figure 2.8(a), the clamping force is monitored by force sensors and position control is used to obtain extra accuracy in the position of the tip of the clamp as force and static displacement are proportional to the effective stiffness of the part-fixture system. Nee *et al.* in Ref. [115, §6.5.2] apply system identification to establish models for the dynamic control of the IFS, contrary to the proposals in Refs [168, 169]. In Figure 2.8b(b) it can be observed that the approach by Nee *et al.* shows a promising increase of surface quality after machining, this increase has also been observed in the experimental results by Papastathis [119]. Similar to the IFS design by Nee *et al.*, a test-bed - where stepper motors are applied for the active control of clamping forces - has been developed within the AFFIX project [5, 22].

2.6.4   Mechatronic System Design Synthesis

Now that the requirements for IFS are specified, the process variables are made explicit, and related works have been studied, it is clear that active control of part-fixture systems seeks to improve the mechanical behaviour of the system. Related applications can be found in the field of **active control of structures**, where structural dynamics and control engineering are combined to improve the behaviour of structures. Applications can be found in the traditional areas of interest of structural engineering. Buildings and bridges should not collapse when they are hit by earthquakes nor by wind. The hull and wings of aeroplanes should be capable of bearing the aerodynamic forces. Large, hence flexible space structures, such as satellites and space-stations are in constant need of correction with respect to their orbit and orientation. Correction comes in the form of (small) thrust pulses and vibrations should be kept to a minimum for reasons of "comfort" for personnel as well as instruments, and structural integrity of the space craft. Furthermore, fluid-structure interaction in pipelines in (nuclear) industry can cause undesired noise and vibrations [29]. Improvement of the behaviour of buildings, aero-

wings and space structures by means of active control has enjoyed considerable research effort in the 1970s and 1980s [102] and recently regained attention because of the advance of smart materials and advanced (modern) approaches to control [61, 69, 71, 128, 130].

The mechatronic system design for IFS can hence be established taking the active structural control approach as described above as a starting point. One of the major differences between "conventional" structures studied in structural engineering and part-fixture systems is that the more conventional structures have a supporting structure that is usually taken as the fixed world, whilst the part, which is the structure of interest, is fastened to the "fixed world" in the form of a base plate by compliant fixture elements that tend to be single, geometrically dispersed points in traditional fixture designs. Another difference is that in smart fixture design the fixture elements are the only active elements.

Structural control comprises the structured approach in the study of the four following fields: sensing, actuating, mechanical modelling and control. The mechanical modelling of part-fixture systems has been reviewed in Section 2.5 already. In the following sections we will therefore pay attention to the remaining three fields after analysing the application of (basic) structural mechanics in fixture design.

2.6.4.1 Approaches to Structural Mechanics

Applications of structural mechanics methods in fixturing design can be found in both fixture layout design and in verification. Specific attention has been paid to contact mechanics at the part-fixture interface: friction and local deformation. Friction introduces hysteresis on the level of micro- and macro-slippage. Friction and hysteresis on micro-level are usually observed in the form of higher than expected damping. Furthermore, as it is hard to model friction from first principles [15, 72], it is often assumed that friction can be adequately modelled as Coulomb friction.

Any occurring friction will introduce nonlinearity to the system behaviour and, furthermore, changes the distribution of the reaction forces. For this reason, often friction is taken into account to verify the existence of force closure during the fixture layout design. During the fixture verification stage the influence of the contact compliance on the reaction forces is studied.

The actual underlying contact mechanics to calculate this deformation are hard

to model from first principles, as many parameters play a role [15, 72]. A frequently applied model in fixture development is the Hertzian contact theory [122]. However, the applicability of the *classical* Hertzian contact theory is limited, as factors such as such as plasticity, kinematic hardening and surface hardness are not taken into account [122, 145, 146, 175], but play a large role within fixturing. Furthermore, since the Hertzian theory assumes that one of the bodies is an infinite half-body, one can only make some approximate calculations for prismatic parts with relatively small contact points and low contact stresses. Experiments by Shawki and Abdel-Aal [145, 146] and Phuah [122] revealed significant discrepancies between the Hertzian theory and the experimental results. Moreover, results of Phuah and Shawki and Abdel-Aal do not show mutual agreement as well. For this reason, based on the experimental results published by Shawki and Abdel-Aal [145, 146], empirical approaches have been adopted by Daimon *et al.* [32] and Mittal *et al.* [109] who established a model whereby spring-dashpot elements are used to describe the (contact) stiffness of the clampers and locators. Thus avoiding "computationally expensive" contact mechanics in their models. The approach to model contact stiffness with (non-)linear springs and dashpots has been widely investigated and compared with experimental results and subsequently adopted in the manufacturing research community and spring-dashpot elements are added to rigid as well as flexible models of parts [67, 93, 107, 139, 142, 153, 175]. Two examples of spring-dashpot elements are shown in Figure 2.9. The element shown in Figure 2.9(a) is used to model contact friction, and axial and radial contact stiffness. This element is not only used to model the contact mechanics in a part-fixture system, but systems consisting of a certain number of these elements are also widely applied in structural dynamics to model bolted joints in structures, see e.g. Ref. [79] and the references therein. Nee *et al.* [142] provide a further description of both models shown in Figure 2.9.

Additionally, friction and contact compliance have a detrimental influence on the locator performance. As a result of nonlinearity in contact phenomena, different clamping sequences give differently positioned workpieces in the same part-fixture systems. Computational mechanics, usually by the application of the finite element method [29], has not only been applied to study the locator performance but also workholding stability. Many industrial parts are actually not as rigid as the prismatic parts studied in academic

research papers and often possess complex shapes, see e.g. [32, 83, 104, 115, 133]. There is a need to carry out verifications that study the deformation of flexible part during fixturing and processing. The strong increase in computational power over the last two decades has allowed for analyses that take into account the compliance of part-fixture systems. The advantages of conducting detailed finite element analyses are that one can analyse stresses, deformation, reaction forces, fixture compliance, compute tool path compensation [106, 118, 122, 134, 138].

It should be observed that machining means material removal, which in some cases should be accounted for [39]. Most authors, see e.g. Refs [59, 78, 118, 133], propose the use of special elements in the finite element environment to take care of the material removal. In addition, Deng [39] studies the influence of material removal on fixturing stability and proposes to optimise the clamping by taking into account the material removal. Zhang *et al.* [178] propose to apply matrix perturbation techniques to update the mass and stiffness matrices to accommodate for material removal.

2.6.4.2 Actuation

Clamps can be actuated by means of the following actuation methods [54, 61, 70, 71, 127]:

- Hydraulic actuation has the advantage that hydraulic systems are often installed and applied in manufacturing environments. Due to their stiffness and large stroke hydraulic actuators can be applied to actuate PKM- or Cartesian-based reconfigurable fixture designs, e.g. [17, 47, 88]. The drawback of hydraulic systems are the extra requirements such as pumps, reservoir, pipelines, accumulators etc. which take up space and are costly systems. The velocity of hydraulic actuators is highly depended on the pump capacity and maximum flow rate of the servo-valve. For applications in adaptive structures, piezo-hydraulic actuation and use of magneto- and electro-rheological fluids have replaced the mechanical servo-valves. In manufacturing, small, modular hydraulic clamps have been developed for use in flexible fixtures [35, 45, 140].

- Pneumatic actuation is a concept that is closely related to hydraulic actuation. A pneumatic infrastructure is probably even more commonly installed than its

hydraulic equivalent. Pneumatic actuation has the following severe drawbacks which render this actuation principle to be only a useful concept for low force applications, e.g. [7, 162]. Due to the compressibility of gasses, the stiffness of pneumatic actuators is low. For the same reason, the supply pressure is also low and large piston areas are required compared to hydraulic actuation.

- Electromechanical actuated clamps; electromechanical actuation for linear motion using ball screws (or lead screws) is commonly applied to actuate the swivel tables in manufacturing machinery where reliability, accuracy and stiffness are also required [74]. Several actuation principles can be used, such as DC or AC motors, or even a rotary piezomotor. Electromechanical actuation has the advantage over hydraulic actuation that no auxiliary equipment and infrastructure is needed in the form of pumps and pipes. The disadvantage is that a relatively large electric motor and gearbox use extra valuable space which reduces the accessibility of the fixture.

- Other electromagnetic actuation principles such as voice-coil motors, solenoids, electrostatic actuation, an actuation principle often applied in MEMS systems and the electromagnetic dual of solenoids, or linear motors.

- Piezoelectric actuators (PEAs) have the advantage that they offer a very stiff actuation principle, moreover, PEAs can exert high forces. PEAs have very small actuation stroke, which may be increased by a motion amplifier. In contrast with hydraulic and electromechanical actuation, PEAs do not suffer from friction, backlash and play and have a high bandwidth.

- Other applications of smart materials based actuation principles may be used, such as: piezohydraulic actuation, electrostrictive and magnetostrictive actuation.

- Shape-memory-alloy actuators have at the moment two major drawbacks: they are often made of brittle materials and have relatively low bandwidth compared with other actuation methods.

- Dual actuation methods were initially proposed for application in the precise positioning of the read/write head in hard discs [46]. Dual actuation methods make

use of two actuators that are mounted on top of each other along the same axis of actuation (piggyback configuration). One actuator is used for coarse motion and the other actuator is used for precise positioning or for the force stroke. This actuation principle is often applied for ultra-precision stages that are utilised in atomic force microscopes (nano-scale precision), or in wafer stepper machines for micro-lithography (IC manufacturing). More recently, dual actuation found its way in other micro-manufacturing applications for precise part positioning [44, 64, 154][5] or positioning of the cutting tool [49, 80]. Neelakantan *et al.* [117] studied the utilisation of a lead screw for the positioning stroke and a PEA for the force stroke for application in brakes and clutches.

- Other Principles, such as pneumatic or electrostrictive polymer artificial muscles, pneumatic bladders and magnetic clamps.

Actuators are selected on basis of demands regarding price, operational costs, actuator bandwidth, required stroke, required force or torque, and power output relative to its size/mass (power density).

2.6.4.3 Sensors

The forces and displacements in a part-fixture system can be measured with different sensing principles.

Cutting forces are often measured using dynamometers [63, 81] that measure the three components and possibly a torque of the machining force. The dynamometer is mounted on the machine table and functions as baseplate for the fixture. Dynamometers tend to be costly and limited in size, to overcome these difficulties, Hameed *et al.* [63] propose an inverse mechanics based method to calculate the cutting forces on basis of the measured reaction forces at the clamps, supports and locators. Reaction forces at the locators can be measured relatively cheaply with piezoelectric force transducers or strain-gauge based sensors [40, 71, 115, 122].

Displacements are commonly measured with linear variable differential transformer sensors, ultrasonic proximity sensors, eddy current sensors, (contactless) [71, 106] and

---

[5]Many micro-manufacturing technologies actually rely on technologies developed in the IC fabrication industry.

at present state-of-the-art displacements can be measured using optical techniques such as video- and photogrammetry [57]. Actuators often come with built-in sensors such as encoders or force transducers.

Sensors are based on different physical principles, such as piezoelectric, ultrasonic, optic, resistive and the physical principle has its influence on the dynamic behaviour of measurement systems [71]. Sensors should therefore be selected on basis of bandwidth, measurement range, resolution, and price. The actuator-sensor combination should have enough resolution to deliver sufficient accuracy. The sensor signal generally needs conditioning with filters and amplifiers.

2.6.4.4   Controller Design

The model of the part can be coupled to that of the actuators, sensors and the structural model of the fixture. Several control strategies have been developed or are applied in the field of structural control [71, 102]. Typically, a part-fixture system is a multi-input multi-output (MIMO) system. In "flexible systems", i.e. systems where the stiffness of the actuator-fixture is much higher than that of the part, one can apply collocated control[6] [102]. When the system is stiff, the control inputs can give undesired interference at outputs which are controlled by other control inputs. In this case application of more advanced, model-based control techniques - such as $\mathcal{H}_\infty$, $\mathcal{H}_2$, Linear-Quadratic-Gaussian (LQG) control or μ-Synthesis - are required [151]. These controllers can be based on mathematical or empirical models (system identification).

2.6.4.5   Model Reduction

In case when e.g. a complex, flexible part is fixtured, the part-fixture system needs to be modelled with discrete techniques, such as the finite element method. These models typically comprise thousands if not millions of degrees of freedom. In this case the model becomes too large for real-time application in model-based control. In order to avoid excessive computational effort, model order reduction techniques have been proposed to reduce the size of the mass and stiffness matrices [132] and are sometimes applied

---

[6]Collocated control refers to a configuration where sensor and actuator are placed in the same position, i.e. one directly controls the measured variable or output.

to establish "superelements" for dynamic substructuring [29, 132]. Dynamic substructuring is used to analyse the behaviour of large systems such as buildings, airplanes, spacecraft. These model reduction techniques developed for computational structural mechanics analysis work well with proportional damping models, in case of non-classical damping, one will have to establish reduced models in state-space using iterative methods to establish the condensation matrix [132].

Other approaches of condensation techniques of state-space models have been developed in the area of systems and control [144]. Furthermore, many transient analysis of physical models are carried out with models cast in state-space formulation. Computational fluid dynamics models of jet engines, models of integrated circuits (IC), MEMS devices [144] or bolted structures / joints [79] are computationally extensive, and typically, contain 10^5-10^9 degrees of freedom. Physical phenomena that do not play an important role on macro-scale, strongly affect the behaviour of MEMS devices or the ever further miniaturised IC designs and require large-scale multi-physics modelling. Other model reduction techniques have been developed to execute analyses of these systems with limited resources and time, such as proper orthogonal decomposition, which has been developed for nonlinear systems (fluid dynamics) [144].

2.6.5 Conclusion

The fixture design process has been analysed and the important design parameters that play an important role in the fixture performance have been established. These process variables are the part displacement and the reaction forces at the locators. The state of the art regarding the control of these parameters has been reviewed. Furthermore, a brief survey of related applications revealed that the integration of actuators and control to enhance the performance of a mechanical structure has been extensively studied in the area of structural control. It should be concluded that the knowledge and methodology developed for structural control can provide the necessary underpinning tools for the mechatronical design of an intelligent part-fixture system. From the literature it can be observed that a structural approach is seldom taken in fixture design. For example, Refs [3, 87, 93, 105, 148] give some examples of studies where model reduction techniques have been applied in part-fixture modelling, and e.g. Refs [3, 60] are examples of papers

where a structural control approach is taken in the modelling and control of (part-)fixture behaviour, whilst a myriad of scientific publications can be found on fixturing taking other approaches.

2.7   Summary and Knowledge Gaps

In the last post of this chapter a review is held of the several relevant aspects of the design of an IFS. The relevant capabilities for an IFS have been established regarding its reconfigurability for flexible utilisation of the fixture and adjustability for increased locating performance. During the manufacturing process the deformation of the workpiece should be minimal. This can be achieved by controlling the part displacement and vibration, or the reaction forces at the locators. These process variables and control objectives are strongly related to those considered in the related field of structural control.

Based on the relevant needs in the area of application of active control of intelligent fixturing systems during the machining process, the knowledge gaps can be identified as follows:

1. There is still a lack of "computationally efficient dynamic models to represent the dynamic response of the workpiece during machining" [104].

2. Regarding "the interaction between the workpiece, fixture and the cutting forces" [104], there is a lack of a systematic approach and applications of techniques developed in the related area of structural mechanics.

3. Existing concepts of actively controlled fixtures mostly make use of the adaptive control strategy or compensators that require online tuning of the settings. Today's emphasis on virtual prototyping requires accurate models that can be utilised in the hardware-in-the-loop (HIL) approach [71] of model-based control. Doing HIL simulations of actively controlled part-fixture systems has the advantages that the number of required prototypes can be strongly reduced and the mechanical and control design can be carried out in parallel, thus saving money and lead-time in the design process.

4. In today's virtual enterprise oriented manufacturing environment, R&D, design, process and setup planning may be carried out on dispersed locations. This requires a formalised methodology to establish the design of an actively controlled intelligent fixturing system.

2.8 Table

Table 2.1: Overview of applied control strategies.

Reference	Applied trategy
[3]	hardware-in-the-loop (HIL) approach
[20]	measure frequency behaviour of fixture, compensated by a filter
[43]	adaptive control
[53]	composite control with PID compensators
[115]	model-based control using system identification
[121]	composite modal controller to control fast and slow dynamics
[135]	filtered X-LMS adaptive control algorithm
[176]	numerical control in combination with PID servo control
[177]	adaptive control

2.9 Figures

(a) A fixture design process-oriented flowchart. Source: Ref. [142], Fig. 2.2.

(b) A fixture design outcome-oriented flowchart. Source: Ref. [115], Fig 6.2.
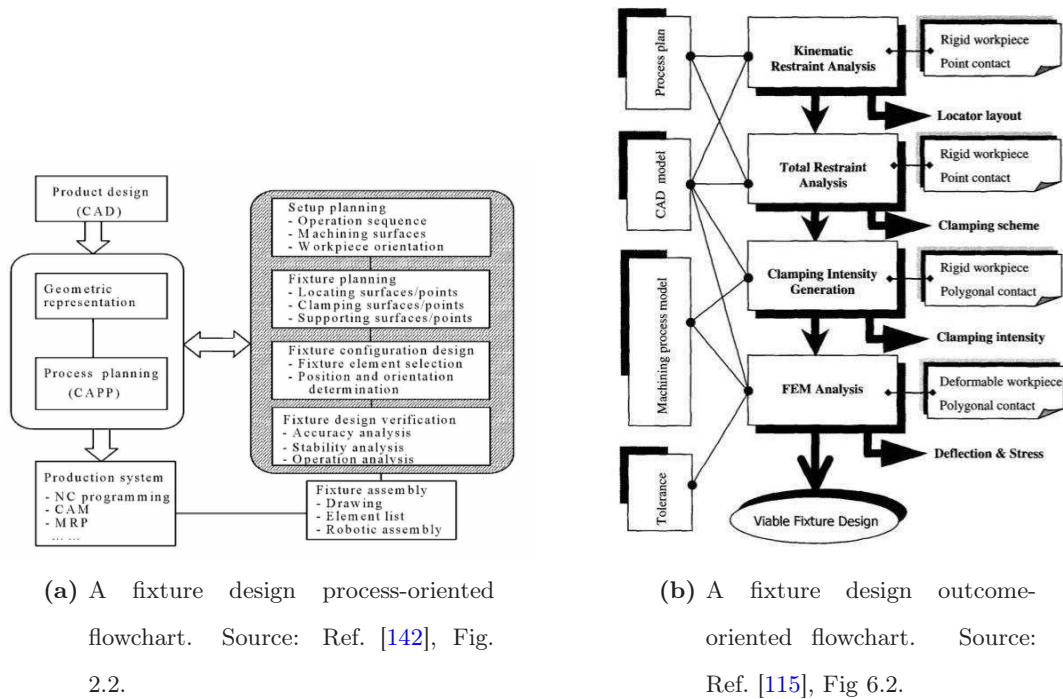
Figure 2.1: Fixture design process flowcharts.
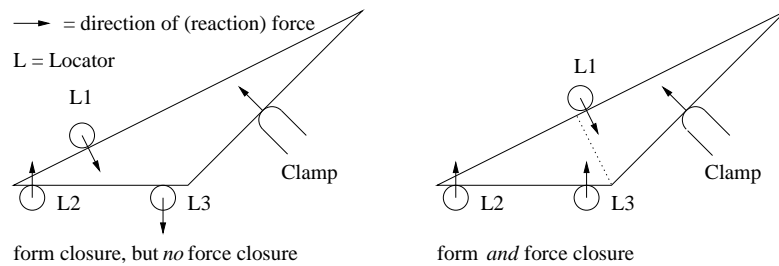
Figure 2.2: Difference between form and force closure, adapted from [115, Fig. 3.1].
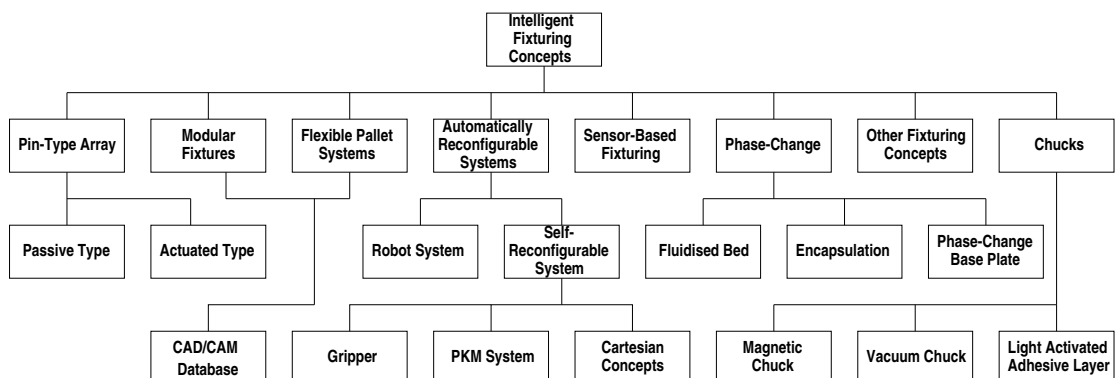
Figure 2.3: Taxonomy of flexible fixturing concepts.
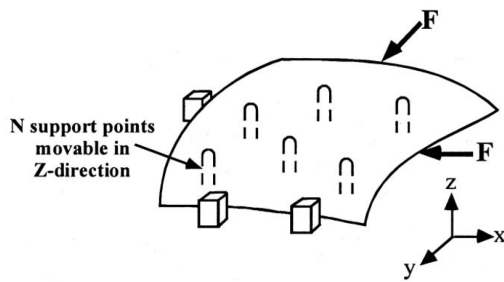
(a) Compliant part fixtured using a pin-type array fixture N-2-1 locating scheme. Source: Ref. [165], Fig. 1(a).
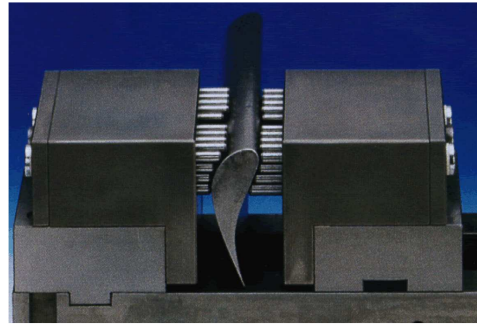
(b) Example of pin-type array fixture that is used for locating and clamping. Source: Ref. [122], Fig. 2.2.

Figure 2.4: Examples of pin-type array fixtures.
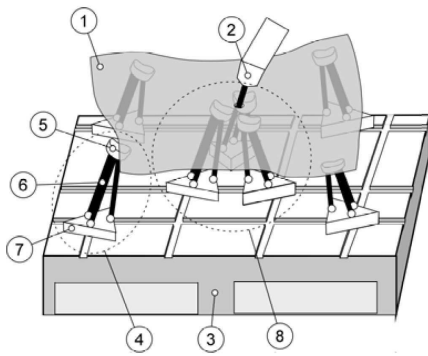
(a) "Conceptual schematic of self reconfigurable swarm fixture: (1) part; (2) manufacturing equipment; (3) bench; (4) agent; (5) support head; (6) positioning mechanism; (7) mobile bases; (8) concentration of agents in the manufacturing region." Source: Ref. [112], Fig. 2.
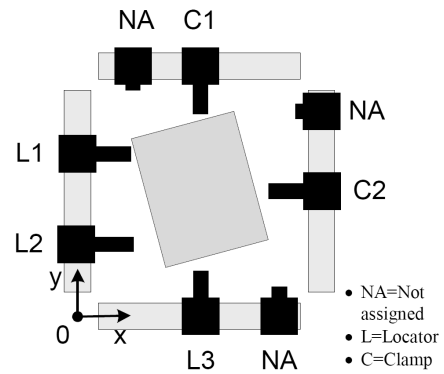
(b) Schematic concept of self-reconfigurable fixture presented in Refs [120, 143]. Source: Ref. [120], Fig. 9.

Figure 2.5: Design concepts for self-reconfigurable fixtures with the ability to reconfigure during machining process.

WORKPIECE ERRORS   APPEARANCES   SOURCE OF ERRORS
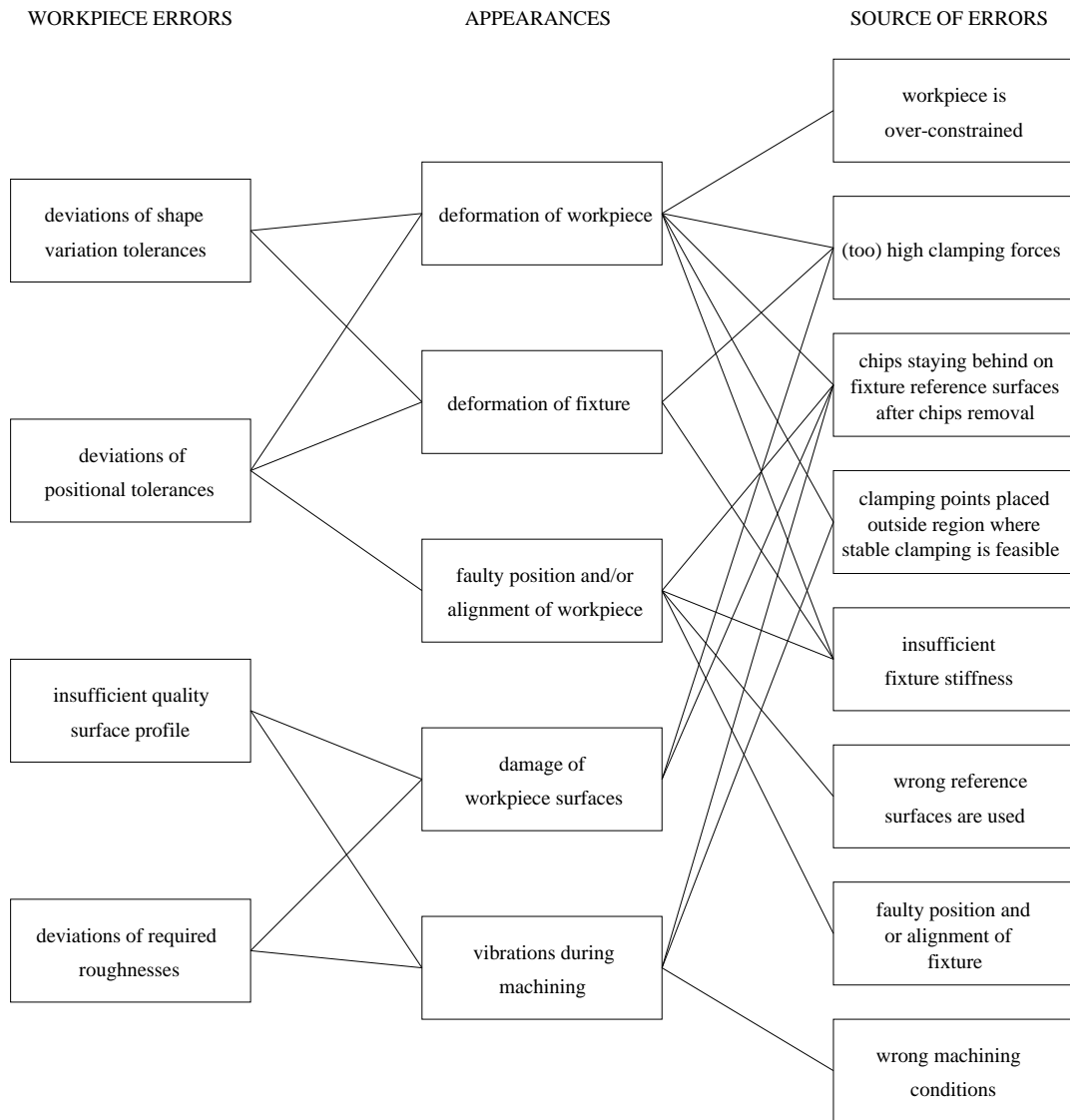
Figure 2.6: Analysis of workpiece errors with associated phenomena and sources, translated from [84, Tab. 1]
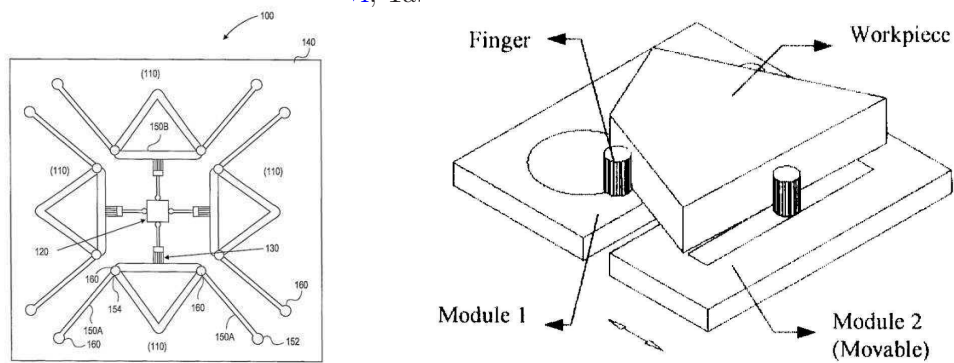
(a) Adaptive fixture concept developed by Wiens *et al.*. Source: Ref. [171], Fig. 1.

(b) Three fingered reconfigurable fixturing system presented in Ref. [42], Fig 1.

Figure 2.7: Concepts of force controlled fixtures.
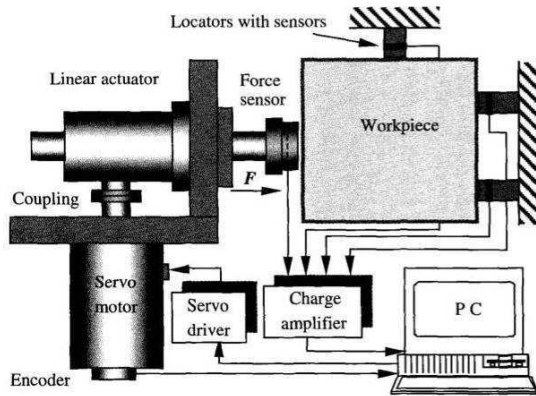
(a) Schematic architecture active fixture developed by Nee *et al.*. Source: Ref. [115], Fig. 6.14.
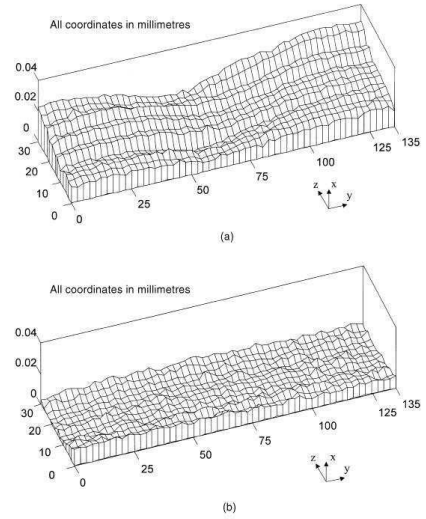
(b) Measured machined surface profiles, under (a) passive clamping and (b) active clamping. Source: Ref. [114], Fig 7.

Figure 2.8: Concepts of force controlled fixtures.
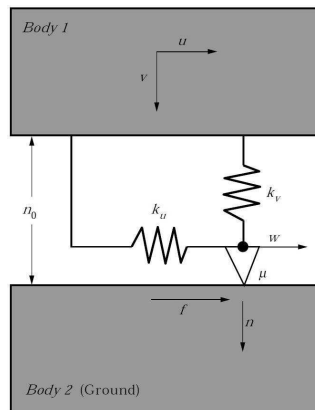
(a) Contact modelling by Yang *et al.*. Source: Ref. [174], Fig. 2.
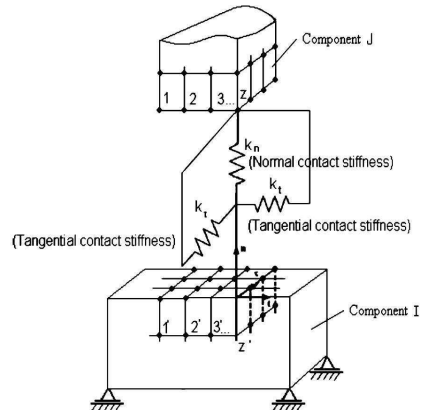
(b) Fixture-part interface contact model presented in Ref. [180], Fig 4.

Figure 2.9: Contact models

40

Research Methodology

3.1 Introduction

The aim of this chapter is to explain the research methodology applied in the thesis in order to address the knowledge gaps discussed at the end of the literature review in Chapter 2. In the literature survey, process variables and input–output relationships, present in the part-fixture system and useful for the active control of clamping forces to minimise the part displacement during machining, were identified. They will be revisited and herewith their use in the establishing control design will be studied. Secondly, all decisions made during the work will also be explained. The intended knowledge contributions of this research and key assumptions will be made explicit. Thirdly, the methodology used to establish the models, needed for fixture control design and founded upon this research approach, is discussed. Followed by the evaluation of the proposed methodology.

3.2 Research Approach and Key Assumptions

In Figure 3.1, one can see a generic block diagram for fixture control. Four levels can be identified in the figure:

1. The plant, in this study a part-fixture system, inclusive senors and actuators.

2. Low-level control, this is the form of control that is studied in the standard text-books on control systems in engineering, such as [41, 48, 50, 102]. A reference value

r is set on the controller which interacts somehow with the plant to cause the plant to behave in a desirable manner. Interaction with the plant goes in both directions, steering signals are sent to the plant and information from the sensors in the plant is processed in the controller. The two basic principles of control are feed-forward and feed-back control. These control principles have been studied extensively and many controllers have been designed for these two control strategies.

3. High-level control can consist of several levels. One of the highest levels where this type of control is applied, is that of the factory. Signals from a central server are sent which e.g. initiate the fabrication process of a certain product. On a lower level, commands are sent to a fixture to change its reconfiguration. During the reconfiguration process high-level control ensures that the fixture elements do not collide. Furthermore, high-level control can communicate with low-level controllers of the machine and then decide on how to change the reference signal r, e.g. to change the clamping forces such that they remain minimal during the machining process. Often, high-level control possesses some form of intelligence and, to a certain degree, can work autonomously.

4. The engineer, who designs the fixture and the control architecture and monitors and supervises the systems. The high-level control control is instructed with commands c given by the engineer.

This study considers only the dynamics of the part-fixture system, i.e. the plant, and the low level control. This is the area that is boxed with the dashed line in Figure 3.1. The high-level control for part-fixture systems has been studied at The University of Nottingham by the authors of [120, 143], and others, in the AFFIX research consortium [5] (see also Section 1.1).

The part displacement and the reaction forces at the locators have been identified as key process variables and the clamping forces/displacements have been identified as the control inputs in the literature review. Furthermore, it was observed that in many cases it is difficult to measure part displacements. These variables can also be projected on the block diagram shown in Figure 3.1. The part displacements and the reaction forces at the locators are the outputs y of the plant and the reference r sets the desired

reaction forces or part displacements at the controller. The controller on its turn sends a steering signal to the actuated clamps.

Hardware-in-the-loop (HIL) control and other modern controllers for advanced systems such as $\mathcal{H}_\infty$, $\mathcal{H}_2$ and μ-Synthesis rely on mathematical models of the plant for real-time simulations, or models for the plant-model-based compensator. In Figure 3.1 on the top of the boxed area, which is the focus of research effort in this study, one can see a typical example of a system where a HIL control design is applied. A computer (microprocessor) is connected via some control device, that is the interface between the virtual model and the real plant: the part-fixture system with the four actuated clamps in Figure 3.1. On basis of the mathematical model, steering signals for the actuators are calculated and are fed into the real system. In the mean time the virtual system (simulation) is updated with sensor signals form the real part-fixture system. In first instance these simulations are done with more generic software as MATLAB [101] and when the system goes into production by more dedicated means.

The mathematical models above must be accurate, such that the actuation signals calculated on basis of the model yield the desired system output and the error between measured and calculated variables is minimal. Secondly, these models should be fast enough to keep ahead of the update rate of the digital sensor signals.

In the literature review a stage in the fixture design process has been identified where detailed part-fixture models are built: the fixture design verification. The finite element method (FEM) [14, 52, 182] is applied for computational analyses of the deformation, stress, locating performance and workpiece stability in the system. These verifications are done at the end of the design cycle of the fixture, as e.g. illustrated in Figure 2.1(b) by the fixture design process scheme of Nee *et al.* [115]. Furthermore, in the literature it was recognised that the optimal place of the clamps, clamping intensity and location of the supports can be established on basis of finite element analyses (FEA) in conjunction with additional optimisation techniques.

It is therefore logical to make the FEA a more prominent element in the fixture design process, as shown in Figure 3.2, especially, when one thinks of the computational power that is at the engineer's disposal and the need for fast design process and the accuracy of the models required currently. Similar to the design process shown in Fig-

ure 2.1(b), the process starts with a kinematic restraint analysis to establish form closure for a viable locator layout. The next element in the design process is the tolerance sensitivity analysis, as proposed by Rong *et al.*, see Ref. [142, §4.2] and the references therein, which depends solely on the combination of locator tolerances and placement, and the part tolerances. The next step is then the FEM-based modelling of the part-fixture system to establish/verify the deformation, stress, the locating performance, workholding stability, the optimal support and clamping layout, and the clamping forces. Furthermore, the finite element (FE) models can be utilised to establish forms of model-based control, such as HIL control.

Depending on the geometric complexity, FE models typically contain in the order of $10^5 - 10^6$ degrees of freedom and are currently too computationally expensive in system simulation for real-time control. As found in the literature survey, model reduction techniques have developed in the fields of structural mechanics, control engineering and computational physics. The aim of model reduction is to condense the size of the model, whilst preserving the characteristic dynamics of that model. One of the model reduction techniques that is commonly applied in structural dynamics, and also widely implemented in commercially available FE software, is the Craig-Bampton method [28, 29, 149].

An important issue in model reduction is the selection of the remaining degrees of freedom. These degrees of freedom should be selected from the areas of the part that are of special interest. These areas fall into two categories: the regions where contact between workpiece and fixture occurs, and the machining areas. A key assumption that plays a pivotal role in establishing small models is the classical Saint-Venant's principle [95, 159]. In simple terms this principle states that a complex, distributed load applied on an area that is away from the area of interest can be substituted by an equivalent concentrated load without significantly changing the stress/strain state at the area of interest. This means that it is sufficient to select only a limited number of degrees of freedom from the machining areas. In addition, the concentrated loading at these nodes yields larger displacements locally than the original load would, i.e. the model is always a conservative model.

Another finding of the literature review is that the contact between part and fixture can be modelled with spring-dashpot elements. This approach has been taken in the modelling presented in the further chapters. This results in a favourable outcome: it suffices to select only a small set of degrees of freedom, namely those of the nodes where these spring-dashpot elements are attached to the part. A further assumption in this study is that the fixture (layout) design has been established previously.

Numerical contact modelling requires a large number of degrees of freedom at and below the contact surfaces. At the beginning of this PhD study, attempts have been made to reduce the contact problem to the contact area, by retaining only those degrees of freedom at the contact surfaces. This has proved to be an invalid approach, as still a great number of degrees of freedom is needed to describe the contact problem correctly. Secondly, the mode shapes that are required for a Craig-Bampton reduction are linearised mode shapes and as a result the nodes of workpiece and fixture are stuck together, resulting in unrealistic part-fixture contact models.

Subsequently, the reduced model can be exported, so it can be used for real time simulation, as mentioned above in e.g. Matlab. Some interfacing work is needed to import the saved file with the reduced mass and stiffness matrices in Matlab. The dynamic accuracy of the Craig-Bampton reduced model comes from dynamic mode shapes, the so-called fixed interface modes, that are added as additional degrees of freedom to the preserved physical degrees of freedom. These fixed interface modes (the mode shapes of the model where the physical degrees of freedom selected to be retained) are constrained during the modal analysis. When an increasing number of these modes is added to the reduced model, the accuracy of the reduced model increases. The standard verification of the accuracy of the model is to perform a modal analysis to ensure that the eigenfrequencies of the reduced model match those of the full model. The selection criteria for fixed interface modes in this work relies on this criterion. The eigenfrequencies of the full and the reduced model are compared for model analyses with no imposed boundary conditions. In addition, the fixed interface modes are studied visually, as in some cases a set of fixed interfaces modes represents the "first order modes".

In parallel, the actuator models for the clamps are established. Dynamic actuator models can be found in general textbooks, such as Refs [41, 48, 54, 77, 129], and / or

in specialised monographs, e.g. [103, 110, 111]. In this study, it has been assumed that sensors and actuators already have been selected. Most of the modelling work has been undertaken within the framework of the Affix project [5]. Three different actuators have been used within the Affix research consortium: hydraulic actuators, electromechanical cylinders and piezoelectric actuators.

Dynamic models for the sensors can be established based on the physical principle used to transduce the variable into an electric signal. At the time when most of the modelling work has been carried out, the sensors in the fixtures had not been selected yet. It has been assumed that the sensor therefore can be mathematically modelled as a constant gain. Another assumption is that the selected sensors and actuators are robust enough to function in the harsh machining environment.

The next, crucial, step is the coupling of all models and integrating the controller(s). The fixture elements and the workpiece are connected with the springs-dashpot elements. Workpiece stability is required and the part and the fixture elements are to remain in contact at all times. In this study, it has been assumed that the fixture stiffness is much higher than the part stiffness, as a result the fixture can be modelled with spring-dashpot elements. In addition, no friction has been included in the model - which means that tangential contact stiffness is not needed in the mathematical model. Also, the contact stiffness is assumed to be linear. This results in a completely linear model. The linear model has two advantages: firstly, the computational times are lower than a nonlinear model, and secondly, controllers for the linear part-fixture system can be designed with the Matlab Toolboxes for the Affix project [5], simple forms of PID control - which is frequently applied in industry - and other forms of compensators have been investigated. The methodology followed in this study allows for and easy expansion to incorporate other forms of controller design and nonlinearity for increasing the accuracy of the model.

Finally, the machining process should be studied, to establish a model for the machining forces. The calculated forces can be corrected by measurements with a dynamometer, or e.g. the method proposed by [63]. In the literature, models can be found for calculating the cutting forces. In this study, the dynamic grinding forces in several publications have been analysed, and an empirical dynamic grinding force model has

been established.

As stated above, the work undertaken herewith can be found in the block "FEM Analysis" in Figures 2.1(b) and 3.2. In Figure 3.3, an expanded version of this block "FEM Analysis" is shown with the dashed line. In this box the main items of the the research approach are shown in individual blocks. Arrows connect the individual processes. The vertical column shows the steps that rely on structural mechanics and control. The main contributions that should fill the first three knowledge gaps defined in Chapter 2, regarding the modelling of part-fixture systems and the design of controllers, are identified in this column.

3.2.1 Summary of Key Assumptions

In this section a brief summary is given of the key assumptions and choices made in this research.

Modelling

- The Craig-Bampton model reduction technique [28, 29] will be applied to condense the FE models of the workpieces studied in the part-fixture systems considered in this work.

- Saint-Venant's principle has been utilised to obtain a reduced set of degrees of freedom at the machining areas.

- Spring-dashpot elements are used to model the fixture stiffness and damping.

- The contact mechanics have been modelled with spring-dashpot elements, a linear spring stiffness has been assumed. The methodology applied in the thesis allows for easy implementation of more complex models to increase the accuracy of the mathematical representation of the part-fixture system.

- The part-fixture system is assumed to be frictionless, as a result there is no tangential stiffness and damping present in the part-fixture contact interface.

- The assumptions described above yield small, linear models which can be used for the design of controllers with the MATLAB Toolboxes.

- Models for hydraulic, electromechanical and piezoelectric actuators, as utilised in the AFFIX project [5], are established in this study.

Control

- This work considers only the application of low-level control of clamping forces; models for the servo-control of actuated clamps are established.

- Dynamic models for the measurement systems have not been built as sensors had not been selected yet in the AFFIX project at the time of establishing the essential models presented in this work.

Verification of Control Design

- For the verification of the control design, a simple empirically-based machining force profile has been established.

Methodology

- It has been assumed that the design of part and fixture layout has been established previously. Furthermore, in the thesis it has been assumed that actuators and sensors have already been selected during earlier stages of the fixture design and that these are robust enough to work under harsh machining conditions.

Methodology and its Limitations in Wider Manufacturing Perspective

- Fixturing research falls in a larger context of manufacturing research, where a wide range of subjects is studied. However, in this thesis, only a limited number of research topics can effectively be covered. In the previous sections and in the literature survey (Chapter 2) a number of issues affecting the performance of intelligent fixturing systems have been mentioned. This work has the following position relative to these wider issues:

    – Fixture reconfigurability, and adjustability, manipulation and realignment capabilities to deal with respectively different parts and part tolerances are not considered in this thesis. Instead, the focus of the work lays on model-based

control design for active fixturing systems for error compensation during the machining of a single part.

– Part tolerances are not considered here, and, furthermore, perfect part dimensions are assumed. As a result, the influence of tolerance spread in a batch, or the influence of tolerances on individual parts are not studied.

– The research work undertaken in the AFFIX-project concentrates on the fixturing of compliant parts. The stiffness of these workpieces is sufficiently low to prevent interference between the inputs (active clamps); hence, this application of collocated control results in a stable system. Furthermore, the methodology presented in this thesis focuses on *combining* structural analysis, model reduction, mechatronics and control design. For this reason, feedforward control and/or advanced controllers, such as robust control, $\mathcal{H}_\infty$ etc., are not considered in this work. Elaborating further on this and the previous bullet point, advanced measurement systems as CMM and photogrammetry applications are not considered in this work as sensing methods. It is assumed that sensing can be done with displacement and force sensors.

3.3   Development of Methodology

A concept towards a practical design methodology, based on the research (approach) presented above, can be outlined as follows. In Figure 3.4, a general methodology to obtain a reduced model for control of the part-fixture system and a suitable control strategy is presented. It starts with the system design of fixture and part. In the process design, the manufacturing engineer determines which manufacturing (machining) operations are needed and in what sequence they are performed [142]. The drawings of the part and the fixture are usually prepared in 3D CAD software. The drawing of the part and (possibly) the arrangement drawing of the fixture can then be exported to a commercially available FE software platform. In some cases an intermediate exchange file format, such as the `.step` [149] format, needs to be used to import the data from the drawing(s) to the FE software. In case the part is geometrically complicated, a carefully simplified geometry that has a similar mechanical behaviour, e.g. by removing some

curved shapes, can be established. This is sometimes called a "parametric model", can be used [90] and is discussed in more detail in Section 6.4.1. The parameterisation of the part geometry is shown in Figure 3.4 as a parallel route.

Following the flow in Figure 3.4, when the part is imported into the FE software program, the material properties, element size and element type are specified by the user. The software assembles the overall mass and stiffness matrices. The Craig-Bampton reduction [28, 29] is used to reduce the model to the specified size. The Craig-Bampton reduced matrices then are exported from the FE software into an export file. MATLAB and the MATLAB Toolboxes are then used to load the matrices and create a state-space representation of the part-fixture dynamics. An actuator and a suitable controller are modelled and coupled to the system. This model *can* then be applied to control a real part-fixture system using appropriate computer-actuator-sensor interfaces and software. This research is concerned with the building of small models only, not with the actual application of control design such as HIL.

3.4 Evaluation

An evaluation covering the work undertaken in this study is carried out in seven parts.

1. The finite element method is an established modelling technique, it can be assumed, that when modelled correctly, the FE model is a correct computational representation of the corresponding system. The Craig-Bampton model reduction technique is an established and proven method. The reduced workpiece models are verified by comparing results from static, dynamic and modal analyses with the results obtained with the corresponding full models of the part.

2. The modelling of the part-fixture system, as done with the linear spring, is verified against studies that consider the reaction forces at the locators found in the literature.

3. Dynamic actuator models are established on basis of widely accepted models found in the literature. The models established here are verified with the examples found in the literature.

4. A numerical analysis will be made of the coupled models previously established in the thesis.

5. The methodology, as established in this work, has been verified against a near-industrial test-case, as studied within the framework of the Affix project. This is the fixture system shown on the top in Figure 3.1. The applicability of the methodology has been studied against this complex case involving a 3D part and four active clamps.

6. In the work-related PhD thesis by Papastathis [119], reconfigurable fixturing systems have been designed, and an approach of active control of the clamping forces has been considered.

   - In that work, a similar approach has been taken regarding the modelling, *based* on the work carried out for *this* thesis.

   - An experimental validation of the mathematical models has been accomplished successfully *by* Papastathis [119].

   - The difference in the applied modelling approach between this thesis and the work by Papastathis [119], is that the latter does not consider the application of a model reduction method.

7. The hardware-in-the-loop approach, which has been identified as a possible control design in the thesis, has been successfully tested within the Affix project: a physical demonstrator of the system studied in the thesis (shown Figure 3.1) has been built. This system has the layout shown at the top of Figure 3.1 and has been used to validate the HIL control design approach to compensate for a distortion in the form a static load.

3.5 Conclusion

The research approach taken in this study has been explained and the intended contributions to address the current knowledge gaps have been highlighted. A concept towards a practical design methodology has been proposed. This methodology will be used throughout the work. Furthermore, the stages for partial-verification, covering the

intended contributions in this research have been outlined for future reference in the thesis.

This research approach is worked out in the main body of the thesis as follows. The main items of the research methodology: FE-modelling and model reduction of the workpiece, building actuator models, control design coupling of the models and adding the fixture stiffness are worked out in Chapter 4, as well as establishing of machining force models. These individual tools are verified in Chapter 4, subsequently, two simple compliant part-fixture systems actuated by hydraulic and electromechanical actuators are modelled in Chapter 5 with the methods set out in this chapter and Chapter 4. The simulation of these simple systems forms the next step in verification of the methodology. Chapters 6 and 7 mirror Chapters 4 and 5 in some respect. As a second step in the verification of the methodology and as an illustration of its applicability, the more complex, near-industrial part-fixture system shown in Figure 3.1 is considered. The system is modelled in Chapter 6 and a simulation of this system is presented in Chapter 7.

3.6   Figures
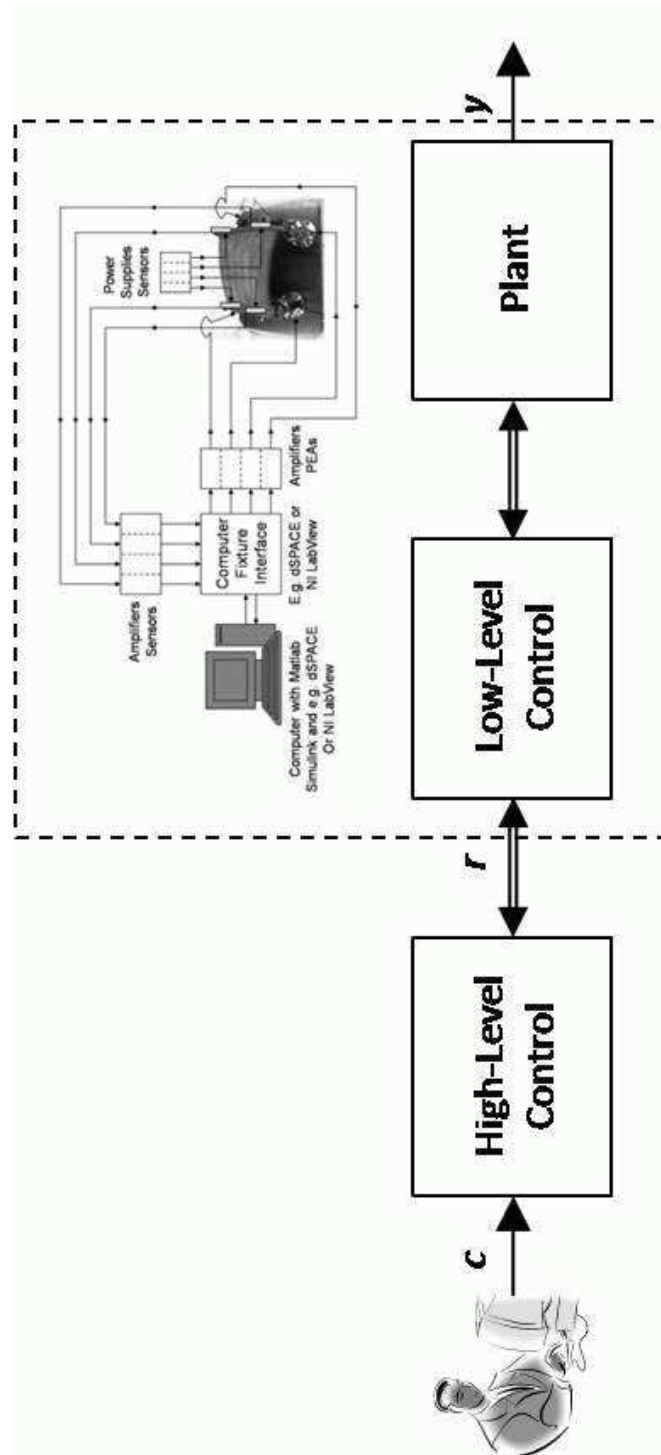
Figure 3.1: Canonical control block diagram for control of active fixtures.
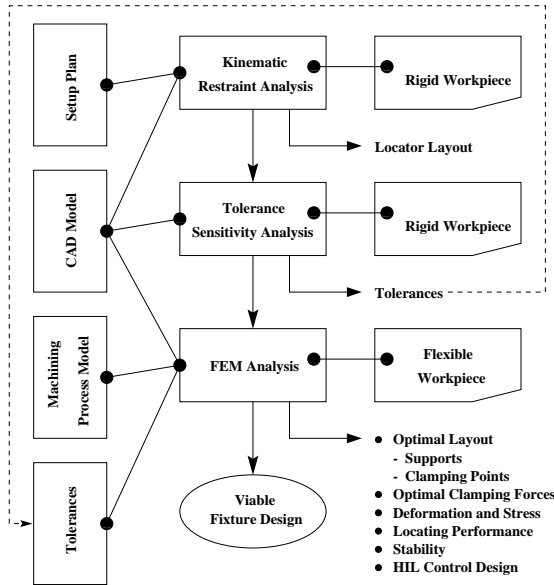
Figure 3.2: An active fixture design outcome-oriented flowchart adapted for early-on integration of finite element analysis.
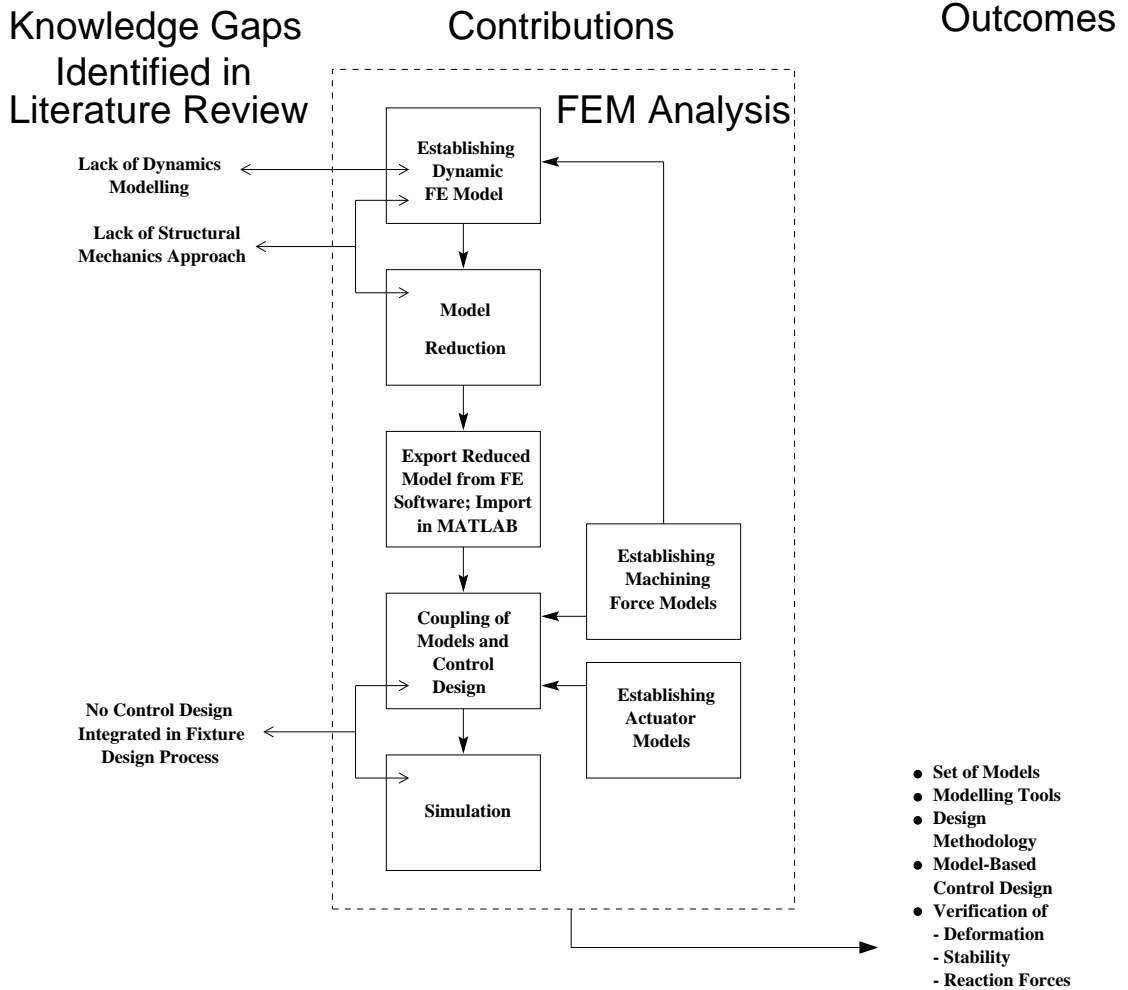
Figure 3.3: Research methodology in the framework of active fixture design.
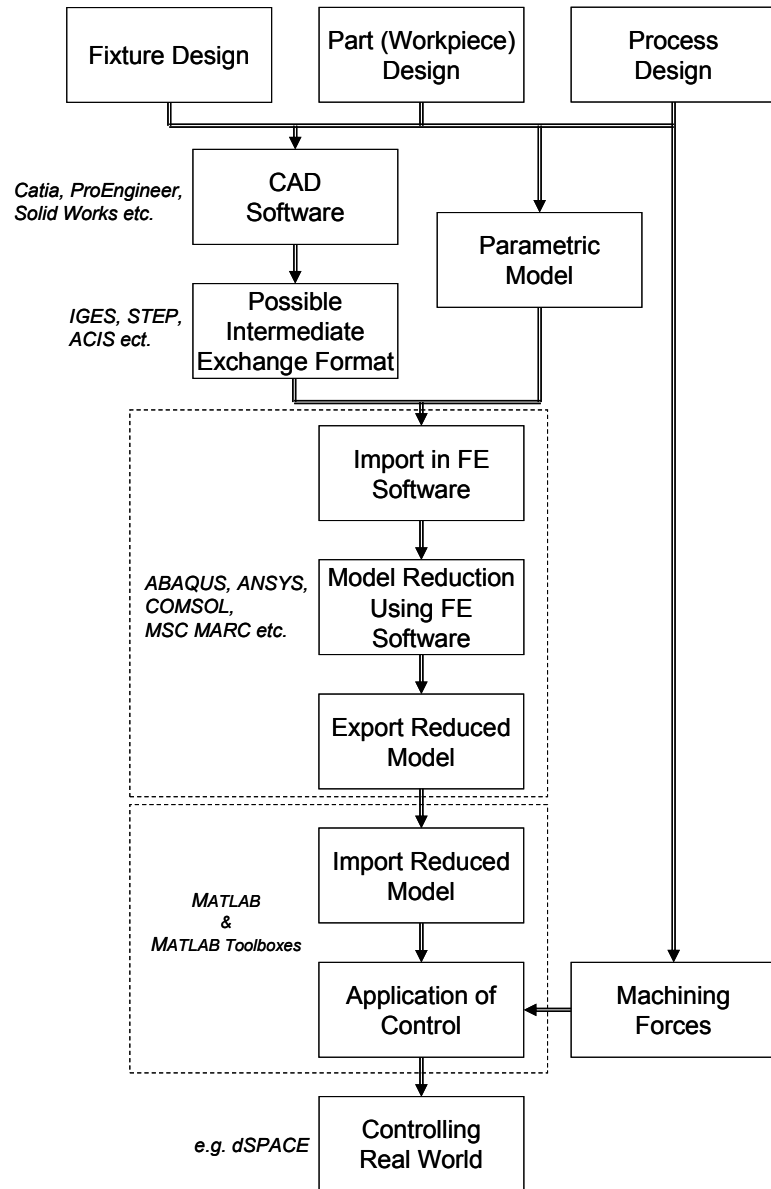
Figure 3.4: Proposed approach towards a methodology for design of an actively controlled part-fixture system.

Analysis of Active Fixture Subsystems

4.1   Introduction

Fixtures are used to fixate, position and support workpieces, and form a crucial tool in manufacturing. And furthermore, they have a significant impact on manufacturing costs. A vast amount of research has been made on fixturing technology (see Chapter 2 and e.g. Refs [115, 142]). The main focus of research in part-fixture mechanics, however, has been in the static deformation and part constraints [115, 142]. Little attention has been paid to the dynamic behaviour of these systems. Nevertheless, the dynamics of the system largely determines the obtained precision during the machining processes.

For a good performance, the designed fixture (layout) should provide sufficient restraint and support. Furthermore, the fixture needs to be stiff. Especially compliant parts might need additional support, such that the part undergoes minimal deformation due to the machining process. The deflection of the part-machine system comes from clamping and machining forces, and determines the obtained precision of the manufacturing process. Controlled actuators are integrated in e.g. modular clamps or automatically reconfigurable fixtures. These actuators can be used to minimise the deformation of the part during machining in an effective manner. This concept is called active fixturing. According to the best knowledge of the author of this thesis, little attempts (see Section 2.6.3 in the literature survey) have been made for systematic approach for the control design in active fixturing systems.

The work presented here, draws on Refs [10, 11, 12]. In these papers, the subsys-

tems are integrated into a simple, yet full active part-fixture systems. These full systems are studied in Chapter 5. Here, the research methodology established in Chapter 3 is applied to analyse the subsystems of an active fixturing system. On basis of a function analysis, one can dissect the active fixturing system in the following subsystems:

1. The workpiece (the part).

2. The part-fixture interface (the part-fixture contact).

3. Passive fixture elements.

4. Actuated clamp(s).

5. Sensors and control system.

These subsystems are studied in subsequent order in this chapter. Firstly, the structural modelling of the part is studied in respectively Section 4.2. In addition, it is discussed how models with a small number of degrees of freedom, which accurately describe the compliant part as distributed-parameter system, can be established using a model reduction technique. The fixture is used to firmly hold the workpiece in one position during the manufacturing process. This support and restraint is offered at certain points and surfaces[1], where the fixture elements are in contact with the workpiece.

Mittal *et al.* [109] established a model whereby spring-dashpot elements are used to describe the (contact) stiffness of the clampers and locators, based on the papers by Shawki and Abdel-Aal [145, 146]. The approach avoids "computationally expensive" contact mechanics in the model. Furthermore, it has been widely adopted in the manufacturing research community, see e.g. [142], and is farther worked out in Section 4.3. Subsequently, the modelling approach of part and fixture elements is compared with benchmark results presented in the literature in Section 4.4.

Active clamping forces are generated by several actuation methods. Hydraulic and electromechanical actuators are amongst the actuation principles mentioned in Chapter 2. These actuators are widely used in applications for precision positioning systems

---

[1]In this thesis, one of the key assumptions is that support and restraint is offered through point contacts, see Chapter 3.

and force-feedback applications [54, 103, 163]. In Section 4.5, hydraulic and electrome-chanical actuators are analysed for application in an active fixturing system.

The fifth and last subsystem identified above are the sensors control system. The process variables that are candidate for control were identified in Chapter 2, as the reaction forces at the fixture elements and the displacements of the part and fixture. In Chapter 3, it was explained that within the larger research framework on fixturing (the AFFIX project) sensors had not been selected yet when the work for this thesis was carried out, for this reason it is assumed that the bandwidth of the sensors is much larger than the frequencies of the dominant modes of the structural components (the workpiece and fixture elements). The clamping forces are controlled by means of a closed-loop controller. In Section 4.6, the design of several compensators for closed-loop servo-control are discussed.

In this methodology, the subsystems are modelled as models with a certain input and some mechanical or electrical output. However, the subsystems are not intercon-nected yet. To establish an overall model of the actively controlled part-fixture system, the established mathematical models of the subsystems need to be integrated. The in-tegration of the models for the part, the contact interface, the fixture, the actuated clamp(s) and the controller is then discussed in Section 4.7.

For the control design verification and for the application of real-time simulation of part-fixturing system, a realistic machine force model is required. One of the active fixture designs established within the AFFIX project, is a design for a grinding fixture. For this reason, a transient grinding force will be established in Section 4.8.

The *research methodology* outlined in Chapter 3 is based on systematically breaking down the active fixturing system into subsystems by analysing the functions and compo-nents of an active fixturing system. Based on the research methodology, a *methodology for the model-based design of controllers* for active fixturing systems was proposed that consistently models all the subsystems of the active fixture. As a result of the analyses carried out in this chapter, tools are developed to establish small, yet accurate models of the dynamic behaviour of a part-fixture system, two practically applicable models for actuated clamps are developed, a methodology for the design of compensators for low-level servo-control is discussed, and mathematical tools for the integration of all the

subsystems into the overall model of an active fixturing. All of which can be directly used in the control design methodology.

4.2 Part Modelling

The equations governing the mechanics of a workpiece are hard to establish analytically, since the part is elastic and its geometry is arbitrary and often complex. Only very few analytical solutions exist to describe the load-displacement relationships of an elastic body of complex geometry [51, 159]. For this reason, elastic bodies are often modelled with the finite element method (FEM) to find an approximate solution for the load-displacement relationships. In Section 4.2.1, the underlying principles for the derivation of the equations of motion for a discretised system will be explained. The general dynamics of a body are described by the wave equation. Generally, standing waves dominate the dynamic response of a structure. For this reason the standing (modal) waves are generally studied in structural dynamics, notable exceptions are soil dynamics and certain aero-elastic phenomena such as wing flutter.

Modal systems are governed by the following set of equations of motion:

$$\boldsymbol{M}\ddot{\boldsymbol{x}} + \boldsymbol{C}\dot{\boldsymbol{x}} + \boldsymbol{K}\boldsymbol{x} = \boldsymbol{f}.$$

Here is $\boldsymbol{M}$ the mass matrix, $\boldsymbol{C}$ the damping matrix, $\boldsymbol{K}$ the stiffness matrix, $\boldsymbol{x}$ the displacement vector and $\boldsymbol{f}$ the applied force vector.

4.2.1 The Finite Element Method

The finite element method was developed to solve the complex structural analysis and design problems encountered in civil and aerospace engineering. Thanks to its successful application in this area, FEM is now widely used in numerical analyses to find approximate solutions of discretised partial differential equations (PDEs) or integral equations. Approximate solutions for structural, thermal, electromechanical, fluid and other physics problems can be found with the finite element method and this is the method of choice to solve problems in the field of structural mechanics and elliptic PDEs. The solution approach is based on the mesh discretization of a continuous domain. This means a division of the continuous domain into discrete sub-domains: the elements. The finite

element method allows this domain to take arbitrary shapes, which makes the finite element method a suitable tool to analyse complex structures, such as cars and airplanes. Furthermore, the results, e.g. distribution of stresses and displacements of a structure can be visualised and studied with the so-called post-processing software. As observed in Chapter 2, finite element analysis is a powerful design tool for virtual prototyping and design optimisation and, hence, it accelerates product development.

The underlying basic principles of the finite element method regarding structural analysis can be outlined as follows. To analyse the displacements of a certain body caused by a load applied on that body, the body is divided into elements as mentioned above. These elements are interconnected at the 'nodes', this is illustrated in Figure 4.1. In this Figure an arbitrary 2D domain is shown, for the work presented in this study, the body under consideration is typically the workpiece. Figure 4.1 shows that the mesh discretization approximates the geometry of the domain. The most important assumption underlying the finite element method is that the displacement is distributed over the element in a predefined manner and can be calculated by the so-called interpolation function. Typically, linear, quadratic or trigonometric interpolation functions are applied in the finite element method. This means that the mesh discretization needs to be fine enough to give an accurate approximate description of the real displacement field. For more information on the topic mentioned above, see the classic texts on FEM, such as Refs [14, 52, 182], and also the excellent review by Nikov [118].

The next step is to calculate the element stiffness and mass matrices. One of the advantages of the finite element method is that these matrices have a constant format, only depending on the nodal coordinates and the stiffness coefficient. For the stiffness matrix the governing equations are the constitutive relations between applied loading and displacement. These equations are established as follows. From the relation between stress and displacement in a certain element the expression for virtual work can derived as function of the displacements. The potential energy can be derived from the expression for virtual work. When a load is applied on a part and it comes in a state of equilibrium, this state requires the presence of minimal potential energy. This minimum is found by differentiating the expressions for potential energy by the displacements. Similarly, the mass matrix can be established [14, 182]. However, alternatively, the mass

of an element can be considered to be lumped on its nodes. This results in a simple mass matrix that is only populated on its diagonal. This mass matrix gives results that are almost as good as a 'properly' established matrix [182] and is often applied in finite element (FE) software, e.g. [149].

4.2.2 Model Reduction

Typically, in the order of $10^6 - 10^7$ degrees of freedom (DOFs) are needed to establish accurate FE-models for complex 3D parts. These systems are too large to use for real-time applications. It has been established in Chapter 2 that reaction forces and part displacements are the main process variables for control. As a result, the degrees of freedom describing the displacements at the machining areas and the clamping, locating and support points are the relevant degrees of freedom. Model reduction techniques, which condense the redundant degrees of freedom out of the model, can be used to establish small yet accurate problems that can be used to establish the relevant displacements and reaction forces.

As established by the literature survey held in Chapter 2, there are many different model reduction techniques, established within different disciplines: structural mechanics, control engineering, mathematics and modelling of different physical problems such as fluid mechanics and electronic circuits. (See also Ref. [144] for a more extensive review.) As discussed in Chapter 3, the Craig-Bampton model reduction technique [28, 29] will be applied in the thesis. The Craig-Bampton model reduction technique has been developed for application in structural dynamics (substructuring) problems [28], furthermore, this model reduction technique is a well defined, established and widely used method and is implemented in many commercially FE software packages, such as ABAQUS [149].

Obviously, the retained degrees of freedom in this reduction are those at the machining regions and part-fixture interfaces (the contact points). In case the machining regions are described by many degrees of freedom, it may be necessary to reduce the model even further. This is done by a smart application of Saint-Venant's principle [95, 159]. In simple terms this principle states that a complex distributed load applied on an area that is away from the area of interest can be substituted by an equivalent concentrated load without significantly changing the stress/strain state at the area of interest. The

implication is that it is sufficient to select only a limited number of degrees of freedom from the machining areas. Loads can only be applied at the remaining degrees of freedom of the reduced model. Hence equivalent loads, which act on the retained nodes surrounding the area where the load is applied, need to be found to represent the (distributed) loading. Establishing the equivalent loads for reduced models goes in the same fashion as finding equivalent loads for distributed loading acting on normal (not reduced) FE-models [14, 182]. These equivalent concentrated loads applied in the reduced model yield larger displacements locally than the distributed loads applied in the full model applied, i.e. the reduced model is always a conservative model in the sense that it tends to over-predict displacements.

An in depth technical discussion of the Craig-Bampton model reduction technique is given in Appendix A. At this place it is sufficient to know that the dynamic accuracy of the Craig-Bampton reduced model comes from dynamic mode shapes, the so-called fixed interface modes, that are added as additional degrees of freedom to the preserved physical degrees of freedom. The fixed interface modes are found by a modal analysis where the physical degrees of freedom selected to be retained are constrained. The higher the number of the fixed interface modes in the reduced model, the higher the accuracy of the reduced model; the number of needed fixed interface modes is determined by the desired accuracy. For this reason, modal analyses of the reduced model need to be carried out to ensure that the first number of eigenfrequencies of the reduced model closely match those of the full model. Furthermore, when the fixed interface modes are studied visually, it can be established that in some cases a set of fixed interfaces modes represents the $1^{\text{st}} - n^{\text{th}}$ order (where $n \in \mathbb{N}_1$: $1, 2, 3, \ldots$) modes.

4.3 Fixture Modelling

4.3.1 Contact Stiffness

In the literature review held in Chapter 2, it was found that Daimon *et al.* [32] and Mittal *et al.* [109] established models whereby spring-dashpot elements are used to describe the (contact) stiffness of the clampers and locators, based on earlier papers by Shawki and Abdel-Aal [145, 146]. Thus "computationally expensive" contact mechanics models

are avoided. This approach has been widely adopted in the manufacturing research community, see e.g. [142], and is applied in the work.

The contact stiffness is dependent on two materials that are in contact [15, 72], e.g. because of its lower modulus of elasticity, a contact where at least one of the bodies is of aluminium arise comparatively much more compliant than steel-steel contacts. Additionally, the shape of the contact (point, line and flat contact) and hence the shape of the fixel[2] and the size of the contact area determine the contact stiffness as well. This means that for the comparison of the steel-steel and aluminium contact above, the shape and dimensions of the bodies in contact must be the same as well. Furthermore, when modelling the contact mechanics (analytically) from first principles, it proves to be very hard to consider effects such as surface hardening and plasticity.

From the experimental results presented in Refs [122, 137], one can make an estimate for the contact stiffness of realistic fixture elements. In Figure 4.2 the stiffness of a steel-steel contact for a clamping element is shown. This is a representative illustration from the results presented in Refs [122, 137]. The results presented in Ref [137] show that for this design locators and clamps have the same stiffness and that steel-steel and aluminium contacts both have stiffnesses of the same order of magnitude. Furthermore, the experimental results in Refs [122, 137] show a larger stiffness and a larger spread than predicted by the Hertzian theory, even when upper and lower limits are calculated on basis of margins in the modulus of elasticity and margins in the radius of the contact point (due to the dimensional tolerances). The average force-displacement relationship in Figure 4.2 is shown with a curve, and, as illustrated by the added red line, is nearly linear.

The observed near-linearity is a justification to utilise linear springs for initial/preliminary calculations, as is in the literature [122]. Since this work is devoted to an initial methodology for the design of actively controlled part-fixture systems, spring stiffnesses are assumed linear. The contact stiffness presented in Refs [122, 137] ranges from $7 \times 10^6 - 7 \times 10^7$ N/m. This range for the contact stiffness has applied in the thesis.

---

[2]Or: fixture element.

4.3.2 Fixture Stiffness

The modelling of fixture stiffness can be split into two categories: the clamp stiffness that is determined by the actuator stiffness, and the stiffness of the locators, supports and fixture body. The actuator stiffness is modelled in Section 4.5. In this work it has been assumed that the fixture body is the fixed world and has an infinite stiffness. In case the lowest eigenfrequency of the passive fixture elements is less or equal to that of the part, the fixture element has to be modelled with finite elements as described above for the part. Subsequently, a model reduction for the element is carried out reducing the size of the dynamic model. Alternatively, a lumped-parameter model may be established in certain cases. The resulting dynamic models give a good description of the frequency dependent dynamic stiffness of the support or locator. On the other hand, when the eigenfrequencies of the supports and locators are much higher than the lowest eigenfrequencies, the dynamic stiffness of the locator or support is constant in the frequency domain and has the same magnitude as the static stiffness of the element. In this case the fixture element can simply be modelled by a spring-dashpot element, that has the equivalent spring stiffness and damping of the element.

In case the fixture stiffness is modelled by spring-dashpot elements and the stiffnesses of both the contact and passive fixture elements are modelled as linear stiffnesses, one can even model both elements conveniently as one effective element; the spring stiffnesses are in series. It is realistic to assume that the stiffness of the fixture element is of the same magnitude or larger than the contact stiffness. For fixture element stiffness that is, $a \in \mathbb{R}$, for $a \geq 1$ and $\mathbb{R}$ is the set of real numbers, a, times larger than the contact stiffness k_{cont}, the effective stiffness k_{eff} is calculated as follows.

$$\frac{1}{k_{\text{eff}}} = \frac{1}{k_{\text{cont}}} + \frac{1}{ak_{\text{cont}}}. \tag{4.3.1}$$

Then, k_{eff} has a proportional relation with k_{cont}:

$$k_{\text{eff}} = \frac{a}{a+1}k_{\text{cont}}. \tag{4.3.2}$$

Using the expression in (4.3.2), it is shown that the effective stiffness k_{eff} is of the same order of magnitude as the contact stiffness k_{cont}, as is illustrated by Figure 4.3.

4.3.3 Friction

Friction is present in the contacts between part and fixture. As one requirement for a fixture design is that the fixture does not damage the workpiece, it can be assumed that the friction may be modelled with the classic friction laws, such as the Coulomb friction law [15, 72]. In this work, friction is not included in the analysis for the following reasons. The friction coefficient is not known a priory [108]. Furthermore, in the case of point contacts in the fixture layout, friction does not change the distribution of the forces radically [108], as shown by the model evaluation in Section 4.4. Frictionless fixture layout planning is considered to be conservative and for that reason frictionless calculations are accepted and used. Another reason is that friction introduces nonlinearity into the model. The work here is carried out with the application of the MATLAB$^{\circledR}$ Control Toolbox$^{\text{TM}}$ for linear models in mind. For this reason, friction cannot directly be taken into account. The methodology to make (sub-)models of part-fixture systems allows for extension of the models to include friction. This will increase the accuracy of the modelling, but also significantly increases the computational costs due to the introduction of nonlinearity into the model.

4.4 Verification of Reduced Part and Passive Fixture Models

4.4.1 Introduction

In Chapter 2, it has been observed that one of the main objectives of the fixture design verification is to find out the reaction forces at the locators. For example, the fixture design provides stable workholding only when the directions of all reaction forces at the locators are aimed inward to the workpiece at all times during the whole manufacturing process. Additionally, workholding stability depends on the clamping force. Whether the clamping intensity has been given a set minimal allowable value, or the intensity is controlled with a dynamic scheme, off-line modelled workholding stability depends on correctly computed clamping and reaction forces. Furthermore, for an optimal locating performance it is crucial to have an even distribution of the reaction forces at the locators. It is therefore essential to have part-fixture models that are accurate representations

of the real system. Many approaches for the mathematical modelling of part-fixture systems can be found in the literature, e.g. [104, 108, 153, 155, 169]. For these reasons, it is important to compare the modelling approach applied in this work with results that can be found in the established publications. Not all studies presented in the literature are suited for this comparison; some results are irreproducible because the full set of dimensions of the part are not given, the positions of locating and clamping points are not specified, cutting forces are poorly described, or results such as stresses and strains[3] are presented which can be calculated with the method presented in the thesis, but only after more extensive interfacing between ABAQUS and MATLAB. The following studies have been identified as suitable candidates for the verification of the established modelling as used in this research. These are the studies by Meyer and Liou [108], Tan *et al.* [153], Tao *et al.* [155] and Wang *et al.* [169]. In these publications relatively simple 2D and 3D systems are studied. These case studies can easily be reconstructed with a model that is representative of the modelling as carried out in this research. In Section 4.3.3 and also in Chapter 3 it has been explained that friction is not incorporated in the modelling presented in the thesis. It can be easily shown that the frictionless reduced models behave in the same way as frictionless models presented in the literature. For this reason, firstly, Case Study 1 from Ref. [108] will be studied. Meyer and Liou [108], present a model consisting of a rigid part, fixtured with rigid contacts. Subsequently, the influence of friction is analysed by comparing the modelling approach followed in this thesis with the results from the 2D case study presented in [155]. In this study, Tao *et al.* [155] use rigid contacts, and a rigid body to model the part. Hereafter, one of the 3D models studied in [153, 155] will be considered. In [153], an FE-model of the part is used and Tan *et al.* [153] compare models with soft and hard contacts with experimental results. It should be noted here, that the rigid body models and unreduced FE-model found in the literature are compared with the soft contact, reduced part models developed in this thesis. Despite the appearance of the word 'dynamic' in these publications, the studies

---

[3]The models established for the real-time control of active fixturing systems, find their basis on the extensive FEA carried out during e.g. the fixture layout design (see Chapter 3, Figs 2.1(b) and 3.2). It is assumed that during these analyses sufficient study of the stresses and strains occurring during machining has been made. An online retrieval of these results slows down the whole real-time simulation and is therefore not considered in this work.

are actually quasi-static: a static load is travelling over the part and transient effects are not included in the analysis. Hence, for comparison, there is only a need for statically reduced models to be constructed.

4.4.2 Case Study I

4.4.2.1 Description of Part-Fixture System

The first case study analysed by Meyer and Liou [108], involves a $15 \times 10 \times 5$ cm rectangular prismatic part that is fixtured with a 3-2-1 locating scheme and three clamps, as shown in Figure 4.4. Meyer and Liou [108] studied a new method for the optimal placement of clamps and locators. Friction is not considered in their study. In Figure 4.4(b) the fixture layout, as optimised by Meyer and Liou [108], is shown. It can be seen that the positions of locators L5 and L6 and clamps C1 and C2 are optimised for the given tool path and machining forces, as they are not placed in the standard equally-distributed locations which maximises the inter-element distance. The machine force is a vector that consists of three components,

$$\boldsymbol{F}_{\mathrm{m}} = \{100, -100, -50\}^{T} \quad \text{N}. \tag{4.4.1}$$

The part itself has a weight of 25 N, which corresponds to a density between that of aluminium and titanium. The three clamps, labelled as C1, C2, and C3 in Figures 4.4 and 4.5, each exert a clamping force of 20 N.

4.4.2.2 Modelling of the Part-Fixture System

A corresponding FE model of the part has been built and is shown in Figure 4.5. The model consists of $10 \times 20 \times 30$ linear brick elements (C3D8) [149] and 21483 DOFs. The material properties are chosen to be between those of aluminium and titanium: $E = 90$ GPa and $\nu = 0.33$. The nodes which are the fixturing points and the centre of gravity are retained in the model reduction. Furthermore, for demonstration purposes, all the nodes on the tool path are kept. These nodes are highlighted and labelled in Figure 4.5. A spring stiffness $k = 3 \times 10^{7}$ N/m has been applied to model the locators.

4.4.2.3 Comparison of Results

The statically reduced model has been exported to MATLAB, and the clamping, gravity and machining loads have been applied to the reduced model. Since friction is not incorporated in the model by Meyer and Liou [108] and in the model built with the methodology established in this thesis, the reactions at the locators are (of course) identical, as shown in Figure 4.6. The main difference between the two models is that part and fixture are rigid in the paper by Meyer and Liou [108], but are modelled as flexible elements here. Since the part is a rectangular prismatic part, its stiffness is high. The low compliance of the workpiece does not significantly change the distribution of the reaction forces.

4.4.3 Case Study II

4.4.3.1 Description of Part-Fixture System

Tao *et al.* [155] held an initial study leading to a dynamic scheme for minimal clamping forces for the Intelligent Fixturing System designed at the National University of Singapore [114, 115]. In this study, a general 2D part is considered. The part is fixtured by three locators and one clamp, shown in Figure 4.7. Tao *et al.* [155] take into account the effect of friction in their study. The workpiece is made of aluminium, with the following material properties: $E = 70$ GPa and $\nu = 0.33$. The machining load is given by (see Figure 4.7):

$$\boldsymbol{F}_{\mathrm{m}} = \{F_{\mathrm{m}x}, F_{\mathrm{m}y}, T_{\mathrm{m}}\}^{T} = \{250 \text{ N}, 300 \text{ N}, 3 \text{ Nm}\}^{T}. \tag{4.4.2}$$

The tool path on the workpiece has a length of 145 mm [155] and the coordinates of the clamping and locating points are given in Figure 4.7 and Table 4.1. Note that clamping point coordinate provided by Tao *et al.* lays outside the part geometry in the given coordinate system, the correct coordinate is given righthand side of the Table 4.1 by ((35,31.58)). The dimensions of the part can be derived from length of the tool path and the coordinates of the fixturing points.

4.4.3.2   Modelling of the Part-Fixture System

A FE-model of the workpiece, presented in Tao *et al.* [155], has been made with the commercially available FE software ABAQUS [149]. The part is modelled with linear, triangular plane strain elements (CPE3). The mesh of the part is shown in Figure 4.8. A static model reduction [62] has been carried out. The retained DOFs of the full FE-model come from the nodes that are highlighted as bigger dots in the mesh shown in Figure 4.8. The machining nodes on the tool path can easily be identified by the dots that form a horizontal line in Figure 4.8. In Figure 4.8. There are four dispersed dots at the bottom and top of the workpiece. From bottom left, clockwise, in Figure 4.8, these nodes are the 'Clamp', 'Locator 1', 'Locator 2' and 'Locator 3' respectively, c.f. Figure 4.7. The coordinates of these nodes are given in Table 4.1. From Figure 4.7 it can be observed that the reaction forces normal to the part at the Locators 2 and 3 act in the $\pm 45°$ directions. Hence, the spring stiffnesses of these elements are in the same directions. To incorporate these springs a new coordinate system for the displacements of the part at Locators 2 and 3 has been introduced. Hence, a $\pm 45°$ rotation of the displacements or degrees of freedom at Locating points 2 and 3 is needed. This can be achieved by means of a transformation matrix that rotates only these degrees of freedom. The global transformation matrix $\boldsymbol{T}$ for this transformation is:

$$
\boldsymbol{T} = \begin{bmatrix}
\boldsymbol{I} & \boldsymbol{0} & \boldsymbol{0} & \boldsymbol{0} & \boldsymbol{0} & \boldsymbol{0} \\
\boldsymbol{0} & \cos\theta & -\sin\theta & \boldsymbol{0} & \boldsymbol{0} & \boldsymbol{0} \\
\boldsymbol{0} & \sin\theta & \cos\theta & \boldsymbol{0} & \boldsymbol{0} & \boldsymbol{0} \\
\boldsymbol{0} & \boldsymbol{0} & \boldsymbol{0} & \cos\theta & -\sin\theta & \boldsymbol{0} \\
\boldsymbol{0} & \boldsymbol{0} & \boldsymbol{0} & \sin\theta & \cos\theta & \boldsymbol{0} \\
\boldsymbol{0} & \boldsymbol{0} & \boldsymbol{0} & \boldsymbol{0} & \boldsymbol{0} & \boldsymbol{I}
\end{bmatrix},
$$

where θ is the rotation angle of $-135°$. This matrix transforms the reduced displacement vector $\boldsymbol{p}$ as follows:

$$
\boldsymbol{p} = \boldsymbol{T}\boldsymbol{p}^*.
$$

Hence, the new, reduced system becomes:

$$
\boldsymbol{T}^T \boldsymbol{K}_{\mathrm{G}} \boldsymbol{T} \boldsymbol{p}^* = \boldsymbol{T}^T \boldsymbol{f}_{\mathrm{G}}.
$$

69

Here, $\boldsymbol{K}_{\mathrm{G}}$ is the reduced stiffness matrix, $\boldsymbol{f}_{\mathrm{G}}$, is the reduced force vector. In this case, Locators 2 and 3 are modelled as springs with spring stiffness 7×10^8 N/m in y'-direction and x'-direction respectively, directions as shown in Figure 4.8. Locator 1 is modelled as a spring with spring stiffness 7×10^8 N/m in y-direction.

The clamp is modelled as a force. The normal of the clamping clamping surface, as can be seen in Figure 4.7, is not in x- or y-direction. On basis of the geometric ratios, the normal of clamping surface can be established in the x, y coordinate frame. The clamping force, which is in the negative normal direction, has the following components:

$$F_{\mathrm{c}} = 0.465746433 F_{\mathrm{c},x} + 0.884918222 F_{\mathrm{c},y}.$$

Force closure is present in the fixture design and the clamping force produces reaction forces at the three locators. To fulfil the requirement for stable workholding, a variable clamping force is applied, such that contact between the part and the locators is always present.

An approximate model for the applied torques has been established as follows. The exerted 3 Nm machining torque in Equation (4.4.2) is transformed into equivalent concentrated loads, that have opposite sign in the y-direction. The load is applied to the neighbouring nodes of the node where the concentrated machining forces are applied. When the two nodal distances of the neighbouring in the machining tool path are unequal, a compensating load in y-direction is applied. This compensating load ensures that the sum of the equivalent forces in y-direction is zero. For the comparison between the model established here and the one presented in the the literature, it is sufficient to compare a relatively few points. For this reason, only 17 calculations are made, such that the force components in Equation (4.4.2) are only applied the internal nodes of the tool path. As a result, the nodes at the extreme left and right of the workpiece, are used only to apply the equivalent loads of the torque component in Equation (4.4.2).

4.4.3.3   Comparison of Results

The calculated minimal clamping and reaction forces for the model established above are presented in Figure 4.9. In Figure 4.9, also the results from the study by Tao *et al.* [155] are shown. As a result the model as established above can easily be compared with results

presented in Ref. [155]. Tao *et al.* [155] considered the part, clamps and locators to be rigid, for this reason they only study the static reaction forces. Furthermore, in their analysis, friction is present. In the model established with the methodology developed for this thesis, the part, and clamps and locators are flexible and, additionally, friction is not taken into account.

The model developed here has been thoroughly checked for force equilibrium. It can be seen that, although the trends in the figure are qualitatively the same, the quantitative results are not. Firstly, the reduced flexible model predicts a lower clamping force than needed in the model by Tao *et al.* [155]. Secondly, the lowest minimal clamping forces needed in the flexible model, occurs at cutter position $x = 85$ mm and the lowest minimal clamping forces in the model by Tao *et al.* occurs at $x = 110$ mm. Thirdly, the flexible model predicts that higher clamping forces are needed, to ensure that contact exists between the workpiece and Locator 2, when the cutting tool is near the end. Furthermore, it is striking that the reaction forces at Locator 3 in the flexible model are consistently higher than the reaction forces as calculated by the rigid model. This is due to a different distribution of the reaction forces in the two models, which is caused by the absence of friction in the flexible model. Springs, that have a lower spring stiffness, can be added in the tangential direction. This can be seen as a first step towards the modelling of the tangential stiffness of the locators in case friction is incorporated in the model of the part-fixture system. In this case, the magnitudes of the reaction forces in the flexible model become more similar to the reaction forces of the rigid model. However, this is an incorrect way of modelling, as slip is not taken into account. For this reason, the results for this case cannot be presented here. The results obtained in case tangential springs were added, still exhibit the same lowest point for the minimal clamping forces at $x = 85$ mm. To make the model which incorporates friction more accurate, the clamp should be modelled as a spring. This spring is then loaded with the clamping force. Another tangential spring stiffness can then be added and the distribution of the reaction forces will agree better with the rigid model.

The methodology developed in Chapter 3 allows for a proper implementation of friction, but this is really beyond the scope of the current work.

4.4.4 Case Study III

4.4.4.1 Description of the Part-Fixture System

The 2D case study presented in Ref. [155] and studied in Section 4.4.3 has been extended to a 3D case study in Refs [153, 155]. In Figure 4.10(a) a $112 \times 122 \times 220$ rectangular prismatic aluminium part is shown. The workpiece is located with a 3-2-1 locating scheme (L0-L5) and two side clamps, P1 and P2, are used to constrain the part on the locators. The aluminium alloy used for the workpiece has the following material properties $\rho = 2700$ kg/m^3, $E = 68.9$ GPa and $\nu = 0.33$. The machining area is the centre line in z direction at the top of the part, as shown in Figure 4.10(a) (see also the line of dots on the corresponding FE-model in Figure 4.10(b)). The machining force is modelled as a force vector with the following components:

$$\boldsymbol{F}_{\mathrm{m}} = \{-55, 131, -60\}^{T} \quad \text{N.} \tag{4.4.3}$$

Tan *et al.* [153] present a FE-model, where both part and fixture elements are modelled elastically and compare this with the initial FE-model by Tao[4] where the contacts are modelled as hard contacts, with an infinite contact stiffness, resulting in zero displacement boundary conditions in the normal directions of the workpiece surface at the fixturing points. Furthermore, this system has been analysed by Qin *et al.* [131], who built a model consisting of a rigid part and elastic fixture elements. The models, as presented in Refs [131, 153, 155], take into account the friction between workpiece and fixture.

4.4.4.2 Modelling of the Part-Fixture System

A 8349 DOF, $10 \times 10 \times 22$ linear hexagonal (C3D8) element model has been built for the part. The six locators have each a spring stiffness of $k = 1 \times 10^{7}$ N/m. The FE-model and the highlighted nodes, of which the DOFs are retained in the statically reduced model, are shown in Figure 4.10(b).

---

[4]Tao's model is presented in: Z.J. Tao, A. Senthil Kumar, A.Y.C. Nee and M.A. Mannan, 'Modelling and Experimental Investigation of a Sensor-Integrated Workpiece-Fixture System', *International Journal of Computer Applications in Technology*, **10** (33), pp. 236–250, 1997.

4.4.4.3 Comparison of Results

In Ref. [153] the FE-model by Tan *et al.* is compared with the previously established FE-model by Tao *et al.* and with experimental results. In Figure 4.11, these results are shown. On the top of Figure 4.11, one can see the experimental results obtained for the case study. On the left- and righthand sides of the Figure, a sort of run-in and run-out effect seems to occur. This effect is not modelled in the FEM model, where the load is applied quasi-statically. Locator 3 (L3) has a constant reaction force of about 725 N. Although, one might object against this and argue that the trend is actually that of a slightly increasing reaction force. L4 starts at 430 N and decreases to 310 N, and L5 does exactly the opposite. The locators at the bottom of the part, L0, L1 and L2, have very low experimental values and are not in close agreement with the FE model by Tao *et al.* and the one by Tan *et al.*. A possible explanation for this might be that this is probably due to a crude or wrong model for the clamping sequence. Furthermore, the rigid-part-soft-contact model of the part-fixture system by Qin *et al.* [131] predicts again different reaction forces as seen in Figure 4.12.

The model, as established with the methodology as presented in this thesis, can be compared with results of the models presented in [153]. A linear contact and fixture stiffness of $k = 1 \times 10^7$ N/m is assumed. First, the results for locators L3, L4 and L5 are discussed. When F_x, the force applied in x-direction, is 55 N and the clamping force at P2 is -670 N then, since there is no friction incorporated in the modelling in the thesis, the reaction force on L3 becomes 615 N, if the force in x-direction is -55 N, then the reaction force at L3 becomes 725 N. Both results are remarkably matching with Fig. 9 and Fig. 7 respectively in Figure 4.11, which respectively show constant reaction forces at L3 of 615 N and 725 N.

The results for L3, L4 and L5 in Figs 7, 8 and 9 of Figure 4.11 do not agree very well. Whereas one should expect the predictions to become increasingly accurate when a more detailed model is established, as the difference between the early model by Tao *et al.* and later model by Tan *et al.* is that the latter are taking into account the stiffness of the contacts and the fixture. However, in the range of fixture and contact stiffnesses in practice, the reaction force does not depend so much on these stiffness. In

fact the reaction forces are almost equal to those in the case of an infinite contact and fixture stiffness. Hence one should expect the results of Figs 8 and 9 of Figure 4.11 to be indistinguishable when presented graphically. However, when P2 exerts a clamping force of -640 N and $F_x = $ -55, then a reaction force of 695 N can be expected.

There are some other reasons to put doubts on the results presented in Ref. [153]: something strange appears to be happening at the bottom of the system in the 3D case study, presented in Section 4.4.4. Is the configuration of the locators really as shown in Figure 4.10(a) or is it as shown in Ref. [155, Fig. 10]? It seems that the reaction forces at locators L0, L1 and L2 in the 3D case study discussed in Section 4.4.4 in z-direction are relatively sensitive to the friction forces compared to the reaction forces at locators L3, L4 and L5.

In Figures 4.13(b), 4.14(b) and 4.15(b), the reaction forces at L4 and L5 decrease from 458 N to 314 N and increase from 314 N to 458 N, respectively. When the cutter position reaches the centre of the workpiece, at 110 mm (or at $t = $ 66 s) the reaction forces L4 and L5 are the same as can be observed in Figures 4.13(b), 4.14(b) and 4.15(b). This seems logical: the clamps and locators are placed in locations of symmetry with respect to the centre. It is therefore odd that the corresponding reaction forces, as shown in Figure 4.11, are intersecting at least 10 s before, however, this is dependent on contribution of the the friction friction forces to the force equilibrium.

When extra springs in the tangential directions are attached to the locators to simulate stiffness that is due to the friction in the tangential directions, the intersecting point, where the reaction force of L1 becomes larger than L2, changes, but it moves to the right, beyond 110 mm (or 66 s). As mentioned above: this is not an exact modelling of the displacements and (friction) forces in tangential direction. In this case, also the reaction forces for L0, L1 and L2 start to look like the results in Figs 8 and 9 of Figure 4.11, except that the results converge for increasing cutter position (or time) instead of diverge. However, this is strongly dependant on the direction of force F_x. Furthermore, the reaction force L3 in the direction normal to the surface of the part decreases when the position of the cutter decreases.

In addition, as observed in Figures 4.13(a), 4.14(a) and 4.15(a), when gravity and top clamping are considered and the load F_z reduced, the reactions at the bottom

locators can be changed, such that they show more resemblance to the experimentally obtained reaction forces. From this observation it can be concluded that frictionless modelling yields conservative results. Furthermore, the experimental results and the model-based predictions presented in Refs [131, 153] are not consistent. This shows that models incorporating friction not necessarily yield consistent results and results that are in close relation with the experimental results. The predictions made on basis of the frictionless models, as established in this thesis, yield results which show the same level of agreement with the experimental results as those presented in Ref [153]. In addition, according to the frictionless models top clamping is needed, which has *not* been used in the experiments discussed in Ref [153].

4.4.5 Conclusions

The developed methodology yields results that are in close agreement with models presented in the literature that do not consider friction. Given the conservative nature of frictionless fixturing modelling, the overall conclusion is that part-fixturing modelling, as established by this research, is a valid way of modelling. Even without friction, the modelled magnitude of the reaction forces comes close to the experimental values and the models that consider friction. This means that the models can be utilised to tune controllers, using e.g. the MATLAB$^{\circledR}$ Control Toolbox$^{\text{TM}}$. Secondly, the developed methodology can be expanded and fine-tuned by incorporation of a (empirical) model for the friction, which avoids the difficulties of modelling friction from first principles. Additionally, the torque modelling can also be refined by creating and selecting more nodes around the tool path. This results in a more accurate modelling of the torque and the related displacements. Thirdly, since a static reduction is made, the displacements for the reduced model are the same as those of the unreduced FE model. Finally, as a recommendation, in order to increase the accuracy of the predicted values of the part displacements and reaction forces, small non-linear models containing friction should be established in future work.

4.5 Clamping Force Modelling

4.5.1 Hydraulic Actuator

As remarked in Chapter 2, hydraulic systems are utilised in manufacturing and hydrauli-cally actuated clamps can be connected to the existing hydraulic infrastructure available at the shop floor. Special hydraulic clamps are commercially available [35, 45, 140], which are relatively small compared to the actuators that are applied in e.g. the tri-, hexapods, which are widely applied in manufacturing and elsewhere. In this section, a dynamic model of a hydraulic actuator for the generation of dynamic clamping forces is built. In Figure 4.16 the components of a hydraulic servo-system consisting of a three-way-servo-valve and an asymmetric actuator are shown. The actuator is called asymmetric as the piston surface areas at both sides of the plunger are different. Oil at supply pressure P_s is pumped into the system. At one side of the piston in Figure 4.16, the oil flows directly into the cylinder at the supply pressure P_s. If P_1 is assumed $\frac{1}{2}P_s$, for the system shown in Figure 4.16, and the viscous friction force $w\dot{y}_0$ of the oil, the Coulomb friction force F_μ and the external force F_e are not present, then a force equilibrium exists. The viscous friction force is the product of piston velocity $\dot{y}_0$ and viscous friction coefficient w, which is related to the viscosity of the oil. This force equilibrium is the case when there is no change in the piston speed. Hence the amount of oil $Q_1 - Q_2$ flowing into the cylinder determines the velocity and displacement of the actuator. The amount of oil flowing in and out of the cylinder is controlled with a valve displacement x. The dynamics of such a hydraulic system are modelled, based on the methodology presented in standard textbooks such as [103, 163]. From [163], a linearised ordinary differential equation can be obtained for the actuator displacement y_0, where the stiffness of the oil in the cylinder has been accounted for higher model accuracy. Using the same notation as shown in Figure 4.16, this gives the following expression

$$\dot{y}_0 A = C_d \sqrt{\frac{P_s}{\rho}} \left[a_1 - a_2 - (a_1 + a_2)\frac{P_L}{P_s} \right] - \frac{V_0}{E}\dot{P}_L. \qquad (4.5.1)$$

Here, C_d is the (von Mises) discharge coefficient for turbulent flow through a narrow orifice, P_s is the supply pressure, ρ is the density of the oil, P_L is the excess pressure that is caused by the external load and E is the bulk modulus of the hydraulic oil. Coefficients

a_1 and a_2 are described in [163] and are related to the valve displacement x as follows

$$a_1 - a_2 = bx; \qquad a_1 + a_2 = b|x|. \tag{4.5.2}$$

Using Newton's second law, a force balance for the piston can be established

$$M_0 \ddot{y}_0 = P_c A - P_s \frac{A}{2} - F_e - F_\mu - w\dot{y}_0, \tag{4.5.3}$$

where M_0 is the mass of the plunger, P_c is the pressure in the cylinder, A is the piston surface area, F_e is the external force, F_μ is the Coulomb friction force and w is the viscous friction coefficient. This viscous friction coefficient is hard to model [163, p. 25] from first principles. Solving for P_c yields

$$P_c = \tfrac{1}{2}P_s + P_L, \tag{4.5.4}$$

where P_L is

$$P_L = \frac{F_e + F_\mu + w\dot{y}_0 + M_0 \ddot{y}_0}{A}. \tag{4.5.5}$$

If the cylinder is assumed to be equipped with a hydrostatic bearing the Coulomb friction force F_μ can be ignored. The viscous friction force $w\dot{y}_0$ is not known exactly, but is chosen to have a realistic value in this thesis. If pole placement is used as the control method, then system damping can be changed by the desired amount.

4.5.1.1 Linearising the actuator model

In order for the state equations to be linear, inputs and states should not be coupled. However the equations derived in the last section are coupled. In this section the state equation is linearised. Viersma [163] identifies the following coefficients for a system consisting of an asymmetric actuator with a critical-centre[5] three-way valve:

$$K_m = \frac{b}{A}C_d\sqrt{\frac{P_s}{\rho}}; \quad c_h = \frac{AP_s}{|x|}; \quad c_o = \frac{EA}{L}. \tag{4.5.6}$$

In Equation (4.5.6), K_m is the velocity gain, L is the length of the oil cylinder, c_h is the hydraulic stiffness of the valve, and c_o is the oil cylinder spring stiffness. The

---

[5]Critical-centre: when the valve in Figure 4.16 is in the centre position, i.e. $x = 0$, then there is no leak flow: $Q_1 = Q_2 = 0$; for $x > 0$ in the definition of Figure 4.16 there is a flow Q_1, but $Q_2 = 0$; and for $x < 0$ there is a flow Q_2, but $Q_1 = 0$.

cylinder volume V_0 can be expressed as: $V_0 = AL$. Obviously $L = y_0$, however, in the clamped position, y_0 and therefore L will not vary significantly: $y_0 \pm \Delta y_0 \approx y_0$. Therefore the length of the oil cylinder L can be considered to be constant. Valve displacement x will be typically naught or around zero, and c_h can therefore be assumed to be infinite. In this way the nonlinearity introduced by having $c_h(x)$ coupled to the states and the coupling between the states $(y_0 \dot{y}_0, y_0 \ddot{y}_0)$ in the state equations is removed. Using (4.5.5) and (4.5.6), Equation (4.5.1) can be reformulated as follows

$$\dot{y}_0 = K_m x - \frac{\dot{F}_e + M_0 \ddot{\ddot{y}}_0 + w \ddot{y}_0}{c_o}, \tag{4.5.7}$$

$$\ddot{\ddot{y}}_0 = K_m \omega_o^2 x - \frac{\dot{F}_e}{M_0} - 2\beta\omega_0\ddot{y}_0 - \omega_o^2\dot{y}_0, \tag{4.5.8}$$

where the coefficients β and ω_0 are defined as:

$$\beta = \frac{w}{2\sqrt{M_0 c_0}}; \qquad \omega_0^2 = \frac{c_o}{M_0}. \tag{4.5.9}$$

4.5.1.2 Modelling the connection force

The connection force F_e is a function of the relative displacements and velocities, and the values of the connecting spring stiffness and damping are *constant*

$$F_e = c(\dot{y}_0 - \dot{y}_1) + k(y_0 - y_1). \tag{4.5.10}$$

The time derivative in Equation (4.5.10) can be substituted into the rearranged equation of motion displayed by Equation (4.5.8)

$$\ddot{\ddot{y}}_0 = K_m\omega_0^2 x - \frac{d_1}{M_0}(\ddot{y}_0 - \ddot{y}_1) - \frac{k_1}{M_0}(\dot{y}_0 - \dot{y}_1) - 2\beta\omega_0\ddot{y}_0 - \omega_0^2\dot{y}_0. \tag{4.5.11}$$

4.5.1.3 Valve Dynamics

It is assumed that the actuator of the electro-hydraulic servo-valve has a very small time constant compared to the bandwidth of the valve and the valve dynamics can be described with a second order transfer function between reference value r and actual valve displacement x in Laplace form [103, 163]

$$\frac{x}{r} = \frac{1}{\dfrac{s^2}{\omega_v^2} + \dfrac{2\beta_v}{\omega_v} + 1}. \tag{4.5.12}$$

78

For a valve controlled by an electric actuator the transfer function $V(s)$, modelling the dynamical behaviour of the servo-valve, becomes

$$V(s) = \frac{x}{r} = \frac{1}{\left(\dfrac{s}{K_{\mathrm{v}}} + 1\right)\left(\dfrac{s^2}{\omega_{\mathrm{v}}^2} + \dfrac{2\beta_{\mathrm{v}}}{\omega_{\mathrm{v}}}s + 1\right)}, \tag{4.5.13}$$

where the actuator gain K_{v} is expressed as

$$K_{\mathrm{v}} = \frac{1}{\tau_{\mathrm{v}}}.$$

Hence, if the actuator time constant τ_{v} increases, the gain decreases, and the time needed for the start up of the actuator increases.

4.5.2 Electromechanical Linear Actuator

Another actuation principle for the generation of clamping forces that can be utilised is by electromechanical linear actuation, which e.g. has been applied in the fixture designs in Refs [25, 30, 42, 115], and the design by Papastathis and Ryll (see Papastathis [119]) developed at The University of Nottingham. Electromechanical linear actuators, sometimes called ball-screw actuators or electromechanical cylinders, are based on a ball-screw, driven by a standard rotary electromechanical actuators, such as a permanent magnet DC motor (PMDC). Despite the apparent drawbacks of PMDCs, like wear of the brushes and relatively low power density compared to other electric motors, DC motors are often utilised because of the fine characteristics and great controllability compared to other types of electric motors. PMDCs are modelled from first principles, and the standard electromechanical equations for a PMDC are given by [41, 48, 54, 77, 110]

$$J_{tot}\ddot{\theta} + f_r\dot{\theta} = k_{\mathrm{T}}i + T_{\mathrm{e}}, \tag{4.5.14}$$

$$L\frac{\mathrm{d}i}{\mathrm{d}t} + Ri + k_{\mathrm{bemf}}\dot{\theta} = V_{\mathrm{C}}. \tag{4.5.15}$$

In these equations, i is the current, J_{tot} - the total inertia as seen by the motor, f_r - viscous friction coefficient, θ - angular displacement, k_{T} - torque coefficient, T_{e} - external torque, L - motor inductance, R - motor resistance, k_{bemf} - back-emf constant, and V_{C} is the voltage output of the controller.

The contact stiffness and damping are modelled by spring-dashpot elements. Based on [137], the clamp and locator have a spring stiffness $k = 3 \times 10^7$ N/m and a damping

constant $c = 960.12$ Ns/m. The connection forces F_e between part and the electromechanical actuators is a function of the relative displacements and velocities:

$$F_e = c(\dot{y}_0 - \dot{y}_1) + k(y_0 - y_1). \tag{4.5.16}$$

The relation between angular displacement θ of a PMDC and the translational displacements of the tip of the ball-screw x_{act} is

$$x_{act} = \theta p, \tag{4.5.17}$$

where p is the ball-screw pitch.

From the principle that work over a distance in translational direction equals work over the equivalent distance in angular displacement follows, that the external torque T_e is proportional to the connection force F_e and the ball-screw pitch p

$$T_e = pF_e. \tag{4.5.18}$$

An example of an electromechanically actuated fixture is given Section 4.7.4.

4.6   Servo-Control

In Figure 4.17, a control loop for a generic active fixturing system can be seen: the actuator displacement x_{act}, the part displacement x_n and the actuator forces F_{act}, can be measured. These quantities are called the system outputs. One of these outputs can be selected and used to create a feedback loop. This works as follows. A reference value r is given for a desired output, e.g. the actuator force. This value is compared with the actual value of this output - called the state - as measured by the sensor. The difference ε, called the error signal, is sent to the controller. A controller compensates its input signal for the system dynamics, it can e.g. amplify an input signal in case when the system response would be undesirably small. The controller feeds the steering signal(s) into the actuator(s). The relative actuator displacements and velocities determine the actuator force, which is measured by the force sensor and is fed back and compared with the input reference signal. In this work the actuators are assumed to be controlled by means of a classical controller. The controller has to function within a closed-loop system.

4.6.1 Control strategies

Investigations have been made to the use of position feedback: firstly, the actuator displacement feedback (ADFB), secondly, the part displacement feedback (PDFB), and, thirdly, force feedback (FFB). In practice, it is attractive to have multiple active clamps. As a result, the system becomes a multi-input multi-output(MIMO) system. Collocated control, where in the case of a fixturing system, the actuator displacement or nearby part displacement or the actuator clamping force is controlled, is one of the practical control strategies. For this reason, collocated control is used as a control strategy. In this case, a reference value that ensures stable workholding should be set on the clamp. As can be seen from Figure 4.17, one of the outputs is taken and used for negative feedback. This study does not concern feedback or parallel compensation [102]. For the AFFIX project several classical control strategies have been investigated and compared in the form of series compensation. This involved the three term proportional-integral-derivative control [48, 50, 102] (PID-control) and the use of lag filters (LaFs) and lead filters (LeFs) [48, 50, 102]. For the classical three term PID controller, the transfer function $C(s)$ is defined as [48]

$$C(s) = K_p \left(1 + \frac{1}{T_I s} + T_D s \right). \tag{4.6.1}$$

The lead and lag filters have a transfer function of

$$C(s) = K_p \frac{s + \omega_{\mathrm{LF}}}{\alpha_{\mathrm{LF}} s + \omega_{\mathrm{LF}}},$$

where the proportional gain K_p, the settings for the corner frequencies $\omega_{\mathrm{LF}}/\alpha_{\mathrm{LF}}$, and ω_{LF} need to be tuned appropriately. These settings determine respectively the corner frequency for the maximum controller response and the minimum response from the compensator. The design rules for the LeF and the LaF can be found in classic textbooks such as [48]. In case

$$\alpha_{\mathrm{LF}} > 1$$

the compensator is a LaF, and when

$$\alpha_{\mathrm{LF}} < 1$$

the controller has the properties of a LeF.

81

Finally, for mathematical modelling, the controller will have to be connected to the rest of the model. This issue is discussed in Section 4.7.4.

4.7 State-Space Realisation

For increased readability the index "CB" has been dropped from the notation in the equations for the mass and stiffness matrices as derived in Equation (A.2.6). The damping matrix C can be established using proportional damping

$$C = \alpha M + \beta K.$$

The springs and the dashpots representing the clamps and locators need to be attached to the part. The corresponding spring stiffness and damping must be added according to their respective variables in the damping and stiffness matrices. This can be modelled likewise as a mass-spring-damper system, with n masses and n coordinates. Since the fixture is considered to be a rigid body, this comes down to adding the positive damping and spring stiffness value to the diagonal of the damping and the stiffness matrices in their respective rows.

The fixture elements are not included in the FE-model of the workpiece. The damping and stiffness matrices should be updated with the values of the equivalent damping and stiffness coefficients of the passive fixture elements on the diagonal. Separate stiffness and damping matrices K^* and C^* are made, including all the equivalent values for the stiffness and damping of the active clamps, such that a difference stiffness matrix δ_K and a difference damping matrix δ_C are can generated

$$\delta_C = -(M^{-1}C - M^{-1}C^*), \quad \delta_C = -M^{-1}(C - C^*); \tag{4.7.1}$$

$$\delta_K = -(M^{-1}K - M^{-1}K^*), \quad \delta_K = -M^{-1}(K - K^*).$$

Note that $C - C^*$ and $K - K^*$ are diagonal matrices, which have non-zero entries on the diagonal for the degrees of freedom at the active clamping points[6].

---

[6]Active clamping point: these are points that are clamped by *active* clamps.

4.7.1 State-Space

The standard state-space formulation for an arbitrary system is derived as follows. The second order system

$$M\ddot{p} + C\dot{p} + Kp = f$$

is written in matrix notation. If one substitutes the generalised coordinates $p_1 = \dot{p}$ then the system can be rewritten as a first order system:

$$M\dot{p}_1 = -Cp_1 - Kp + f.$$

Obviously:

$$\dot{p}_1 = -M^{-1}Cp_1 - M^{-1}Kp + M^{-1}f.$$

Then the state-space notation for this system is:

$$\left\{ \begin{array}{c} \dot{p}_1 \\ \dot{p} \end{array} \right\} = \left[\begin{array}{cc} -M^{-1}C & -M^{-1}K \\ I & 0 \end{array} \right] \left\{ \begin{array}{c} p_1 \\ p \end{array} \right\} +$$

$$\left\{ \begin{array}{c} -M^{-1}f \\ 0 \end{array} \right\}. \tag{4.7.2}$$

Hence, a generic second order system can be written in state-space notation. In the context of this thesis, the second order system is the reduced part model. The next step in establishing an overall model for the control, is to couple the part model to the fixture. As a result, state-matrix A is containing the damping and stiffness matrices C^* and K^*, where the damping and stiffness coefficients of the equivalent values of the fixture elements are added. When the state matrix A, is extended for the actuator(s) - for the present with zeros - it becomes the following matrix

$$A = \left[\begin{array}{ccc} -M^{-1}C^* & -M^{-1}K^* & 0_{act}^T \\ I & 0 & 0_{act}^T \\ 0_{act} & 0_{act} & 0_{aa} \end{array} \right]. \tag{4.7.3}$$

The damping and stiffness matrices C^* and K^* have additional entries on their diagonals, the physical implication of this is, that the reduced system is "fixtured" with spring-dashpot element to the 'ground'. In order to connect the active clamping points with the actuated clamps, the rows in the state matrix containing the equations of

motion of the workpiece must be updated with the selected columns corresponding to the degrees of freedom of the active clamping point from the difference matrices $\boldsymbol{\delta}_K$ and $\boldsymbol{\delta}_C$ from (4.7.1). This gives the state matrix to be

$$
A = \begin{bmatrix} -\boldsymbol{M}^{-1}\boldsymbol{C}^* & -\boldsymbol{M}^{-1}\boldsymbol{K}^* & \boldsymbol{\delta}^* \\ \boldsymbol{0} & \boldsymbol{0} & \boldsymbol{0}_{\text{act}}^T \\ \boldsymbol{0}_{\text{act}} & \boldsymbol{0}_{\text{act}} & \boldsymbol{0}_{aa} \end{bmatrix}.
$$

Where $\boldsymbol{\delta}^*$ is a combination of the selected columns from matrices $\boldsymbol{\delta}_C$, $\boldsymbol{\delta}_C$ as defined in Equation (4.7.1) and the zero columns which correspond to (possible) other states of the actuator. Finally, the actuator model(s), as established in Section 4.5, should be added to the bottom row of the partition in (4.7.3). Now that $\boldsymbol{A}$ is established, the whole state-space model $\{\boldsymbol{A}, \boldsymbol{B}, \boldsymbol{C}, \boldsymbol{D}\}$ can then be established on the basis of Equation (4.5.11) and the transfer functions of the compensator, as developed in Section 4.6.1. The machining forces are modelled in the reduced FE model of the part.

4.7.2 Transformation to Modal Coordinates

In some cases it is desirable to run the model in modal coordinates. This enables potentially faster simulations, introducing modal damping and avoiding the sometimes ill-posed product $-\boldsymbol{M}^{-1}\boldsymbol{K}$ of the reduced mass and stiffness matrices. Consider the general equation of motion in Cartesian coordinates in matrix notation

$$
\boldsymbol{M}\ddot{\boldsymbol{x}} + \boldsymbol{C}\dot{\boldsymbol{x}} + \boldsymbol{K}\boldsymbol{x} = \boldsymbol{f}.
$$

In MATLAB the eigenvalues and eigenvectors of a system are established by the following command:

$$
[\boldsymbol{\Phi}, \boldsymbol{\Lambda}] = \texttt{eig}(\boldsymbol{K}, \boldsymbol{M}).
$$

The dimensionless eigenvectors of the system ϕ_i are scaled such that:

$$
\boldsymbol{\Phi}^T \boldsymbol{M} \boldsymbol{\Phi} = \boldsymbol{I}, \text{ and } \boldsymbol{\Phi}^T \boldsymbol{K} \boldsymbol{\Phi} = \boldsymbol{\Lambda}.
$$

The transformations between the Cartesian coordinates $\boldsymbol{x}$ and the modal coordinates $\boldsymbol{\eta}$ and load $\boldsymbol{F}$ in the Cartesian frame and the equivalent load in modal coordinates $\boldsymbol{P}$ are

$$
\boldsymbol{x} = \boldsymbol{\Phi}\boldsymbol{\eta}; \quad \boldsymbol{P} = \boldsymbol{\Phi}^T \boldsymbol{F}.
$$

Assuming damping can be modelled by proportional or modal damping [29] and making use of linearity, in case of proportional damping, the equations of motion can be rewritten in modal coordinates as [29]

$$I\ddot{\boldsymbol{\eta}} + (\beta I + \alpha \Lambda)\dot{\boldsymbol{\eta}} + \Lambda \boldsymbol{\eta} = \boldsymbol{P}.$$

Making use of the property of the identity matrix that the inverse of the identity matrix is identity matrix itself [56], equations of motion can be rewritten in state-space notation as follows:

$$\left\{\begin{array}{c} \ddot{\boldsymbol{\eta}} \\ \dot{\boldsymbol{\eta}} \end{array}\right\} = \left[\begin{array}{cc} -(\beta I + \alpha \Lambda) & -\Lambda \\ I & 0 \end{array}\right] \left\{\begin{array}{c} \dot{\boldsymbol{\eta}} \\ \boldsymbol{\eta} \end{array}\right\} + \left\{\begin{array}{c} \boldsymbol{P} \\ \boldsymbol{0} \end{array}\right\} \qquad (4.7.4)$$

$$\left\{\begin{array}{c} \dot{\boldsymbol{x}} \\ \boldsymbol{x} \end{array}\right\} = \left[\begin{array}{cc} \boldsymbol{\Phi} & 0 \\ 0 & \boldsymbol{\Phi} \end{array}\right] \left\{\begin{array}{c} \dot{\boldsymbol{\eta}} \\ \boldsymbol{\eta} \end{array}\right\} + [\boldsymbol{0}].$$

4.7.3 Connecting a System in Modal Coordinates to a System in Cartesian Coordinates

The transformation from Cartesian to modal coordinates is a linear transformation. Therefore the connection of reduced part-fixture system in modal coordinates to an actuated and controlled clamp only requires the equations to be written out diligently. This is demonstrated with the following example. Consider the simple three mass-spring system shown in Figure 4.18. The equations of motion for this system are given by

$$\left[\begin{array}{ccc} m_a & 0 & 0 \\ 0 & m_1 & 0 \\ 0 & 0 & m_2 \end{array}\right] \left\{\begin{array}{c} \ddot{x}_a \\ \ddot{x}_1 \\ \ddot{x}_2 \end{array}\right\} + \left[\begin{array}{ccc} k_1 & -k_1 & 0 \\ -k_1 & k_1 + k_2 & -k_2 \\ 0 & -k_2 & k_2 + k_2 \end{array}\right] \left\{\begin{array}{c} x_a \\ x_1 \\ x_2 \end{array}\right\} = \left\{\begin{array}{c} F_a \\ F_1 \\ F_2 \end{array}\right\}.$$

When the system is cut open between m_a and m_1, the equations of motion for the subsystem m_1 and m_2 become:

$$\left[\begin{array}{cc} m_1 & 0 \\ 0 & m_2 \end{array}\right] \left\{\begin{array}{c} \ddot{x}_1 \\ \ddot{x}_2 \end{array}\right\} + \left[\begin{array}{cc} k_2 & -k_2 \\ -k_2 & k_2 + k_2 \end{array}\right] \left\{\begin{array}{c} x_1 \\ x_2 \end{array}\right\} = \left\{\begin{array}{c} F_e + F_1 \\ F_2 \end{array}\right\},$$

where F_e is the connection force between m_a and m_1, defined as

$$F_e = -k_1(x_1 - x_a). \qquad (4.7.5)$$

The equations of motion in modal coordinates of this subsystem are

$$\begin{bmatrix} 1 & 0 \\ 0 & 1 \end{bmatrix} \begin{Bmatrix} \ddot{\eta}_1 \\ \ddot{\eta}_2 \end{Bmatrix} + \begin{bmatrix} \lambda_1 & 0 \\ 0 & \lambda_1 \end{bmatrix} \begin{Bmatrix} \eta_1 \\ \eta_2 \end{Bmatrix} = \mathbf{\Phi}^T \begin{Bmatrix} F_\mathrm{e} + F_1 \\ F_2 \end{Bmatrix}. \tag{4.7.6}$$

Where the modal matrix $\mathbf{\Phi}$ is denoted as follows

$$\mathbf{\Phi} = \begin{bmatrix} \phi_{11} & \phi_{12} \\ \phi_{21} & \phi_{22} \end{bmatrix}.$$

Equation (4.7.5) is rewritten as

$$F_\mathrm{e} = -k_1(\phi_{11}\eta_1 + \phi_{12}\eta_2 - x_a). \tag{4.7.7}$$

Then, Equation (4.7.7) can be substituted into (4.7.6), and the equations of motion of both subsystems can be rewritten in state-space notation:

$$\begin{Bmatrix} \ddot{\eta}_1 \\ \ddot{\eta}_2 \\ \dot{\eta}_1 \\ \dot{\eta}_2 \\ \ddot{x}_a \\ \dot{x}_a \end{Bmatrix} = \begin{bmatrix} 0 & 0 & \lambda_1 + k_1\phi_{11}^2 & k_1\phi_{11}\phi_{12} & 0 & -\phi_{11}k_1 \\ 0 & 0 & k_1\phi_{21}\phi_{11} & \lambda_2 + k_1\phi_{21}\phi_{12} & 0 & -\phi_{21}k_1 \\ 1 & 0 & 0 & 0 & 0 & 0 \\ 0 & 1 & 0 & 0 & 0 & 0 \\ 0 & 0 & -\frac{k_1}{m_a}\phi_{12} & -\frac{k_1}{m_a}\phi_{12} & 0 & \frac{k_1}{m_a} \\ 0 & 0 & 0 & 0 & 1 & 0 \end{bmatrix} \begin{Bmatrix} \dot{\eta}_1 \\ \dot{\eta}_2 \\ \eta_1 \\ \eta_2 \\ \dot{x}_a \\ x_a \end{Bmatrix} + \begin{Bmatrix} \phi_{11}F_1 + \phi_{21}F_2 \\ \phi_{12}F_1 + \phi_{22}F_2 \\ 0 \\ 0 \\ \frac{F_a}{m_a} \\ 0 \end{Bmatrix}.$$

4.7.4 Connecting a Controller

The last subsystem to be connected to the model in state-space is the controller. This is done by substituting the input variable(s) of the actuator(s) by the state equations describing the dynamics of the controller. The following representative example will illustrate the connection of a controller. Consider the simple active fixturing system shown in Figure 4.19. A 1D part modelled as a rigid mass is clamped with an electromechanical actuator on a locator. The equation of motion of the part can easily be established on basis of Figure 4.19

$$M\ddot{x}_2 = c\dot{x}_1 - 2c\dot{x}_2 + kx_1 - 2kx_2 + F_\mathrm{m}. \tag{4.7.8}$$

Obviously, the connection force between the part and the ball screw is

$$F_\mathrm{e} = -c\dot{x}_1 - kx_1 + c\dot{x}_2 + kx_2.$$

Since $x_1 = p\theta$ the external torque as seen by the motor is expressed by the following relationship

$$T_{\text{e}} = pF_{\text{e}} = -cp^2\dot{\theta} - kp^2\theta + cp\dot{x}_2 + kpx_2. \tag{4.7.9}$$

A proportional-integral (PI) controller is a representative controller and is added to the part-fixture system shown in Figure 4.19. The equation for the PI controller is given by

$$C(s) = K_p \left(1 + \frac{1}{T_i} \right).$$

Rewritten in state-space notation:

$$\{\dot{V}_{PI}\} = [0]\{V_{PI}\}\} + [1]\{V_r\}, \tag{4.7.10}$$

$$\{V_C\} = \left[\frac{K_p}{T_I} \right] \{V_{PI}\} + [K_p]\{V_r\}.$$

Where V_r is the reference voltage, V_C is the controlling voltage over the DC motor and V_{PI} is a state variable introduced by the PI controller.

Substituting the expression for the external torque (4.7.9) and the expression for the controller (4.7.10) into the equations of motion for the ball-screw (4.5.14) and (4.5.15), and combining with (4.7.8) and rearranging, yields the following set of expressions that are ready to be used in state-space notation

$$J_{tot}\ddot{\theta} = -(f_r + cp^2)\dot{\theta} - kp\theta + cp\dot{x}_2 + kpx_2 + k_Ti,$$

$$M\ddot{x}_2 = cp\dot{\theta} - 2c\dot{x}_2 + k\theta - 2kx_2 + F_{\text{m}}, \tag{4.7.11}$$

$$L\frac{\mathrm{d}i}{\mathrm{d}t} = -Ri - k_{\text{bemf}}\dot{\theta} + \frac{K_p}{T_I}V_{PI} + K_pV_r,$$

$$\dot{V}_{PI} = V_r.$$

The MATLAB$^{\circledR}$ Toolboxes$^{\text{TM}}$ [100, 101] provide the designer with a tool for this with the commands `append` and `connect` that do the algebraic substitutions and rearrangements described above automatically.

4.8 Machining Force Modelling for System Verification

The system performance can be analysed in the frequency and in the time domain. Some of the system characteristics can exclusively be studied with transient analyses.

For example, analysis of the step response is a standard tool to establish the following quantities: overshoot, rise time, settling time. For this reason, a realistic machine force needs to be established to verify the design of the controller. In this section the following machining force models are considered: a step force and a simplified grinding force profile.

4.8.1 Step Force

In control engineering step responses are extensively studied. It is important to know how a system responds to a sudden input as large, sudden and fast changes can occur on one of the system inputs. If the system is at rest (steady-state) this can have extreme effects on the system and in case the system is part of larger system it can affect the overall system. The step response of an active fixturing system can be studied as a step placed on the actuators and as a step-shaped machining force. Applying a step input as the machining force forms an input that is composed theoretically by all frequencies. Therefore all eigenfrequencies present in the system will be excited which makes the step a good and "cheap" alternative representation for a real machining process like cutting, milling or grinding. Most importantly, an analysis for the step response of an active fixturing system gives information on the system stability and indicates of the safety factor needed in the applied clamping forces for dynamically stable workholding.

4.8.2 Grinding Force Modelling

The aim of this section is to establish a simplified empirical grinding profile based on experimental results. For the last fifty years, the grinding process has been the subject of extensive research [99]. However, the grinding process depends on many parameters, and as some of those are not fully investigated and understood, the grinding process should be considered to a certain extend as a black box process. Interested readers can find more information in the recent monographs on the grinding process that discuss current research, for a deeper understanding of the trends and the development of the manufacturing process [99].

4.8.2.1 On a Model for Cutting Forces

The modes of part-fixture system get excited by the contact and cutting forces that transmit self-generated and forced vibrations. The cutting forces themselves depend on many parameters [19, 68, 99]. One factor of specific interest here is: the shape of the wheel, as it is one of the most substantial factors contributing to the build-up of grinding forces. The unroundness of the wheel and the grit on the wheel affect the machining forces. From the literature, e.g. [9, 27], it is clear that specific geometric features such as cracks leave their signature in the force profile. The geometry of the grains on the grinding wheel and the shape of the wheel itself due to wear are unknown a priori, unless measured, and will change over time due to wear. This places severe limitations on the accuracy of the predictions of cutting forces established by FE models that take the individual grain on the grinding wheel into account, such as [8, 86]. More exact results are provided by empirical models, but these results due to their empirical nature are less generic [19]. The latter models are built to reduce the complexity of the grinding process model. To establish these traditional empirical models, empirical relations are sought for a reduced number of variables from the whole set of variables that govern the grinding process [19].

In this section an empirical model is established for the description of a grinding force profile. The empirical model established is not based on a mathematical description of the relations between certain dominant and tunable variables in the grinding process. For the purpose of active fixture design verification by means of a transient simulation, it is sufficient here to generate a generic force profile. This profile should provide a mathematical description of the typical characteristic transient grinding forces, based on a wide range of empirical results. Some experimental results are shown in the following figures. In Figure 4.20 one can see transient tangential grinding forces from an experiment and a corresponding simulation of a face grinding process. Figure 4.21 shows the transient normal force profile for a cylindrical grinding profile. Although both processes and directions are different, a similarity in the force profile can easily be observed: there is a force peak related to the wheel revolution and some "noise" in between those peaks; a similar observation can be made from [58, Fig. 4]. Furthermore, from the literature,

e.g. [86, 99], it can be established that the relation between tangential and normal forces is almost linear. This gives another argument for the validity of a comparison of the force profile plots.

Figure 4.22 shows the frequency spectrum of the force plot shown in the time domain in Figure 4.21. It can be observed that the rotational speed of the wheel together with its multiples form a major component in the frequency spectrum.

In [27, Fig. 7] the normal force is shown as fixed pattern around the wheel. In [68, Fig. 4.1] the Talyrond roundness plot[7] of a grinding wheel is shown. It can be that the wheel is not perfectly round, but has multiple equally distributed lobes, that give the wheel the profile of a pointed star. Also Thompson, [157] observes a relation between wheel lobes and frequency components in his results. Multiples of the rotational speed are also mentioned as sources of chatter in Ref. [99]. It can henceforth be concluded that the macro-geometry of the wheel in terms of wheel lobes and eccentricity largely determines the force profile, and spindle speed orders due to the unroundness of the wheel are likely to be present in the force signal.

A clear trend can be observed in the grinding force profiles, namely there is a strong relation with the (multiples) of the spindle speed. Acknowledging this trend, the next step is to construct a force signal that has sinusoidal components with a base frequency - the angular velocity of the grinding wheel - and multiple higher harmonics of this frequency. This is done on basis of the experimental results presented in [27]. In Table 4.2 the amplitude of the (six multiples of the) spindle speed shown, in Figure 4.22, are given in mN and in a scaled amplitude.

It should be noted that in Ref. [27] no information is given for the phase of the frequency components, hence no information on the individual amplitudes of sine or cosine components of the signal can be established. However for a machine force profile $F_\mathrm{m}(t)$, only consisting of cosine components, the following expression can be established

$$F_\mathrm{m}(t) = c_1 \left(c_2 + c_3 \left[\cos \omega t + 0.4464 \cos \omega 2t + 1.1875 \cos \omega 3t + 0.6786 \cos \omega 4t + \ldots \right. \right.$$

$$\left. \left. \ldots 0.8036 \cos \omega 5t + 0.1786 \cos \omega 6t \right] \right), \tag{4.8.1}$$

---

[7]A Talyrond roundness measurement is standardised roundness measurement of an object is named after the trade name of a sphericity-measuring device from Taylor Hobson.

where c_1, c_2 and c_3 are coefficients that can be used to tune the magnitude of the machining force, such that it matches the experimental grinding force measurements, ω is the angular velocity of the grinding wheel, in the case of example shown in Figure 4.20

$$\omega = \frac{v_\mathrm{w}}{\pi d} 2\pi.$$

Here, v_w is the wheel speed, d the wheel diameter and ω is the rotational velocity of the wheel in rad/s. For the coefficients $c_1 = 100$, $c_2 = 2.8526$ and $c_3 = 0.5$, the signal is graphically shown in Figure 4.23(a). In this specific case the approximated force profile shows good resemblance with the experimental force profile shown in Figure 4.20, as can be seen in Figure 4.23(b), regarding its proportions in the constant component of the force and the oscillations.

Some closing remarks need to be made regarding the universality of the grinding force profile generated above. This considers the ratio of the amplitude of the oscillatory component in the signal set against the constant component in the force profile, governed by constants c_2 and c_3 in (4.8.1). When constant c_1 in (4.8.1) is used to scale down the signal, as shown in Figure 4.23(a) to the amplitude shown in Figure 4.21, the ratio used for Figure 4.23(a) is slightly larger than the ratio as shown in Figure 4.21, but still not too far off, despite the difference in process parameters. The oscillations in Figures [58, Fig. 4] and 4.23(a) show good resemblance as well. Furthermore, from other results presented in the literature, it can be observed that within the same grinding process the "noise" to the average value of the machining force remains at a fixed value [27, 99].

It can be concluded that a generic model for the force profile of a grinding process has been established. The empirical model presented here does not predict the magnitude of the forces in the way traditional empirical models do [19]. Instead, the model developed above is based on the dominating trend that is observed in machine force measurements for grinding wheels with wheel lobes in the macro-geometry.

4.9 Conclusions

It can be concluded that the analysis of the several subsystems in an actively controlled part-fixturing system yielded models that can be further refined and can be integrated into one overall model representing the part-fixture system. Further verification is done in

Chapter 5, where simple part-fixture systems are studied. The analysis of the subsystems of an active fixturing system can be summarised as follows:

- Small, yet accurate dynamic models of compliant workpieces are established by modelling the flexible part with the finite element method and subsequently reducing the size of the model with the Craig-Bampton model reduction technique [28, 29]. In addition, Saint-Venant's principle is used to obtain a condensed selection of the DOFs describing the machining region.

- In this work, the part-fixture contacts are assumed frictionless. In addition, it was shown that the contact stiffness can reasonably be modelled as a linear stiffness. In order to provide enough dynamic stiffness, good design practice requires the natural frequencies of the fixture elements to be well above those of the part. This means that the fixture elements can be modelled with spring-dashpot elements that have an equivalent stiffness and damping. Furthermore, springs-dashpot elements are used to connect the active clamp with the workpiece.

- Comparison of part-fixture modelling, as done in the thesis, with part-fixture models presented in the literature, leads to the conclusion that the models, established with the methodology presented here are in good agreement with results found in the literature.

- Dynamic models for hydraulic and electromechanical actuated clamps that are integrated with the overall part-fixture system can be established on basis of relevant models presented in the literature.

- A part-fixture system is a MIMO system by nature. For this reason, the design of the controller in the thesis is focussed on collocated servo-control, which is an appropriate control strategy for flexible MIMO systems, since interference between the clamping forces on a single sensing point is avoided [102].

- For dynamic simulation, the separate subsystems are integrated into one overall dynamic system in a state-space formulation.

- A generic and easy tunable force profile of a grinding process has been empirically established. The model does not predict the magnitude of the forces, but it shows a trend for grinding wheels with wheel lobes in the macro-geometry.

4.10   Tables

Table 4.1: Coordinates of fixture elements.

Fixture element	Tao *et al.* [155]	FE model
Clamp	(35, 32.5)	(35, 31.58)
Locator 1	(15, 100)	(15, 100)
Locator 2	(135.36, 85.36)	(130.36, 85.36)
Locator 3	(135.36, 14.64)	(135.36, 14.64)

Table 4.2: Read and worked out spindle speed orders with a ruler from the x-axis in Figure 4.22.

Multiple of Spindle Speed	Normal Force [mN]	Relative Amplitude
1	89.6	1.0000
2	40.0	0.4464
3	106.4	1.1875
4	60.8	0.6786
5	72.0	0.8036
6	16.0	0.1786

4.11   Figures
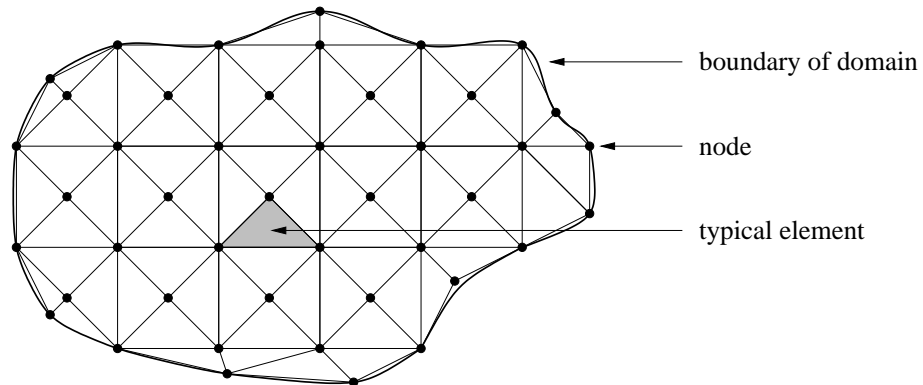
Figure 4.1: Finite element mesh for an arbitrary 2D domain, highlighting the domain boundary, a typical node and element.
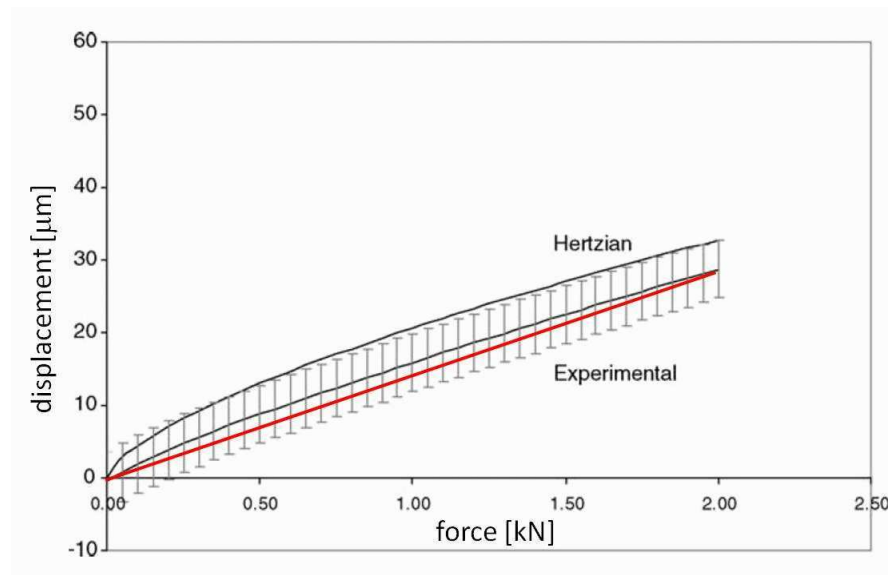
Figure 4.2: Experimental force-displacement relationship clamping elements compared with Hertzian contact theory, from [137, Fig. 11] labels on axes and red line added.
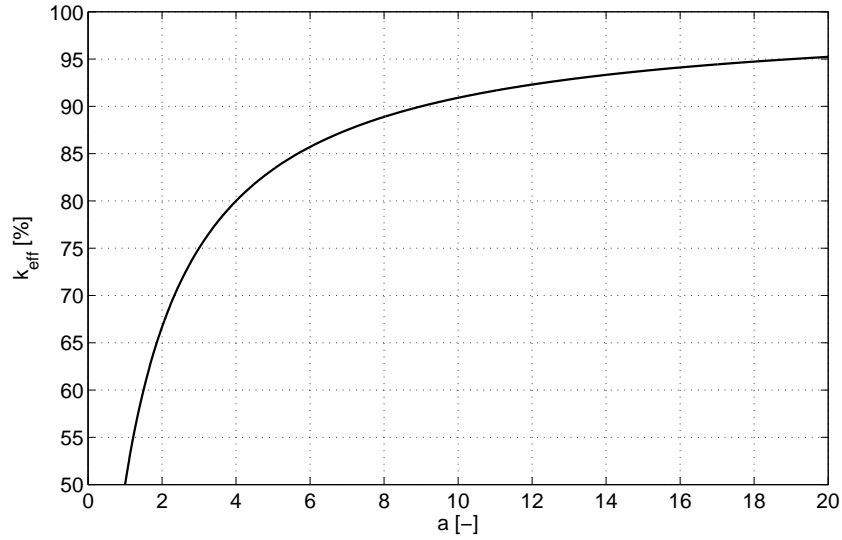
Figure 4.3: Effective fixture stiffness k_{eff} as a percentage of the contact stiffness k_{cont} for realistic range of coefficient a, where the coefficient is used to relate the equivalent stiffness of the contact to that of the fixture element as used in (4.3.1) and (4.3.2).

(a) Workpiece with tool path, machining forces and centre of gravity. Source Ref. [108], Fig. 2.

(b) Workpiece with tool path and fixturing points. Source: Ref. [108], Fig 4.
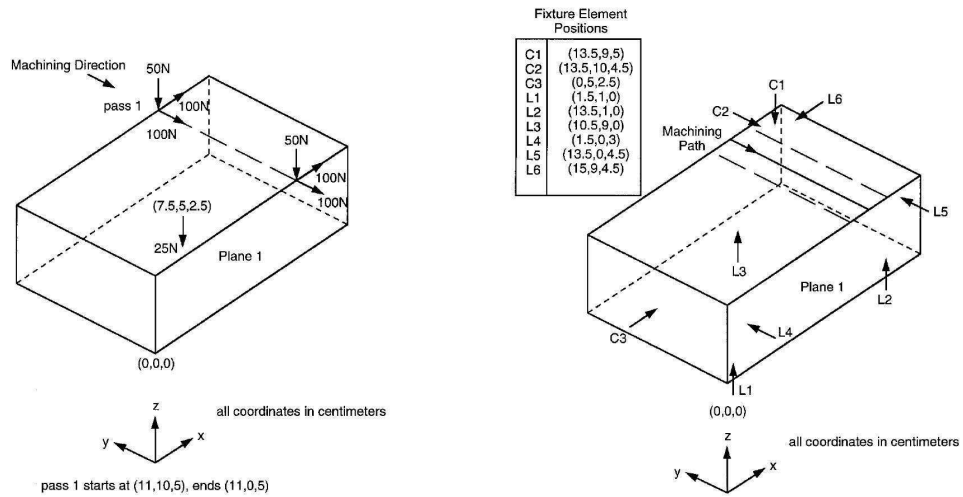
Figure 4.4: Case study 1, taken from Ref. [108].
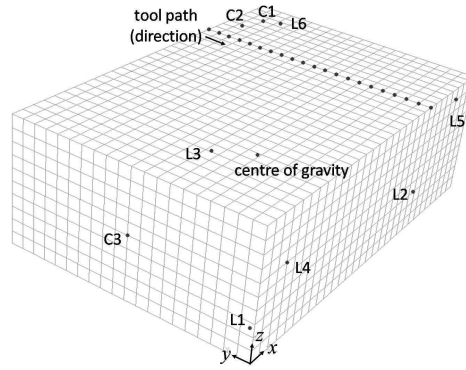
Figure 4.5: Finite element model built to model case study 1 in Ref. [108], showing the mesh, fixturing points, centre of gravity and tool path, c.f. Figure 4.4.
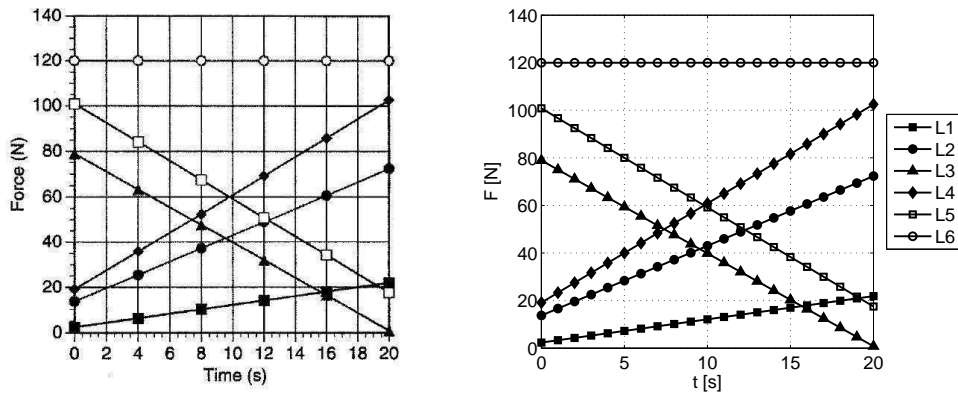
(a) Reaction forces at the locators L1-L6 as shown in Ref. [108], Fig. 5 (legend same as (b)).

(b) Reaction forces at the locators L1-L6 calculated with the developed methodology.

Figure 4.6: Case study 1, taken from Ref. [108].
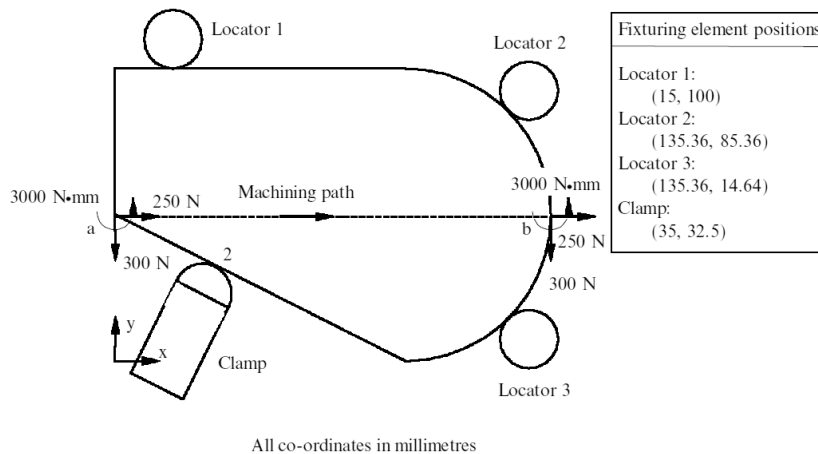
Figure 4.7: Part-fixture system for the 2D case study in Tao *et al.* [155, Fig. 8(b)].
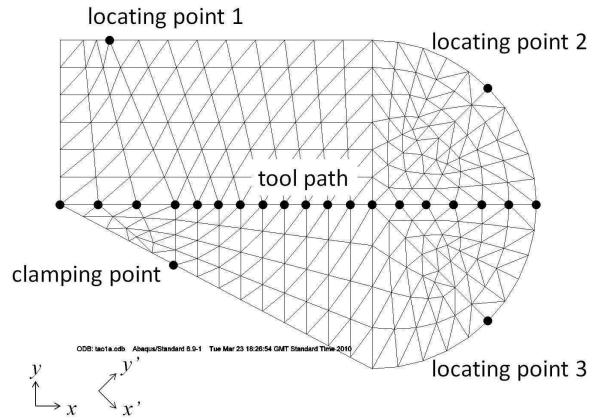
Figure 4.8: Mesh of workpiece for the 2D case study in Ref. [155].
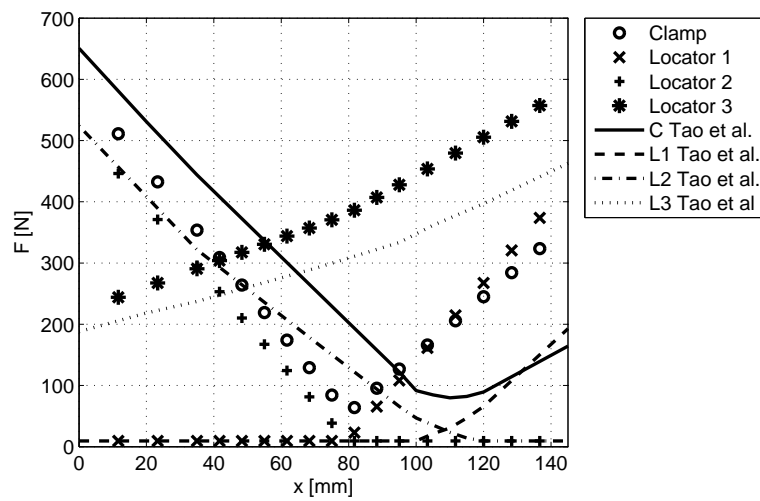
Figure 4.9: Clamping and reaction forces for case study presented by Tao *et al.* [155] and the reduced compliant model established in this study.
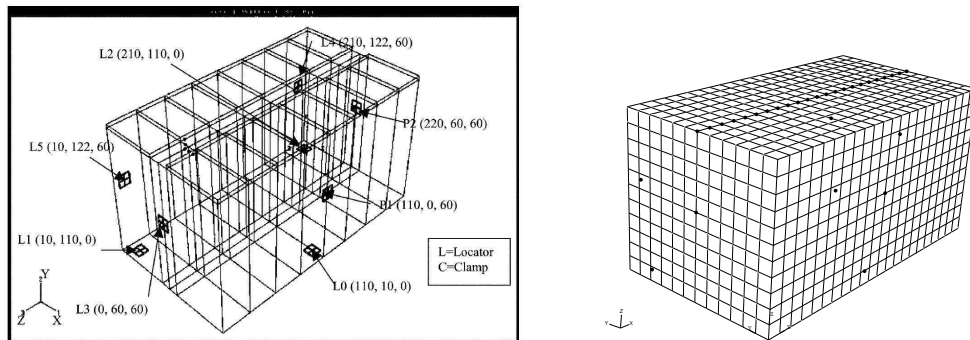
(a) FE-model presented in [153], Fig. 6.

(b) Established FE-model based on the case study presented in [153].

Figure 4.10: FE models for subcase study I in [153].
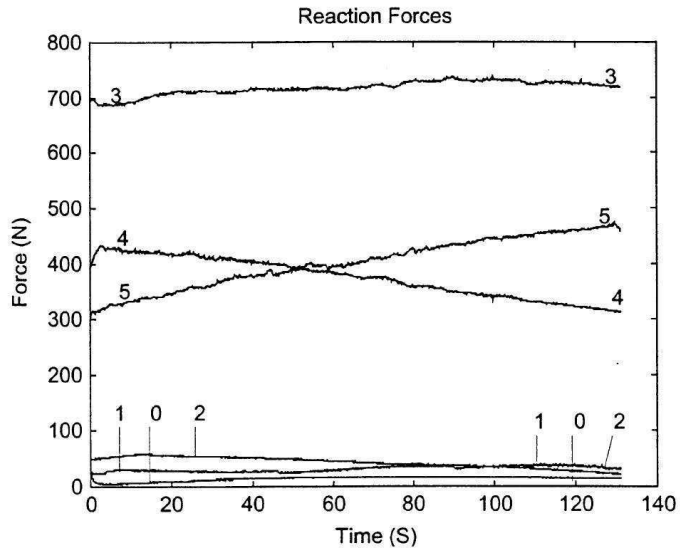
Fig. 7.   Reaction force versus time obtained in Tao's experiment.
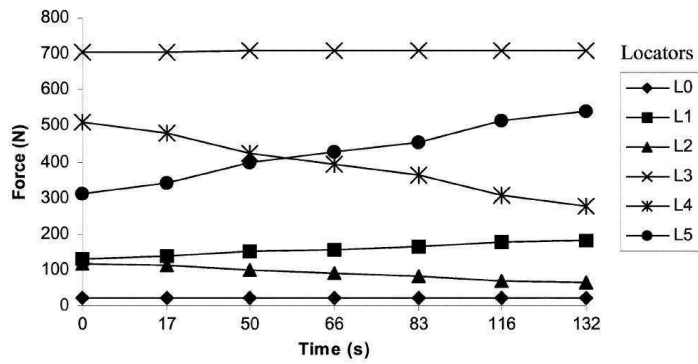
Fig. 8.   Finite-element results for Tao's model (without fixture-element stiffness).
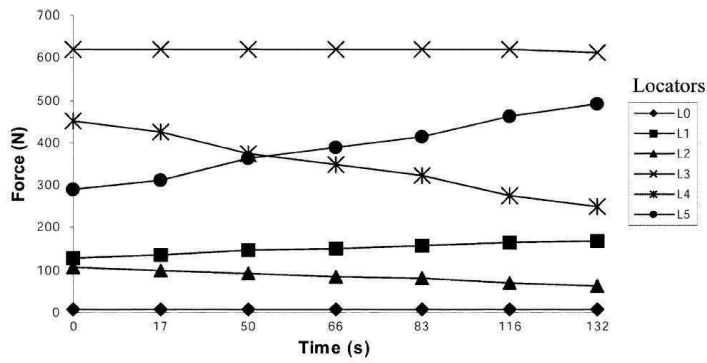
Fig. 9.   FEM results from developed model (with fixture-element stiffness).

Figure 4.11: Results presented in Ref. [153, Figs 7-9].
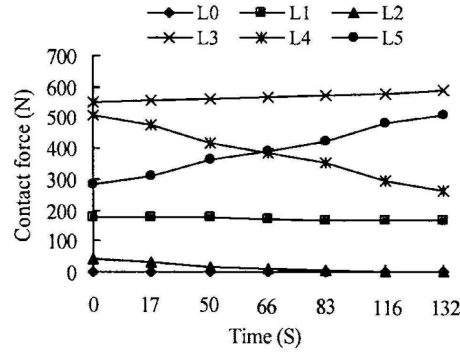
Figure 4.12: Reactions from the model presented in Ref. [131, Fig.12].
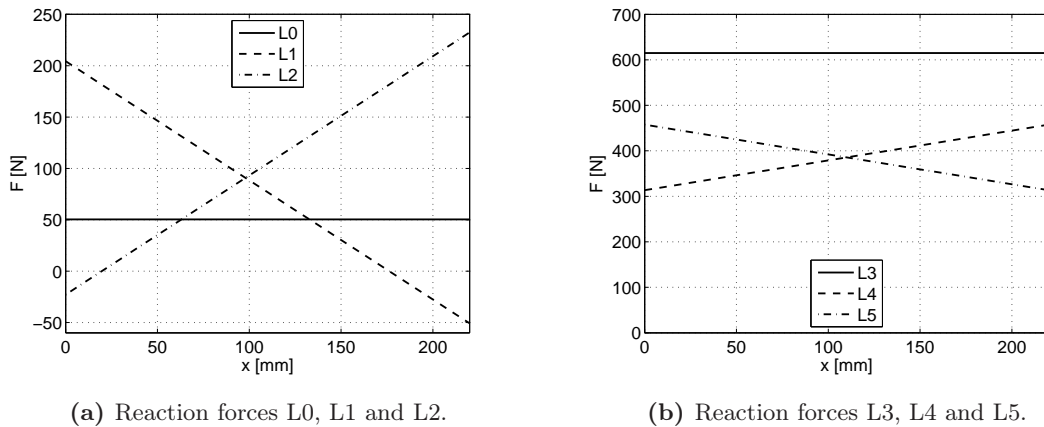
(a) Reaction forces L0, L1 and L2.

(b) Reaction forces L3, L4 and L5.

Figure 4.13: Reaction forces in the locators for F_x=55 N, F_y=131 N, F_z=-232 N, no gravity force applied, and clamping force P1 = 640 N and P2 = -670 N.
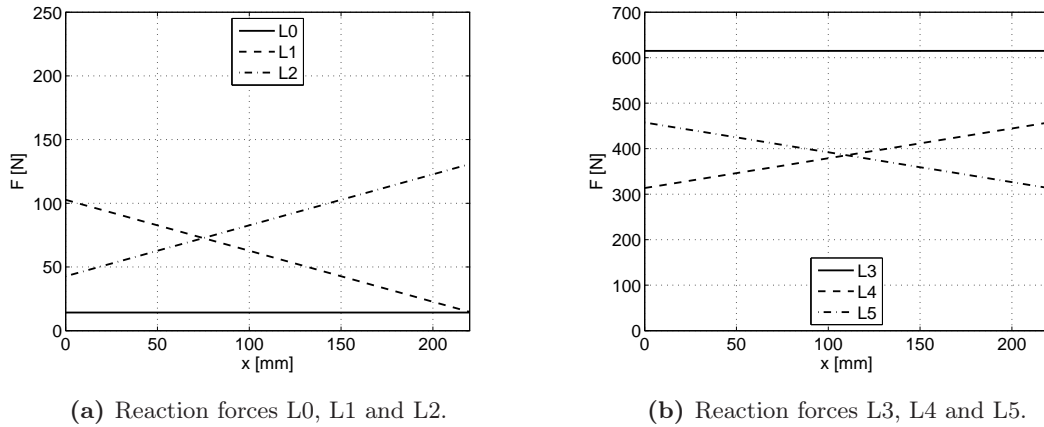
(a) Reaction forces L0, L1 and L2.

(b) Reaction forces L3, L4 and L5.

Figure 4.14: Reaction forces in the locators for F_x=55 N, F_y=131 N, F_z=-232 N, gravity body force applied, at L0, L1 and L2 of -39.811 N, -19.9055 N -19.9055 N, respectively, and clamping force P1 = 640 N and P2 = -670 N.

(a) Reaction forces L0, L1 and L2.

(b) Reaction forces L3, L4 and L5.
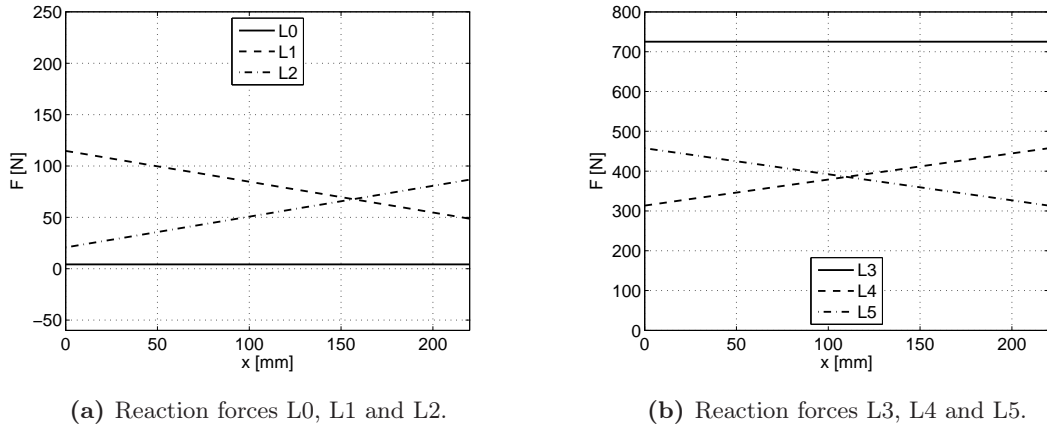
Figure 4.15: Reaction forces in the locators for F_x=-55 N, F_y=131 N, F_z=-60 N, top clamping force applied in the form of equivalent forces at L0, L1 and L2 of -60 N, -40 N, -40 N respectively (these equivalent forces approximate the gravity body force + an additional 20 N clamping forces per locator) and clamping force P1 = 640 N and P2 = -670 N.
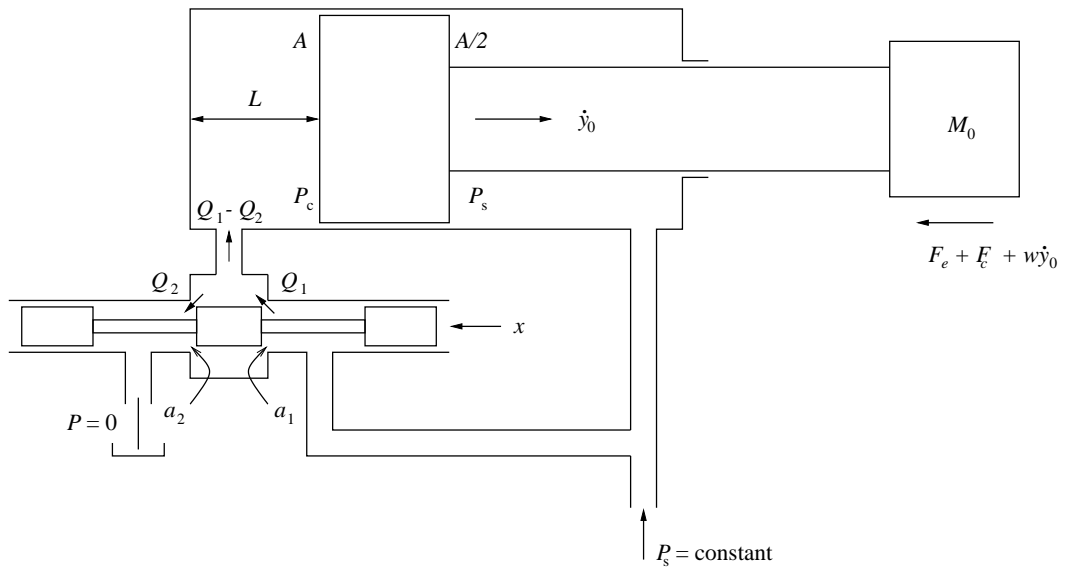
Figure 4.16: Three-way-valve-controlled asymmetric hydraulic actuator system; Figure assembled from Ref. [163, Figs 1.1 and 2.4].
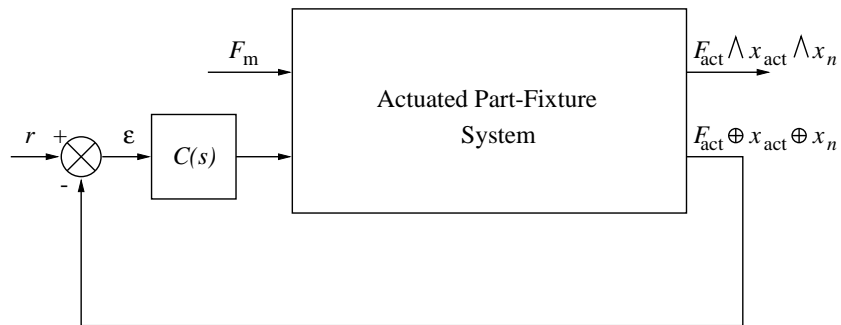
Figure 4.17: Block diagram of control system; $\wedge$ = "and", $\oplus$ = "or".
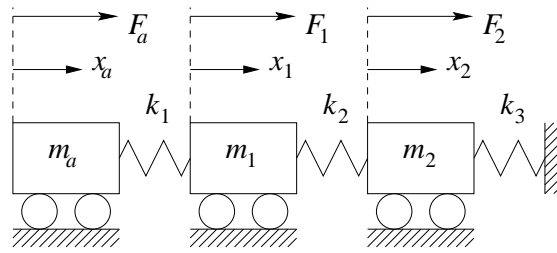
Figure 4.18: A simple 3 mass-spring system.
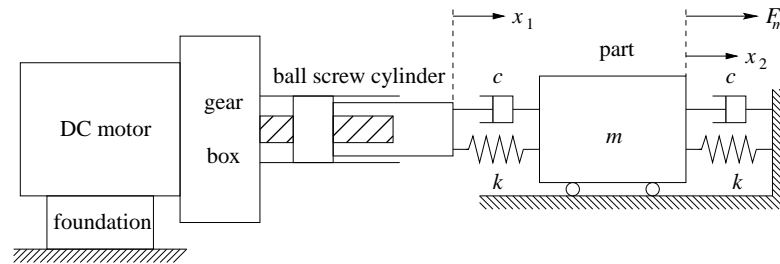
Figure 4.19: Simple model of active fixture with electromechanical actuator.
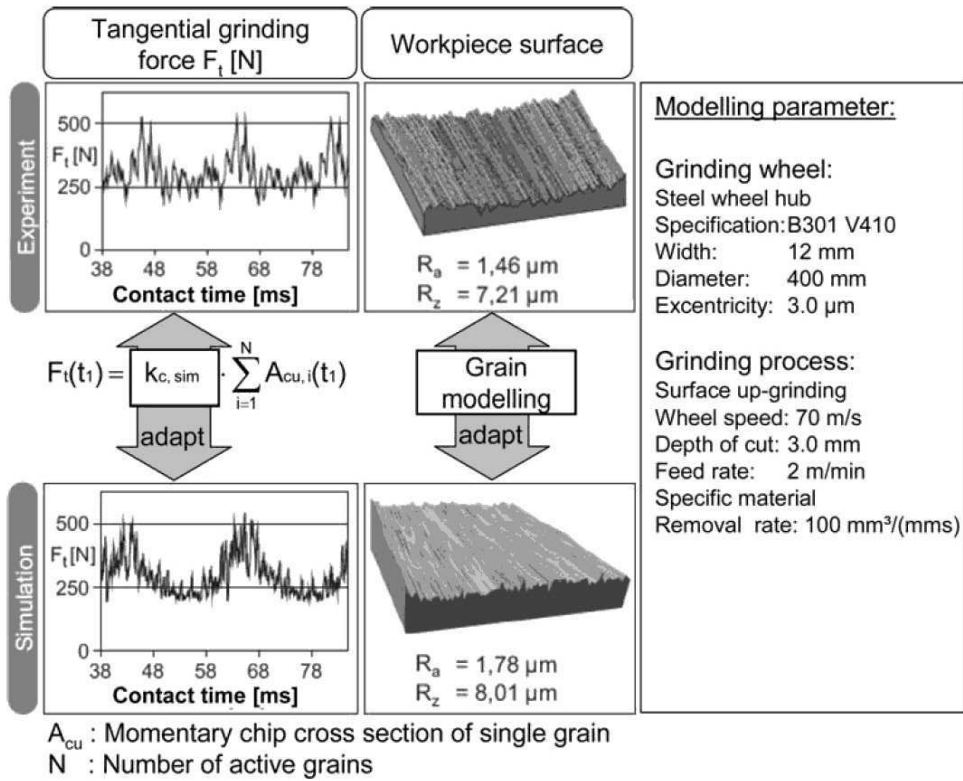
Figure 4.20: Transient tangential grinding forces face grinding; source: [8, Fig. 3].
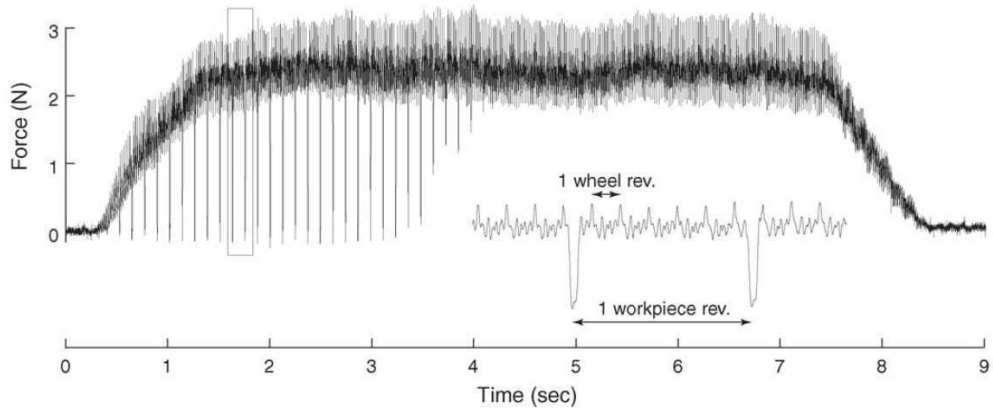
Figure 4.21: Transient normal grinding forces cylindrical grinding; source: [27, Fig. 8].
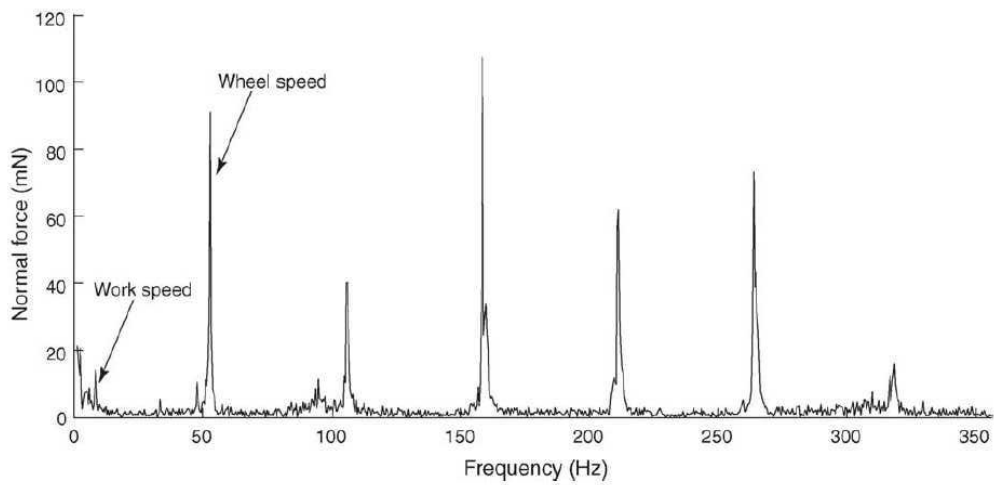
Figure 4.22: Frequency spectrum of grinding forces cylindrical grinding; source: [27, Fig. 6].
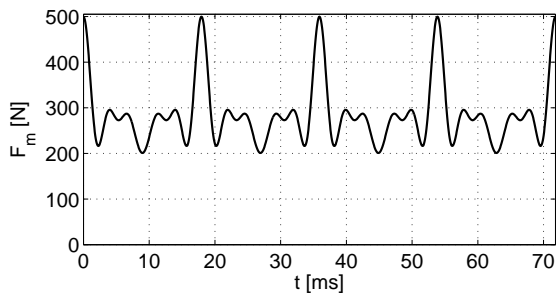
(a) Reconstructed machine force profile F_m, $\omega = 350$ rad/s.
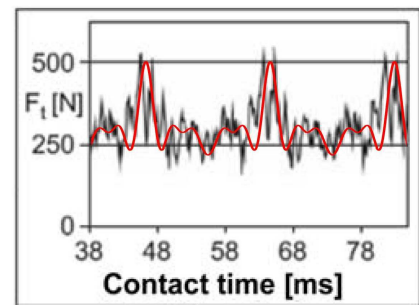
(b) Match of reconstructed machining force profile with experimental measurements as presented in [8].

Figure 4.23: Empirically established machining force profile.

Analysis of Simple Fixture Systems

5.1 Introduction

After the motivation for this work given in Chapter 1, in Chapter 2 a survey into fixturing technology and the modelling of active fixtures was made. On basis of that survey, knowledge gaps were identified. In Chapter 3, the applied research approach to address these gaps has been outlined. Tools for the modelling of fixture elements, actuators, the workpiece, the design of a controller and the state-space realisation of the total model have been established in Chapter 4. As a successive step in the research work carried out for the thesis, two practical examples of simple active fixtures are studied in this chapter.

Both examples are study models made to assess the performance of active fixturing capabilities of actuation concepts for an intelligent fixturing system (IFS) technology demonstrator. An IFS is characterised by automatic reconfiguration and active fixturing capabilities. During early stages of the design, hydraulic actuation was investigated. In this chapter, the model of a simple active fixturing concept is investigated: one actuated clamp and one locator are applied to fixture a 2D workpiece. Secondly, the performance of a more mature design of the demonstrator, comprising an electromechanically actuated clamp and a thin walled part is investigated.

The control design for both systems is established on basis of the methodology proposed in Chapter 3 (and worked out in Chapter 4). Firstly, a finite element (FE) model of the part is build. The machining areas, clamping and locating points are

identified - support points are absent in the studies presented here. The nodes in the mesh discretization that are at the locations of these points, are retained in the subsequent model reduction. The model reduction technique applied in this thesis, is the Craig-Bampton method [28, 29]. The number of dynamic modes, the so-called 'fixed interface modes' (FIMs), added to the model reduction determines the accuracy of the dynamic behaviour. The dynamic accuracy regarding the first low frequency modes of the model reduction has been assessed and the minimal number of FIMs has been added to the reduced model.

The part-fixture contacts are assumed frictionless and are modelled by linear spring-dashpot elements. In these study models, the stiffness of the fixture elements is considered to be much higher than than the equivalent spring stiffness of the contact areas. Furthermore, it is assumed that the natural frequencies of the passive fixture elements are higher than those of the part. This means that the dynamic behaviour of the fixture is governed by the contacts.

Models of the actuators that provide the active clamping forces have been established previously in Section 4.5, and are used here. In addition, compensators have been designed for several closed-loop controllers on basis of the models and methodology presented in Section 4.6. And finally, small, yet accurate enough overall models of the active fixturing systems are established.

The structure of this chapter is as follows. A more detailed description of the active fixturing system is provided in Sections 5.2 and 5.5 for the hydraulically actuated (HA) and electromechanically actuated (EMA) systems respectively. A numerical model containing all the relevant equations of the actuator models and compensators is given in Sections 5.3(HA) and 5.6(EMA). A set of simulation results of each of the systems is then given in Sections 5.4(HA) and 5.7(EMA). The overall conclusions for the chapter can be found in Section 5.8.

5.2 Description of Hydraulically Actuated Fixture System

Concepts for intelligent fixturing systems have been studied extensively within the research framework of the AFFIX project. One of these concepts is the technology demon-

strator described in [120, 143], and shown in Figure 2.5(b). One of the actuation methods for the active fixture elements that has been considered initially is hydraulic actuation. For this reason, a study model of an hydraulically actuated clamp, that fixtures a geometrically simple flexible structure has been established. For this reason, the actuator is larger than the small clamps such as available by Enerpac or Roemheld (see Section 2.6.4.2, and Refs [35, 45, 140]). This study model and parts of the research described in Sections 5.2, 5.3 and 5.4 are published in Ref. [10, 11]. The part considered here, is the prismatic part used for experimental work in [122], a $25.4 \times 35 \times 70$ mm aluminium cuboid. The fixturing system is shown in Figure 5.1.

In this study model, the mechanical behaviour of the workpiece is described by a 2D FE-model. The locating point, at the righthand side of Figure 5.1, is constrained by a locator. This locating element, modelled by a spring-dashpot element, has an equivalent stiffness k and a damping coefficient c to model the behaviour at the contact interface. At the left hand side of the part, there is a clamping point. Both at the clamping and the locating point, the displacement perpendicular to the actuator displacement are constrained, as shown by the "roller support" condition in Figure 5.1. For this reason, the clamping point is denoted by y_1 There is one machining point, where a machining force F_m acts in the horizontal plane, that is the y-direction. The clamping force is generated by a hydraulic cylinder. The hydraulic actuator has an actuator displacement y_0. The actuator *velocity* is controlled by the amount of hydraulic oil that flows into the cylinder through the hydraulic servo-valve. The flow oil through the valve is controlled by the valve *displacement* x, which is steered by an electric actuator. For this reason, the transfer function between actuator and valve displacement can approximately be described as an integrator

$$\frac{y_0}{x} = \frac{K_m}{s},$$

where K_m is the velocity gain of the actuator and s is the Laplace variable. However, in real life hydraulic oil is not perfectly incompressible. The model for hydraulic actuators developed in Chapter 4 takes this compressibility into account and is used here to model the behaviour of the hydraulic actuator.

5.3 Numerical model

5.3.1 Finite Element Model Part

A 2D finite element (FE) model with lumped mass elements [182, pp. 473-474] of the part has been made. In order to establish this model, plain strain [182, Chapter 4] has been assumed. The mesh consists of 24 linear triangular elements, shown in Figure 5.2. As discussed in Chapters 3 and 4, the Craig-Bampton model reduction technique [28, 29] has been applied to condense the workpiece model to a small, yet accurate enough model. The nodes at the machining point, the clamping and locating point are kept (see Figures 5.1 and 5.2) and on basis of the methodology set out in Section 4.2.2, six fixed interface modes are retained in the model. This allowed for a good approximation of the lowest free vibration modes - using the concept that the dynamics of a system is determined by the lowest frequency modes [29], as the first four non-zero (i.e. elastic) eigenfrequencies of the unsupported part have respectively percentile errors of 1.2 %, 2.2 %, 1.2 % and 8.8 % compared to the FE model.

5.3.2 Fixture Model

After Refs [122, 137], the spring-dashpot elements used to model the part-fixture contacts, as shown in Figure 5.1, have a spring stiffness $k = 3 \times 10^7$ N/m and a damping constant $c = 960.12$ Ns/m. The connection force F_e in the contact between clamp and actuator, is a function of the relative displacements and velocities, and the values of the contact spring stiffness and damping given by Equation (4.5.10)

$$F_\mathrm{e} = c(\dot{y}_0 - \dot{y}_1) + k(y_0 - y_1).$$

5.3.3 Clamp Model

5.3.3.1 Hydraulic Cylinder

The ordinary differential equation that models the behaviour of the hydraulic actuator and the servo valve developed in Chapter 4 is given by Equation (4.5.8) to be

$$\dddot{y}_0 = K_\mathrm{m}\omega_0^2 x - \frac{\dot{F}_e}{M_0} - 2\beta\omega_0\ddot{y}_0 - \omega_0^2\dot{y}_0,$$

where y_0 is the actuator displacement, F_e the external force acting on the cylinder, as displayed above (and by (4.5.10)), M_0 the mass of the cylinder, velocity gain K_m, hydraulic stiffness c_h, and the stiffness of the oil column c_o are as defined in (4.5.6)

$$K_m = \frac{b}{A} C_d \sqrt{\frac{P_s}{\rho}}; \quad c_h = \frac{AP_s}{|x|}; \quad c_o = \frac{EA}{L}.$$

Based on these coefficients, the damping coefficient β and the eigenfrequency of the actuator ω_0 are defined in (4.5.9) as

$$\beta = \frac{w}{2\sqrt{M_0 c_0}}; \quad \omega_0^2 = \frac{c_o}{M_0}.$$

The properties of the hydraulic oil are given in Table 5.1. The damping factor of the oil w is assumed to yield a relative damping coefficient of $\beta = 0.4$, see Equation (4.5.9).

5.3.3.1.1 Dimensions of the Hydraulic Cylinder

The dimensions of the hydraulic actuator are calculated on basis of the required clamping force. If one considers that a force of 2000 N needs to be delivered, then with a safety factor of 2, the cylinder must to be capable of delivering 4000 N. The maximum effective pressure is half of the supply pressure. The piston surface area needed is then: $A = 4000/100 \times 10^5 = 4 \times 10^{-4} \text{m}^2$. This comes down to a plunger radius of 11.2 mm.

To provide some (limited) reconfigurability capabilities, the maximum stroke of the cylinder is 10 cm. Assuming the cylinder operates around the equilibrium position where the piston displacement is half of the maximum stroke. Length L will then be of the order of 5 cm.

For an actuator that is ten times as stiff as the fixture stiffness: $10kL/E = A = 0.015 \text{ m}^2$, hence a radius of 69 mm. The cylinder that has to reduce the piston surface area by a factor two, hence has a diameter of 48 mm.

The piston is made of steel. With a density of 7900 kg/m^3, and for the piston a plunger length of 1.5 cm and a rod length of 20 cm, the mass of the cylinder will be 13.5885 kg. The valve coefficient b is chosen to be equal to 1. The eigenfrequency of the actuator is then according to Equation (4.5.9):

$$\omega_0 = \sqrt{\frac{EA}{LM_0}} = 4691.9 \text{ rad/s} (= 746.75 \text{ Hz}). \tag{5.3.1}$$

Note that this eigenfrequency is of the same order of magnitude as that of the hydraulic valve which is modelled in Section 4.5.1.3. Furthermore, the models of the hydraulic actuator, servo valve, part, locator and clamp stiffness and the controller are connected as described in Section 4.7.

5.3.3.2 Hydraulic Servo-Valve

The transfer function $V(s)$ of a valve controlled by an electric actuator is given by Equation (4.5.13):

$$V(s) = \frac{x}{r} = \frac{1}{\left(\dfrac{s}{K_\mathrm{v}} + 1\right)\left(\dfrac{s^2}{\omega_\mathrm{v}^2} + \dfrac{2\beta_\mathrm{v}}{\omega_\mathrm{v}}s + 1\right)},$$

where ω_v and β_v are the eigenfrequency and relative damping of the valve, the actuator gain K_v is expressed as

$$K_\mathrm{v} = \frac{1}{\tau_\mathrm{v}}.$$

The bandwidth ω_v of the hydraulic servo-valve of 3770 rad/s (600 Hz) in Table 5.1, is a value that has been found in Ref. [163], it is (perhaps optimistically) assumed that this valve can handle sufficient flow rate for the oil. Likewise, it is assumed that the constant pressure pump can supply sufficient oil.

5.3.4 Controller Design

Closed-loop servo-controllers have been designed. Compensators have been designed in the form of a proportional controller and lead and lag filters, which have a transfer function of

$$C(s) = K_p \frac{s + \omega_\mathrm{LF}}{\alpha_\mathrm{LF}s + \omega_\mathrm{LF}},$$

where the proportional gain K_p, the settings for the corner frequencies $\omega_\mathrm{LF}/\alpha_\mathrm{LF}$, and ω_LF need to be tuned appropriately. These settings determine respectively the corner frequency for the maximum controller response and the minimum response from the compensator. Furthermore, when $\alpha_\mathrm{LF} > 1$, the compensator is a LaF; and when $\alpha_\mathrm{LF} < 1$ the compensator is called a LeF. The controller has been tuned appropriately and some of the characteristics of this active part-fixture system are discussed in Section 5.4. In Section 5.4, the following closed-loop control strategies are investigated: force feedback

(FFB) in combination with with a proportional controller (P-control) and a LeF; actuator displacement feedback (ADFB) and part displacement feedback (PDFB) with P-control and a LaF compensator.

5.4 Simulation of the Hydraulically Actuated Fixture

5.4.1 Frequency Response Plots

A frequency response plot shows the amplitude of the response of a system output to a harmonic excitation with a fixed frequency of an input to the system. This response is measured or computed for a whole range of input frequencies, that allow the construction of a frequency response diagram for this range [48, 50, 102]. The frequency response can have a delay that can be expressed as a certain number of degrees in phase change: input $\sin(\omega t)$, output: $\sin(\omega t + \varphi)$, where φ is the phase change. This phase change can be better interpreted when depicted in a Nyquist plot. This is done in Section 5.4.2. The frequency response diagrams can be seen in Figure 5.3. For the plots in Figure 5.3(a) and (c) the response follows the desired input value r until the eigenfrequency of the valve is reached and then declines rapidly. In Figure 5.3(b) and (d) it can be seen that the position feedback control systems work: for the actuator displacement feedback in Figure 5.3(b) the response is for most of the frequency range is quite small and only large around the clustered eigenfrequencies. A similar fact holds for the part displacement feedback in Figure 5.3(d) where response in most of the frequency range is quite small. Using force feedback this behaviour cannot be observed, part and actuator will always have a response to excitation by machine force F_{m} for the frequency range below the cluster of first eigenfrequencies. After tuning it was found that for control using LaF, it was possible to create sufficiently damped systems that fall in the ± 3 dB bandwidth, at the expense of reducing the bandwidth. The stability of force feedback can be observed, adding a LeF as controller creates a small increase in bandwidth. Due to its nature FFB is inherently stable for this system, this is of great practical advantage. The overshoot for the position feedback systems using P-control only is introduced by adding the servo-valve to the system. It is therefore essential to add the dynamical behaviour of the valve to the model [103, 163].

5.4.2 Nyquist Diagrams

As remarked in Section 5.4.1, the frequency response of a system consists of the amplitude of system's response and the phase change. The Nyquist diagram combines this frequency response with the phase change. The amplitude of the response is the distance from the origin and the phase is expressed by the angle in polar coordinates. The frequency information itself goes lost, but one can obtain valuable information concerning the stability. The point (-1,0) in the Nyquist diagram is usually linked with instability. The control engineer can design a controller such that the response always has a certain distance from this point. According to standard (-1,0) rules for control design, the system response in a Nyquist diagram should never encircle the (-1,0) point [48]! The most certain information concerning instability comes from studying the eigenvalues of the system: the real part of the eigenvalue should be equal or smaller than zero for the system to be (marginally) stable. Refer for further information e.g. to [48, 50, 102]. The Nyquist diagrams can be seen in Figure 5.4. Most of the responses start with a unity response and zero phase change in the vicinity of (1,0) and spiral their ways to a small response at (0,0), except for actuator displacement (position) feedback in combination with proportional control in Figure 5.4(a) and (c). In this case a suitable gain margin ($\sim$ 2) and phase margin ($\sim$ 45°) have been found. It has to be mentioned that all the poles are strictly in the left half of the complex plane. All the real parts of the system eigenvalues are smaller than 0: $\lambda_\Re < 0$.. Hence, even though in Figure 5.4 one can see that the curves for the systems using part displacement for feedback start from the (-1,0) point, it does not mean that the system is instable.

5.4.3 Machining

Two steps and a ramp are given to simulate the machining force F_m as shown in Figure 5.5. The step separation and the ramp duration are each of 0.01 s. The transient response can be found in Figures 5.6 and 5.7. In Figure 5.6 the initial valve setting x is chosen such that the part displacement never becomes smaller than zero, i.e. there is no lift off between part and clamp or locator, which is the essential condition for stable workholding. In Figure 5.7 the initial clamping force is chosen such that it is 980 N and

the actuator and part displacements are compared.

As the poles of the part-fixture system and the actuator are far apart from each other, there is no interference and application of only P-control is sufficient to obtain a good transient response. It should be observed that using the standard margins for stability from the standard literature on control design such as [48, 50, 102] allows for more overshoot than Nee *et al.* [114, 115] allowed for their design. Note also that force feedback control allows for the largest part displacement. There is a potential trade off here between part displacement and minimisation of contact stress, thus avoiding unnecessary plastic deformation.

5.5 Description of Electromechanically Actuated Fixture System

In Section 5.2, 5.3 and 5.4 a fixturing system with a hydraulically actuated clamp has been studied. This system consists of one actuator, a 2D part and one locator. Here, a more advanced system is studied. This system has been initially designed as a concept demonstrator within the framework of the AFFIX project. A design for this concept demonstrator has been established and described in Refs. [120, 143], and shown in Figure 2.5(b) and has been assembled by the authors of these papers, see e.g. PhD thesis by Papastathis [119]. The concept demonstrator can perform all the functions of an intelligent fixture as described in the literature review (Section 2.6.1): the fixture can be automatically reconfigured into a new planar configuration (layout); since all the fixturing elements are active, it can reposition and realign parts; furthermore, the active fixture elements can be used as active clamps. One of the aims of the AFFIX concept demonstrator described in [120, 143] is to demonstrate its ability to handle "compliant" parts. Therefore, it was decided to have a five-sided box or a container (or open box) as 'workpiece'. In the rest of these sections, for the sake of brevity this part will be further referred to as "five-sides" or "part". The part has the dimensions of $150 \times 100 \times 30$ mm and a wall thickness of 3 mm. Here, only the active fixturing capabilities of the fixture are investigated by means of an initial study to establish a control strategy for a simplified version of this design. This design is shown in Figure 5.8.

In the simplified fixture design in Figure 5.8, one can see that the five-sides is located with the classical 3-2-1 locating scheme. There are 3 locators at the bottom at points x_6, x_7 and x_8. Here, x denotes the coordinate vector. The origin of the system is taken in the lower left vertex in Figure 5.8. These three points are given the zero displacement condition in z-direction, but can slide frictionless in the x, y-plane. Two other locators at x_3 and x_4, locate the five-sides in y-direction. The form closure of the fixture is obtained with a locating point at x_5, which constrains the motion in x-direction. A passive clamp clamps the part in x-direction at point x_2 in Figure 5.8. Clamping force – and hence, workholding stability – in the x-direction is investigated, for this reason, the clamp is just modelled by a spring-dashpot element to take the contact stiffness into account. An actively controlled clamp clamps in y-direction at x_1, x_{13} is the coordinate of the actuator tip. As explained in Chapters 3 and 4, the contact stiffness in the normal direction is modelled with a linear spring-dashpot element. The contacts are assumed to be frictionless. Points x_9, x_{10}, x_{11} and x_{12} are points where machining takes place. The exact coordinates of these nodes can be found in Table 5.2. Parts of the research described in Sections 5.5, 5.6 and 5.7 are published in Ref. [12].

5.6 Numerical Model

5.6.1 Finite Element Model Five-Sides

In order to ensure the quality of the model, it has been decided to build a model of quadratic brick elements [149, 182], with 2 elements in the direction of the wall thickness. This comes down to 414255 DOFs distributed over 24864 elements. A careful comparison of several reduced models for accuracy resulted in the model reduction, as introduced in the Section 5.5, to the 12 nodes at x_1 to x_{12}, which equals 36 DOFs combined with 10 fixed interface modes. This means a reduction of the model to 46 DOFs, a reduction over 9000 times without significant loss of accuracy for the purposes of this investigation.

5.6.2 Clamp Model

Weight and power (speed and power density) demands put restrictions on the selection of an electro-motor that drives the ball-screw. For this reason a permanent magnet

synchronous motor (PMSM) has been selected for the AFFIX intelligent fixturing technology demonstrator, which has been built on-site at the University of Nottingham by the authors of [120, 143]. Modelling PMSMs from first principle is rather complex, a more empirical approach to establish models for the AC electric motor family is worked out in several books on control systems, e.g. Ref [48]. Franklin *et al.* [48, pp. 43 and 44] present the torque-speed curves for low and high rotor resistances. In case of high rotor resistance the torque-speed curve shows a(n) (almost) linear relationship between torque and speed [48, pp. 43 and 44]. On basis of these (experimental) performance characteristics it is argued that PMSMs with high rotor resistance can be modelled as the standard permanent magnet DC motor (PMDC) using the empirical model outlined in Ref. [48, pp. 43 and 44] rather than from first principle. The transient behaviour of this "crude" model shows good agreement with the more rigourous modelling and experimental work by Pillay and Krishnan, e.g. [125]. For this reason, the authors of [120, 143] have selected the combination of an AKM23C with a S20260 servo drive from Danaher Motion. This combination approaches the performance curve of a DC motor, as shown in Figure 5.9. As a result, an effective [34] back-emf constant, inductance and resistance can be defined. Hence the motor can be modelled as a standard PMDC. The standard electromechanical equations for a PMDC have been given by Equations (4.5.14) and (4.5.15)

$$J_{tot}\ddot{\theta} + f_r\dot{\theta} = k_\mathrm{T}i + T_\mathrm{e},$$

$$L\frac{\mathrm{d}i}{\mathrm{d}t} + Ri + k_\mathrm{bemf}\dot{\theta} = V_C.$$

Here, i is the current, J_{tot} - the total inertia as seen by the motor, f_r - viscous friction coefficient, θ - angular displacement, k_T - torque coefficient, T_e - external torque, L - motor inductance, R - motor resistance, k_bemf - back-emf constant, and V_C is the voltage output of the controller. The connection forces F_e between part and the electromechanical actuators has been established in (4.5.16) as

$$F_\mathrm{e} = c(\dot{y}_0 - \dot{y}_1) + k(y_0 - y_1).$$

The relation between rotary displacement θ of actuator and the translational displacements of the tip of the ball-screw in y-direction y_{13} is

$$y_{13} = \theta p, \tag{5.6.1}$$

where p is the ball-screw pitch.

In Section 4.5.2 it was derived from the principle that work over a distance in translational direction equals work over the equivalent distance in angular displacement, that the external torque T_e is proportional to the connection force F_e and the ball-screw pitch p

$$T_e = pF_e.$$

The constants for the modelling of the Danaher AKM23C [33, 34] are given in Table 5.3. The motor behaviour matches quite reasonably the documentation. It should be noted that for a PMDC k_T and k_{bemf} are equal, this is not the case for PMSM modelling. The controller that is needed to run the PMSM only has a bandwidth specified by Danaher [33] and is modelled with the following relation between applied control voltage V_{CC} and the voltage V_C that comes from the Danaher controller:

$$\frac{V_C}{V_{CC}} = \frac{1}{\dfrac{s^2}{\omega_v^2} + \dfrac{2\beta_v}{\omega_v}s + 1}, \tag{5.6.2}$$

where s is the Laplace variable, ω_v is the specified bandwidth of the controller (800 Hz [34]) and β_v is the damping coefficient, which is chosen such that the Danaher controller has no overshoot: 0.65.

5.6.3 Fixture Model

The fixture stiffness and damping are modelled as spring-dashpot elements. Some typical values for the stiffness and the viscous damping as discussed in Chapter 4 are used. The clamp and locator have a spring stiffness $k = 3 \times 10^7$ N/m and a damping constant $c = 960.12$ Ns/m.

5.6.4 Controller Design

An investigation has been made to the application of several forms of feedback: firstly, ADFB, secondly, the PDFB at the clamping point, and, thirdly, FFB. These quantities, called outputs, can be practically measured by appropriate sensors and one of these outputs is taken and used for feedback. To avoid problems with backlash and friction in the electromechanical actuator, the force has been taken as output, rather than the

current going into motor. In the case when the stiffness of the fixture and clamp are in the order of (or lower than) the stiffness of the part, the part displacement can possibly be measured by placing a sensor in the (proximity) of the clamp [40, 106]. In this study the clamp and fixture stiffness is much higher than the relatively thin walled part. The aim of this work is to investigate and compare several classical control strategies in the form of series compensation. Applications of proportional control (P-control), proportional integral control (PI-control), the classic three term PID-controller described by Equation (4.6.1):

$$C(s) = K_p \left(1 + \frac{1}{T_I s} + T_D s \right).$$

and a lag filter (LaF)

$$C(s) = K_p \frac{s + \omega_{\mathrm{LF}}}{\alpha_{\mathrm{LF}} s + \omega_{\mathrm{LF}}}, \quad \text{for } \alpha_{\mathrm{LF}} > 1$$

are studied. In these expressions, K_p is the proportional gain, T_I the integral gain, T_D the derivative gain, ω_{LF} the corner frequency of the LaF and α_{LF} the LaF coefficient.

Establishing a feedback loop can lead to instability when the feedback signal is too large. The signal in the feedback loop therefore is amplified with a gain K_{fb}, which in fact equals adding a compensator in feedback loop, which is not uncommon practice [48]. In case of FFB this gain had to be smaller then unity! The control designer can tune this gain using the root-locus technique [48].

5.7 Simulation of the Electromechanically Actuated Fixture

A representative selection of the most important results from the aforementioned investigation into control strategies is given below.

5.7.1 Frequency Response

A frequency response plot shows the amplitude of the response of a system output to a harmonic excitation with a fixed frequency of an input to the system. This response is measured or computed for a whole range of input frequencies, that allow to construct a frequency response diagram for this range [48]. For most of the controlled systems an output has the same amplitude for a whole range of frequencies. This output is scaled

to unity (1^0) and the frequency for which the frequency response gets for the first time below 0.5 (-3 dB), determines the bandwidth of the system. The frequency response can have a delay that can be expressed as a certain number of degrees in phase change: input $\sin(\omega t)$, output: $\sin(\omega t + \varphi)$, where φ is the phase change. This phase change can be better interpreted when depicted in a Nyquist plot. This is done in the next section.

In Figure 5.10 the responses of the following outputs are taken: the displacements in y-direction of the clamping point $\boldsymbol{x}_1$, (y_1) and the actuator displacement of point $\boldsymbol{x}_{13}$ in y-direction (y_{13}). These responses are plotted versus the excitation inputs of applied controller voltage V_{CC} and machining force F_{m} over a range frequencies. Note that there is no displacement in x- or z-direction for the actuator. It can be seen that the application PI or PID control gives a significant increase in bandwidth when any form of position feedback is used. Also in Figure 5.10(b) and (d) it can be seen that the response for the lower frequencies goes to zero, this means that for lower frequencies the machining force that acts as a disturbance is effectively cancelled. A second important observation can be made: since the fixture is much stiffer than the five-sides, the part closely follows the ball-screw tip. Hence diagrams (a) and (c) are very similar.

5.7.2 System Stability Analysis

As remarked above, the frequency response of a system consists of the amplitude of system's response and the phase change. The Nyquist diagram combines this frequency response with the phase change. The amplitude of the response is the distance from the origin and the phase is expressed by the angle in polar coordinates. The frequency information itself is lost, but one can obtain valuable information concerning the stability. The point (-1,0) in the Nyquist diagram is usually linked with instability. The control engineer can design a controller such that the response always has a certain distance from this point. According to standard (-1,0) rules for control design, the system response in a Nyquist diagram should never encircle the (-1,0) point [48]! The most certain information concerning instability comes from studying the eigenvalues of the system: the real part of the eigenvalue should be equal or smaller than zero for the system to be (marginally) stable, which is the case for all systems.

Nyquist plots of the part-fixture system are given in Figure 5.11. Most of the

responses start with a unity response and zero phase change in the vicinity of (1,0) and spiral their ways to a small response at (0,0). Overall the systems have a good margin with respect to the (-1,0) point. The Nyquist diagrams are in agreement with what was learned from analysis of the eigenvalues of the system.

5.7.3 Transient Response

The system's transient behaviour is analysed in this section. Applying a step input as the machining force forms an input that is composed by all frequencies. Therefore all eigenfrequencies present in the system will be excited which makes the step a good and "cheap" alternative representation for a real machining process like cutting, milling or grinding. The part displacement at the clamper location y_1, the total displacement $x_{10} = \sqrt{x_{10}^2 + y_{10}^2 + z_{10}^2}$ of node 10, the point where the machining is applied and the clamping force of the active clamper are considered as output for a step of 750 N.

Several observations can be made. The most important is that the system responds quite slowly for open loop and force feedback control. This is because of the elasticity present in the system. As the part has a relatively low stiffness the electromechanical actuator needs more time to reach the steady-state situation. This can be easily verified with a simple model of an electromechanical actuator connected by a spring-dashpot element to a rigid part (mass) that is connected to the earth by another spring-dashpot element. The higher the stiffness of the elements, the faster the response of the actuator. This can be compensated for by a PI or PID controller; applying a lag filter compensates only partially for it.

A second very important result from this simulation is that position feedback control yields a smaller displacement of the point where machining is applied, hence the machining results would be more accurate. This comes at the cost of having higher clamping forces, which can cause plastic damage to the part. The Von Mises equivalent stress in the part can *only* be calculated with the recovery matrix. The Von Mises equivalent stress can be used to check if the local contact stresses do not exceed the yield stress of the workpiece material. As spring-dashpot elements are used to model the contact interface, only approximate predictions can be made.

Application of a PI- or PID-controller does not work well in combination with

force feedback. Only small proportional and derivative action can be applied and no significant benefit can be obtained. These systems basically show the same response for this step input, however when a clamping force is applied, they will respond differently. A lag filter and proportional control, not shown here, do not remove the steady-state error. This is in agreement with the frequency response. In the section considering the frequency response it was observed that since $y_1 \approx y_{13}$ the results for part or actuator position feedback give similar results.

5.8 Conclusions

The main findings following from the analyses of the two fixture systems above are that the mathematical sub-models needed for an active part-fixture system can be integrated successfully into a single state-space system model, describing the overall model. In addition, the reduced workpiece model is a representation accurate enough for the full system dynamics, allowing for real-time simulation of the system. Furthermore, position feedback can be used to minimise unnecessary displacement of the workpiece, as it yields a smaller part displacement at the clamping point and the machining region when compared with FFB control.

Other conclusions can be summarised as follows:

- The clamp-workpiece contact is much stiffer than the part, hence part-clamp relative displacement is almost zero, as a result actuator and part position feedback have similar results.

- Several feedback control techniques are compared in this study and their advantages and disadvantages are considered in the application to active clamps.

- Parameter studies have been conducted to investigate the chatter suppression in the frequency domain, and the absolute and workholding stability of the system.

- For the *electromechanically* actuated system:

    - Applying PI- and PID-control removes the steady-state error.

– The study shows that the stiffness of the total system is an important factor concerning the bandwidth of an electromechanical actuator. The stiffer the system is the greater the actuator's bandwidth.

– The application of a derivative action in PID-control is rather limited because of an overshoot in the transient behaviour, too much action present also causes instability.

– Application of PI-control leads to the best results: a significant increase in the bandwidth of the actuator, and therefore a faster response in the time domain when machine forces are applied.

• For the *hydraulically* actuated system:

– The application of a LeF for force feedback is very limited for position feedback because of an overshoot in the transient behaviour, and this can even cause instability.

– LeF and classical three-term PID control are in practice not feasible for this part-fixture system using position feedback.

– Reducing the bandwidth by increasing the α_{LF}, or decreasing the ω_{LF}, in the LaF makes the system more stable but less responsive.

– Although FFB control is naturally stable, it has a lower bandwidth than position feedback control.

– The application of only proportional control for position feedback control can be successfully used to stabilise the part-fixture system.

– For good control performance, it should be ensured that the hydraulic actuator is of one order of magnitude stiffer than the rest of the system. Note that the commercially available hydraulic clamps from e.g. [45, 140] are relatively stiff due to their short length L of the hydraulic spring in the cylinder.

5.9   Tables

Table 5.1: Properties of hydraulic oil.

Property	Symbol	Unit
Supply pressure	P_s	200×10^5 Pa
Bulk modulus oil	E	10000×10^5 Pa
Density	ρ	800 kg/m^3
Discharge coefficient	C_d	0.611 [-]
Actuator gain servo-valve	K_v	7540 s^{-1}
Eigenfrequency servo-valve	ω_v	3770 rad/s
Damping value servo-valve	β_v	0.6 s

Table 5.2: Nodal coordinates and material properties of five-sides.

Description	Symbol	Numeric Value
Young's modulus	E	71.7 GPa
Poison's coefficient	ν	0.33
Density	ρ	2700 kg/m^3
Node	$\boldsymbol{x}_1$	(0.075,0,0.015)
Node	$\boldsymbol{x}_2$	(0,0.05,0.015)
Node	$\boldsymbol{x}_3$	(0.008,0.1,0.015)
Node	$\boldsymbol{x}_4$	(0.142,0.1,0.015)
Node	$\boldsymbol{x}_5$	(0.15,0.05,0.015)
Node	$\boldsymbol{x}_6$	(0.142,0.008,0)
Node	$\boldsymbol{x}_7$	(0.142,0.092,0)
Node	$\boldsymbol{x}_8$	(0.008,0.05,0)
Node	$\boldsymbol{x}_9$	(0.0375,0,0.03)
Node	$\boldsymbol{x}_{10}$	(0.1125,0,0.03)
Node	$\boldsymbol{x}_{11}$	(0.0375,0.1,0.03)
Node	$\boldsymbol{x}_{12}$	(0.1125,0.1,0.03)

Table 5.3: Properties AKM23C PMSM + S20260 drive amplifier.

Description	Symbol	Numeric Value
Total inertia seen by motor	J_tot	4.3232×10^{-5} kgm^2
Motor inductance	L	0.0407 H
Motor resistance	R	20.3 Ω
Supply voltage	V_s	120 V
Viscous friction coefficient	f_r	6.207×10^{-5} Nms/rad
Torque constant	k_T	0.8 Nm/A
back-emf constant	k_bemf	0.5348 Vs/rad

5.10 Figures
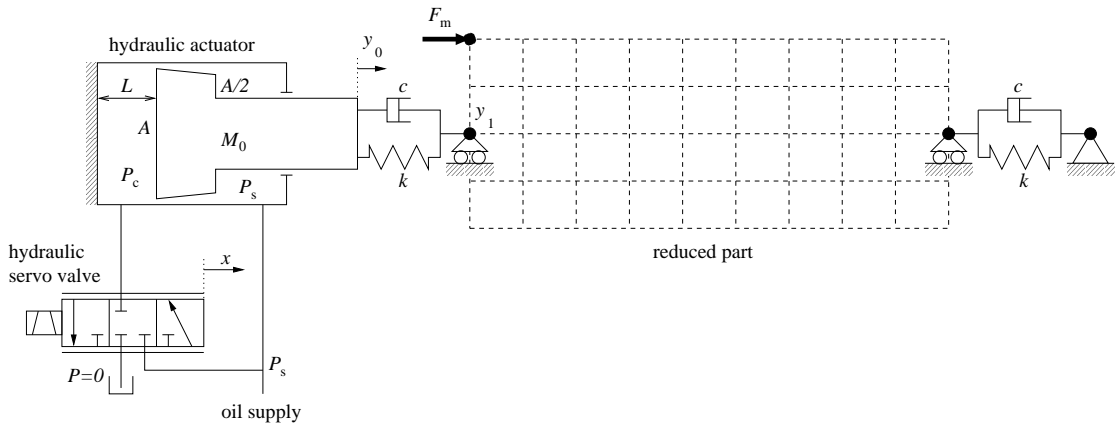
Figure 5.1: Active fixture consisting of a hydraulic actuator, a critical centre three way hydraulic servo-valve (i.e. no over- or underlap, see Footnote 5 in Section 4.5.1.1) [103, 163], and a part; the part is connected to the ground and the actuator by means of spring-dashpot elements.
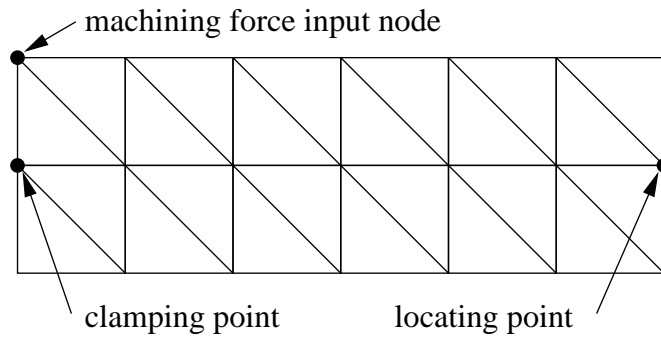
Figure 5.2: Finite element mesh.
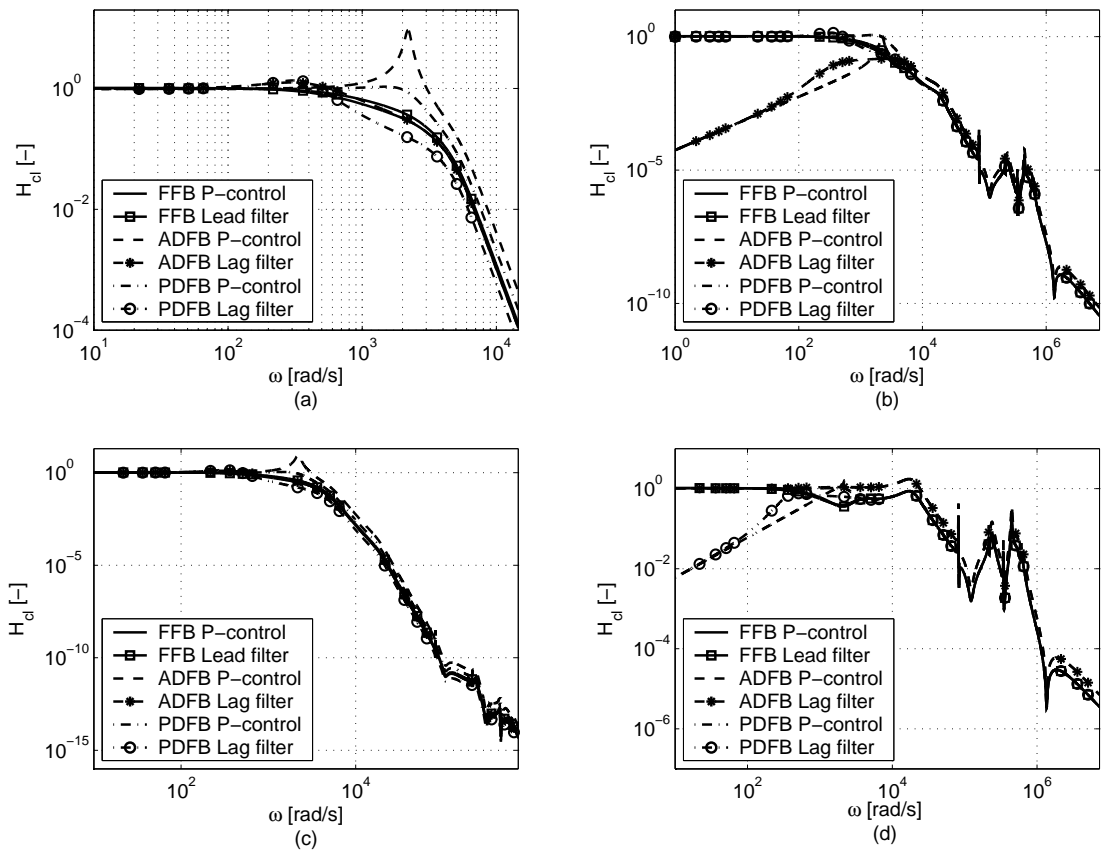
Figure 5.3: Closed-loop frequency response diagram; with (a) response y_0/r, (b) response y_0/F_m, (c) response y_1/r, (d) response y_1/F_m.

122
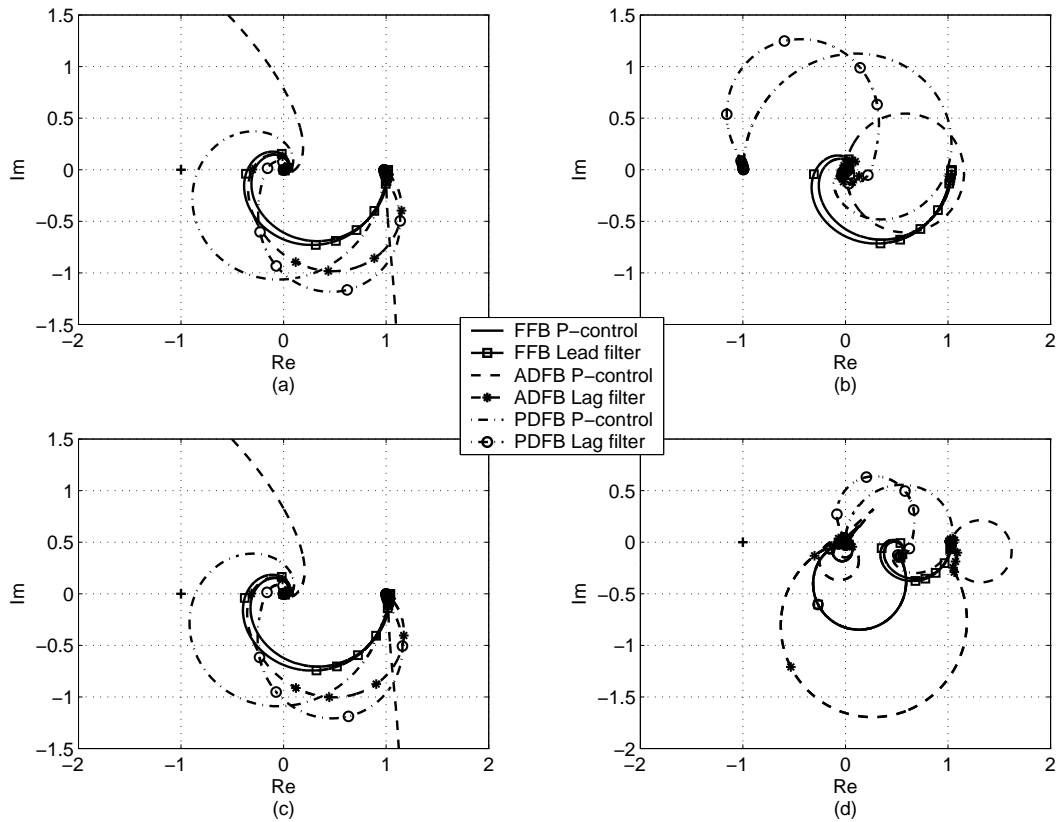
Figure 5.4: Closed-loop Nyquist diagram; with (a) plot of y_0/r, (b) plot of y_0/F_m, (c) plot of y_1/r, (d) plot of y_1/F_m.
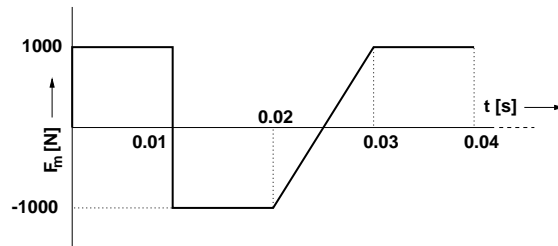
Figure 5.5: Machine force profile.
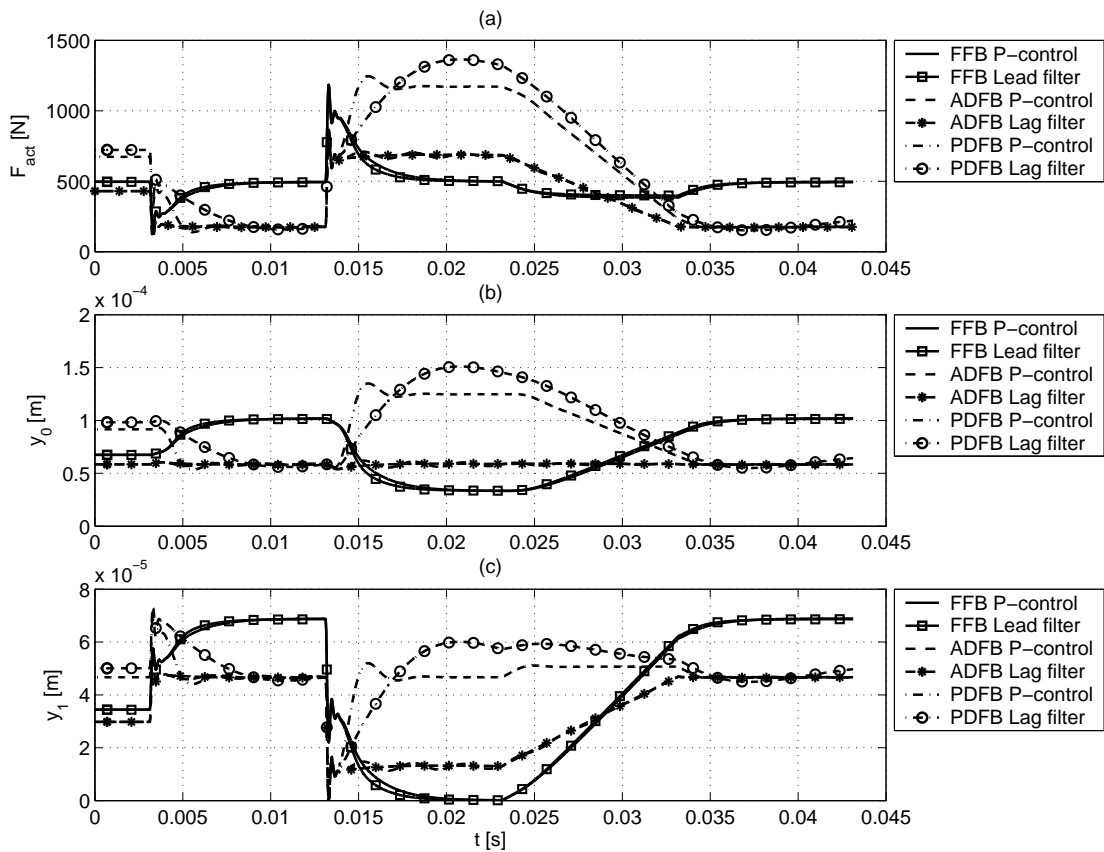
Figure 5.6: Comparison for minimum clamping force for $y_1 > 0$; machining time 0.04 s; with (a) dynamic response F_{act} to F_{m}, (b) dynamic response y_0 to F_{m}, (c) dynamic response y_1 to F_{m}.
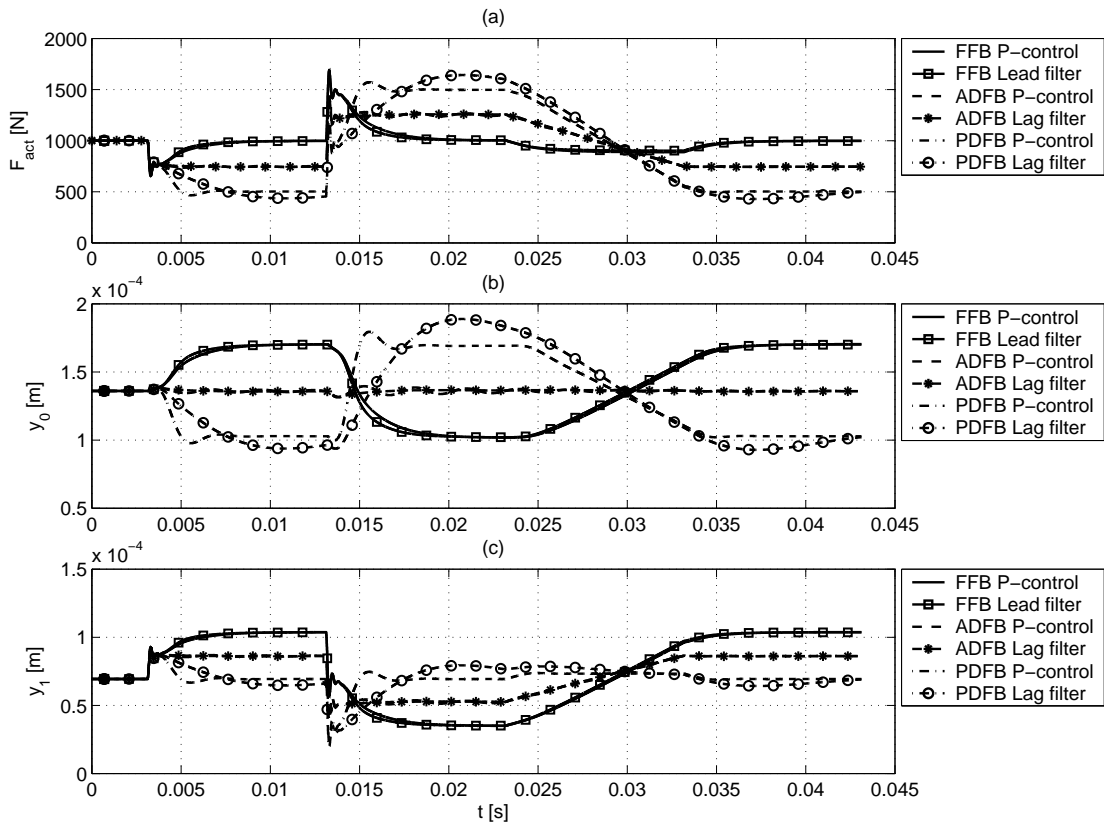
Figure 5.7: Comparison for displacement for same clamping force; machining time 0.04 s, clamping force at $t = 0$ s, $= 980$ N; with (a) dynamic response F_{act} to F_{m}, (b) dynamic response y_0 to F_{m}, (c) dynamic response y_1 to F_{m}.
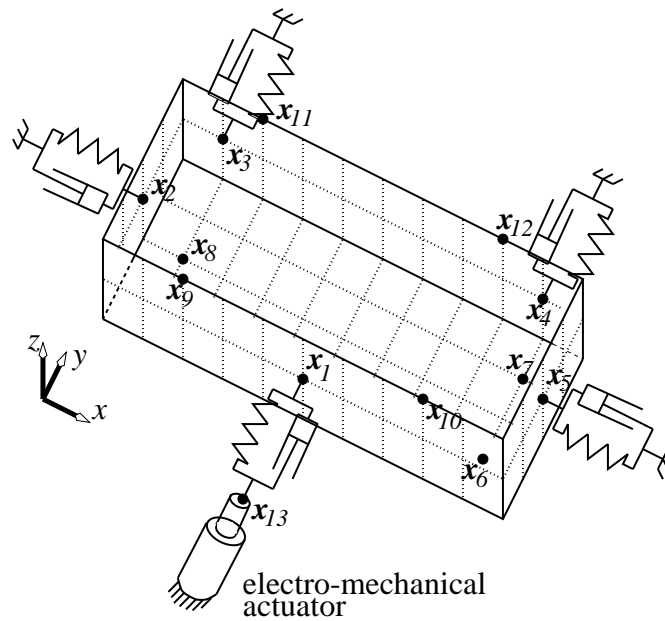
Figure 5.8: Sketch of the system under consideration, not to proportion.

125
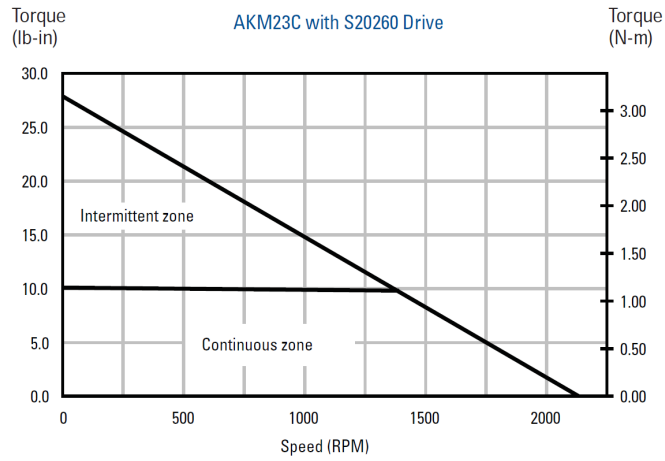
Figure 5.9: Torque-speed characteristic AKM23C PMSM + S20260 drive amplifier.
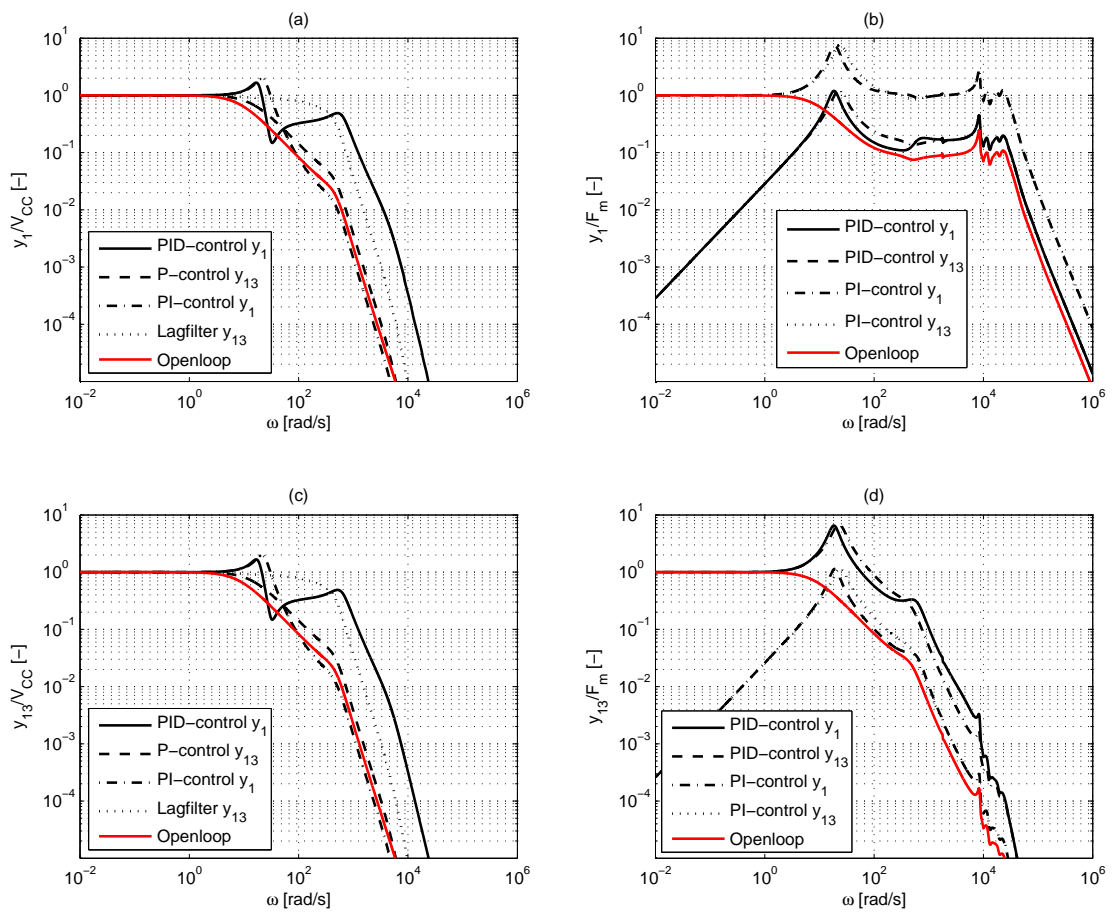
Figure 5.10: Frequency response diagrams; with (a) response y_1/V_{CC}, (b) response y_1/F_{m}, (c) response y_{13}/V_{CC}, (d) response y_{13}/F_{m}.
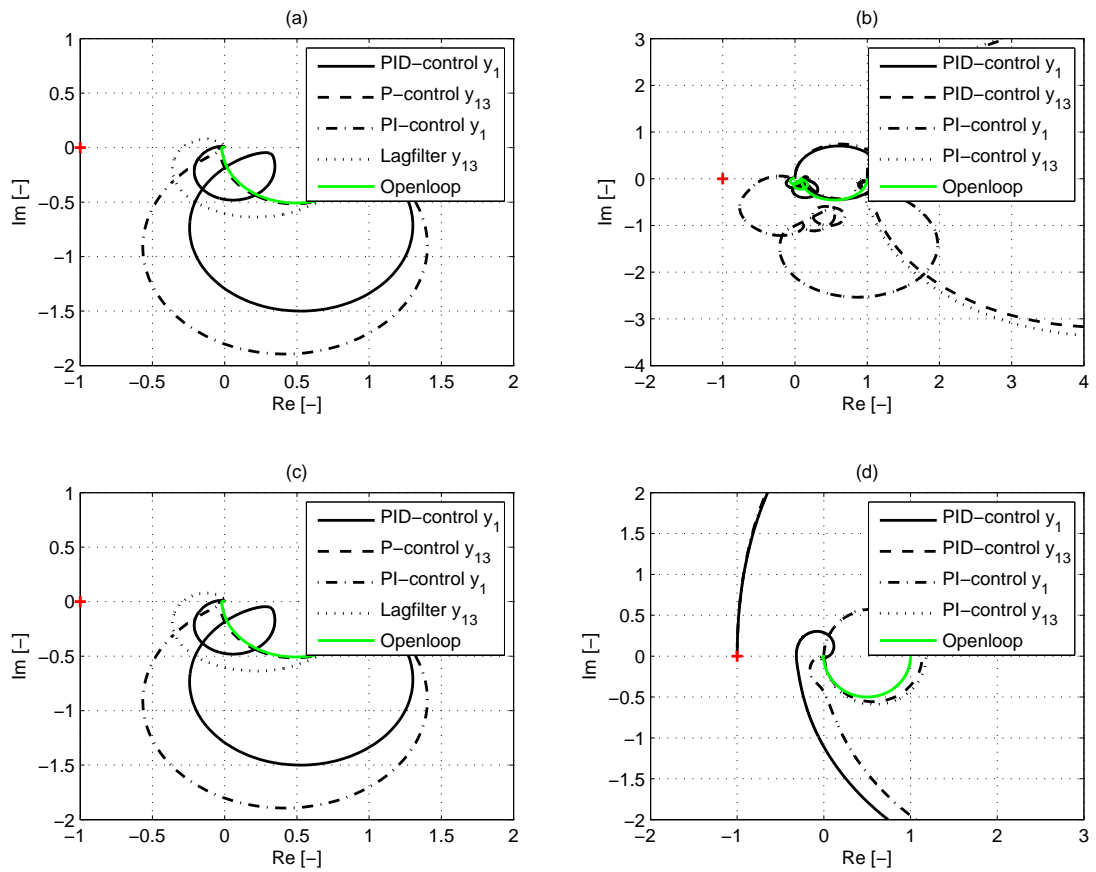
Figure 5.11: Nyquist diagrams; with (a) response y_1/V_{CC}, (b) response y_1/F_{m}, (c) response y_{13}/V_{CC}, (d) response y_{13}/F_{m}.
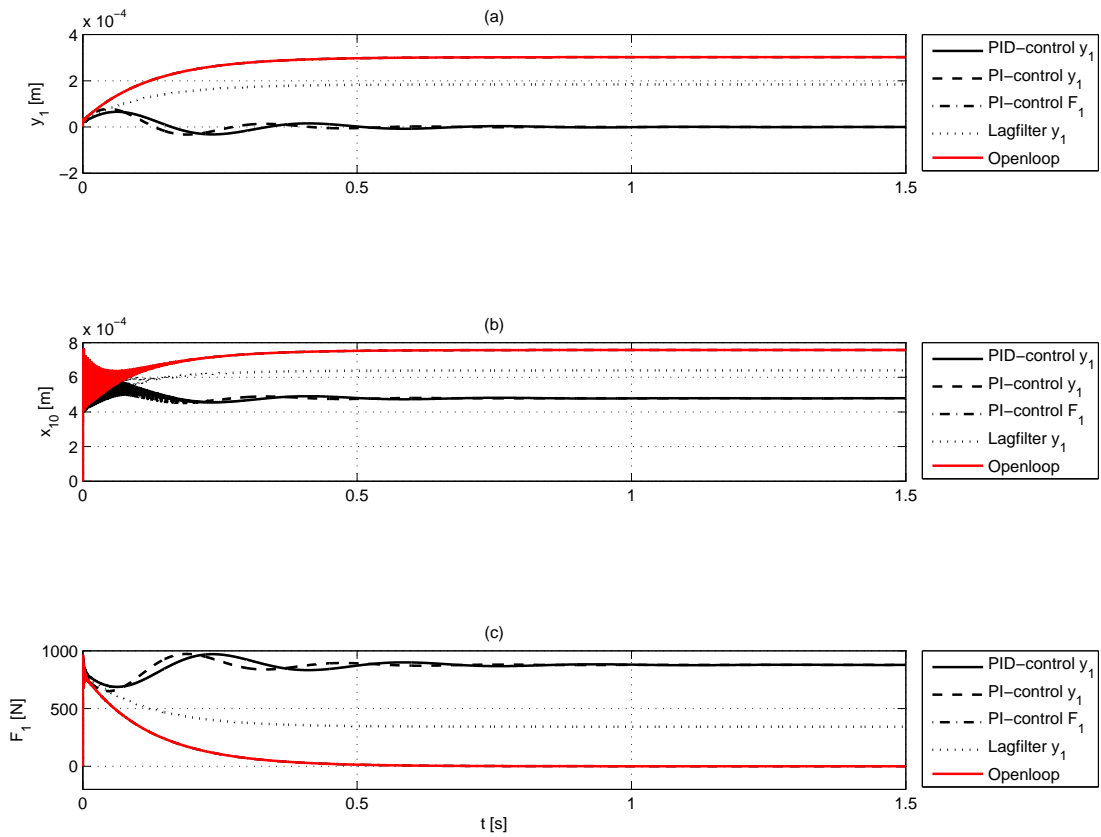
Figure 5.12: Comparison of a step input of 500 N as machining force, with (a) dynamic response F_1 to F_m, (b) dynamic response y_1 to F_m, (c) dynamic response $\boldsymbol{x}_{10}$ to F_m.

Industrial Case Study: Modelling

6.1 Introduction

In this chapter an application of the methodology and models established in this thesis is made for a complex, near-industrial fixturing system for a compliant part. Within the AFFIX research consortium the design of an existing machining fixture has been studied [5, 83, 90]. This case study involves the redesign of a grinding fixture for a family of nozzle guiding vanes (NGVs), as utilised by an aerospace manufacturer. This manufacturer makes gas turbines and is a subcontractor for aero-engine components. NGVs and aerospace components are typical low-volume high-value parts and generally are designed with tight tolerances. This requires accurate and reliable fixtures. The low number of parts manufactured, renders dedicated fixture designs economically inviable. For this reason a reconfigurable fixture design for the NGV family is desirable. The new fixture design also should deliver reduced setup times, an increased locating performance (positioning and aligning of the workpiece during the setup process), and minimal distortion due to clamping forces. These problems encountered by industry have, as can be observed in Chapter 2, received serious attention in scientific publications. The study carried out by the AFFIX research consortium focused mainly on the reduction of the setup times and the positioning and aligning of the NGV in the fixture. Actively controlled minimal clamping forces are kept outside this case study and form a goal beyond the horizon of the current time line for this case study. The work resulted in a guidelines for the redesign and a technology demonstrator. Despite not being the focus of

the case study, the developed system can also be used to minimise the distortion due to the clamping forces, and therefore this demonstrator will be analysed in detail in this chapter.

The modelling tools and methodology developed in Chapters 3 and 4 will be applied to model the subsystems of this actively controlled fixturing system. The major contribution of this work is the proof of concept that models with a low number of degrees of freedom can be established for real-time control. For this reason, control settings have not been exhaustively investigated here. Additionally, the most important control objective is to minimise the reaction forces at the locators, rather than damping oscillations, which can be done with a PI controller, for example. Furthermore, adding derivative action proved to make the systems unstable. The application of the methodology in the work presented here, is illustrated in Table 6.1. The work in the chapter is then presented as follows. Firstly, an analysis of the whole part-fixture system will be held in Section 6.2 and its subsystems will be identified. These systems will be considered in more detail. A short description of the development of the finite element model of the NGV by Klärner *et al.* [83] will be given, which subsequently will be reduced here to smaller size using a model reduction technique in Section 6.4.2. Thirdly, a mechatronic model of the active clamps will be established, which comprises the mechanical model of the clamp housing and a actuator model for the piezoelectric actuator (PEA) in Section 6.3. After this, a model for the locators is established and control strategies are considered. Detailed simulations have been carried out and the results of these simulations are presented in Chapter 7. Parts of this chapter and Chapter 7 are based on Ref. [13].

6.2 Analysis of Fixture Design

6.2.1 Current Design

In order to establish design for an actuated clamp and working technology demonstrator, the aerospace components manufacturer identified a specific fixture design and NGV from the whole family of NGVs and fixtures as a representative design regarding dimensions and clamping and machining forces. A limited view of this current nozzle guiding vane (NGV) grinding fixture design is given in Figure 6.1, c.f. [91, Fig. 1]. In this figure, the

following components can be identified. Firstly, it can be seen that the NGV geometry can be divided in three parts: the inner and outer bounds and the wings. In the assembled gas turbine the wings have a radial direction with respect to the turbine shaft, which is the main axis of revolution. For this reason, the inner bound is shorter than the outer bound, as the radial distance to the shaft is larger at the outer bound than at the inner bound. In the bottom right, a Cartesian coordinate system is shown. Obviously, this system does not match with a cylindrical coordinate system, but it is chosen such that the y-direction is more or less parallel with the vanes or wings of the NGV, hence this is more or less parallel with the radial direction in the turbine and the z-direction is parallel with the axial direction of the turbine. The direction of this system with respect to the part is kept throughout Chapters 6 and 7, which makes comparison between the several figures easy. The part has six datum points: 1 in x-direction, 2 in y-direction and 3 in the z-direction. Hence, the current fixture is designed with the classic 3-2-1 locating scheme. Furthermore, the fixture has 1 clamp in x-, 1 clamp in y- and 4 clamps in z direction. All are mechanical clamps. Additional supports are placed underneath the four clamping points in z-direction. In Figure 6.1, the visible fixture elements are labelled.

6.2.2 Design Technology Demonstrator

Following the analysis of the case study [5, 83, 90], the AFFIX research consortium came with the recommendation for a modular design. Furthermore, an adaptive modular clamp has been designed to replace the four mechanical clamps in the z-direction [5]. A technology demonstrator, which can demonstrate the capabilities of the adaptive clamps has been designed for the same NGV (part) as shown in Figure 6.1, has been designed. A solid and a finite element (FE) model of this design are shown in Figure 6.2. A physical demonstrator has been assembled and can be seen in Figure 6.3.

In order to establish the demonstrator, the full fixture design has been reduced in complexity: the part is now only located in the x, y-plane, three locators are used. The locators are numbered as well, as can be seen in Figure 6.2(b). There is neither locating nor clamping force provided in x- or y-direction. This has some implications for modelling of the boundary conditions and the applied machining force which will be discussed

in Section 6.6 and Chapter 7. The four mechanical clamps acting in the z-direction in Figure 6.1 have been replaced by four actuated clamps that provide clamping forces in the z-direction and, additionally, can (re-)position the part using the actuator displacements during the part-fixture setup. These clamps can dynamically compensate for part displacements due to dynamic machining forces. They are numbered, respectively, as "clamp 1", "clamp 2", "clamp 3" and "clamp 4", as shown in Figure 6.2(b). This adopted numbering will be used consistently in Chapters 6 and 7. Hence the fixturing system can be dissected in three (actuated) mechanical components. These are respectively the actuated clamp, the NGV and locators. A fourth subsystem can be identified as well: the controller.

As shown in Table 6.1, FE models of the clamps and locators have been established [5]. An assembly of the individual FE models of the fixture components as a representation of the whole part-fixture system is shown in Figure 6.2(b). The model of the NGV has been previously established and analysed by Klärner *et al.* [83] in order to model the grinding forces and predict the reaction forces. The parametrisation process carried out by Klärner *et al.* [83] involved several simplifications of the geometry of the NGV, which can be observed when Figure 6.2 (b) is compared with Figure 6.2(a). The parametrisation process is discussed in more detail in Section 6.4.1.

6.3 Clamp Modelling

The modelling of the four identical adaptive clamps is a crucial step in the analysis. In this model, actuation is combined with a mechanical model. As mentioned in Section 6.4, real-time model-based control of the part-fixture system requires small, though accurate enough models. The adaptive clamp is a relatively complex model compared to the clamp models studied in Chapters 4 and 5 and consists of a clamp housing and an integrated piezoelectric actuator. These two subsystems have been modelled independently and an overall model of the clamp has been established. From the structural analysis of the clamp housing it followed that the clamp housing can be modelled as a lumped-parameter system. A lumped-parameter system describing the dynamic behaviour of the PEA has been established as well by combining the PEA models presented in Refs [4, 55]. The

section is organised as follows. Firstly the working of and the general methodology to model the clamp are discussed in Section 6.3.1. A detailed derivation of the properties of the lumped-parameter models is presented in Section 6.3.2.

6.3.1 General Methodology Clamp Modelling

One can see the clamp without actuator as a FE model with many degrees of freedom in Figure 6.4(a). Extensive analysis of this FE model revealed that the dynamics of the clamp can accurately be described by the simplified, discrete model (including the actuator) containing only 1 degree of freedom shown in Figure 6.4(b). In the discrete model shown in Figure 6.4(b), z_i is the workpiece displacement at node i of the NGV model in direction of the actuator displacement. This node is connected to the active clamp with a spring-dashpot element, which has respectively a spring stiffness k_c. This spring-dashpot element is applied to model the properties of material that is above the actuator-flexure mechanism, inclusive the gripper mechanism, only shown in Figure 6.2(a). The corresponding spring stiffness of this region has been derived by static FE analysis of the model shown in Figure 6.4(a). The rod-shaped element in the centre of the clamp housing in Figure 6.4(a) is the actuated part of the adaptive clamp and is shown here with an upward displacement and has an effective mass m_c; its displacement is denoted by z_f. This element is guided by a flexure mechanism consisting of two parallel diaphragms that only allow for motion of the "rod" in the actuated direction as can be seen in Figure 6.4(a). The equivalent stiffness k_f of the discrete flexure mechanism in Figure 6.4(b) has been extracted from this static FE analysis of the model shown in Figure 6.4(a). Eigenfrequency and mode shape analysis of the model shown in Figure 6.4(a), revealed that there is a mode shape in which the clamp shows displacement in the actuated direction only, and the corresponding frequency matches closely the frequency that belongs to the discrete mass spring model $\sqrt{k_f/m_c}$ of which the elements are shown in Figure 6.4(b). From this detailed analysis it follows that, the dynamic behaviour of the clamp can be modelled as a single degree of freedom system. The values of the viscous damping coefficients c_c and c_f of the discrete model are estimated on basis of an educated guess, as described in Section 6.6. A discrete model of the clamp without actuator has

now been established, its equation of motion reads

$$m_c\ddot{z}_f + (c_c + c_f)\dot{z}_f + (k_c + k_f)z_f = c_c\dot{z}_i + k_c z_i. \qquad (6.3.1)$$

The clamps are actuated by stacked piezoelectric actuators. This PEA is not shown in Figure 6.4(a). This type of actuators can be modelled as a discrete mass-dashpot-spring model, which have respectively an effective mass m_p, a viscous damping coefficient c_p and a spring stiffness k_p, as is shown in Figure 6.4(b). The discrete model of the PEA is actuated by a force F_p, which is generated by the conversion of electric power into a force by the piezoelectric effect. This model has been established as follows.

The coupled electromechanical behaviour of a stacked PEA is usually modelled by the standards established by the IEEE [1], this approach can be found in many publications and monographs such as [54, 111].

The linear model mentioned above does not consider the dynamic behaviour of the hysteresis that occurs in the PEA [4, 54, 55, 111] and nonlinearities that occur over large displacements. For model-based dynamic feedback control design it is essential to establish a model that describes the dynamics of a PEA. The piezoelectric materials in PEAs, show hysteresis nonlinearity between electrical input and actuator displacement. The hysteresis effect has a great impact on the dynamic performance of the PEA [4, 54, 55, 111, 117]. Several mathematical models are used to describe the hysteresis [4, 55, 117]. When charge feedback is applied on the PEA, or the PEA is within closed-loop control, the hysteresis effects are effectively cancelled [4, 111, 123]. In this study charge feedback is applied and it is assumed that the hysteresis effects do not need to be modelled.

Here, an approximate [126], but *linear* dynamic model can be established based on [4, 55]. Although linear models as this one exist, one would normally model a PEA as nonlinear for the reasons mentioned above. The reason for omitting a nonlinear model in the thesis is that the thesis doesn't deal with making accurate models of actuators, but about the general methodology. Goldfarb and Celanovic [55] present a lumped-parameter model to model the mechanical behaviour of PEA, a similar model has been used by Neelakantan *et al.* [117], whereas Adriaens *et al.* [4] and Craig and Kurdila [29] establish their model by solving the governing PDE for axial vibration of a truss. Furthermore, Craig and Kurdila [29] extend their overall PEA model into a FE-model. The lumped-

parameter model presented in Ref. [55] forms the basis of the model presented in this section. It is assumed that the piezoelectric stack actuator can be modelled by a lumped mass and a linear material stiffness and damping for the following two reasons. Firstly, it is advisable to keep the bandwidth of the steering voltage over the PEA below the the first mechanical mode of vibration, therefore the frequency band of interest is below this first eigenfrequency. Secondly, in order to keep the model as small as possible, the variable of interest here is only the actuator tip displacement. Starting by combining Eqns (15) and (20) from Ref. [55] (c.f. [4, Eq. (58)]) yields the following equation of motion for a PEA:

$$m_{\mathrm{p}}\ddot{z}_{\mathrm{p}} + c_{\mathrm{p}}\dot{z}_{\mathrm{p}} + \left(k_{\mathrm{p}} + \frac{T_{\mathrm{em}}^2}{C}\right) z_{\mathrm{p}} = F_{\mathrm{e}} + F_{\mathrm{p}}, \qquad (6.3.2)$$

where z_{p} is the actuator displacement, C is the capacitance of the PEA, T_{em} is the piezoelectric transformer coefficient and F_{p} is the actuation force. Actuation force F_{p} is then established by substituting [4, Eq. (56)] with the lumped parameter system from Eq. (6.3.2) and executing the same algebraic substitutions and rearrangement as described in Ref. [4] between Eq. (56)–(59) ([4, p. 340]). As mentioned above, charge feedback is applied to steer the PEA. This means that the the actuation force F_{p} is the same as the expression at the righthand side of [4, Eq. (60)], where the actuation force is proportional to the steering voltage V_{pea}:

$$F_{\mathrm{p}} = \frac{T_{\mathrm{em}}C_{\mathrm{e}}}{B_2 C}V_{\mathrm{pea}}.$$

Here, V_{pea} is the steering voltage over the PEA, C_{e} and B_2 are respectively the external capacitance and an amplification value in the charge feedback scheme.

Furthermore due to the open-lead (or, galvanically open) configuration that occurs when the PEA becomes part of an electronic circuit there is an increase in actuator stiffness [4, 54, 55, 111, 126] by T_{em}^2/C [4, 55]. It should be noted that the actuator stiffness quoted in the PEA vendor specifications is this overall stiffness $k_{\mathrm{p}} + T_{\mathrm{em}}^2/C$ and not stiffness k_{p} [123, 124]!

In order to be able to generate both push and pull forces with a PEA, the actuator needs to be preloaded, otherwise the ceramic material gets cracked, rendering the PEA defective [54, 111, 123]. For the modelling of the clamp this is a favourable condition:

the flexure and actuator displacement effectively coincide

$$z_\mathrm{f} = z_\mathrm{p},$$

which means that the spring-dashpot elements with indices 'f' and 'p' as shown in Figure 6.4(b) are acting in parallel.

The external force F_e that works on the actuated clamp is the force exerted by spring-dashpot element at the top of discrete clamp model in Figure 6.4(b) due to the relative motion of the part with respect to the clamp:

$$F_\mathrm{e} = c_\mathrm{c}(\dot{z}_i - \dot{z}_\mathrm{p}) + k_\mathrm{c}(z_i - z_\mathrm{p}), \tag{6.3.3}$$

and is readily incorporated in the equation of motion of the clamp without actuator (6.3.1).

$$(m_\mathrm{c} + m_\mathrm{p})\ddot{z}_\mathrm{p} + (c_\mathrm{c} + c_\mathrm{f} + c_\mathrm{p})\dot{z}_\mathrm{p} + \left(k_\mathrm{c} + k_\mathrm{f} + k_\mathrm{p} + \frac{T_\mathrm{em}^2}{C}\right)z_\mathrm{p} - c_\mathrm{c}\dot{z}_i - k_\mathrm{c}z_i = \frac{T_\mathrm{em}C_\mathrm{e}}{B_2 C}V_\mathrm{pea}. \tag{6.3.4}$$

6.3.2 Details of the Structural Analysis Clamp Housing and PEA

Detailed FEA has been made of the clamp housing in order to establish its stiffness and modal properties. After having established the working of the clamp, the right boundary conditions for FEA are easily determined. The degrees of freedom of the nodes at the bottom of the base are completely constrained: this is a reasonable approximation as the base of the clamp housing is bolted onto the fixture base. Furthermore, the precise effects at the bottom of the base are not of interest in this analysis. An intuitive approach regarding the loading has been taken. Initially, the top of the rod has been given a displacement downward. This is equivalent to an external load being applied on the rod. Analysing the stresses and displacements, it was observed that the displacements at the outer casing and base are very small compared with the displacements of the clamp components as can be seen in Figure 6.7(a). In fact, the flexural displacements of the outer casing are all smaller than 3 μm. Furthermore, most of the flexural motion was taken by the top of the rod and the diaphragms. This lead to the idea that the mechanical behaviour of the clamp can be modelled by lumped-parameter model. This idea has been tested with a more extensive static and modal analyses presented in Sections 6.3.2.1 and 6.3.2.2 respectively.

6.3.2.1 Establishing Stiffness k_c and Flexure Stiffness k_f

With static analyses, the stiffness of the rod k_c and the stiffness of the flexure mechanism k_f theoretically can been established by two different load cases. However, there is some material between the two diaphragms, hence there is a third unknown stiffness. As a results three load cases are needed to identify the values of the three stiffnesses.

- FE housing 1: displacement condition of 0.1 mm of the top of the rod (Figure 6.5),

- FE housing 2: the top surface of the rod and the top pad are both given a displacement of 0.1 mm (Figure 6.5),

- FE housing 3: a displacement condition of 0.1 mm for the top pad (Figure 6.5).

Here, load case FE housing 1 is the approach taken initially and the computed displacements for this load case are shown in Figure 6.7(a). On basis of the calculated reaction forces at the bottom of the clamp for these three load cases, a stiffness for each load case is calculated and presented in Table 6.3. The values for the stiffness presented in Table 6.3 are normalised on load case FE Housing 3, which has stiffness k. The components of the clamp housing are made from steel and its material properties are given in Table 6.2.

6.3.2.1.1 Flexure Stiffness k_f

In case a PEA is driving the clamp, but the gripper is not holding a part, the stiffness as seen by the actuator is that of load case FE Housing 3.

6.3.2.1.2 Stiffness of Material Between Diaphragms

The stiffness of the material between the two diaphragms can be established on bases of the difference between the stiffness for load case FE Housing 2 and 3. On first instance, the displacement boundary conditions at the top surface of the rod in load case FE Housing 2, see Figure 6.5, appears misplaced. However, this is the only appropriate place for a boundary condition: the components surrounding the rod and the flexure form a fastening mechanism to fasten the rod onto the flexure and it is hard to establish in the FE model which components are connected. However, since the stiffnesses for load cases FE Housing 2 and 3 are almost identical, it means that the deformation between

the two diaphragms is very limited compared to the 0.1 mm prescribed displacement and stiffness of the material between the two diaphragms is much larger than the stiffness of the diaphragms.

6.3.2.1.3 Calculation of Stiffness k_c

Since the stiffness k_c of the rod and the stiffness k_f of the flexure act in series, and the stiffness of the material between the two diaphragms reasonably can be assumed as infinite, the stiffness of the rod is then given by

$$k_c = \frac{1}{\dfrac{1}{0.82990k} - \dfrac{1}{k_f}} = \frac{1}{\dfrac{1}{0.82990k} - \dfrac{1}{k}} = 4.8788k.$$

This is almost five times stiffer than the diaphragms in the flexure and much stiffer than the effective stiffness of the clamp housing limited by the stiffness of the diaphragms. It should be realistically estimated on basis of Figure 6.2(a) that the total stiffness of the gripper is lower than that of the rod and flexure. The overall high stiffness of the clamp is actually intentionally achieved: the reason for this will be discussed in Section 6.5.

6.3.2.1.4 Verification of FE-Model Clamp Housing

It is observed that the reaction forces as presented for the three load cases are higher than would be reasonably expected for a flexure mechanism. Therefore, the stiffness for a circular disc with centric hole, has been analysed as well. This disc has the same inner and outer radii and thickness as the diaphragms in the FE-model. The stiffness of outer casing and the material between the diaphragms is much higher than the stiffness of the diaphragms. As a result, the boundary conditions for these discs may be given by:

$$u_z\big|_{r=\frac{1}{2}d_2} = u_r\big|_{r=\frac{1}{2}d_1} = u_r\big|_{r=\frac{1}{2}d_2} = \left.\frac{\partial u_z}{\partial r}\right|_{r=\frac{1}{2}d_2} = \left.\frac{\partial u_z}{\partial r}\right|_{r=\frac{1}{2}d_1} = 0, \qquad (6.3.5)$$

$$u_z\big|_{r=\frac{1}{2}d_1} = 0.1 \text{ mm}.$$

The material properties are those given in Table 6.2. The diaphragms in the FE-model have a measured thickness t and an inner diameter r_1 and outer diameter r_2. In order to fulfill the boundary conditions, a reaction force and a reaction moment will occur. For the verification only the reaction force is of interest. This reaction force is the sum of the reaction forces at all the nodes. An analytical model has been established and

several models were built in ABAQUS. Details on the analytical model can be found in Appendix C. A number of different elements from the element library in ABAQUS [149] has been used to build disc spring models. Single disc models have been built with general purpose 3D shell elements, general purpose axisymetric shell elements, thin shell elements, axisymetric linear and quadratic solid elements. Quarter disc models have been established with linear and quadratic 3D continuum elements. The equivalent stiffnesses for a structure consisting of two disc serial disc springs have been established and are presented in Table 6.3.

Comparison of the stiffness of 'FE Housing 3' with these models reveals that the stiffness of load case FE Housing 3 is higher than those of the simplified disc-with-hole models models, apart from the models that are based on the thin shell theory. The calculated stiffnesses for the general purpose shell elements and the solid elements, however show great consistency. The boundary conditions given to the disc models are not entirely realistic, as the rod and the casing not purely rigid. Hence, the boundary conditions given to the simple FE-models introduce extra stiffness and the reaction forces should be higher than the forces that are needed for the same displacements in the model of the whole clamp housing. The reason for this is the low number of elements in the thickness direction of the diaphragms of the flexure. This low number of elements in thickness direction has a negative impact on the predictive quality of the mesh. This will be discussed further in Section 6.3.2.4.

6.3.2.2   Modal Properties of the Clamp Housing

An eigenfrequency and mode shape analysis has also been carried out. The only boundary condition is the zero displacement condition for the nodes at the bottom of the base of the clamp housing, as shown in Figure 6.4(a). Firstly the mode shapes have been analysed. One of the mode shapes involves only a parallel deflection of the flexure mechanism, the base and outside almost do not undergo any deflection and the rod in the centre undergoes a translation (= rigid body motion) in axial direction as shown in Figure 6.7(b). From Figure 6.7(c) it can be established that the flexural motion of the rod goes up to a maximum of 5.4 % of the overall motion, likewise it can be established that the flexural motion of the casing does not exceed 4.5 % of the overall motion of

this mode. This is within the accuracy brackets of predictions of a FE-model. However, in the FE-model, this is not the first mode. There are two pair of modes of free transverse vibration of the rod inside the housing, where the flexure mechanism provides the cantilever boundary conditions. These vibrations can cause damage to the PEA and a small mechanical patented device is placed on the rod to increase its stiffness and damp the transverse vibrations.

Hence, it can be concluded that the mode involving only flexural motion of the flexure mechanism, is the dominant mode. For this reason, the stiffness as established with the static analysis can be used to calculate the effective mass m_{eff}, since

$$\omega = \sqrt{\frac{k_{\text{eff}}}{m_{\text{eff}}}}.$$

The effective mass has been compared the mass of the moving parts in the FE-model. It appears that the effective mass is equal to the sum of the effective mass of the diaphragms m_{ds} and the mass M of the wedges, the rod, some other components and the part of the flexure that show non-flexural motion in this mode. From Figure 6.6 it is easy to establish why the two diaphragms have the effective mass of one. The radial coordinate $\bar{r}$ of the centre of mass of one element $r_2 - r_1 \mathrm{d}\varphi$ is:

$$\bar{r} = \frac{\displaystyle\int_{r_1}^{r_2} r 2\pi r \mathrm{d}r}{\displaystyle\int_{r_1}^{r_2} 2\pi r \mathrm{d}r}.$$

Then $\bar{r}$ is only 2.2 % larger than $(r_1 + r_2)/2$. At $r = (r_1 + r_2)/2$, the diaphragm travels around 50 % (47 % for the analytical thin plate model) of the maximum motion. Hence, a lumped mass at that point has only 50 % of the accelerations of the mass in the centre. For this reason, Figure 6.6 shows only two lumped *effective* masses at either side of the centre mass, each having the mass of a quarter diaphragm.

6.3.2.3 Establishing a Simplified Model

The static and modal analyses lead to the conclusion that the dominant mechanical behaviour of the clamp housing can be modelled as a moving rod having a lumped mass that is constrained in all but the axial direction by the two diaphragms. Since a system consisting of two parallel disc springs is the structural equivalent the diaphragm-based

flexure mechanism, a simple system may be describing the mechanical behaviour of the clamp housing can be established, this is shown in Figure 6.6(a) and (b). As the spring stiffness of the diaphragms is assumed to be linear, Figure 6.6(c) shows an equivalent system to the system shown in Figure 6.6(a) and (b) in a more "canonical form".

6.3.2.4 Mesh Size Inspection and Maximum Stroke Clamp Housing

The predictive quality of FEM is directly related to the mesh discretization. The solution of the problem is approximated by the linear combination of the simple basis functions of the elements and, hence, the finer mesh is, the better the approximation. On places with steep stress/strain gradients (local stress concentrations) the FE mesh should be fine. For this reason, the Von Mises stresses occurring in clamp housing have also been studied. Since the Von Mises stress is the invariants of the stress deviator tensor, it used as a yield criterion [51]: when the Von Mises stresses exceed a certain value, called the yield stress, at a certain point, plastic deformation occurs at that point.

In Figure 6.8, it can be observed that most of the stresses occurring in the clamp are located near inner and outer diameters of the diaphragms. Furthermore, it can be seen in Figure 6.8 that only three linear elements are used to model the diagram in the thickness direction. Most of the stresses and strains occur in the diaphragms, therefore the quality of the mesh should be increased in this area to give reliable qualitative description of the real displacement field. This can be done by two methods. Either the mesh should be refined in the area, or one can, by placing special transition elements [182] around the diaphragms, change the elements describing the diaphragms into higher order elements, as higher order elements yield usually good predictions.

From the calculated Von Mises stresses, the yield stress for spring steel (1,000 MPa) is reached in the diaphragms when the top pad moves up or down for 0.135 mm. In order to avoid plastic deformation, which causes lasting failure the flexure mechanism, the maximum actuator displacement should be below 0.135 mm.

6.3.2.5 Design Consideration

If one looks closely at Figure 6.4(a), one can see the base of the housing is mounted on the fixture base with a pad: a shaded area reveals the shape of a small recess. This recess

has a strongly adverse effect on the stiffness of the clamp housing. In case the constraint is only placed on the bottom of this edge, there is an extra pair of modes before the mode that only involves deflection of the flexure mechanism. This is a tilting motion for the whole casing. In case the other nodes that are on the bottom of the recess area are constrained as well, these modes do not occur. Furthermore, the PEA will push on the centre of the base as well, causing undesired deflection and thus limiting the efficacy of the actuator. It is therefore advisable to make the bottom of the base very flat and to leave the recess out of the design.

6.3.3 Conclusions of Analysis of Clamp Housing

The findings of this analysis can be summarised as follows:

- Static calculations have been used to determine the stiffness of the rod and of the diaphragms of the clamp housing.

- FEA confirmed that the stiffness of the case is higher when compared with the stiffness of the flexure mechanism and the rod. As a result, the stiffnesses of the rod and the flexure dominate the mechanic behaviour of the clamp and, hence, statically, the clamp can be modelled as a lumped-parameter system. Furthermore, as the stiffness of the case and the material of the fastening mechanism (between the diaphragms) are much higher, the diaphragms can be modelled with simple FE-models as, shown in the summary of the analyses in Table 6.3.

- Eigenfrequency and mode shape analysis revealed that the first mode, whereby the top pad moves, shows the same displacement as in the case when the top pad is actuated statically (load case: ''FE housing 3). This also proved to be the dominant mode. As a consequence, the clamp can be modelled as a lumped-parameter model.

- Stress analysis revealed in which areas mesh refinement should be applied.

- Furthermore, on basis of the the stress analysis the maximum allowable displacement could be calculated to be 0.135 mm.

- A design rule has been established. There is a recess at the bottom-side of the base of the clamp housing. The design of the clamp housing becomes significantly

stiffer when this recess is left out of the design.

6.4 Workpiece (NGV) Model

6.4.1 Obtaining a Parametric Model

Klärner [82] and Klärner *et al.* [83] have found a parametric model of the NGV. Firstly, a solid model of the NGV geometry has been studied. Subsequently, this model has been split in three parts as shown in Figure 6.9. After this the three parts have been reunited in commercially available FE-software (MSC.Marc$^®$Mentat$^®$). This model is further referred to as the 'full' or 'complex' model. An initial model, consisting of 542,788 linear tetrahedron (tet) and hexahedron (brick) elements was established. Subsequently, this 542,788 element model was reduced to a 117,963 element, 109,506 DOF model, shown in Figure 6.10. This model consists entirely of linear tetrahedron (tet) elements are used to build the model. As can be seen in Figure 6.10, e.g. on the outer bound, bottommost in the figure, the mesh is too coarse in cross sectional thickness direction (just one element) to make accurate calculations. It is worth considering the mesh of the 542,788 element model here. A part of the mesh of the outer bound of the 542,788 element NGV model is shown in Figure 6.11. This model already consists of 121,110 tet elements, comprising 96,996 DOFs. Based on these numbers, the 542,788 element complex model has an estimated 500k DOFs. However, as can be observed in Figure 6.11 also this mesh is too coarse for accurate calculations: more layers of elements are needed in wall thickness direction t in the region labelled in Figure 6.11 to provide an accurate approximation of the mechanical behaviour of the wall. When and if quadratic elements are applied, the accuracy of the model should increase drastically. When modelling with continuum solid 3D elements, it is reasonable to expect an accurate model of the NGV to have in the order of ten millions DOFs.

As the computational demands for such large models are high, for this reason, a parameterised model comprising a lower number of DOFs has been established by Klärner [82] and Klärner *et al.* [83]. This model has been established by studying the geometries of the three parts of the NGV as shown in Figure 6.9. The geometries of the cross-sections of the inner and outer bound have been simplified as shown in Figure 6.12.

Altogether a set of 30 parameters was used to describe the parameterised model. The second moments of inertia related to the centre of area I_{yy}, I_{zz} and I_{yz}, the principal moments of inertia I_1 and I_2, and their orientation γ, and the area A of the simplified cross-sections were compared with those of the full model. Because of the simplifications of the model, the seven mentioned evaluation criteria - the five inertias, orientation and cross-sectional areas - cannot all have the same values as the full model at the same time. Therefore, an optimisation has been carried out, to minimise the discrepancies between the magnitudes of the criteria and the full and the in the parameterised model.

This resulted in a final parametric FE-model consisting of 9696 linear brick elements or 50013 DOFs. The simplified model is shown in Figure 6.13. From Figure 6.13 two important observations can be made. Firstly, the geometry of blades or wings of the NGV, that have crescent-like cross-section in the complex model, is reduced to a parallelogram-like cross-section in the parameterised model. Furthermore, it can be observed that in most regions in the inner and outer bounds of the NGV, the mesh is too coarse in the y-direction. Since the geometry of the parameterised model is not as chamfered and smooth as the geometry of the complex model, the thin-walled character of the NGV is clearly revealed. It is therefore advisable, if another parametric model is to be made, to consider general shell elements that solve the Reissner-Mindlin and Koiter-Sanders plate problem [149, 150].

6.4.2 Establishing a Reduced Model

The parametric NGV model established by the authors of Refs [82, 83] has been used within the AFFIX project and within this work as FE-model of the NGV. The specific NGV studied in the AFFIX case study is assumed to be made of Rene 95 [91]. The latter is a nickel-based superalloy. Nickel(-based superalloy) crystals have orthotropic elastic properties. When parts are made of single crystal material, or when the part is directionally solidified after the casting process, which results in columnar crystals, the orthotropic nature of nickel is apparent. In these two cases the material has to be modelled as an orthotropic material. Rene 95 is a so-called equiaxed or poly-crystalline nickel-based superalloy. Which means that the component is made of many crystals that each have a random orientation and as a result, on a macroscopic scale, the material can

be modelled as an isotropic material [26]. The relevant material properties of Rene 95 as found in the CINDAS aerospace structural materials handbook [26] are given in Table 6.2.

In the viewing perspective of Figure 6.13, the 7 nodes at the clamping and locating points are within the inner and outer bounds (or: frames) of the NGV. These nodes are shown as if the NGV were transparent. Furthermore, six nodes were selected from the grinding area. This is a practical application of Saint-Venant's principle [159]. This principle states that as long as the region where load is applied, is far enough from the region where the reaction forces are studied, a complicated, distributed load can be substituted by an equivalent point load. In this case the load is applied at the machining region, which is sufficiently far away of the regions of interest: the clamping and locating points. The machining force input nodes are shown with a label in Figure 6.13. The degrees of freedom at these six nodes are to be retained in the reduced model. Subsequently, the model has been reduced by the Craig-Bampton method [28, 29] (see also Appendix A), which is commonly implemented in commercially available FE software, e.g. [149]. As the number of the so-called 'fixed interface modes' (FIMs) added to the model determines the quality of the modelled high(er) frequency behaviour [28, 29], further study of the FIMs of this particular case has been made. A more detailed description of this analysis can be found in Appendix B. It has been established that when 12 FIMs are included in the reduced model, an accurate model describing the static and the "low" frequency (up to ~ 1.5 kHz) dynamic behaviour of the fixtured NGV has been found. Each individual FIM adds another degree of freedom to the reduced model. Thus a model containing only 51 degrees of freedom has been established consisting of $(7 + 6) \times 3$ degrees of freedom from the retained nodes and 12 additional degrees of freedom from the FIMs.

6.4.2.1 Conclusions for Model Reduction of NGV

- A reliable low degrees of freedom model has been established that will be used for the setting of a model-based control for the clamps.

- FE model reduction for the NGV reduces the order from 10^6 (complex) or 50013 (simplified) to 51 DOF.

6.5   Controller Design

One of the objectives of applying an active fixture is to achieve minimal surface deformation during the machining process. During the grinding process it will be nearly impossible to obtain reliable measurements of the displacements in the machining areas. A good measure for the deformation of the part during the machining process caused by the grinding forces are the reaction forces caused by workpiece deflection as seen by the locators. In this study the control criterion is therefore the minimisation of reaction forces at the locators. For this reason, in this work it is assumed that the clamps and locators are equipped with force sensors. The scheme that is applied to control the force at each locator is shown in Figure 6.14.

Figure 6.14 shows the architecture of closed-loop force-feedback control for each active clamp. As there are four active clamps, there are four control inputs. The reaction forces at the three locators are the outputs. The active clamps and locators are all part of a single system: the part-fixture system. This means that the actively controlled part-fixture system is actually a multi-input multi-output (MIMO) system. A further discussion of MIMO systems would be inappropriate in the study of this particular application, however, some remarks on this subject are necessary. In the general case, proper multivariable controllers will have to be designed, as the controlled input variables can interact in an undesired manner with the other system variables [102, 151]. Only small interaction occurs between the controlled input variables, when the system is relatively flexible. In this case, the actuator output can be taken as the controlled system output (collocated control) and individual, nearly decoupled single-input single-output (SISO) feedback loops can be established [102, 151]. In this specific design the stiffness of the active clamps is much higher than the stiffness of the NGV. This means that the clamps do not interact with each other. Secondly clamp 1 and locator 1, and clamp 2 and locator 2 are nearly collocated. For this reason, this specific application shows that the system can be split into individual SISO subsystems. The loops of clamps 1 and 2 are established by measuring the reaction force at locators 1 and 2: $F_{\mathrm{loc},1}$, $F_{\mathrm{loc},2}$. These measured forces are compared with the reference values r_1 and r_2 that are set for clamps 1 and 2. The error signals go into the controllers, labelled as "block C" in Figure 6.14,

which steer the respective actuators until the desired outputs for the reaction forces at the locators, $F_{\mathrm{loc},1}$ and $F_{\mathrm{loc},2}$, are reached.

The closed-loops for clamp 3 and 4 are established as follows. The reaction force in locator 3 is measured and, as shown in Figure 6.14, compared with the reference values r_3 and r_4 respectively. The error signals are sent to the respective controllers, shown again as "block C" in Figure 6.14. Both clamps work with a force-control criterion for the same locator. In order to maintain a stable SISO system the reference values and control settings for both clamps must be the same: $r_3 = r_4$, as the system is only a SISO system, then the inputs of clamps 3 and 4 are the same.

In this study the main objective is to establish a model-based controller for a part-fixture for real-time control. In order to achieve this, a proportional (P) and a proportional integral (PI) controller have been investigated. In Chapter 7 their performance will be compared. As for the current fixture layout design, modal control [48, 50, 102] is not feasible, as modes of the part-fixture system are not easily observed and controlled. Moreover, one should ensure that the actuator is not exciting the uncontrollable modes of the fixtured NGV. These are, as revealed by the detailed study of the FIMs (see Section 6.4.2 and Appendix A), the vibrations of the wings. For this reason, proportional controllers combined with low pass filters (double-lag filters) have been established to ensure the stability at higher proportional gains and hence increase the performance of the P-controller. The transfer function $C(s)$ of the P-controllers including the double-lag filter reads then [48]:

$$C(s) = K_{\mathrm{p}} \frac{(s + \omega_{\mathrm{LF}})^2}{(\alpha_{\mathrm{LF}} s + \omega_{\mathrm{LF}})^2}, \quad \alpha_{\mathrm{LF}} > 1,$$

where the proportional gain is K_{p}, and the settings for the corner frequencies of the low pass filter $\omega_{\mathrm{LF}}/\alpha_{\mathrm{LF}}$, and ω_{LF} need to be tuned appropriately. In this study, the settings for the corner frequencies of the low pass filters have been taken the same for each clamp.

The second controller considered in this study is the PI controller. The transfer function $C(s)$ of the classical PI-controller is the following [48]:

$$C(s) = K_{\mathrm{p}} \left(1 + \frac{1}{T_{\mathrm{I}} s} \right),$$

where the proportional gain K_{p} and the integration time constant T_{I} can be adjusted to establish a controller that fulfills the requirements of the control system design. One of

those requirements is that the amplification for a higher range of frequencies is smaller than 1; such that the PI-controller limits the bandwidth of the active clamp, not to excite the uncontrollable wing vibration modes, as was mentioned above in the description of the design of the P-controller.

Applying PI control yields zero steady state errors. This results in one zero eigenvalue, meaning that the system is only marginally stable. This zero eigenvalue is related to the fact that clamps 3 and 4 both use the reaction force at locator 3 as their reference. As mentioned above, the condition to maintain a stable SISO system is: $r_3 = r_4$. It is imperative to apply this condition in order to avoid excitation of the mode belonging to the zero eigenvalue.

6.6 State-Space Realisation

Apart from the locators, most of the mathematical models that describe the actively controlled part-fixture system have now been established. When the locators are modelled, the models can be integrated and a state-space model can be established. Since the locators are considerably stiffer than the part, they can be modelled as spring-dashpot elements that are connected to single nodes, selected to be the locating points in the model reduction process, as is described in Section 6.4 and shown in Figure 6.13.

Although, the compliance (flexibility) of the part requires an over-constrained (statically indeterminate) design, to increase the stiffness of the part-fixture system, Figure 6.2 shows that the NGV is only clamped and located/supported in the z-direction, which is sufficient for the requirements of the demonstrator, where only loads in the z-direction are to be applied. The over-constrained system is created by the application of the four clamps and the locators, as can be seen in Figure 6.2(b). Since the NGV is a flexible part, there are no computational problems caused by the statically indeterminate state of the part-fixture system. For the requirements of this demonstrator sufficient constraint in x- and y-direction is provided by the friction present in the real world between the clamps and the part. A conservative approach is taken, it is assumed that friction does not contribute to the constraint provided by the fixture and therefore can be omitted. To avoid numerical difficulties caused by rigid body motion in the x, y-

plane, it was necessary to provide this constraint by removing the degree of freedom in the x-direction at clamping point 3 and the degrees of freedom in the x- and y-directions in clamping point 4, shown in Figure 6.13. (In this figure, the convention for the axes of the coordinate system is also illustrated.) These imposed boundary conditions are the most significant differences between the mathematical model of the demonstrator considered in this paper and the real industrial fixture being designed for the machining of the NGV. For the latter, the fixture design should provide ample constraint in x- and y-directions to sustain real-world machining loads that act in all directions.

The reduced NGV model has been coupled with the active clamp model established in Section 6.3 and the locators. A modal damping matrix has been established and the damping ratio β has reasonably been assumed 0.2 for all modes. This damping ratio has been estimated as an average value, due to the internal friction in the stack PZT elements in the PEA. The PEA will have a higher damping value and the friction in clamping and locating points will give several system modes larger damping ratios as well, however, for some modes this damping ratio will be an "optimistic" estimation. The overall model has been put into a state-space formulation and the differential equations that describe the transfer functions of the controllers have been rewritten into a first order system and added to the part-fixture model using the MATLAB® Control Systems Toolbox™ [100].

6.7 Conclusions

The conclusions and main findings of the modelling and analysis of the industrial case study thus far can be summarised as follows:

- Instead of using the raw power of model reduction techniques, for certain designs consisting of stiff and relatively compliant parts, careful analysis of the system allowed for the precise lumped-parameter models that describe a single (or a few) dominant mode(s). The numerical values of characteristic stiffness and lumped masses are then established based on FE- and/or analytical modelling.

- A low degrees of freedom and reliable dynamic model of the workpiece is established, using the methodology developed in the thesis.

- This reduced model is coupled with the mechatronic models of actuators (and sensors) and subsequently a model for controller design is established.

- The analyses of the clamp housing and the workpiece revealed the importance of establishing detailed dynamic models. Model reduction techniques are used to create condensed models, whilst preserving the characteristics of the system. The reduced model is an accurate enough representation of the full system dynamics, and the reduced models are of importance for real-time control.

- A design rule has been established with respect to the design of the clamp: for increased stiffness of the clamp, the clamp base should be designed without a recess, which is present in the current design.

- A dynamic model for the generation of clamping forces with PEAs has been developed in the chapter. The PEA model has been connected to the overall system model and controlled using the methodology set out in Chapter 3. This shows that this methodology is generic and easily expandable.

6.8   Tables

Table 6.1: Summary table for application of control design methodology in active fixturing.

step	description
	previous work
1	definition and design of the demonstrator: [5, 90]
2	establishing of a (parametric) FE model NGV (workpiece) by Klärner *et al.* [83] for verification of active fixture design
3	active clamp design and FE model: Ce.S.I. [5]
	current work
4	further FEA modelling clamp housing for establishing lumped-parameter-model clamp in order to build a small and yet fast and accurate model for model-based control design part-fixture system
5	establishing a sufficiently small dynamic actuator model
6	establishing mechatronic model of clamp by integration of models established in steps 4 and 5 (see above)
7	model reduction of FE-model workpiece (established in step 2) using commercially available FE-software in order to reduce the model size for the model-based control design
8	FEA to determine stiffness locators for equivalent spring-dashpot elements in order to build a small model after Refs [32, 109, 138, 142, 175]
9	selection of controller models
10	integration of models established in steps 6–9 into a single model in a state state-space form

Table 6.2: Material properties evaluated at room temperature of the nickel alloy NGV and the steel used for the fixture elements: the modulus of elasticity E, the Poisson's ratio ν and the density ρ), assembled from .

Material	E [GPa]	ν [-]	ρ [kg/m^3]
Steel	210	0.29	7800
Rene 95 [26]	209	0.31	8190

Table 6.3: Static stiffness of flexure mechanism. (*) g.p. = general purpose element

Model	N/0.1 mm	# Elements	Type [149]
FE housing 1	$0.82990k$		C3D8
FE housing 2	$1.0006k$		C3D8
FE housing 3	$1k$		C3D8
shell g.p.* tri	$0.96177k$	$20 \times 110 \times 2 = 4400$	S3
shell g.p.* quad	$0.96158k$	$20 \times 110 = 2200$	S4
axisym. shell g.p.* linear	$0.95969k$	90	SAX1
quarter disc linear	$0.96704k$	$6 \times 45 \times 137 = 36990$	C3D8
quarter disc quadratic	$0.96990k$	$6 \times 45 \times 137 = 36990$	C3D20
axisymmetric linear	$0.96799k$	$13 \times 90 = 1170$	CAX4
axisymmetric quadratic	$0.96889k$	$13 \times 90 = 1170$	CAX8
Kirchhoff-Love [158]	$1.024174k$	analytical model	
thin shell tri	$1.024174k$	$18 \times 224 \times 2 = 8064$	STRI3

6.9 Figures
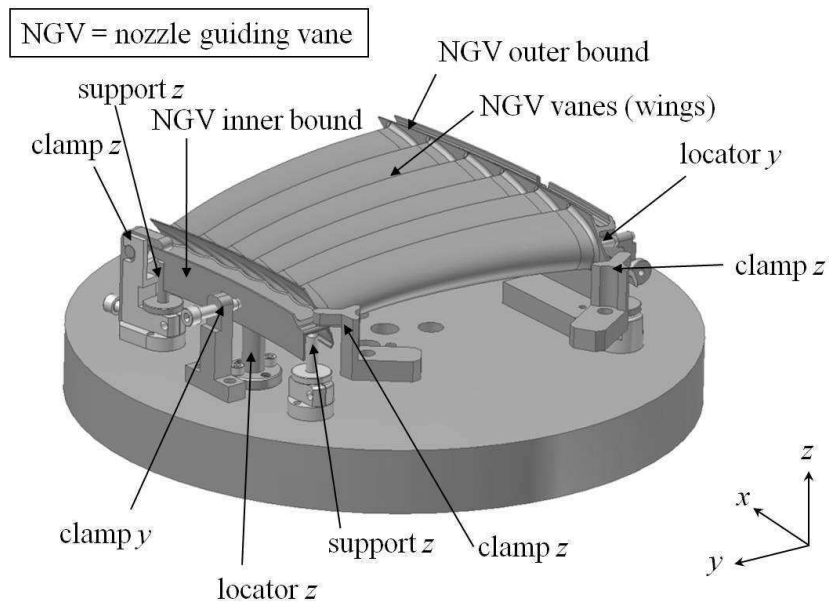
Figure 6.1: Solid model of current design for nozzle guiding vane grinding fixture (labels added). Source: Ref. [5].
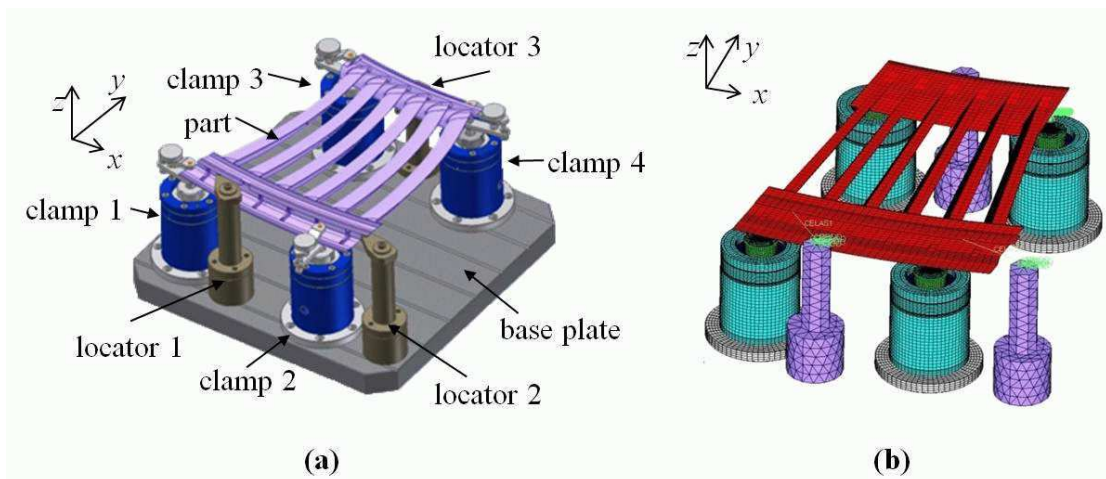
Figure 6.2: Concept demonstrator of adaptive fixture: **(a)** 3D solid model, source: [5]; **(b)** FE model of part-fixture system, source: [5].

Figure 6.3: Realised concept demonstrator, courtesy of Ce.S.I..

(a)   **(b)**
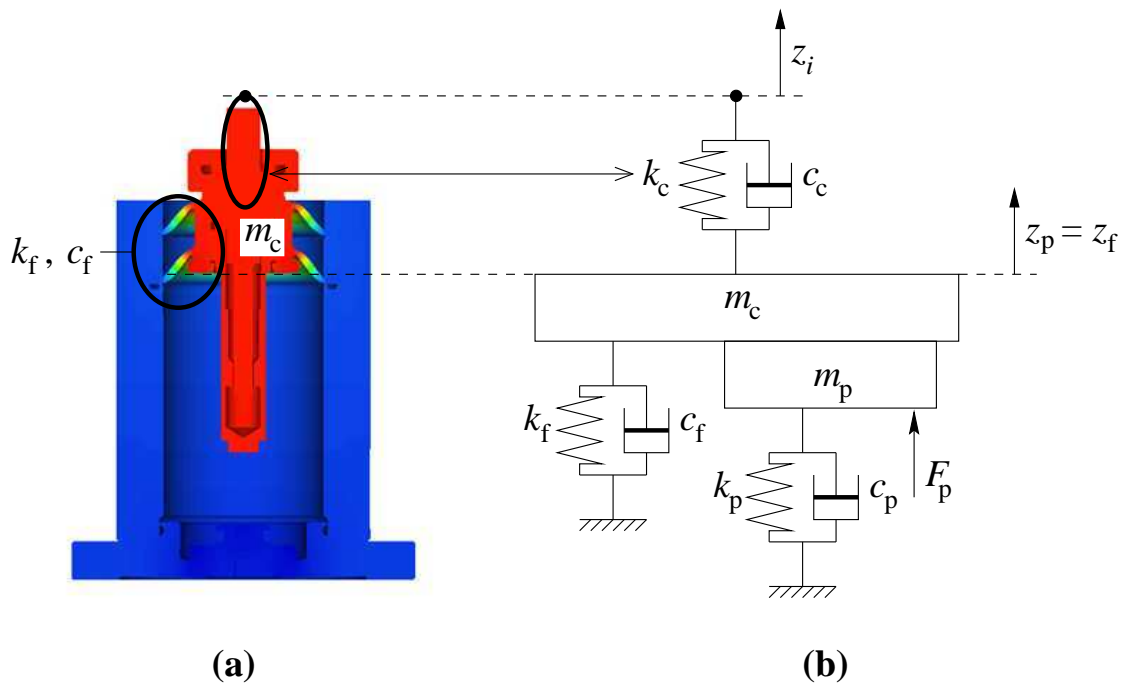
Figure 6.4: Models of the adaptive clamp: **(a)** full FE model, source: [5]; **(b)** simplified, linearised model of adaptive clamp.
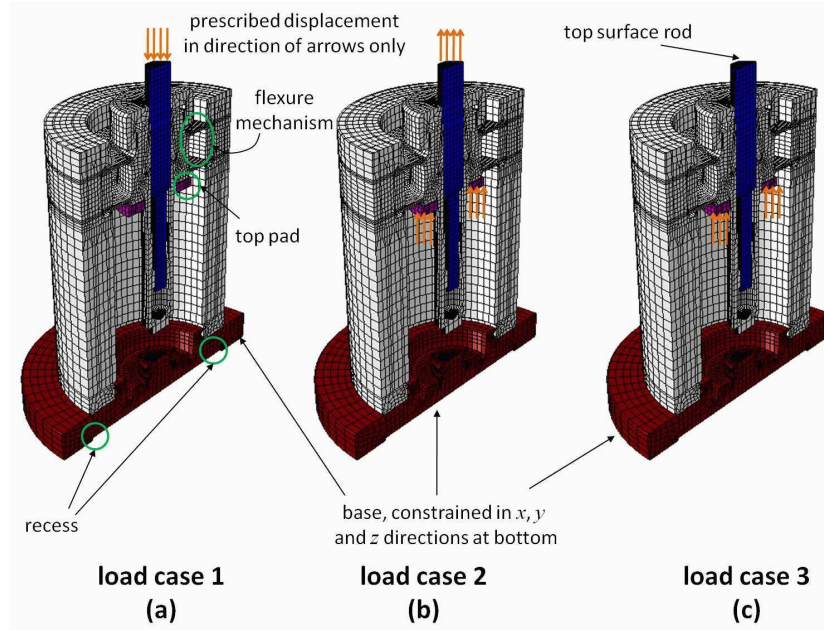
Figure 6.5: Boundary conditions static analyses.
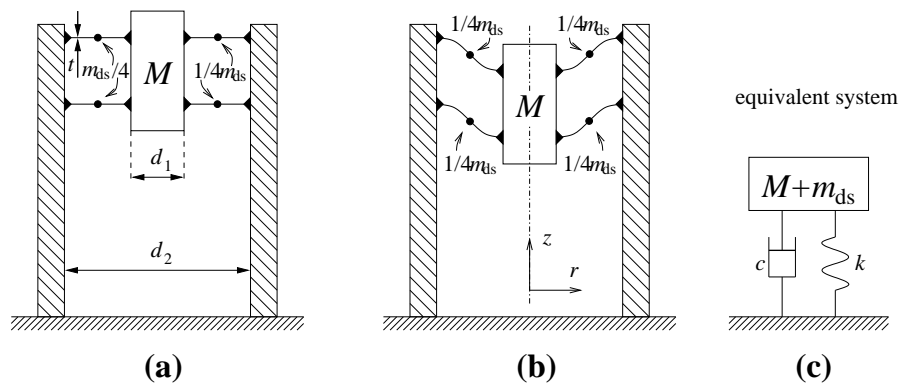
Figure 6.6: Cross-section of simplified model of actuator housing. Left: no deflection/base state, centre: deflection/mode shape, right: equivalent system.
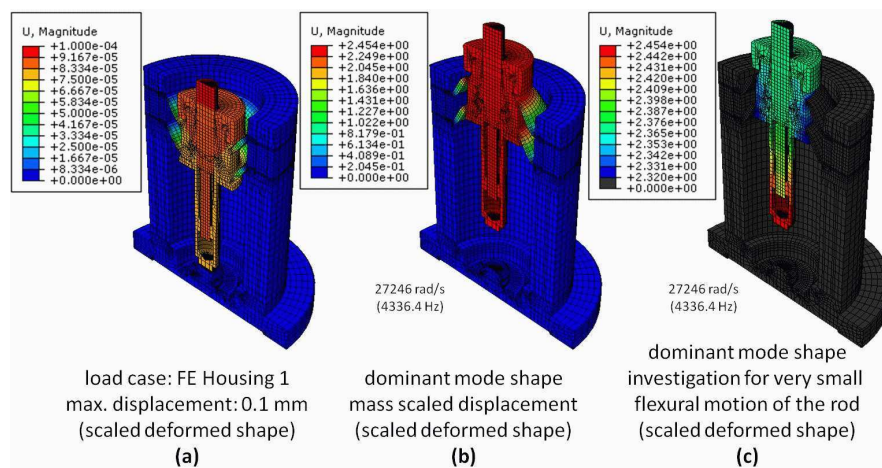
Figure 6.7: Results of FEA of the clamp housing.

155
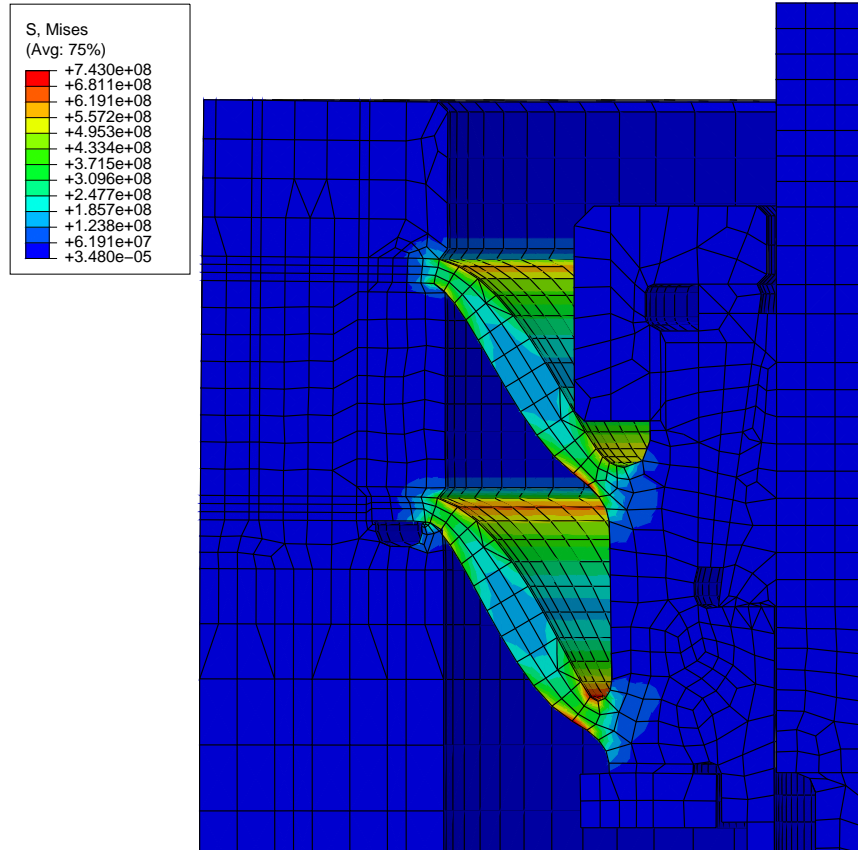
Figure 6.8: Von Mises stress concentrations on diaphragms.
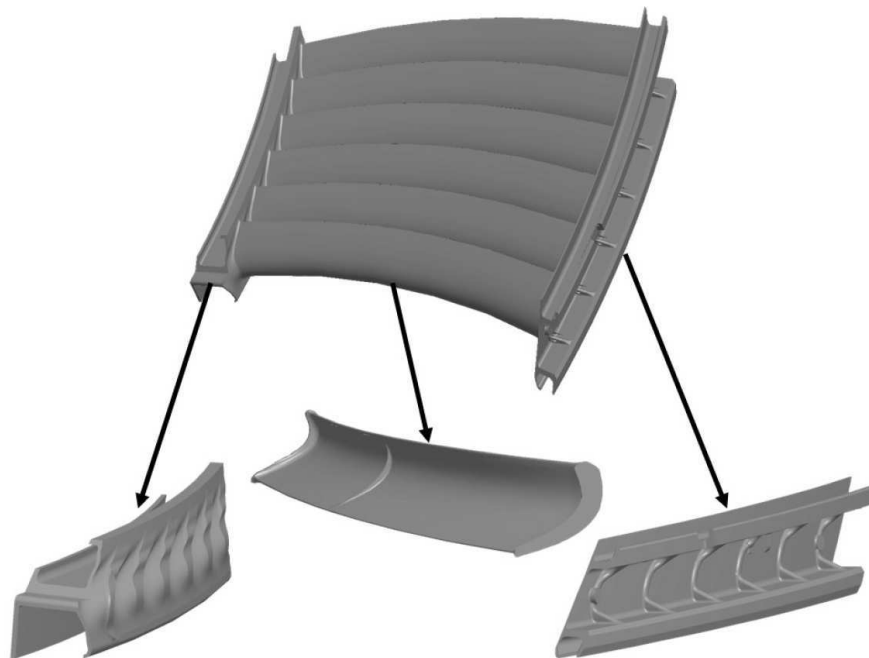
Figure 6.9: "Division of the NGV into three components", taken from [82].

156
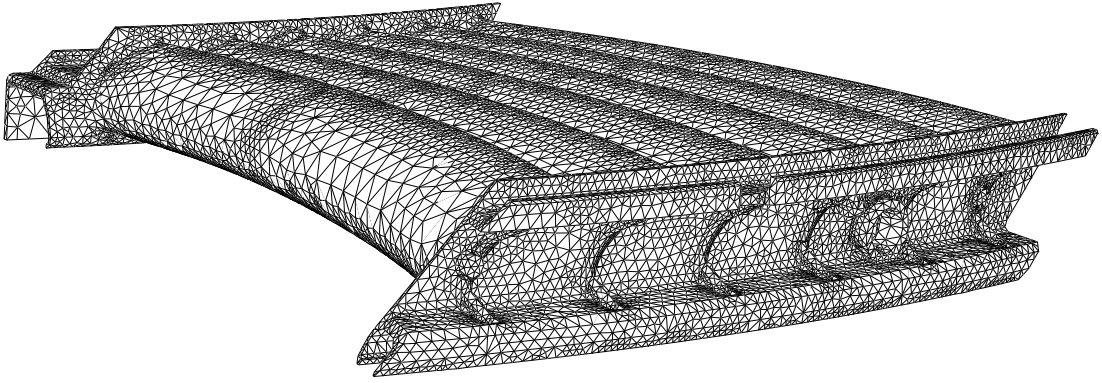
Figure 6.10: Mesh of the full model.
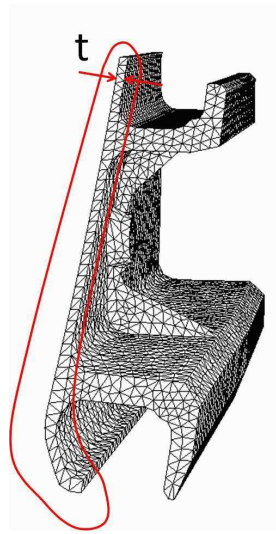
Figure 6.11: Mesh of the outer bound of the NGV, cross-sectional view.
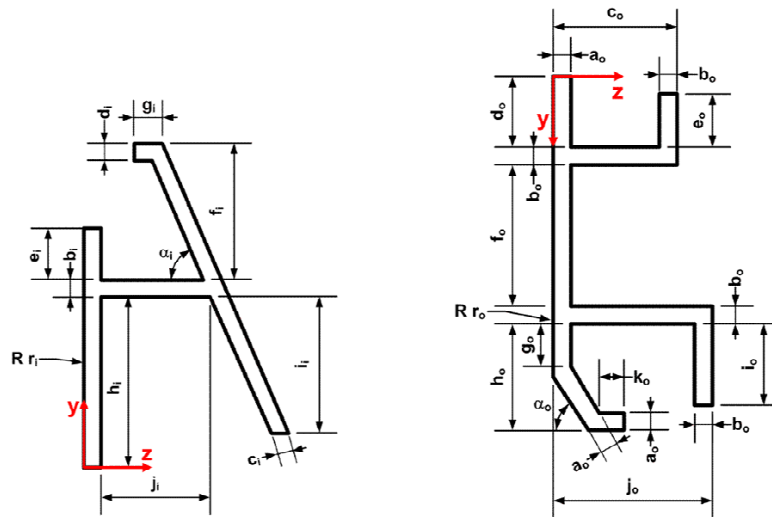
Figure 6.12: Simplified cross-sections, from [82, 83].

157
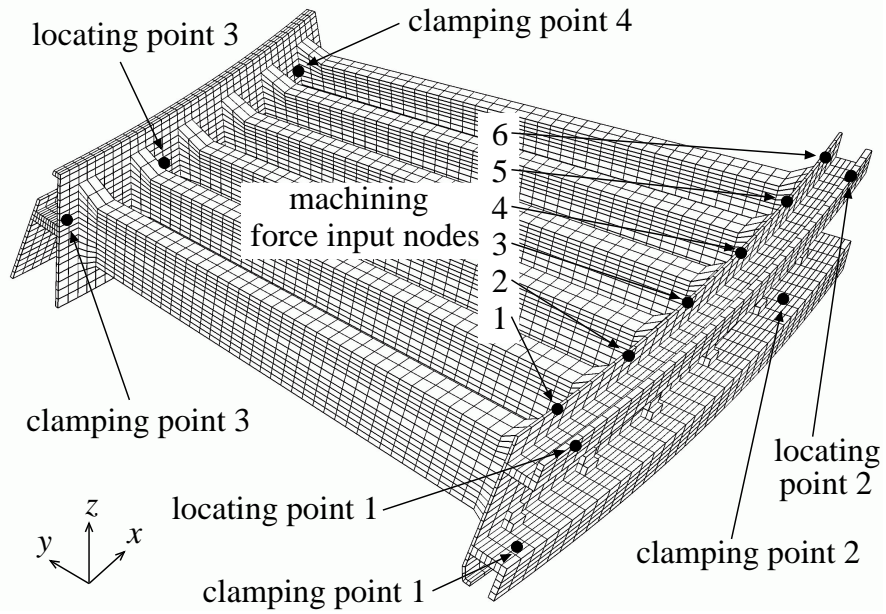
Figure 6.13: Retained nodes of NGV.
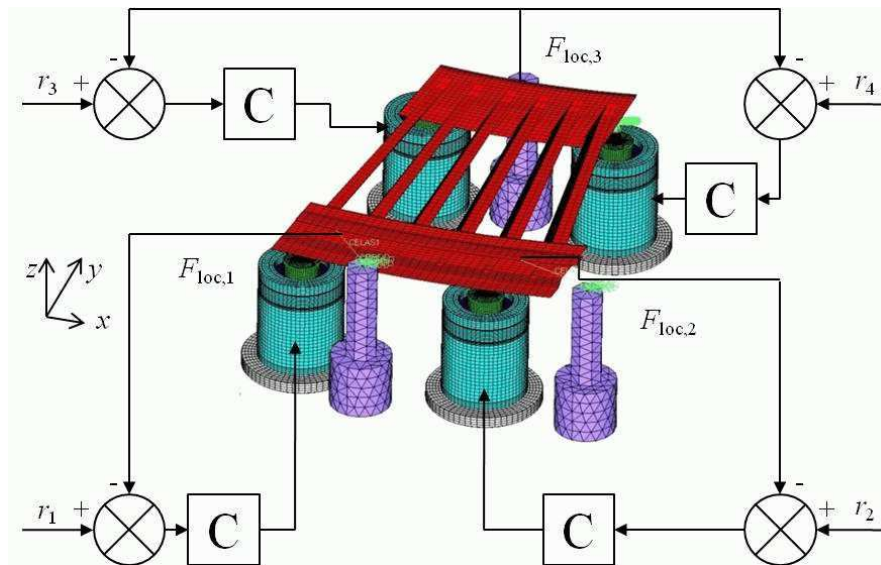
Figure 6.14: Physical representation of the control architecture.

158

Industrial Case Study: Results

7.1 Introduction

In this Chapter the application of the methodology and models established in this thesis is made for a complex, near-industrial fixturing system for a compliant part. In order to make the chapter self-contained, this paragraph is a repetition of the first paragraph of Section 6.1. Within the Affix research consortium the design of an existent machining fixture has been studied [5, 83, 90]. This case study involves the redesign of a grinding fixture for a family of nozzle guiding vanes (NGVs) as utilised by an aerospace manufacturer. This manufacturer makes gas turbines and is subcontractor for aero engine components. NGVs and aerospace components are typical low-volume high-value parts and generally are designed with tight tolerances. This requires accurate, reliable fixtures. The low number of parts manufactured, renders dedicated fixture designs economically inviable. For this reason a reconfigurable fixture design for the NGV family is desirable. The new fixture design also should deliver reduced setup times, an increased locating performance (positioning and aligning of the workpiece during the setup process), and minimal distortion due to clamping forces. These problems encountered by industry have, as can be observed in Chapter 2, received serious attention in scientific publications. The study carried out by the Affix research consortium focused mainly on the reduction of the setup times and the positioning and aligning of the NGV in the fixture. Actively controlled minimal clamping forces are kept outside this case study and form a goal beyond the horizon of the current time line for this case study. The work resulted in

a guidelines for the redesign and a technology demonstrator. Despite not being the focus of the case study, the developed system can also be used to minimise the distortion due to the clamping forces, and therefore the performance demonstrator will be analysed in detail in this chapter by studying a selected set of simulation results.

In Chapter 6, the (sub)systems have been analysed extensively, and small yet accurate models of the subsystems have been established. Subsequently, these systems have been connected into an overall system in a state-space form. This system has a low number of degrees of freedom (DOFs) and can be utilised for real-time simulation and control of the part-fixture system. In this chapter the performance of the demonstrator will be investigated. As has been established in Chapter 2, the fixture performance is determined by the shape variation and positional tolerances, the surface profile and quality (roughness). As the resulting machining process quality is related to the overall deformation of the part, a measure for the overall deformation are the reaction forces at the locators. Logically, more deformation should lead to higher reaction forces [115]. Consequently, the set control objective is to minimise the reaction forces at the locators. Both the clamps and the machining forces cause reaction forces at the locators. As the clamps are subject to control, but the machining forces are not, the machining forces should be considered as "disturbance" (in control engineering terms). Note that for workholding stability, contact between part and locators, hence reactions at the locators, are required. For these two reasons (machining process quality and workholding stability), the reaction forces at the fixture locators and the workpiece displacement at the machining region will be studied here. Additionally, tools developed in the field of control engineering, like step response analysis and frequency response analyses, will be applied to study the performance of different controllers. The outline of this chapter is as follows. Firstly, a recapitulation of the mathematical model established in Chapter 6 will be given. Subsequently, the bandwidth of an adaptive clamp and the disturbance rejection in the frequency domain are studied. After which the transient behaviour of the actively controlled system is studied, followed by discussion of a realistic simulation of a pass of a grinding wheel where the workpiece displacements and the reaction at the locators are considered. Finally, conclusions are given. Parts of Chapter 6 and this Chapter are based on Ref. [13].

7.2   System Description

In Figures 6.2 and 6.3 a solid model, a finite element (FE) model and the physical realisation of the demonstrator and are shown respectively. The demonstrator design is based on a real industrial fixturing system. However, this design involved a small reduction in the complexity of the system: there are no locating, clamping and supporting capabilities in x- and y- directions. The several components that can be distinguished from these Figures are labelled in Figure 6.2(a) and have been identified as subsystems in Chapter 6. In the Figure one can see that the workpiece, a NGV, is located by three locators in the z-direction and four actuated clamps are used to clamp the NGV onto the locators. The fixture base is assumed to be infinitely stiff. In Chapter 6, these subsystems have been analysed and small yet accurate models were established. A controller has been designed for the closed-loop control of the adaptive clamps. In the following sections, a reprise is given of the modelling of the actuated clamp, the workpiece and the design of the controller.

7.2.1   Clamp Modelling

Figure 6.4(a) shows a cross-section of the FE-model of the clamp housing. In this housing a piezoelectric actuator (PEA) is placed on the base of the the housing and is used to control the displacement of the top pad: this is marked as displacement z_p in Figure 6.4. This top pad is attached to a structure that is utilised to hold a rod with a gripper (see Figure 6.2(a)). As shown in Figure 6.4, the gripper is fastened to node i of the workpiece model, its displacement is in z-direction: z_i. This rod-holding structure itself is connected to the outer casing of the clamp housing by means of a flexure mechanism. Extensive finite element analysis has been applied to study the mechanical behaviour of the clamp housing. From this analysis it followed that the stiffness of the outer casing and the rod-holding mechanism is much larger than the stiffness of the rod and flexure mechanism. Hence, the flexure mechanism and the rod will dominate the mechanical behaviour of the clamp housing. A numerical modal analysis of the clamp housing confirmed this: there is a dominant mode whereby the casing does not undergo any motion, the rod-holding structure undergoes a translation and the only flexural motion is found in the flexure

161

mechanism. For this reason, the clamp housing can be modelled as a lumped-parameter model with a mass m_c, flexure stiffness k_f and k_c the equivalent stiffness of the rod and gripper.

On basis of Refs [4, 55] a lumped-parameter model for a charge feedback steered PEA was established. Since the clamp will have to provide force and displacement in positive and negative direction along the z-axis, a preloaded is placed on the PEA, and the lumped mass of the rod-holding mechanism and the lumped mass of the PEA can considered to be always in contact [4], as is shown in Figure 6.4(b). The equation of motion for the equivalent lumped-parameter system shown in Figure 6.4(b) is then given by Eq. (6.3.4) to be:

$$(m_c + m_p)\ddot{z}_p + (c_c + c_f + c_p)\dot{z}_p + \left(k_c + k_f + k_p + \frac{T_{em}^2}{C} \right) z_p - c_c\dot{z}_i - k_cz_i = \frac{T_{em}C_e}{B_2C}V_{pea}.$$

$$(7.2.1)$$

7.2.2 Workpiece (NGV) Model

The part is made of the heat resistive Rene 95 nickel-based super alloy. This isotropic material has a modulus of elasticity of $E = 209$ GPa, a Poisson's coefficient $\nu = 0.31$ and a density $\rho = 8190$ kg/m^3 [26]. By omitting some of its features such a small holes, and substituting some cross-sections by more regular shapes, a simplified parametric model of the NGV has been established [83]. This model has been established to reduce the computational effort compared with an accurate mesh discretization the solid model for a series of FE analyses of the part-fixture interaction design of the AFFIX case study demonstrator [5, 83]. This within the AFFIX project established parametric model has been used in the work presented in the thesis as well.

This 50013 degrees of freedom model has been reduced to 51 DOFs using the Craig-Bampton model reduction technique [28, 29]. From the full parametric model, the nodes on the locations of the four clamping points, three locating points have been selected. Furthermore, by a smart application of Saint-Venant's principle [159], another set of six nodes have been selected to model the machining area, as can be seen in Figure 6.13. These thirteen selected nodes equalise 39 DOFs. Additionally, twelve fixed interface modes (FIMs) [28, 29] have been added to improve the accuracy of the dynamics of the reduced model.

7.2.3 Controller Design

There are four actuated clamps, all connected to the same mechanical system, the NGV. The typical controlled outputs would be the actuator, clamp or workpiece displacements or the reaction forces on the locators. This makes the active fixture a multi-input multi-output (MIMO) system. In order to remove the cross-interference of the inputs, typically, special controllers are needed to control MIMO systems [151]. However, because of the specific design of the demonstrator, the stiffness of the actuated clamps is much higher than the stiffness of the NGV, (near-)collocated control of the part-fixture system is possible[1] [102]. This means that relatively simple controllers can be designed for this application. Since the locators are close to the clamps, it proved to be possible to apply near-collocated control and design four closed-loop controllers for the clamps. As shown in Figure 6.14, clamps 3 and 4 in Figure 6.2 are controlling the reaction force of only 1 locator. To avoid problems, these two clamps have been assigned the same controller settings. In order to avoid excitation of the high frequency modes of the fixtured system in case of open- or closed-loop controllers with *only* proportional control, the control action of the clamps has been bound in the frequency domain by application of low-pass filters. These designed low-pass filters are double lag filters [48]. In this chapter, the results are presented for an investigation of open-loop control and closed-loop control with classic proportional (P) and proportional-integral (PI) controllers [48, 50, 102].

7.2.4 State-Space Realisation

The models of the clamps and NGV have been connected. In order to accommodate the absence of constraint in the form of fixturing in the x- and y-directions, the constraint has been placed artificially by removing the degree of freedom in the x-direction at clamping point 3 and the degrees of freedom in the x- and y-directions in clamping point 4, with clamp numbering as in Figure 6.13. The physical coordinates of second order system have been transformed into modal coordinates. Subsequently, the controllers have been added, applying the tools as developed in Chapter 4.

---

[1]Calculations to quantify the cross-interference in closed-loop control have been carried out by one of the partners in the AFFIX-research consortium.

7.3 Active Clamp Bandwidth

A stable system requires that all real parts of the individual eigenvalues λ_n are strictly negative: $\Re(\lambda_n) < 0$. As a first step in control design the system stability is verified with an eigenvalue analysis of the system. The next step is to optimise the performance of the control system within the stability boundaries imposed by the system and the requirements set by the engineer. In this thesis, firstly, the response time of the system is considered. As there are many parameters in a complex near-industrial system, and hence a large set of results to present, only the bandwidth of clamp 1 is considered in this study. The bandwidth of a system is an important indicator of its performance.

The Bode plot of clamp 1 is shown in Figure 7.1. A Bode plot shows the amplitude of the response of a system output to a harmonic excitation for a fixed frequency at one of the inputs to the system, see Figure 7.1(a) and the phase change that occurs in this response with respect to the input signal, shown in Figure 7.1. This response is measured or computed for a whole range of input frequencies [48, 50, 102]. The frequency response can have a delay that can be expressed as a certain number of degrees in phase change: input $\sin(\omega t)$, output: $\sin(\omega t + \varphi)$, where φ is the phase change.

Figure 7.1 shows the Bode plot of a transfer function H where the actuator displacement $z_{p,1}$ has been selected as system response (or: output) for the steering voltage V_{pea} as input. In order to make a good comparison between the bandwidths of different control designs possible, the actuator amplitude for zero frequency (i.e. the steady state frequency) has been scaled to unity (1^0).

In Figure 7.1 the closed-loop P- and PI-control designs are compared with the open-loop system. The open-loop system is designed with the same settings of P-controller in series with a double-lag filter as the closed-loop control design. As mentioned above, this double-lag low-pass filter has been designed such that the actuated clamp does not excite the uncontrollable modes of the fixtured NGV. It has to be mentioned that since the active clamp is actuated by a PEA, the bandwidth of the active clamp is an order of magnitude higher than that of the low pass filter. For the design of the real industrial fixture it is advisable to change the layout of the fixture and make the part-fixture system stiffer. In such a way one can make optimal use of the high bandwidth of the PEA inside

the clamp and increase the performance of the whole active fixture system.

The bandwidth of a system is defined as the upper frequency for which the frequency response of the system, which has been scaled to unity for the zero frequency, gets for the first time below 50 %. The bandwidth for the open-loop system is 330 Hz, for closed-loop P-control 670 Hz, for closed-loop PI control 500 Hz. Applying closed-loop control in this case increases the bandwidth of the active clamps by 103 % and 52 %, respectively!

A system becomes unstable, when there is a phase delay of $\varphi = 180°$, and the system response, in this case the actuator displacement, is equal or larger than unity $z_{p,1} \neq (1^0)$. When looking at the phase plot in Figure 7.1, at a delay of $\varphi = 180°$, the actuator displacement is far smaller than unity, which indicates a stable system and this result is backed up by the earlier eigenvalue calculations.

7.4   Disturbance Rejection in the Frequency Domain

The control objective is to maintain the reaction forces at the locators at their set reference values. For this reason, the fixture is designed such that the clamps can elevate the reaction forces from the locators. The machining forces present during the machining process, should be considered as external disturbances.

Previously, the frequency domain analysis the bandwidth of the active clamp was established. The maximum obtainable bandwidth is limited by the construction of the clamp: the stiffness and mass of the flexure and actuator determine the maximum bandwidth. The bandwidth of the clamp when applied in the part-fixture system is further limited by the stiffness of the part. A compliant part such as the NGV limits bandwidth of the clamp below the theoretical maximum obtainable one. In this section the influence of the bandwidth of the active fixturing system is studied with respect to disturbance rejection in the frequency domain. Important characteristics for a part-fixture system can established on the basis of analyses in the frequency domain. For example, the forced response of the system due to sinusoidal machining force components[2] that excite the system at frequencies near or at one of the eigenfrequencies of the part-fixture system can

---

[2]With a Fourier transform all signals can be transformed into a series of sines and cosines.

be determined. Furthermore, the steady-state behaviour of the system can be predicted, by extrapolating the trends found for low frequency inputs in this analysis.

7.4.1 Method

To study the frequency response at these clamps and locators, sinusoidal input forces have been placed at nodes 3 and 6, shown in Figure 6.13, which are taken as representative force input nodes in the machining area. The sinusoidal force at force input node 3 has an amplitude of 6.5359 N. When a static load with this amplitude is placed on this node, the reaction force at locator 1 is exactly 1 N for the open-loop system.

7.4.2 Disturbance Rejection at Locator 1

Figure 7.2 shows the disturbance rejection at locator 1 in Figure 6.2 for a sinusoidal machining force applied at force input node 3 in Figure 6.13. It can be seen, that for the open-loop system the reaction at locator 1 remains 1 N up to a frequency of 300 Hz and due to interference with the natural frequencies of the fixtured NGV reaches a maximum of 2.25 N at 1500 Hz. The response at high frequencies goes to zero. The proportionally controlled system reduces the reaction forces at low frequencies to 0.434 N and on the range $100 - 360$ Hz it rises to 1 N and then up to 2.4 N at 1500 Hz before falling down for input frequencies that are beyond the natural frequencies of the system. The PI-controllers remove the steady state error at low frequencies, as deduced from the trends shown in Figure 7.2. Up to 165 Hz, the performance of the PI-controlled clamps is better than the P-controlled system. But from then onwards the performance of the PI-controlled system is slightly below that of the P-controlled system, when the maximum reaction force at locator 1 for the PI-controlled system becomes 2.8 N at 1500 Hz.

7.4.3 Disturbance Rejection at Locator 2

The frequency response at Locator 2 in Figure 6.2 is shown in the Bode plot in Figure 7.3. As input node 3 in Figure 6.13 is relatively far away from locator 2, the reaction forces at $0 - 100$ Hz are low: 0.074 N for the open-loop system and 0.069 N for the closed-loop, proportionally controlled system. The PI controlled system totally suppresses the

disturbance at 0 Hz (steady-state), but shows the highest response at the dominant resonance frequencies of the fixtured system at 560 Hz and 1925 Hz respectively.

7.4.4 Disturbance Rejection at Locator 3

From Figure 7.4, it can be seen that the amplitude of the reaction force at locator 3 at low frequencies is low for all the three systems. This is logical, as clamps 1 and 2 and locators 1 and 2 bear most of the reaction forces, as was observed earlier. The steady state response for the closed-loop PI-controlled system is zero, as can be observed from the trend in the Bode plots. However, when the input frequency is in the vicinity of the resonance frequencies of the fixtured NGV, the response for all systems becomes considerable.

7.4.5 Disturbance Suppression Action at Clamp 1

The control criterion requires minimal reaction forces at the locators, this means that a favourable system performance is shown by a low frequency response at a large frequency range. The actuated clamps are used to suppress the disturbance. Opposite of the locators, they should have an as large bandwidth as possible.

A static force of 6.5359 N acting in the z-direction at force input node 3 in Figure 6.13 yields a reaction force of 1.7 N at clamp 1 in Figure 6.2. It can be seen in Figure 7.5 that at 500 Hz the open-loop system reaches an peak response of 2.38 N, at 685 Hz the reaction force drops back to 1.7 N after which another peak response of 4 N occurs at 1528 Hz. At high frequencies that are beyond the resonance frequencies, the frequency response drops. In case of proportional closed-loop control, clamp 1 bears 2.2 N. At 525 Hz the reaction force of the clamp reaches 3.0 N and a second major peak response of 4.4 N reaction force occurs at 1528 Hz. The frequency response falls off at high frequencies as can be observed in Figure 7.5. The PI-controlled clamp bears 2.6 N at low frequencies. This is an increase of 0.9 N, hence it can be concluded that clamp 1 takes nearly all the load from locator 1 for steady state and in the lower range of input frequencies. Before the first peak response of 3.2 N at 530 Hz, there is a small decrease of 0.15 N in borne reaction force occurring over the frequency range of $30 - 239$ Hz. A second peak in the frequency response of 5.7 N occurs when the input force oscillates at

1528 Hz.

7.4.6   Disturbance Suppression Action at Clamp 2

In Figure 7.6 the control action at clamp 2 in Figure 6.2 to suppress a disturbance acting at node 3 in Figure 6.13 is shown. The disturbance has the form of a sinusoidal force acting in z-direction. One can see that the reaction forces projected in the frequency domain for the three different systems are rather similar: the lines are almost on top of each other. At low frequencies the reaction force at clamp 2 for the open-loop, the P-controlled and the PI-controlled system have and amplitude of 3.7 N, 3.8 N and 3.9 N respectively. At 500 Hz, 510 Hz and 525 Hz respectively there are small resonance peaks of 4.7 N, 5 N and 5.3 N respectively. At 1480 Hz 2$\times$ and 1510 Hz there are second resonance peaks in the reaction force of 7.4 N, 7.7 N and 9.5 N respectively for the three considered systems.

Bode plots only show the amplitude of forced response at a system output for a given stationary oscillation at an input. For the fixturing system under consideration the Bode plot gives the amplitude of the reaction forces that are purely due to the forced vibration. One has to keep in mind that force equilibrium is always present. If this would not be the case, rigid body displacement for the part would occur and the fixture would not be providing sufficient constraint to hold the NGV properly. The actual magnitude of the reaction forces for the pure forced vibration situation at a given point in the time domain can be smaller or larger than the magnitude of input force due to the phase difference between input and output. It is therefore not possible without precise reading the phase change in the Bode plots to reconstruct the reaction forces and force equilibrium at a certain point in time. A proof of force equilibrium is given in Section 7.4.8. Alternatively and more straight forward, force equilibrium can be studied using transient simulations. This is better way to study the transient behaviour of a system as it considers both free and forced vibration, which in terms of the mathematical model are the homogeneous and particular solutions of the set of ordinary differential equations that form the equations of motion of the system.

7.4.7 Disturbance Suppression Action at Clamps 3 and 4

From Figures 7.7 and 7.8, it can be seen that the amplitude of the reaction forces at clamps 3 and 4 at low frequencies is low for all systems. This is logical, as the machining area is far away from clamps 3 and 4 and locator 3 in Figure 6.2, but takes place in the plane normal to the y-direction, going through clamping point 1 and 2 and locator point 1 and 2. These clamps and locators bear most of the reaction forces, as was observed earlier. Due to deflection and moment around the x-axis only small forces are transmitted to clamps 3 and 4 and locator 3. However, at the resonance frequencies of the fixtured NGV, the response for all systems becomes considerable.

7.4.8 Verification: Force Equilibrium from Bode Plots

The models of the controlled systems can be verified by using the information of the Bode plots to check for force equilibrium. The phase difference shown in the Bode plots above is relative to the phase of the input force. For a sinusoidally shaped machining force F_{m} that is formulated as:

$$F_{\mathrm{m}}(t) = \hat{F}_{\mathrm{m}}\sin(\omega t),$$

the relation between the amplitude of the reaction force and the actual reaction forces $F_{\mathrm{loc},i}$ and $F_{\mathrm{c},i}$ at the locators and the clamps respectively at a given point in time are:

$$F_{\mathrm{c},i}(\omega) = -\sin(\omega t + \phi_i(\omega))\hat{F}_{\mathrm{c},i}(\omega); \quad F_{\mathrm{loc},i}(\omega) = -\sin(\omega t + \phi_i(\omega))\hat{F}_{\mathrm{loc},i}(\omega). \quad (7.4.1)$$

Where $\hat{F}_{\mathrm{m}}$ is the amplitude of the machine force, $\hat{F}_{\mathrm{c}}$, and $\hat{F}_{\mathrm{loc}}$, are the input amplitudes of the reaction forces at the clamp and the locator respectively dependent on input frequency ω, index i denotes the clamp or locator number, t is the time and ϕ is the phase-shift as a function of the input frequency. In Table 7.1, the reaction forces for non-preloaded system are given for sinusoidally shaped input forces at node 3 in the machining area shown in Figure 6.13. The input frequency is at $\omega = 1$ Hz (2π rad/s) and time t is $1/4 + n$ s, where $n \in \mathbb{N}_1$: $1, 2, 3, \ldots$. Force equilibrium in z-direction can be observed. Furthermore, these results are in agreement with the steady-state results obtained with the step responses studied in Section 7.5. The values are then established as follows. The amplitude of the reaction force at clamp or locator is evaluated at

$\omega = 2\pi$ rad/s in the bode-diagram and subsequently the phase is evaluated at $\omega = 2\pi$, after which both values are put in Eq. (7.4.1). For example, the reaction force at clamp 1, for the PI-controlled system is then:

$$F_{c,1}(\omega = 2\pi) = 2.5654 \sin\left(0.5\pi + \frac{1260}{360}2\pi\right) = 2.5654 \text{ N}.$$

When all reaction forces for each of the systems are summed, this equals the instantaneous value of the machine force: $F_m(t = 0.25 \text{ s}) = 6.5359 \sin(0.5\pi) = 6.5359$ N.

7.5 Step response of the part-fixture system

The part-fixture system under consideration is not a SISO second order system, but a MIMO system of much higher order, which makes the order of the system dependent on the transfer function one is studying. As a result, a study of a step response to this system cannot be directly compared with standard second order step response analyses [48, 50, 102]. Still, much information regarding the system performance can be extracted from a step response analysis. Firstly, all frequencies are present in a step, which means that a step can excite all modes in the system. Secondly, since the part-fixture system can be described as a system of second order differential equations. This means that the system comes to a steady state when excited by a step force, namely all the states of the system do not change over time: $\frac{d}{dt} = 0$. By comparing the reference values for the controlled states with the actual steady state values they have reached, one can evaluate and compare the steady state errors of the different control designs.

In (active) fixture design, the response of the system to machining forces is of special interest, as it determines the usefulness of the fixture. In this study even more, since the control criteria are the reaction forces at the locators. Therefore this study focuses on the input of a step shaped "machining" force F_m of 200 N downward in in z-direction on one of the force input nodes shown in Figure 6.13. The selected node for the step force input is the third node when counting the force input nodes from left to right in Figure 6.13. This node has been selected as it is in the middle of the machining area and, therefore, a representative selection from the set of force input nodes. The selected system responses are the reaction forces at the clamp and the locators, which can easily be measured with the force sensors in the clamps and the locators. The reaction force

$F_{c,i}$ at the clamp has the same value as the external force in Eq. (6.3.3), but the opposite sign.

As the machining area is between clamps 1 and 2, it follows that clamps 1 and 2 and locators 1 and 2 will have to take most of the reaction forces. This can be observed in the step response for the open-loop system, Figure 7.9, the step response for the proportionally-controlled closed-loop system, Figure 7.10, and the PI-controlled system in Figure 7.11.

Furthermore as expected, a force equilibrium can be observed in Figures 7.9, 7.10 and 7.11: the sum of all the reaction forces in the individual figures is 200 N all the time. In the closed-loop systems, the active clamps (mainly clamps 1 and 2) sustain extra force, changing the force equilibrium. It is therefore interesting to see what the magnitudes of the reaction forces at the clamps are.

Although strictly speaking, one cannot use the term settling time, in Figures 7.9, 7.10 and 7.11 one can observe that all the systems are coming within a 5 % bound of the steady state value within $5 - 6$ ms.

In Figure 7.9 the reaction forces at the locators and clamps for the open-loop system are shown. It can be seen that the step force is mainly borne by clamps 2 and 1, which is logical, as the clamps are stiffer than the locators and will attract most of the reaction forces. From the locators, it is mainly locator 1 that provides the reaction force. This force distribution is logical, as can be derived from Figures 6.2 and 6.13: node 3 is in between locator 1 and clamp 2.

In Figure 7.9 the reaction forces at the locators and actuators for the P-controlled closed-loop design can be seen. It is clear that proportional control still leaves a steady state error, as the locators are still delivering reaction forces. When Figure 7.9 and 7.10 are compared, it can be seen that the 14 N relieved from locator 1 have been taken by clamp 1.

In Figure 7.9 the reaction forces at the locators and clamps for the PI-controlled closed-loop system are presented. Applying a PI controller results in a zero steady state error, thanks to the integral action: there are no reaction forces on the locator at steady state. When Figures 7.9 and 7.11 are compared, it can be seen that from the 30 N relieved from locator 1, 20 N have been taken by clamp 1, and 10 N by clamp 2.

When the maximum response at locator 1 is compared, it can be seen that the maximum is of about 40 N for the three different systems. This maximum seems hardly affected by any of the controllers, or when the settings are changed, which is a clear indication of the system being of a higher order. A difference in bandwidth of the actuator was observed when different controllers are applied. Due to the fact that the fixtured NGV behaves as a higher order system, the observed difference in bandwidth of the actuator is not clearly visible. When this "disappearance" of difference in bandwidths is combined with the fact that the PI-controller gives a zero steady error, this makes the PI-controller a preferable choice over the P-controlled clamps, despite the fact that the clamp itself has a higher bandwidth when controlled by a proportional controller. Studying both frequency and step responses, one has to conclude that the system behaviour is effectively limited by the flexibility of the part. As mentioned before, it is advisable that the design of the industrial fixture puts more constraints on the NGV, in order to make the whole system stiffer.

7.6 Disturbance Rejection under Realistic Machining Loads

7.6.1 Modelling of Machining Forces

Here, the performance of the active fixturing system is investigated under more realistic loading conditions. However, the design of the demonstrator does not fully constrain all the degrees of freedom of the rigid body motion of the NGV, as explained in Section 6.6. Therefore extra, artificial constraints are placed by removing some degrees of freedom from clamps 3 and 4. The boundary conditions do not constrain the NGV in the x- and y-direction as the real grinding fixture would. In order to keep the displacements in those directions realistically small, it is better not to apply loads in those directions. However a grinding force has two components: in both normal and tangential directions [21, 68, 83]. It is therefore decided to apply grinding forces normal to the plane defined by the machining area, namely the z-direction, and leave the tangential component out of the simulation.

7.6.1.1 Travelling Load with Constant Amplitude

To compare realistic machining conditions with the previous established results, it has been decided to (a) have the machining force as a constant moving load as benchmark; (b) keep the maximum magnitude of the load at -200 N, which is the same magnitude as the one used for the step load. The observed reaction forces at the clamps and locators are smaller, though are still of the same order of magnitude as the reasonably assumed forces forces in Ref. [83]; (c) a ramp-shaped force is exerted by the grinding wheel on respectively force input nodes 1 and 6 to model the moments of (dis)engagement (or: 'run in' and 'run out') with the workpiece; and (d) as the system dynamics is reasonably fast and steady state is reached rapidly, it makes sense to keep the simulated time span as short as possible, considering the build-up of numerical errors [29, 102]. It has been decided to restrict the simulated machining time to 0.7 s. The results are presented over a time range of 0.8 s. The first 0.05 s show the system at rest and the last 0.05 show the system without forcing. The resulting force profile per force input node in the time domain is shown in Figure 7.12(a).

The resulting force profile can be thought of as a grinding force that is generated by a perfectly centric and perfectly round grinding wheel. The high frequency components that are present in a real grinding force can be reasonably assumed to have a relatively small influence on the system, as they are likely to be well beyond the resonance frequencies of the active clamps and the fixtured NGV in the frequency domain.

The locators work only unilaterally, as can be seen in Figure 6.2. The clamps are used to place a small pre-load on the locators, to ensure contact is always present, for this reason, reaction forces on all the locators are always equal or larger than zero:

$$F_{\text{loc},i} \geq 0.$$

Under these conditions lift-off from the locators does not occur at all times during the machining of the part, which is the essential condition for stable workholding. Furthermore, lift-off can also damage the force sensors, which is another reason for preventing this phenomenon. The necessary minimum clamping forces can be derived with aid of these transient simulations.

7.6.1.2 Travelling Load with Dynamic Amplitude

The transient force profile, described by Eq. (4.8.1) in Section 4.8.2.1, has been adapted such that $c_1 = 40$, $c_2 = 2.8526$ and $c_3 = 0.5$. When the coefficients have these values, the signal is linearly scaled from a maximum of 500 N as shown in Figure 4.23(a) to a maximum of 200 by coefficient c_1. For an input base frequency of $\omega = 350$ rad/s (55.7 Hz or 3342 rpm) the transient reaction force on the wheel and the applied force on each of the six input nodes is shown in Figure 7.12(b).

7.6.1.3 Method

In this Section the influence of the spindle speed on the fixture performance is studied. As benchmark, the fixture performance for the system undergoing a constant moving load ($\omega = 0$ rad/s), as established in Section 7.6.1.1 is compared with the system undergoing a moving load with a transient force profile as established in Section 7.6.1.2. Two realistic spindle speeds are considered here, these are $\omega = 100$ rad/s (15.9 Hz or 955 rpm) and $\omega = 350$ rad/s (55.7 Hz or 3342 rpm) respectively.

In case of a travelling load with constant amplitude, the results come close to the equivalent semi-static load case, as often used to model machining forces for fixture design verification in the literature, e.g. [108, 153, 155, 169] (see also Section 4.4). However, since ramp shaped signals are placed on the machining input nodes and the Fourier analyses of ramps reveals that a ramp signal consists of many frequencies, some modes of the part-fixture system are excited and small ripples in the results can be observed.

In case the spindle speed is 955 rpm, the sixth multiple of the base frequency is 95.5 Hz. This frequency of 95.5 Hz is well below the resonance frequencies and in the frequency range where the PI-controllers deliver a superior performance compared with the P-controllers, as can be seen in the Bode plots presented in Section 7.4.

At a spindle speed of 3342 rpm, the sixth multiple of the base frequency excites the system at 334 Hz. This frequency is still smaller than the resonance frequency which shows a peak in the Bode plots in the range $500-600$ Hz, but an increase in frequency response can be observed for both closed-loop systems, when compared with the results for when the spindle speed is 995 rpm.

7.6.1.4 Study of Forced System Response to Machining Load with Dynamic Amplitude

In this short section the forced response of the system undergoing the machining force with the realistic machining profile is studied. This study is similar to the procedure of establishing a point in the frequency response in a Bode-plot, where the forced response of a harmonic input is studied, in this study the response of the system to a set consisting of a linear combination of multiple harmonics is studied. Initially, this analysis was made to clarify some behaviour of the system that could not be understood straightforwardly. For this reason, the study has focussed on a forced response at machining force input node 6, instead of node 3, which is used as the force input node in Sections 7.4 and 7.5. This study still gives useful insight and representative results. In this section, only the closed-loop PI-controller are considered.

In Figure 7.13 the response of the closed-loop PI-controlled system to the stationary oscillating machine force applied on node 6 given by Eq. (4.8.1) at an input frequency of 100 rad/s (15.9 Hz or 955 rpm) is shown. It can be seen that within 0.01 s the large response of the free vibration is damped out.

This large response is caused by the loading condition, namely at $t = 0$ s, the amplitude of $F_\mathrm{m} = 200$ N and $\dot{F}_\mathrm{m} = 0$ N/s, which is similar to a step-shaped input. The study of step responses and the forced response illustrated in Figure 7.13, shows that the overshoot of the free response to a step-shaped input is quite large. However, this sort of input is not likely occur under real manufacturing circumstances, since the "spark in" and "spark out" of the grinding wheel are best described by a ramp-shaped force profile. A purely forced response occurs from $t = 0.01$ s onward and its amplitude is close to the amplitude found in Figure 7.21 at $t = 0.65$ s.

Furthermore, based on the results for the step response studied in Section 7.5, and the result presented in Figure 7.13, in the light of steep ramps, caused e.g. by an accidental collision between workpiece and tool, it is good to have a safety margin in the applied clamping pre-load. From the result shown in Figure 7.13, the short time-span taken for the machining simulation is justified, as even for this unrealistically short "machining pass" nearly all of the response is the forced response.

175

7.6.2 Open-Loop Response

In Figure 7.14 the reaction forces at the clamps and locators of the fixture for the open-loop system are shown. As could be expected for the open-loop system, the reaction forces at all the individual locators are never zero.

In Figure 7.15 the reaction forces at the clamps and locators of the fixture for the open-loop system are shown. As the system is relatively fast compared to the input frequencies, the maxima in the reaction forces fit in the envelope of the reaction forces for the open-loop system with a moving constant load of 200 N.

Figure 7.16 shows the reaction forces at the locators and clamps for a moving load that oscillates at a base frequency of 350 rad/s (55.7 Hz or 3342 rpm). This input frequency is still below the eigenfrequencies of the open-loop system and the maxima of the reaction forces still coincide with the reaction forces as presented for case the open-loop system is loaded by a moving constant load.

7.6.3 Response of Closed-Loop, P-Controlled System

In Figure 7.17, the reaction forces at the clamps and locators of the active workpiece holder for the closed-loop proportional-control design are shown. When the reaction forces at the locators for this system are compared with those of the open-loop system, it can be seen that the controller gain for clamp 1 is such that at $t = 0.15$ s it reduces a 54 N reaction force on locator 1 in the open-loop system to a 28 N, which is roughly the same reduction as shown for the step response in Section 7.5. Possibly, the controller gain for clamp 1 could be tuned a bit more favourably (read: higher gain), as at $t = 0.65$ as the closed-loop P-controller for clamp 2 reduces the reaction force on locator 2 from 78 N open-loop to 31 N, which is a better performance.

In Figures 7.18 and 7.19 one can see the reaction forces for a transient simulation of moving loads with input base frequencies of 100 rad/s and 350 rad/s respectively. Similarly to the open-loop system, the reaction forces in the closed-loop P-controlled system fall in the envelope of the reaction forces encountered in the P-controlled closed-loop system with a moving constant load of 200 N.

7.6.4 Response of Closed-Loop, PI-Controlled System

The reaction forces at the clamps and supports of the closed-loop PI-controlled system are presented in Figure 7.20. The moving load creates a very small error all the time: small reaction forces are ever present at the supports during machining. However, these forces are of a total different order than the reaction forces at the supports for the open-loop and closed-loop P-controlled systems, as can be seen when Figure 7.20 is compared with Figures 7.14 and 7.17. The reaction forces at the supports are 'funny' looking, step shaped responses. Because of the discrete nature of the model, the travelling machine load is modelled as a series of ramps, as shown in Figure 7.12(a). The closed-loop PI controlled system can almost perfectly compensate for ramp-shaped machine loads: only small piecewise almost-constant deviations from the reference values for the reaction forces at the supports remain. If more force input nodes were retained from the full FE model of the NGV, these steps would become smaller and in the case of the real system, a smooth continuous line will be observed.

From Figure 7.21 it can be seen that applying a PI-controller in the closed-loop system changes the behaviour of the oscillations: the reaction forces at the locators oscillate around a value. Since a pre-load is delivered by the clamps, the reaction force at the locators is always larger than zero:

$$F_{\text{loc},i} > 0,$$

which ensures contact between the locators and the NGV is always present.

In Figure 7.22 the reaction forces of a closed-loop system for a pass of "machining force" with a base frequency of 350 rad/s (55.7 Hz or 3342 rpm) are shown.

7.6.5 Further Discussion

Some more general observations can be made from these figures:

- As observed in Section 7.5, from the results shown Figures 7.14, 7.17 and 7.20 one can see that there is a force equilibrium: the sum of the reaction forces is always equal to 200 N.

- As already observed in Section 7.5, the reaction forces at support 3 and clamps 3 and 4 are relatively small compared to the other reaction forces. For this reason, the reaction forces for clamps 3 and 4 are hardly distinguishable, as shown in Figures 7.17 and 7.20.

- In Figures 7.14, 7.17 and 7.20, it can be observed that the fixed reference values for the reaction forces at the supports are different. Since in this particular 'fixture layout' the clamping and supporting points are more or less equally distributed, the set reference value for the reaction forces at the supports should be the same for every clamp. This will result in a more equal distribution of the workpiece deformation due to clamping forces.

- As mentioned in Section 7.5, the machining load is mainly sustained by clamps 1 and 2 and to some degree by supports 1 and 2, for the open-loop and the proportionally controlled closed-loop systems. The actual magnitude of the load that is borne by individual fixture elements depends on where the load is applied.

- Figure 6.2(a), shows that the clamps constrain the part displacement in both positive and negative directions along the z-axis. As a result, the design allows for the reaction forces at the clamps to become negative. Between 0.52 s and 0.75 s, the distribution of the forces is such that the reaction force at clamp 1 becomes negative for all studied systems. This result can be used to calculate the necessary minimum preload for the actuators.

- A ramp shaped force input does not excite the system as harshly as a stepped shaped force: the overshoots in the systems are negligible as can be seen in Figures 7.14, 7.17 and 7.20. One needs to zoom in strongly to see the overshoots. Also, since the closed-loop systems are faster than the moving load, the dynamic effects of the changing load are hardly observable.

Furthermore, due to the relatively large distance between the force input nodes, the lines in the diagrams are not as smooth as they will be in reality. This can be seen in the discontinuities in the lines between $t = 0.15$ s and $t = 0.65$ s in Figures 7.14, 7.17 and 7.20. Especially the reaction forces at the supports in Figure 7.20 suffer from

this, for the reasons mentioned above. However the simulation still gives a very good indication of what can be expected when a moving load is applied to these systems in the real world.

7.7 Conclusions

The conclusions can be summarised to the following conclusions relevant to the overall work in this thesis:

- Active, feedback-controlled clamps can be effectively used to reduce chatter and to minimise clamping forces.

- The control design methodology has been applied to a complex near-industrial case study, which proves that the subsystem models can be derived and connected into an overall model.

- Extensive parameter studies have been conducted to assess the performance of the control design in terms of absolute and workholding stability and chatter suppression.

- The integration of the PEA model in the overall model of the active fixturing system, shows that the design methodology has wider applications and new actuator models can been added to the overall system.

7.7.1 Case Study Specific Conclusions

Some important conclusions that are more specific to this case study, but that are in a looser connection with the main body of work presented in this thesis, can be drawn. Two main conclusions specifically relating to this case study can be drawn from this results presented above. Firstly, the effectiveness of the control system, i.e. the active clamps is limited by part flexibility and the higher-order dynamics of the part. When the NGV is more constrained, the whole system becomes stiffer, the actuators would still excite the uncontrollable modes, but at much higher frequencies. Generally speaking, stiffer systems are faster systems. In this way one makes optimal use of the large bandwidth provided by the PEAs for actuating the clamps. Secondly, when PI controllers are

179

applied, the errors which are measured as reaction forces at the locators under machining conditions are almost zero and steady-state errors are not present at all. Due to the dynamics of the fixtured NGV, the response of the closed-loop PI-controlled clamps is as fast as that of the open-loop system and the P-controlled system. This makes the PI-control design a far superior and more preferable design choice than the control system design with a P-controller. Some other conclusions can be summarised as follows:

- The reduced model is an accurate enough representation of the full system dynamics.

- The magnitude of the required pre-load, applied on the PEAs inside the clamps, can be established from the result of the dynamic simulations of the intended machining operations.

- The magnitude of the needed pre-load, applied on the locators by the clamps, can be established from the results of dynamic simulations of the intended machining operations.

- Simulation results of the control design confirm the feasibility of a collocated control strategy.

- Regarding the predictable input of the machining forces in case of grinding: feed-forward control is an appropriate candidate to control the reaction forces in a fixture.

As a rule of design, it is advisable for the industrial fixture, that the fixture layout is changed in order to increase the stiffness of the part-fixture system and make optimal use of the large potential bandwidth provided by the PEA.

7.8 Table

Table 7.1: Reaction forces for a machining force 6.5339 N applied in z-direction at force input node 3 oscillating at $\omega = 1$ Hz compared for: OL = open loop system, P = P-controlled closed-loop system, PI = PI-controlled closed-loop system.

$F_{c,i}/F_{loc,i}$	OL [N]	P [N]	PI [N]
clamp 1	1.7055	2.2046	2.5654
clamp 2	3.6765	3.7563	3.9042
clamp 3	0.0213	0.0015	-0.0013
clamp 4	0.0152	0.0426	0.0675
locator 1	1.0008	0.4349	1.42×10^{-5}
locator 2	0.0744	0.0691	7.25×10^{-6}
locator 3	0.0422	0.0269	6.71×10^{-7}
total	6.5359	6.5359	6.5359

7.9 Figures
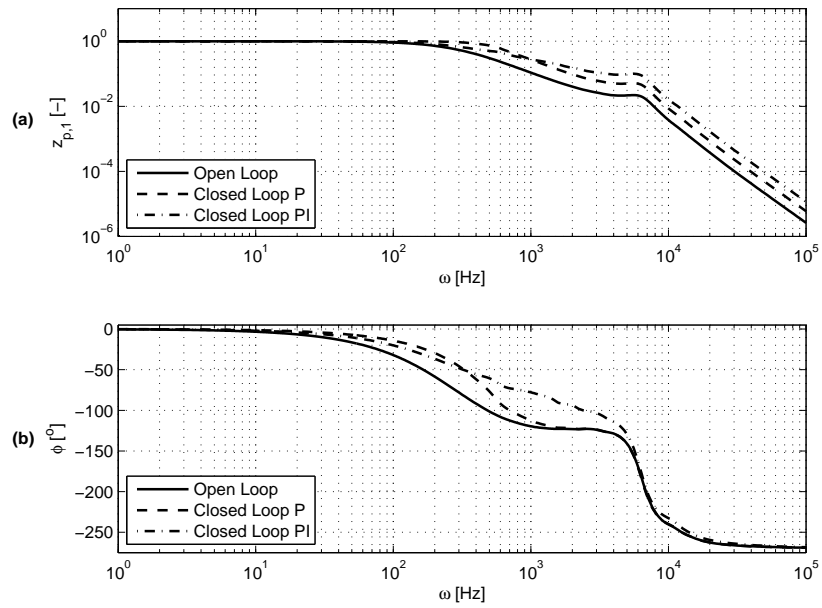
Figure 7.1: Bode plot actuator 1 for $H = \frac{z_{p,1}}{V_{\text{pea}}}$; **bandwidth**: open-loop: 330 Hz; closed-loop P-control: 670 Hz; closed-loop PI-control: 500 Hz.
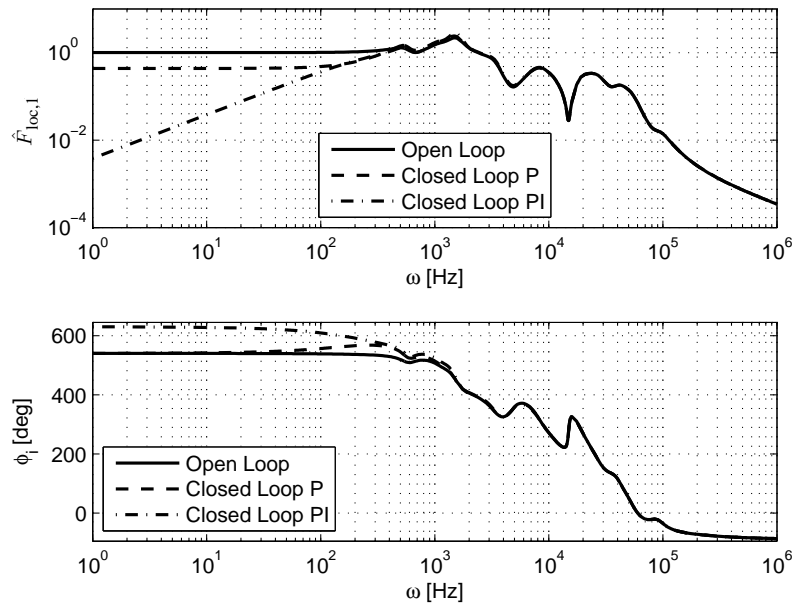
Figure 7.2: Bode plot: input F_{m} of 6.5359 N on third force input node; output: $F_{\text{loc},1}$.
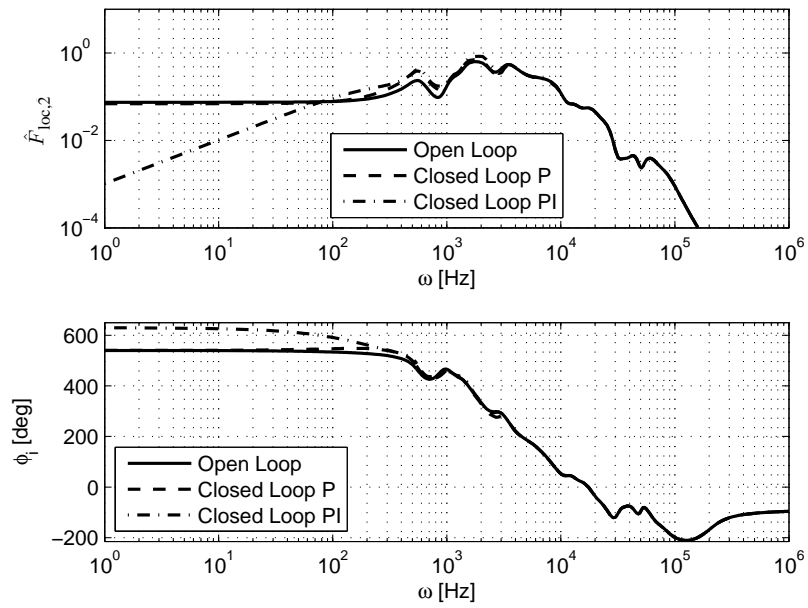
Figure 7.3: Bode plot: input F_m of 6.5359 N on third force input node; output: $F_{\mathrm{loc},2}$.
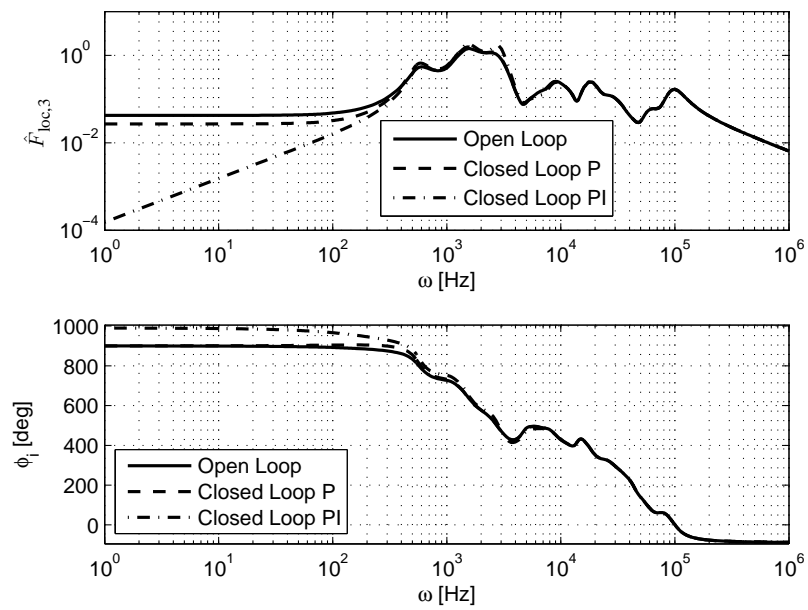
Figure 7.4: Bode plot: input F_m of 6.5359 N on third force input node; output: $F_{\mathrm{loc},3}$.
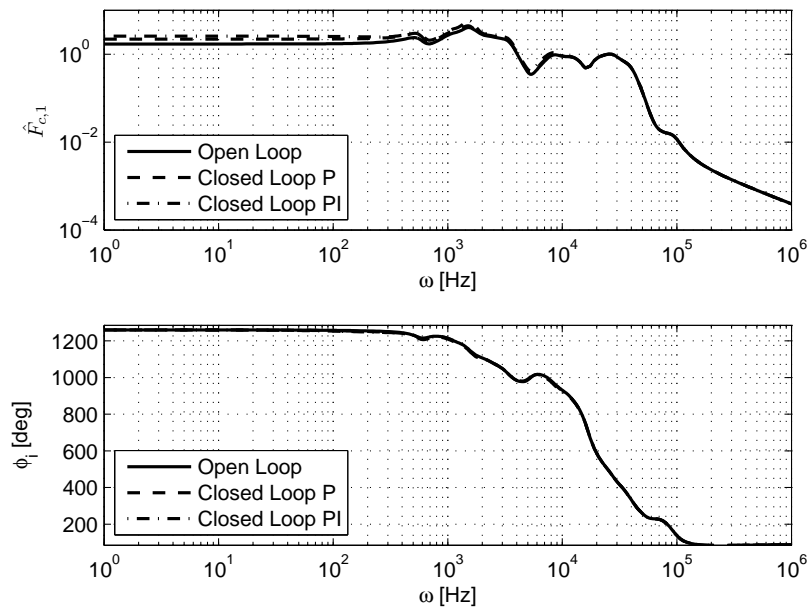
Figure 7.5: Bode plot: input F_{m} of 6.5359 N on third force input node; output: $F_{\mathrm{c},1}$.
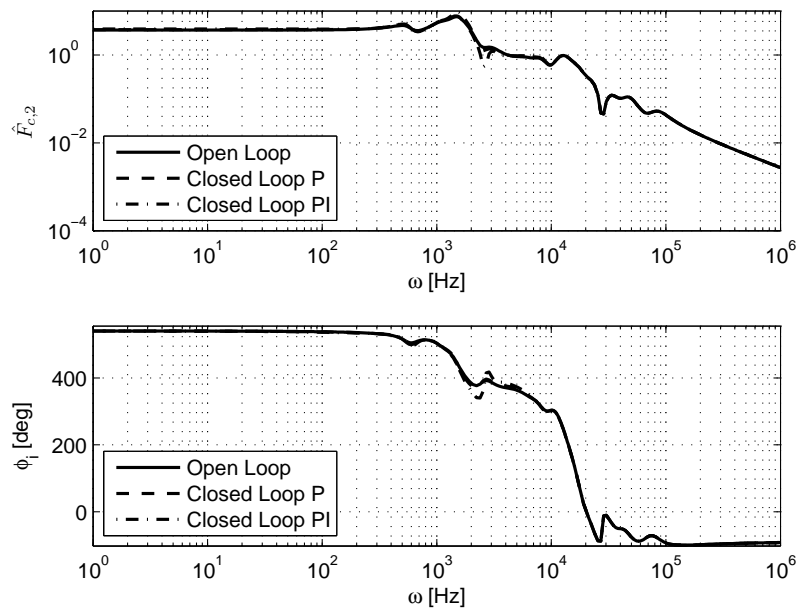
Figure 7.6: Bode plot: input F_{m} of 6.5359 N on third force input node; output: $F_{\mathrm{c},2}$.

184
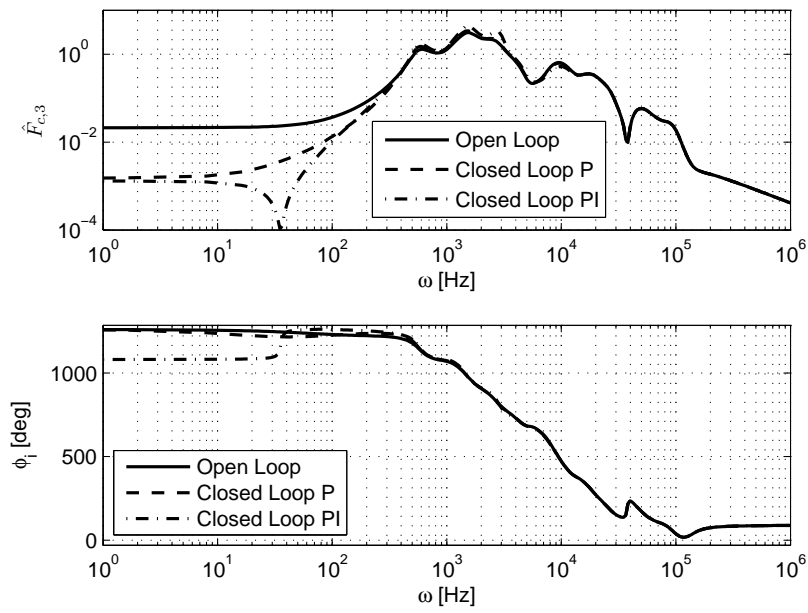
Figure 7.7: Bode plot: input F_m of 6.5359 N on third force input node; output: $F_{\mathrm{c},3}$.
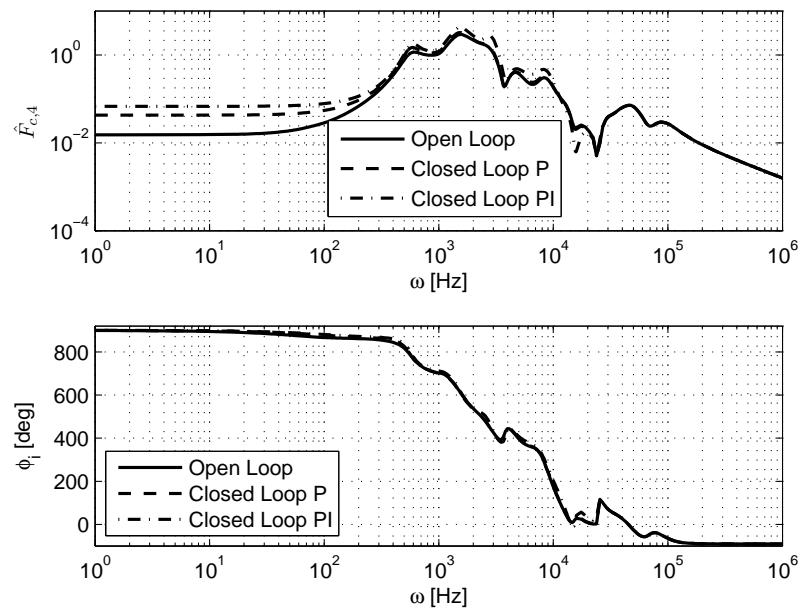
Figure 7.8: Bode plot: input F_m of 6.5359 N on third force input node; output: $F_{\mathrm{c},4}$.
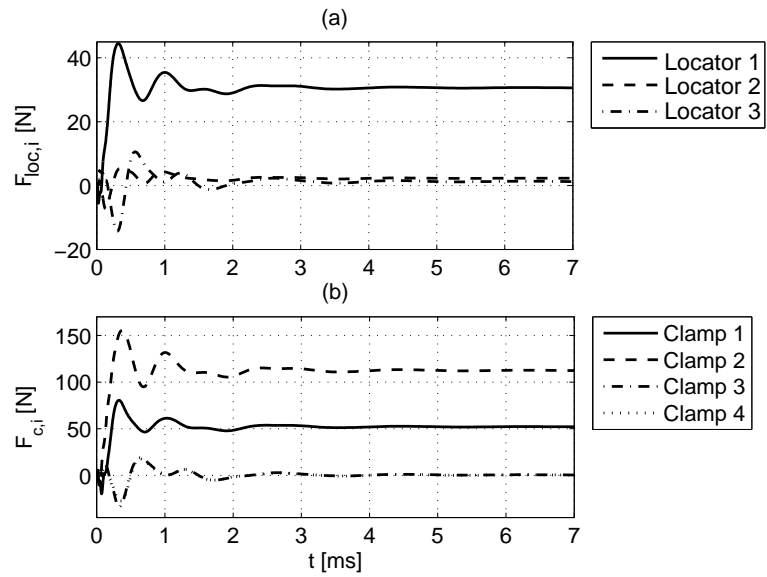
Figure 7.9: Response of the open-loop system to step force $F_\mathrm{m} =$ -200 N in z-direction at node 3; with: **(a)** the reaction forces $F_{\mathrm{loc},i}$ seen by the locator; and, **(b)** the reaction forces $F_{\mathrm{c},i}$ at the clamp. Index i indicates the respective clamp or locator number.
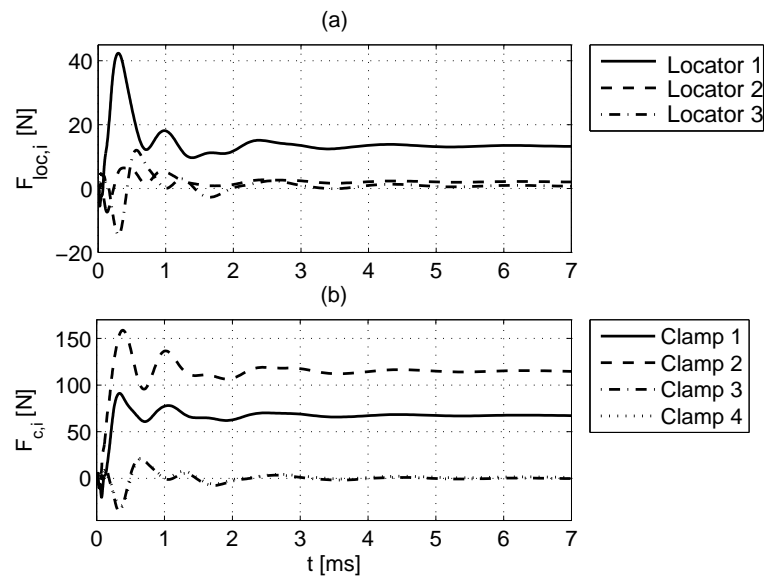
Figure 7.10: Response of the closed-loop system with proportional control to step force $F_\mathrm{m} =$ -200 N in z-direction at node 3; with: **(a)** the reaction forces $F_{\mathrm{loc},i}$ seen by the locator; and, **(b)** the reaction forces $F_{\mathrm{c},i}$ at the clamp. Index i indicates the respective clamp or locator number.
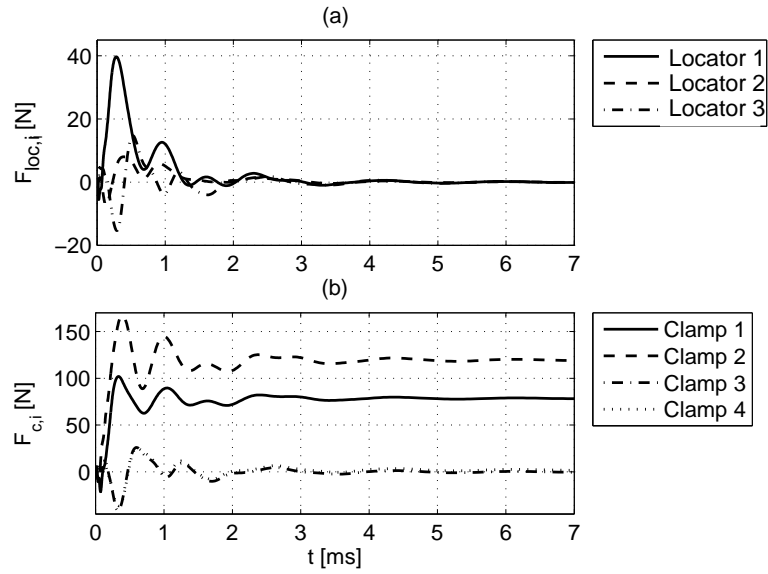
Figure 7.11: Response of the closed-loop system with PI controller to step force F_m = -200 N in z-direction at node 3; with: **(a)** the reaction forces $F_{\mathrm{loc},i}$ seen by the locator; and, **(b)** the reaction forces $F_{\mathrm{c},i}$ at the clamp. Index i indicates the respective clamp or locator number.
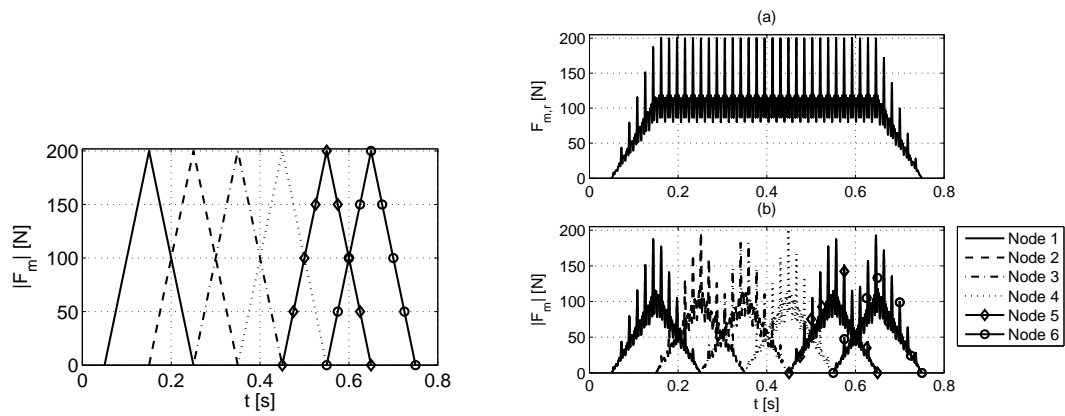
(a) Transient load applied to the nodes, with the same legend as in Figure 7.12 **(b)**, nodes numbers as shown in Figure 6.13.

(b) Reconstructed machine force profile F_m, ω = 350 rad/s (55.7 Hz or 3342 rpm), with: (a) Reaction of the grinding force on the grinding wheel; (b) transient load applied to the nodes.

Figure 7.12: Transient machining load models.
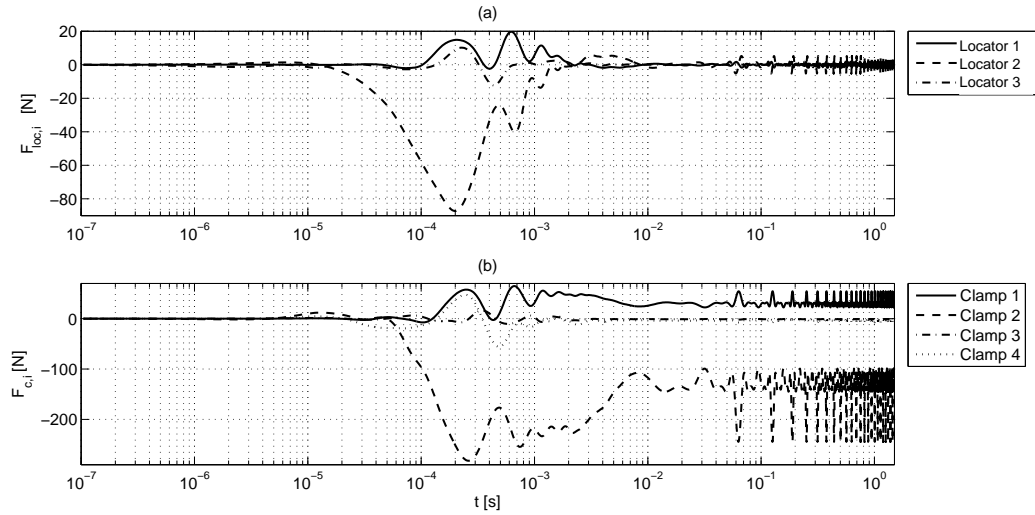
Figure 7.13: Response of a closed-loop system with PI-controller to a stationary "ma-
chining force" at a rotational wheel speed of $\omega = 100$ rad/s (15.9 Hz or
955 rpm) in z-direction on force input node 6 with: **(a)** the reaction
forces $F_{loc,i}$ seen by the locator; and. **(b)** the reaction forces $F_{c,i}$ at the
clamp. Index i indicates the respective clamp or locator number.
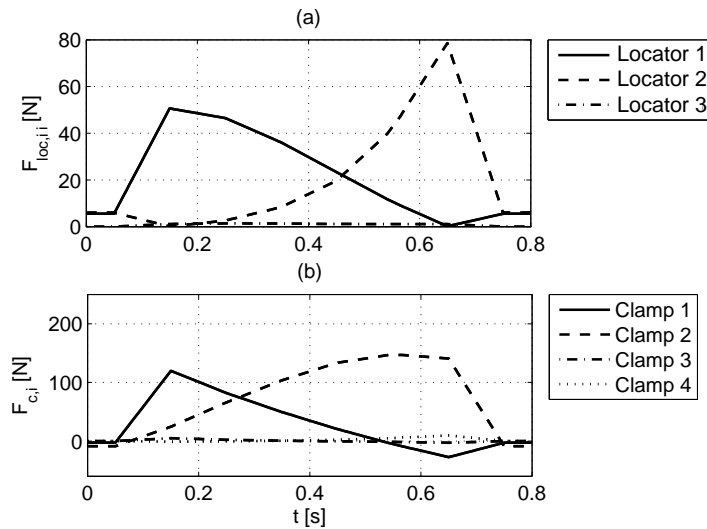
Figure 7.14: Response of the open-loop system to a pass of "machining force" $F_m =$
-200 N in z-direction on the force input nodes, with: **(a)** the reaction
forces $F_{loc,i}$ seen by the locator; and, **(b)** the reaction forces $F_{c,i}$ at the
clamp. Index i indicates the respective clamp or locator number.
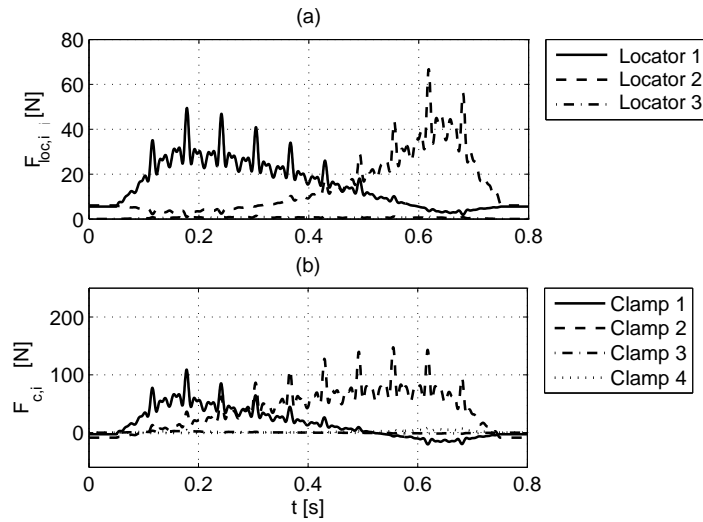
Figure 7.15: Response of a open-loop system to a pass of "machining force" at rotational wheel speed of $\omega = 100$ rad/s (15.9 Hz or 955 rpm) in z-direction on the force input nodes with: **(a)** the reaction forces $F_{\mathrm{loc},i}$ seen by the locator; and. **(b)** the reaction forces $F_{\mathrm{c},i}$ at the clamp. Index i indicates the respective clamp or locator number.
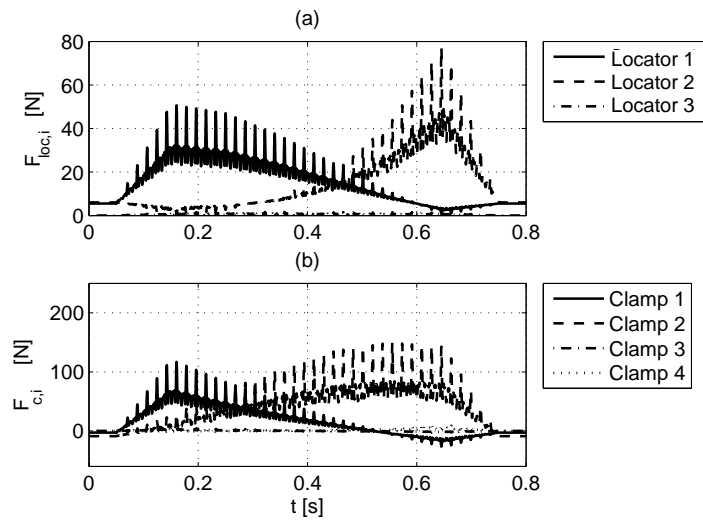
Figure 7.16: Response of a open-loop system to a pass of "machining force" at rotational wheel speed of $\omega = 350$ rad/s (55.7 Hz or 3342 rpm) in z-direction on the force input nodes with: **(a)** the reaction forces $F_{\mathrm{loc},i}$ seen by the locator; and. **(b)** the reaction forces $F_{\mathrm{c},i}$ at the clamp. Index i indicates the respective clamp or locator number.

189
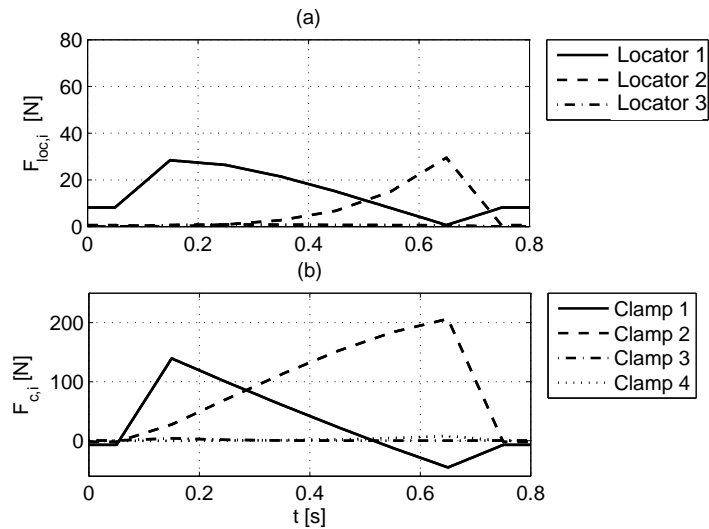
Figure 7.17: Response of a closed-loop system with proportional control to a pass of "machining force" $F_m = $ -200 N in z-direction on the force input nodes with: **(a)** the reaction forces $F_{loc,i}$ seen by the locator; and, **(b)** the reaction forces $F_{c,i}$ at the clamp. Index i indicates the respective clamp or locator number.
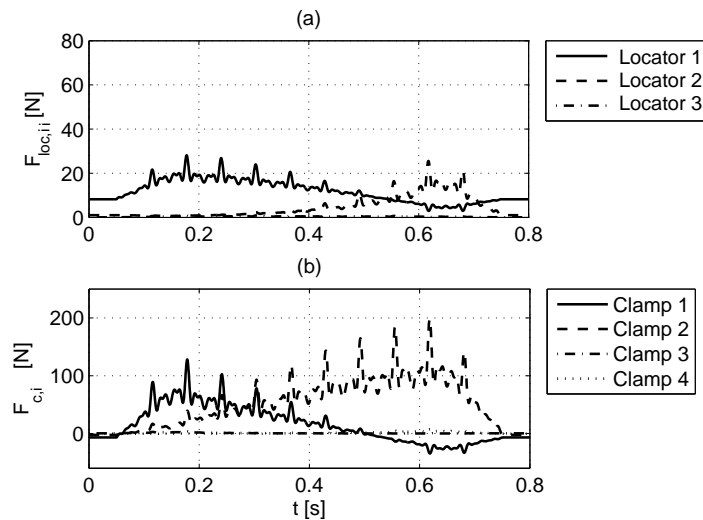
Figure 7.18: Response of a closed-loop system with P-controller to a pass of "machining force" at rotational wheel speed of $\omega = 100$ rad/s (15.9 Hz or 955 rpm) in z-direction on the force input nodes with: **(a)** the reaction forces $F_{loc,i}$ seen by the locator; and. **(b)** the reaction forces $F_{c,i}$ at the clamp. Index i indicates the respective clamp or locator number.

190
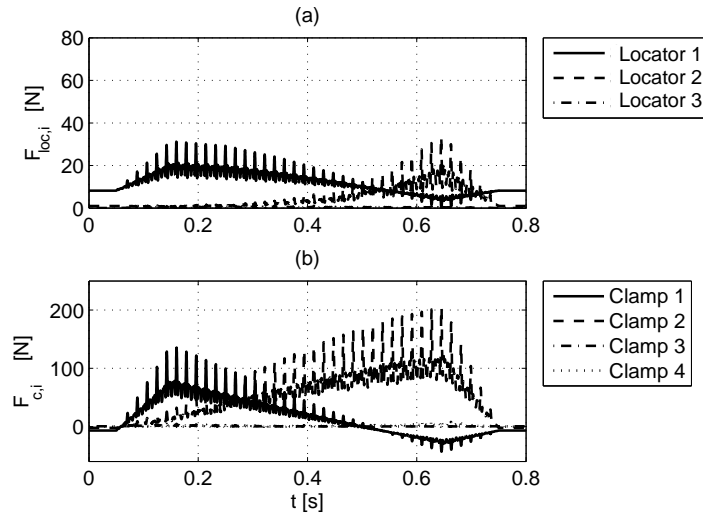
Figure 7.19: Response of a closed-loop system with P-controller to a pass of "machining force" at rotational wheel speed of $\omega = 350$ rad/s (55.7 Hz or 3342 rpm) in z-direction on the force input nodes with: **(a)** the reaction forces $F_{\mathrm{loc},i}$ seen by the locator; and. **(b)** the reaction forces $F_{\mathrm{c},i}$ at the clamp. Index i indicates the respective clamp or locator number.
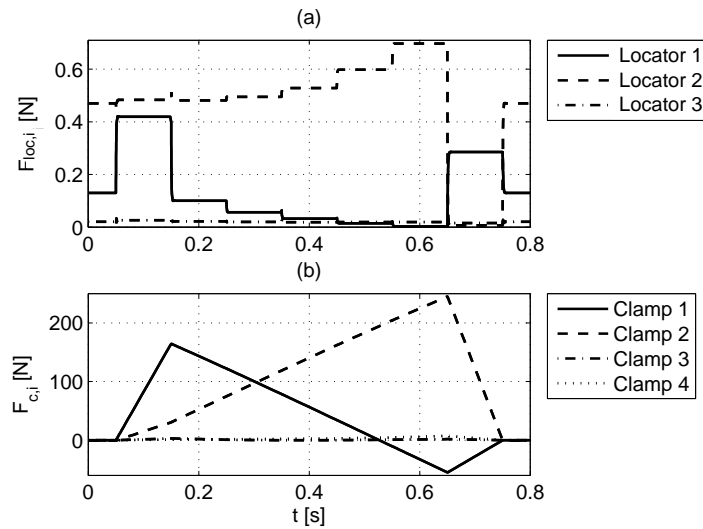
Figure 7.20: Response of a closed-loop system with PI controller to a pass of "machining force" $F_{\mathrm{m}} = $ -200 N in z-direction on the force input nodes with: **(a)** the reaction forces $F_{\mathrm{loc},i}$ seen by the locator; and. **(b)** the reaction forces $F_{\mathrm{c},i}$ at the clamp. Index i indicates the respective clamp or locator number.
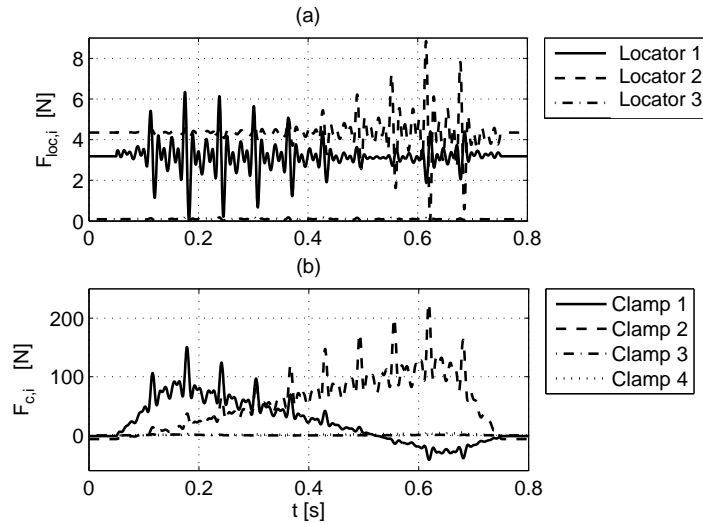
Figure 7.21: Response of a closed-loop system with PI-controller to a pass of "machining force" at rotational wheel speed of $\omega = 100$ rad/s (15.9 Hz or 955 rpm) in z-direction on the force input nodes with: **(a)** the reaction forces $F_{\text{loc},i}$ seen by the locator; and. **(b)** the reaction forces $F_{\text{c},i}$ at the clamp. Index i indicates the respective clamp or locator number.
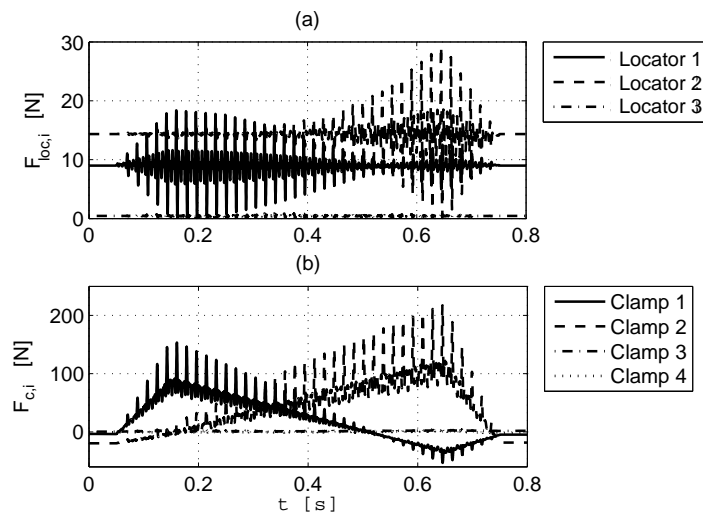
Figure 7.22: Response of a closed-loop system with PI-controller to a pass of "machining force" at rotational wheel speed of $\omega = 350$ rad/s (55.7 Hz or 3342 rpm) in z-direction on the force input nodes with: **(a)** the reaction forces $F_{\text{loc},i}$ seen by the locator; and. **(b)** the reaction forces $F_{\text{c},i}$ at the clamp. Index i indicates the respective clamp or locator number.

Conclusions and Future Work

8.1 Contributions

In manufacturing, fixtures are used to (1) locate, and (2) immobilise a workpiece during the manufacturing process, furthermore, (3) a fixture should provide sufficient support to the part it is holding during the manufacturing operations. This means, the fixture should prevent deflection of the workpiece due to machining and clamping forces. The fixture performance, the degree to which the fixture fulfils the three functions mentioned above, determines the final product quality. Hence, fixtures form a critical component in manufacturing. In machining industry in the Western World, a trend can be observed towards precision manufacturing and the production in small batches. This highly specialised and customised form of manufacturing requires a high level of automation, to enable a quick changeover from one product to another. This form of manufacturing is enabled by the programmability and accuracy of computer numerical control (CNC) machine tools. Traditionally, fixtures are designed for dedicated use, which essentially means that they cannot be adapted to hold other parts. In order to make more 'flexible' use of one fixture, several fixturing concepts have been developed that allow for a reconfiguration of the fixture layout, such that different types of workpieces can be fixtured using the same fixture components. However, the initial novel fixturing concepts had two major drawbacks: low accuracy, and long set-up times. A more recent development is the intelligent fixturing system. The sensors and actuators, integrated in an intelligent fixturing system, allow for the automatic and precise reconfiguration of the fixturing elements. Additionally, the actuated fixture elements can be used to exert optimal clamping forces to minimise the workpiece deflection during the machining process, this is called

active fixturing.

A literature survey has been carried out, in which it has been established that the main process variables to control in active fixturing are: the reaction forces at the contacts where the workpiece is fixated and supported by the fixture (the locating points); and/or the part or fixture displacements. Furthermore, four knowledge gaps were identified:

1. A lack of computationally efficient models of workpiece response during machining.

2. A lack of methodic structural analysis approach of part-fixture interaction.

3. A lack of model-based control design, which can potentially speed up the fixture design process.

4. A lack of control design methodology for active fixturing systems.

To address these knowledge gaps, the research approach taken in the thesis focussed on the analysis and modelling of the active fixturing subsystems. An active fixturing system has been divided into the following subsystems: the part, the part-fixture contact interface, passive fixture elements, the actuated clamp, sensors, and the controller(s). Furthermore, a method to connect these subsystems has been investigated. In addition, a model-based control design methodology has been proposed. On basis of the subsystem analyses, two simple, yet complete, active fixturing systems have been modelled. The performance of the control design of these simple systems has been assessed by means of parameter studies. In addition, the developed control design methodology has been used to analyse an industrial case study.

The research work carried out for the thesis has resulted in key contributions to the following areas in fixturing technology: the structural analysis of part-fixture systems, namely contributions in this area addressing knowledge gaps 1 and 2; actuation modelling and control forces, namely contributions in this area relate to knowledge gaps 2 and 3; control design and performance assessment, namely contributions in this area relate to knowledge gaps 3 and 4; control design methodology, obviously, the established control design methodology relates to knowledge gap 4. The specific knowledge contributions made in these areas will be outlined in the following sections.

8.1.1 Structural Analysis of Part-Fixture Systems

Models describing the dynamic behaviour of the part and the structural elements of the fixture have been established with the finite element method. In this work it was assumed the first natural frequency of the passive fixture elements is higher than the first few frequencies which belong to the dominant dynamic modes of the workpiece. As a result, the dynamic behaviour of the passive elements have been modelled by a spring-dashpot element with equivalent values for stiffness and damping. Furthermore, it was assumed that the contact stiffness and damping occurring in the contact, can be modelled by an equivalent *linear* spring-dashpot element.

The following knowledge contributions are made regarding the structural modelling of part-fixture systems

- Typically, finite elements models have in the order of 10^5 or even higher number of degrees of freedom (DOFs). This number of DOFs is prohibitively high for real-time control applications. It was found that model reduction techniques can be used efficiently to reduce the size of finite element models. In the thesis, the Craig-Bampton model reduction technique [28, 29] is used. The reason for this, is that this method is implemented in most commercially available finite element software packages.

- The dynamic accuracy of models reduced by the Craig-Bampton model reduction method [28, 29] has been studied. The quality of the model reduction depends on the dynamic mode shapes, the so-called fixed interface modes (FIMs), that are added as additional DOFs to the preserved physical DOFs. The desired accuracy determines the number of FIMs needed. The dynamic accuracy of the model reduction has been assessed by a modal analysis of the unsupported part, where for an increasing number of FIMs: (1) the natural frequencies are compared with those of the unsupported full model; (2) a convergence study is conducted of the mode shapes of the physical DOFs of the reduced model; and (3) a visual study is performed with the FIMs.

- The selection of the physical DOFs from the full model has been studied. These DOFs should include all the contact points on the structure. Furthermore, on basis

195

of Saint-Venant's principle [159], it was established that it is not necessary to select all the DOFs that describe the machining regions. It is sufficient to select relatively few degrees of freedom from these regions. As a result, a conservative model of the machining region has been built: the magnitude of the local displacements are over-predicted.

- In some cases it proves possible to establish lumped-parameter models of structures. In this case, it is not necessary to use a model reduction algorithm. The clamp housing studied in Chapter 6 is an example of such a structure.

8.1.2 Actuation Modelling and Control Forces

The following knowledge contributions are made regarding the modelling of controlled clamping forces:

- Active clamping forces are generated by actuators. For this thesis, three actuated clamps are modelled: hydraulically actuated (hydraulic cylinder), electromechanically actuated (electromechanical cylinder / ball screw actuator), piezoelectrically actuated (piezoelectric stack actuator) clamps. These actuator models are general enough to be used directly for other active fixturing systems.

- Spring-dashpot elements are utilised to model the stiffness and damping in the contact interface. The connection force, transferred through the spring-dashpot element is used to couple the actuator with the workpiece.

8.1.3 Control Design Performance Assessment

Compensators for closed-loop servo-control have been applied in the control design. The following conclusions can be drawn regarding the performance assessment of the control design:

- Parameter studies have been carried out to verify the control design. These studies comprised the absolute stability, the workholding stability and the chatter suppression in the frequency domain as achieved by the verified control design. The studies of the simple and the near-industrial active fixturing systems showed that these features could all be achieved.

- Active fixturing systems are multi-input multi-output systems. This means that clamping actions from different clamps can interfere and cause instability. In the case of flexible systems, this can be avoided by applying collocated control. For this reason, collocated control has been investigated as control strategy. Collocated control proved to be a viable control strategy in the case of flexible parts, such as those studied in the near-industrial case study.

8.1.4 Control Design Methodology for Active Fixturing Systems

The following conclusions can be drawn regarding the methodology for control design:

- The applicability of the methodology has been proven with the modelling and simulation of two simple yet complete active fixturing systems, furthermore, the proposed methodology could be directly used for the modelling and control design of a complex near-industrial active fixturing system.

- The methodology can be expanded for model refinement and with other models for control or actuation, this is demonstrated by the addition of the piezoelectrically actuated clamp model which has been established especially for the industrial case study.

8.2 Future Work

The research work presented in this thesis opens up new avenues for advances in technological development and industrial practice. However, due to the number of variables that influence fixture performance, it is impossible to solve all existing issues related to control design for active fixturing systems through the research carried out here. For a farther extension of the methodology for the control design outlined here, contributions can be made in the following areas: (1) modelling, (2) the integration of the model-based control design methodology for active fixture established here with the general design methodology for intelligent fixturing systems.

Regarding the accuracy of the prediction of displacements, an extension of the model of the part-fixture interface subsystem, to include the effects of friction and non-linear contact stiffness can be made. This yields nonlinear models. However, this may improve the accuracy of the prediction for the distribution of the reaction forces, and

hence, the structural deformation of the part-fixture system. Furthermore, an interesting extension for the workpiece-modelling methodology would be the application of model updating techniques, to take the effects of large material removal into account. In certain cases this will also affect the controller settings.

The methodology can be extended with the addition and integration of other models. Within a research or industrial framework these models can even be collected in a database. The database should include a range of actuator and sensor models. In the thesis, a dynamic force profile for a grinding force is established. This model can be extended to a model of a grinding disc with a spindle suspended by spring-dashpot elements in the x-, y- and z-directions, to allow for a more accurate modelling. This would bring the grinding force model more inline with models for the cutting force in a milling process. Additionally, also a database of force-profile models of other machining operations can be established and utilised in a research or industrial environment. Ultimately, the predicted machining forces result in a real-time determination of the displacements and the reaction forces. This means that there can be a real-time change in the reference value set on the actuated clamp, to apply minimal clamping forces.

Control design-wise, regarding low-level control, the methodology can be expanded by extending the current collocated servo-control design to e.g. real hardware in the loop control [54] or multi-input multi-output controllers, such as $\mathcal{H}_\infty$, $\mathcal{H}_2$ and μ-synthesis [151]. Regarding high-level control and high-level control design, there should be an integration of the methodology for low-level control developed in this thesis and methodologies developed for reconfiguration. This concerns: strategies for fixture layouts to minimise the effects of tolerance stack-up, and reconfiguration during the machining process (see Ref. [112]). This will be an important step towards a unified design methodology of intelligent fixtures. As a consequence, avenues will be opened up towards developing robotic fixture design with part-manipulation capabilities during a fixtured grasp operation.

Given the increasing importance of micro-manufacturing for the industry sector in the Western World, it would be interesting to see the methodology established here, expanded to micro-scale and smaller. Already, some work has been undertaken to develop active fixtures for this scale [171].

Model Reduction Techniques and Substructuring

There are several methods in use for model reduction. The commercially available FEA software ABAQUS uses the widely known so called Craig-Bampton [149, 150] method and the Guyan reduction method [149, 150]. In the literature the notion "condensation method" is also used as an interchangeable terminology for "reduction method". These aforementioned methods will be briefly explained here.

A.1   Guyan Reduction Method

In his 1964 paper, Robert Guyan [62] presented a reduction method that is based on the condensation of the stiffness matrix alone; hence the use of the name static reduction. This method is found in widespread use in static analysis. In this section the original notation will not be used, but one based on Craig's notation [29] in order to have a more consistent use of variables within this thesis. The constitutive relations will be re-arranged to start with

$$\left\{ \begin{array}{c} \boldsymbol{R}_{bb} \\ \boldsymbol{R}_{ib} \end{array} \right\} = \left[\begin{array}{cc} \boldsymbol{K}_{bb} & \boldsymbol{K}_{bi} \\ \boldsymbol{K}_{ib} & \boldsymbol{K}_{ii} \end{array} \right] \left\{ \begin{array}{c} \boldsymbol{u}_{b} \\ \boldsymbol{u}_{i} \end{array} \right\}, \tag{A.1.1}$$

for the force and the displacement such that forces $\boldsymbol{R}_{ib}$ become zero. Note that $\boldsymbol{K}_{ib} = \boldsymbol{K}_{bi}^{T}$. The following two equations are obtained:

$$R_{bb} = K_{bb}u_{bb} + K_{bi}u_{ib}, \tag{A.1.2}$$

$$R_{ib} = K_{ib}u_{bb} + K_{ii}u_{ib}. \tag{A.1.3}$$

If equation (A.1.3) is written out for R_{ib} is zero, then it can be solved for u_{ib}:

$$u_{ib} = -K_{ii}^{-1}K_{ib}u_{bb}. \tag{A.1.4}$$

One can now substitute equation (A.1.4) into equation (A.1.2), this yields the following expression:

$$R_{bb} = \left(K_{bb} - K_{bi}K_{ii}^{-1}K_{ib} \right) u_{bb}. \tag{A.1.5}$$

With equation (A.1.4) one can determine the Guyan transformation matrix Ψ_G for $\{u\} = \Psi_G\{u_{bb}\}$:

$$\left\{ \begin{array}{c} u_{bb} \\ u_{ib} \end{array} \right\} = \left[\begin{array}{c} I \\ -K_{ii}^{-1}K_{ib} \end{array} \right] \{u_{bb}\}. \tag{A.1.6}$$

When equation (A.1.6) is substituted into the kinetic energy $\mathcal{T} = \frac{1}{2}\dot{u}^T M \dot{u}$ and potential energy $\mathcal{V} = \frac{1}{2}u^T K u$ one obtains then the following expressions:

$$\mathcal{T} = \frac{1}{2}\dot{u}_{bb}^T \Psi_G^T M \Psi_G \dot{u}_{bb}; \qquad \mathcal{V} = \frac{1}{2}u_{bb}^T \Psi_G^T K \Psi_G u_{bb}.$$

Then with mass matrix M and stiffness matrix K respectively defined as:

$$M = \left[\begin{array}{cc} M_{bb} & M_{bi} \\ M_{ib} & M_{ii} \end{array} \right]; \qquad K = \left[\begin{array}{cc} K_{bb} & K_{bi} \\ K_{ib} & K_{ii} \end{array} \right],$$

the reduced mass and stiffness matrices M_G and K_G become respectively:

$$M_G = M_{bb} - M_{bi}K_{ii}^{-1}K_{ib} - \left(K_{ii}^{-1}K_{ib} \right)^T \left(M_{ib} - M_{ii}K_{ii}^{-1}K_{ib} \right); \tag{A.1.7}$$

$$K_G = K_{bb} - K_{bi}K_{ii}^{-1}K_{ib}. \tag{A.1.8}$$

From this analysis, one can observe two things. Firstly, one can see the result for $\boldsymbol{K}_G$ in equation (A.1.8) already in equation (A.1.5), it is derived here again with a circular reasoning. A second thing to take notice of is that in equation (A.1.7), "combinations of stiffness and mass elements appear. The result is that the eigenvalue-eigenvector problem is closely but not exactly preserved." [62]

A.2   The Craig-Bampton Method

The Wright brothers made their aircraft at the beginning of the 20th century. However the aerospace era saw its dawn in the nineteen sixties. The design of aircraft requires a thorough study of the dynamic behaviour. In that time the computational power was limited while aeroplanes are one of the most complicated engineered systems with order 10^5 components according to Kals *et al.* [74]. This is the driving force behind the rise of model reduction techniques in the nineteen sixties. As concluded from the previous section: the Guyan reduction method preserves the static model, whilst it does not preserve the dynamics because of its mixed mass matrix. Roy Craig Jr. and Mervyn Bampton published in 1968 their so-called Craig-Bampton method in the AIAA Journal [28]. This method can also be found in Craig's book [29].

In this method dynamic modes are added to the reduced mass and stiffness matrices, by means of transformation matrices. This is a kind of logical derivation from the concept of modal expansion under the assumption of small perturbation. There are also several other methods for the use of substructures and model reduction using the aforementioned dynamic modes. The most noted are the methods of Hurty, Rubin, MacNeal and Hintz [29]. The Craig-Bampton method proved itself to be one of the best methods and is therefore still in use today. One can use this method as a standard analysis method in ABAQUS. Let us therefore explore this method in more depth.

For the sake of simplicity the derivation will be made on basis of an example of a simple cantilever beam. The system analysis is simplified by assuming no damping and rigid body motion.

In Figure A.1 (a) one can see that the beam is divided into three components. The middle one is a typical component and is depicted again in Figure A.1 (b). In the

figure the coordinates sets $\mathcal{R}$, $\mathcal{I}$, $\mathcal{E}$ and $\mathcal{B}$ denote respectively the Rigid body coordinates, the Interior coordinates, the excess (i.e.: the redundant coordinates) and the Boundary coordinates (i.e.: the coordinates that are shared with adjacent components).

The matrix vector notation of the re-arranged equations of motions in the notation used in equation (A.1.1):

$$\begin{bmatrix} \boldsymbol{M}_{ii} & \boldsymbol{M}_{ib} \\ \boldsymbol{M}_{bi} & \boldsymbol{M}_{bb} \end{bmatrix} \left\{ \begin{array}{c} \ddot{\boldsymbol{u}}_i \\ \ddot{\boldsymbol{u}}_b \end{array} \right\} + \begin{bmatrix} \boldsymbol{K}_{ii} & \boldsymbol{K}_{ib} \\ \boldsymbol{K}_{bi} & \boldsymbol{K}_{bb} \end{bmatrix} \left\{ \begin{array}{c} \boldsymbol{u}_i \\ \boldsymbol{u}_b \end{array} \right\} = \left\{ \begin{array}{c} \boldsymbol{f}_i \\ \boldsymbol{f}_b \end{array} \right\}. \tag{A.2.1}$$

A.2.1 Fixed Interface Modes

The fixed interface modes are the modes that belong to the component when all boundary coordinates of the component have the zero displacement boundary condition. Hence they are found by solving the following eigenvalue problem:

$$\left[\boldsymbol{K}_{ii} - \boldsymbol{\omega}_j^2 \boldsymbol{M}_{ii} \right] \{\phi_i\}_j = \boldsymbol{0}.$$

Where the infinite degrees of freedom system is reduced to a system with $j = 1$ to n modeshapes and eigenfrequencies. According to the re-arranged equations of equation (A.2.1) one can assemble the eigenvectors as in the following modal matrix, that has n_i, the number of the inner coordinates that are in the modes columns and n rows because of the condensation:

$$\boldsymbol{\Phi}_n \equiv \begin{bmatrix} \boldsymbol{\Phi}_{in} \\ \boldsymbol{0}_{bn} \end{bmatrix}, \qquad \text{for } \boldsymbol{\Phi}_n \in [n \times n_i]. \tag{A.2.2}$$

We then need to normalise them with respect to mass matrix M_{ii}. The modes then satisfy:

$$\boldsymbol{\Phi}_{in}^T \boldsymbol{M}_{ii} \boldsymbol{\Phi}_{in} = \boldsymbol{I}_{ii}, \quad \boldsymbol{\Phi}_{in}^T \boldsymbol{K}_{ii} \boldsymbol{\Phi}_{in} = \boldsymbol{\Lambda}_{nn}.$$

These relations follow from the orthogonality of the modeshapes [29].

Constrained Modes

In order to obtain the constrained modes one needs to rewrite the set of equations in a similar way as for the Guyan reduction. When the equations are re-arranged such that

on the boundary coordinates that a unit displacement is imposed, this gives a reaction force $\boldsymbol{R}_{bb}$ on the boundary coordinates $\mathcal{B}$.

$$\left\{ \begin{array}{c} \boldsymbol{0}_{ib} \\ \boldsymbol{R}_{bb} \end{array} \right\} = \left[\begin{array}{cc} \boldsymbol{K}_{ii} & \boldsymbol{K}_{ib} \\ \boldsymbol{K}_{bi} & \boldsymbol{K}_{bb} \end{array} \right] \left\{ \begin{array}{c} \boldsymbol{\Psi}_{ib} \\ \boldsymbol{I}_{bb} \end{array} \right\}.$$

By writing out the first line of this set of equations, the following expression is obtained:

$$\boldsymbol{K}_{ii}\boldsymbol{\Psi}_{ib} + \boldsymbol{K}_{ib}\boldsymbol{I}_{bb} = \boldsymbol{0}_{ib}.$$

From linear algebra it is known that if an $n \times n$ matrix $\boldsymbol{A}$ is multiplied by an identity matrix of the same size $\boldsymbol{I}$ one has the identity. Hence: $\boldsymbol{K}_{ib}\boldsymbol{I}_{bb} = \boldsymbol{K}_{ib}$. Then solving for $\boldsymbol{\Psi}_{ib}$ gives:

$$\boldsymbol{\Psi}_{ib} = -\boldsymbol{K}_{ii}^{T}\boldsymbol{K}_{ib}.$$

Thus the constraint mode matrix with n_b columns for the boundary coordinates $\mathcal{B}$ $\boldsymbol{\Psi}_c$ is given by the following expression:

$$\boldsymbol{\Psi}_c \equiv \left[\begin{array}{c} \boldsymbol{\Psi}_{ib} \\ \boldsymbol{I}_{bb} \end{array} \right] = \left[\begin{array}{c} -\boldsymbol{K}_{ii}^{T}\boldsymbol{K}_{ib} \\ \boldsymbol{I}_{bb} \end{array} \right], \qquad \text{for } \boldsymbol{\Psi}_c \in [n \times n_b]. \tag{A.2.3}$$

This is a very similar derivation as is seen for the Guyan reduction except for the fact that for the static condensation where a unit displacement is not imposed. The component constraint and fixed interface modes can be seen in Figure A.2

A.2.2 Coupling of the Component Modes

One must now define the component's physical displacement coordinates $\boldsymbol{x}$ into generalised coordinates $\boldsymbol{p}$ of the component. This is in fact a transformation between coordinate systems. The coordinates of the components are denoted with superscript c.

$$\boldsymbol{x}^c = \boldsymbol{\Psi}^c \boldsymbol{p}^c$$

then let:

$$\boldsymbol{x}^c = \boldsymbol{\Phi}_k^c \boldsymbol{p}_k^c + \boldsymbol{\Psi}_c^c \boldsymbol{p}_c^c,$$

where $\boldsymbol{\Psi}$ and $\boldsymbol{\Phi}$ are defined in equations (A.2.3) and (A.2.2) respectively. This yields the following matrix vector expression:

$$\boldsymbol{u}^c \equiv \left\{ \begin{array}{c} \boldsymbol{u}_i \\ \boldsymbol{u}_b \end{array} \right\}^c = \left[\begin{array}{cc} \boldsymbol{\Phi}_{ik} & \boldsymbol{\Psi}_{ib} \\ \boldsymbol{0} & \boldsymbol{I}_{bb} \end{array} \right] \left\{ \begin{array}{c} \boldsymbol{p}_k \\ \boldsymbol{p}_b \end{array} \right\}^c . \tag{A.2.4}$$

The so-called Craig-Bampton transformation matrix is thus:

$$\boldsymbol{\Psi}_{CB}^c = \left[\begin{array}{cc} \boldsymbol{\Phi}_{ik} & \boldsymbol{\Psi}_{ib} \\ \boldsymbol{0} & \boldsymbol{I}_{bb} \end{array} \right]^c . \tag{A.2.5}$$

The reduced mass and stiffness matrices with the transformation matrix defined in equation (A.2.5) become then:

$$\bar{\boldsymbol{M}}_{CB}^c = \boldsymbol{\Psi}_{CB}^{c^T} \boldsymbol{M}^c \boldsymbol{\Psi}_{CB}^c ; \qquad \bar{\boldsymbol{K}}_{CB}^c = \boldsymbol{\Psi}_{CB}^{c^T} \boldsymbol{K}^c \boldsymbol{\Psi}_{CB}^c . \tag{A.2.6}$$

Now, reduced component matrices can be put into larger sets of equations as first step of coupling the components. These sets look as follows:

$$\bar{\boldsymbol{M}}_{CB} \equiv \left[\begin{array}{cc} \bar{\boldsymbol{M}}_{CB}^{\alpha} & \boldsymbol{0} \\ \boldsymbol{0} & \bar{\boldsymbol{M}}_{CB}^{\beta} \end{array} \right] , \quad \bar{\boldsymbol{K}}_{CB} \equiv \left[\begin{array}{cc} \bar{\boldsymbol{K}}_{CB}^{\alpha} & \boldsymbol{0} \\ \boldsymbol{0} & \bar{\boldsymbol{K}}_{CB}^{\beta} \end{array} \right] , \quad \boldsymbol{p} \equiv \left[\begin{array}{c} \bar{\boldsymbol{p}}^{\alpha} \\ \bar{\boldsymbol{p}}^{\beta} \end{array} \right] . \tag{A.2.7}$$

Obviously, the physical displacements at the boundaries of two coupled components must be the same. This is called compatibility. Hence for the set of boundary coordinates $\mathcal{B}$ for components $c = \alpha$ and $c = \beta$.

$$\boldsymbol{x}_b^{\alpha} = \boldsymbol{x}_b^{\beta} . \tag{A.2.8}$$

The compatibility causes the coupled sets of coordinates to be no longer to be linearly independent. One resolves for this by means of a linear transformation with component coupling matrix $\boldsymbol{S}$ and generalised coordinates $\boldsymbol{p}$ from equation (A.2.7)

$$\boldsymbol{p} = \boldsymbol{S}\boldsymbol{q} . \tag{A.2.9}$$

From equation (A.2.4) one learns that interface compatibility becomes:

$$\boldsymbol{p}_b^{\alpha} = \boldsymbol{p}_b^{\beta} = \boldsymbol{q}_b = \boldsymbol{x}_b . \tag{A.2.10}$$

Matrix $\boldsymbol{S}$ and the generalised coordinates in equation (A.2.9) become then:

$$
\left\{
\begin{array}{c}
\boldsymbol{p}_k^\alpha \\
\boldsymbol{p}_b^\alpha \\
\boldsymbol{p}_k^\beta \\
\boldsymbol{p}_b^\beta
\end{array}
\right\}
=
\left[
\begin{array}{ccc}
\boldsymbol{I} & \boldsymbol{0} & \boldsymbol{0} \\
\boldsymbol{0} & \boldsymbol{0} & \boldsymbol{I} \\
\boldsymbol{0} & \boldsymbol{I} & \boldsymbol{0} \\
\boldsymbol{0} & \boldsymbol{0} & \boldsymbol{I}
\end{array}
\right]
\left\{
\begin{array}{c}
\boldsymbol{q}_k^\alpha \\
\boldsymbol{q}_k^\beta \\
\boldsymbol{u}_b
\end{array}
\right\}.
$$

If one has equations of motion built up from the matrices and the vector in equation in (A.2.7):

$$
\bar{\boldsymbol{M}}_{CB}\ddot{\boldsymbol{p}} + \bar{\boldsymbol{K}}_{CB}\boldsymbol{p} = \bar{\boldsymbol{f}}. \tag{A.2.11}
$$

The force input vector $\bar{\boldsymbol{f}}$ is defined as

$$
\bar{\boldsymbol{f}} =
\left\{
\begin{array}{c}
\bar{\boldsymbol{f}}^\alpha \\
\bar{\boldsymbol{f}}^\beta
\end{array}
\right\}
=
\left\{
\begin{array}{c}
\boldsymbol{\Psi}_{CB}^{\alpha^T}\boldsymbol{f}^\alpha \\
\boldsymbol{\Psi}_{CB}^{\beta^T}\boldsymbol{f}^\beta
\end{array}
\right\}.
$$

One can then substitute equation (A.2.9) into equation (A.2.11) and premultiply this expression with $\boldsymbol{S}^T$:

$$
\boldsymbol{S}^T\bar{\boldsymbol{M}}_{CB}\boldsymbol{S}\ddot{\boldsymbol{q}} + \boldsymbol{S}^T\bar{\boldsymbol{K}}_{CB}\boldsymbol{S}\boldsymbol{q} = \boldsymbol{S}^T\bar{\boldsymbol{f}}. \tag{A.2.12}
$$

From this equation (A.2.12) one can distill the coupled Craig-Bampton matrices $\boldsymbol{M}_{CB} = \boldsymbol{S}^T\bar{\boldsymbol{M}}_{CB}\boldsymbol{S}$ and $\boldsymbol{K}_{CB} = \boldsymbol{S}^T\bar{\boldsymbol{K}}_{CB}\boldsymbol{S}$.

$$
\boldsymbol{M}_{CB} =
\left[
\begin{array}{ccc}
\boldsymbol{I}_{kk}^\alpha & \boldsymbol{0} & \bar{\boldsymbol{M}}_{k_\alpha b}^\alpha \\
\boldsymbol{0} & \boldsymbol{I}_{kk}^\beta & \bar{\boldsymbol{M}}_{k_\beta b}^\beta \\
\bar{\boldsymbol{M}}_{bk_\alpha}^\alpha & \bar{\boldsymbol{M}}_{bk_\beta}^\beta & \bar{\boldsymbol{M}}_{bb}^\alpha + \bar{\boldsymbol{M}}_{bb}^\beta
\end{array}
\right]
; \quad
\boldsymbol{K}_{CB} =
\left[
\begin{array}{ccc}
\boldsymbol{\Lambda}_{k_\alpha k_\alpha}^\alpha & \boldsymbol{0} & \boldsymbol{0} \\
\boldsymbol{0} & \boldsymbol{\Lambda}_{k_\beta k_\beta}^\beta & \boldsymbol{0} \\
\boldsymbol{0} & \boldsymbol{0} & \bar{\boldsymbol{K}}_{bb}^\alpha + \bar{\boldsymbol{K}}_{bb}^\beta
\end{array}
\right].
$$

Several convergence tests have been made and one can find the results in [29]. The number of elastic modes with less then a given percentile error relative to all the non-rigid body modes is plotted versus the number of modes used relative to the total coupled degrees of freedom. The Craig-Bampton method shows a good (relative) performance compared with its competitors. It is beyond the scope of this text to discuss further the convergence and performance of the Craig-Bampton method. If one adds the simplicity

in application of this method to this, it is not unexpected that this method is widely used as reduction method.

A.2.3   Reduction Methods Implemented in ABAQUS

The Guyan reduction method is implemented in ABAQUS as a reduction method using the the constraint modes rather than the Guyan method as presented in Section A.1. This is described in the ABAQUS Theory Manual [150] and the ABAQUS User's Analysis Manual [149]. In order to allow for large rotations, the rigid modes are used.

The Craig-Bampton method has a standard implementation in the ABAQUS code. The software engineers of ABAQUS Inc.[1] also implemented a code that allows for large rotations in the dynamic simulations. From the descriptions in the manuals it does not become clear what type of modification is used in addition to the Craig-Bampton method. An educated guess would be that the rigid body modes are also taken into account. In that case the constraint mode matrix $\mathbf{\Psi}_c$ has to be replaced by redundant-interface constrained modes defined by the unit displacements at the redundant or excess set of coordinates $\mathcal{E}$ and the rigid body modes relatively defined to the set $\mathcal{R}$ of the boundary coordinates, such that $\mathbf{\Psi}_c$ is replaced by $[\mathbf{\Psi}_r \; \mathbf{\Psi}_e]$. These sets of modes are constructed in a similar way as the constraint modes matrix.

---

[1] ABAQUS Inc. at present named: Dassault Systèmes SIMULIA

A.3 Figures
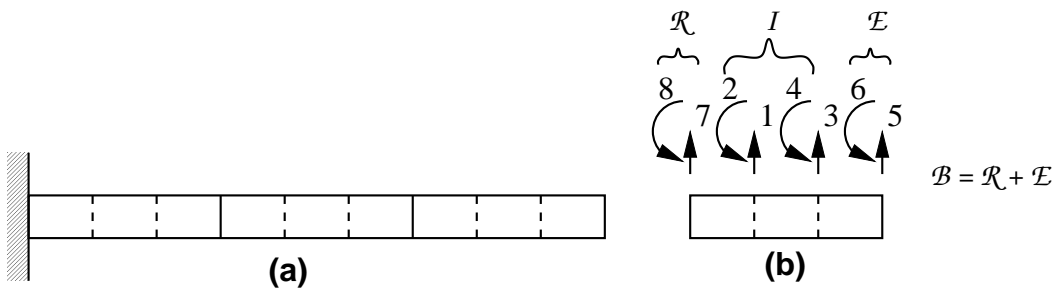
Figure A.1: Typical components, coordinate notation; a): components and coupled system; b): typical component with redundant boundary. After [29]
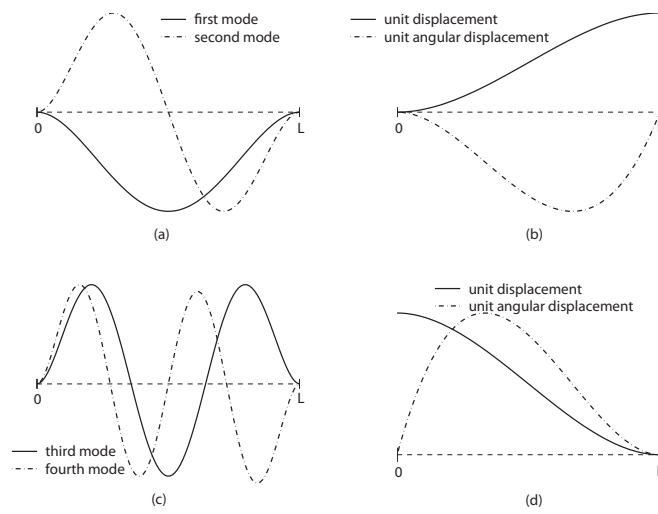
Figure A.2: Example of constraint (A.2 (b) and (d)) and fixed interface modes (A.2 (a) and (c)), after [29].

Model Reduction of NGV

A model reduction of the workpiece, a NGV, in Chapters 6 and 7 has been carried out, in the nodes shown in Figure 6.13 are the retained nodes. The applied model reduction technique is the Craig-Bampton reduction method [28, 29]. Details of this model reduction technique can also be found in Appendix A.

B.1 Analysis

In Tables B.1–B.3 a the results of a convergence study are presented. As has been discussed in Chapter 4, the required number of FIM has been established on basis of the congruity between the eigenfrequencies of the full and reduced order models and a study of the mode shapes.

B.1.1 Visual Study of Fixed Interface Modes

The number of fixed interface modes (FIM) that was added to the transformation matrix has been established to an upper limit of 12 FIM initially. This is not a random number: an important part of the motion in the mode shapes comes from the wings vibrating as "fixed-fixed" beams. The motion of the first twelve mode shapes can be described as a combination of first order modes of the wings, as can be seen in Figure B.1. It should be noted that ultimately the convergence of the eigenfrequencies and mode shapes with respect to the full model is the measure of the number of added FIM. Other visual studies for the FIM have been undertaken regarding the other machining areas of the

NGV, which are the other edges close to the machining area identified in Figure 6.13. From these studies, a set of 12 FIM showing the same "first order" properties as the FIM shown in Figure B.1.

B.1.2 Convergence Study of Eigenfrequencies

Furthermore, the correctness of the model reduction of the simplified part has been studied by means of an eigenvalue analysis of the unsupported reduced model, for an increasing number of fixed interface modes (FIM). Table B.1 shows the eigenfrequencies as resolved from the reduced model. Table B.2 shows the percentile error relative to the full simplified model. From convergence studies of reduced models of the NGV consisting of the other machining areas, it was observed a new "jump" in the accuracy of the reduced model model could be observed, indicating that the visually observed change in properties of the FIM also is clearly observable in the numerical (tabular) results.

B.1.3 Convergence Study of Mode Shape of Physical Degrees of Freedom

In addition, the elastic mode shapes of the reduced model have been studied as well. The reduction included 13 nodes or 39 DOFs. Since the Craig-Bampton model reduction technique [28, 29] does not project these physical degrees of freedom onto another generalised space, one may compare the mode shape of these physical degrees with the corresponding full order system or with other reduced models of the same system consisting at least of the same physical degrees of freedom. This allows to study the influence of the number of FIM on the physical components of the mode shapes of these systems. In order to make a correct comparison, the largest entry of mode shape vector has been scaled to unity and has been taken as positive. The mode shape vectors of the first twelve modes (fourteen in the other studies) the each of the models model have been compared with the vectors of the model that includes the highest number of fixed interface modes - the reference mode shape - by means of an subtraction:

$$\phi_{e,i}^n = \phi_i^n - \phi_{\text{ref}}^n.$$

For example, if the reference mode shape of the nth mode would be

$$\phi_{\text{ref}}^n = [1 \quad -0.45 \ 1 \ 0.3 \ 0.5 \ 0.2]$$

and another mode shape, where index i is the number of the system number with the additional number of FIMs, for same n^{th} mode $\phi_i^n = $ [1 -0.5 1 0.29 0.52 0.17], this would give a maximum absolute error of 0.05. The absolute values of the resulting error vector $\phi_{e,i}^n$ have been summed. These values are the entries in the Table B.3. The total error for each different model has been summed again. This means that the smaller the entry in Table, the higher the convergence level is. Apparently, mode 2 and 3 has been hard to capture, the error summed over all the physical degrees of freedom for these modes remains large compared to the rest of the errors.

From Tables B.1 and B.2 as good convergence can be seen from 6 FIM onwards for the first eight(!) elastic modes of the unsupported NGV. Moreover, from the analysis of the mode shapes it follows also that apparently 6 or more fixed interface mode shapes need to be used to give an approximate description of the elastic mode shapes of the unsupported model of the NGV. The largest contribution in terms of displacements towards the mode shapes belonging to the lower frequency modes comes from the vanes vibrating. Mode 7-12 of the fixed interface modes describe also displacements in the inner and outer bound of the NGV. For this reason it might be wise to keep these fixed interface modes in the model as well, since the machining of the part actually involves certain finishing operations on the inner and outer bounds of the NGV.

B.2   Conclusions

- Given the small error in predicted frequencies: including extra nodes of the full NGV model is not necessary.

- Given the "jump" in accuracy of the prediction of the eigenvalues in case of six or more added fixed interface modes and the fact that modes 7-12 are not really improving the results can lead to a model with as little as 6 fixed interface modes.

- However, given the fact that machining of the NGV takes part on the inner and outer bound of the NGV, it might be wise to include some modes 7-12 as well in the reduced model.

B.3 Tables

Table B.1: Convergence results from model reduction of the NGV.

eigenfrequencies first 12 elastic modes [Hz]						
Mode #	full model	1 FIM	2 FIM	3 FIM	4 FIM	5 FIM	6 FIM
1	478.98	487.06	484.83	484.54	484.46	484.45	483.74
2	584.56	596.86	595.33	594.79	594.79	594.77	594.71
3	651.35	753.72	734.97	654.41	654.4	654.09	651.77
4	678.15	1397.4	966.43	750.96	694.71	693.07	679.55
5	697.12	1856.8	1419.9	983.04	758.31	700.71	697.24
6	700.99	2092.6	1920.1	1488	986.28	758.45	701.04
7	775.55	2244.5	2095.7	1957.8	1493.4	986.39	810.12
8	1044.3	2646.1	2372.4	2095.7	1970.2	1507.8	1065.3
9	1121.5	2704.8	2646.7	2561.4	2098.1	1977.5	1544.1
10	1285.5	3635.6	2765.8	2695	2567.9	2098.1	1995.5
11	1421.4	4009.1	3878.9	3781.6	2698.3	2587.1	2370.9
12	1435.4	4954.5	4593.9	4545.8	3800.6	2710.1	2705.7
13	1453.9	5426.5	4999.7	4888.3	4546	4050.8	3274.3
14	1516.6	5999.4	5992.6	5672.1	4952	4698.3	4300.6
Mode #	7 FIM	8 FIM	9 FIM	10 FIM	11 FIM	12 FIM	
1	483.73	482.84	482.78	482.63	482.58	482.55	
2	594.44	594.44	594.3	594.29	594.19	594.14	
3	651.76	651.76	651.64	651.59	651.53	651.53	
4	679.45	678.38	678.37	678.27	678.26	678.24	
5	697.23	697.2	697.14	697.14	697.13	697.13	
6	701.02	701.02	701.01	701.01	701	701	
7	809.85	781.75	781.75	777.55	776.97	776.71	
8	1064.9	1064.8	1063.6	1063.5	1062.6	1062.6	
9	1470.1	1362.3	1155.3	1149	1130.3	1130.1	
10	1713	1570.4	1426.3	1291.8	1288	1286.8	
11	2039.9	1713.7	1663.3	1478.9	1423	1422.8	
12	2371.2	2063.6	1762.8	1663.5	1480.9	1480.9	
13	2705.8	2656.4	2238.5	1785.3	1665.9	1517.1	
14	3411.4	2731.7	2676.1	2599.5	1792.1	1667.1	

Table B.2: Convergence results from model reduction of the NGV.

$e_\% = \frac{f_r - f_f}{f_f} \times 100\%$					
Mode #	1 FIM	2 FIM	3 FIM	4 FIM	5 FIM	6 FIM
1	1.69%	1.22%	1.16%	1.14%	1.14%	0.99%
2	2.10%	1.84%	1.75%	1.75%	1.75%	1.74%
3	15.72%	12.84%	0.47%	0.47%	0.42%	0.06%
4	106.06%	42.51%	10.74%	2.44%	2.20%	0.21%
5	166.35%	103.68%	41.01%	8.78%	0.51%	0.02%
6	198.52%	173.91%	112.27%	40.70%	8.20%	0.01%
7	189.41%	170.22%	152.44%	92.56%	27.19%	4.46%
8	153.39%	127.18%	100.68%	88.66%	44.38%	2.01%
9	141.18%	136.00%	128.39%	87.08%	76.33%	37.68%
10	182.82%	115.15%	109.65%	99.76%	63.21%	55.23%
11	182.05%	172.89%	166.05%	89.83%	82.01%	66.80%
12	245.17%	220.04%	216.69%	164.78%	88.80%	88.50%
13	273.24%	243.88%	236.22%	212.68%	178.62%	125.21%
14	295.58%	295.13%	274.00%	226.52%	209.79%	183.57%
Mode #	7 FIM	8 FIM	9 FIM	10 FIM	11 FIM	12 FIM
1	0.99%	0.81%	0.79%	0.76%	0.75%	0.75%
2	1.69%	1.69%	1.67%	1.66%	1.65%	1.64%
3	0.06%	0.06%	0.04%	0.04%	0.03%	0.03%
4	0.19%	0.03%	0.03%	0.02%	0.02%	0.01%
5	0.02%	0.01%	0.00%	0.00%	0.00%	0.00%
6	0.00%	0.00%	0.00%	0.00%	0.00%	0.00%
7	4.42%	0.80%	0.80%	0.26%	0.18%	0.15%
8	1.97%	1.96%	1.85%	1.84%	1.75%	1.75%
9	31.08%	21.47%	3.01%	2.45%	0.78%	0.77%
10	33.26%	22.16%	10.95%	0.49%	0.19%	0.10%
11	43.51%	20.56%	17.02%	4.05%	0.11%	0.10%
12	65.19%	43.76%	22.81%	15.89%	3.17%	3.17%
13	86.11%	82.71%	53.97%	22.79%	14.58%	4.35%
14	124.94%	80.12%	76.45%	71.40%	18.17%	9.92%

Table B.3: Convergence of relative error of mode shapes model reduction of the NGV.

maximum absolute error in mode shape normalised on unity (=1)					
Mode #	1 FIM	2 FIM	3 FIM	4 FIM	5 FIM	6 FIM
---	---	---	---	---	---	---
1	0.077487	0.081391	0.091383	0.22657	0.20874	0.15096
2	0.23091	1.7221	0.84471	0.70121	1.5984	1.5984
3	0.22575	0.80856	0.41448	0.29823	1.0416	1.4313
4	0.26201	0.21927	0.16974	0.40504	0.33452	0.16416
5	0.13725	0.067295	0.070477	0.046181	0.13721	0.055331
6	0.054323	0.040624	0.059335	0.035701	0.057612	0.042522
7	1.987	0.037092	0.03023	0.029067	0.029061	0.013582
8	0.13209	0.019541	0.016497	0.016951	0.01691	0.011947
9	1.0041	0.97148	0.22735	0.22393	0.19896	0.037987
10	1.2519	1.9445	0.44348	0.70951	1.969	0.10071
11	1.4335	1.2333	1.2345	1.1974	1.4134	0.05156
12	0.95758	0.97537	1.3515	1.2563	1.036	0.042142
13	1.4763	0.83454	1.6183	1.473	1.9785	0.049106
14	0.94942	1.2277	1.4238	0.98336	0.90195	0.06919
sum of error	10.17962	10.182763	7.995782	7.60245	10.921863	3.818897

Mode #	7 FIM	8 FIM	9 FIM	10 FIM	11 FIM
1	0.18773	0.15955	0.19403	0.040039	0.089768
2	0.48383	1.5873	1.5984	1.5984	1.5984
3	0.28862	0.88638	1.7831	1.2079	1.2167
4	5.39E-01	0.17754	0.17396	0.073024	0.15852
5	2.46E-01	0.071474	0.065784	0.074233	0.070216
6	0.044184	0.046478	0.048218	0.04442	0.035097
7	0.012653	0.0024561	0.0020546	0.000585	0.00020988
8	0.0050533	0.0047815	0.0015929	0.0016577	0.00099579
9	0.037867	0.039114	0.014384	0.009309	0.0026268
10	0.065435	0.012129	0.0084125	0.0025013	0.0034938
11	0.036684	0.02864	0.011797	0.0053916	0.00067296
12	0.020998	0.0087105	0.0077442	0.0031673	9.00E-05
13	0.05107	0.014564	0.014293	0.0048257	0.0026081
14	0.068328	0.069277	0.030219	0.028017	0.0017277
sum of error	2.0873823	3.1083941	3.9539892	3.0934706	3.181126033

B.4   Figure
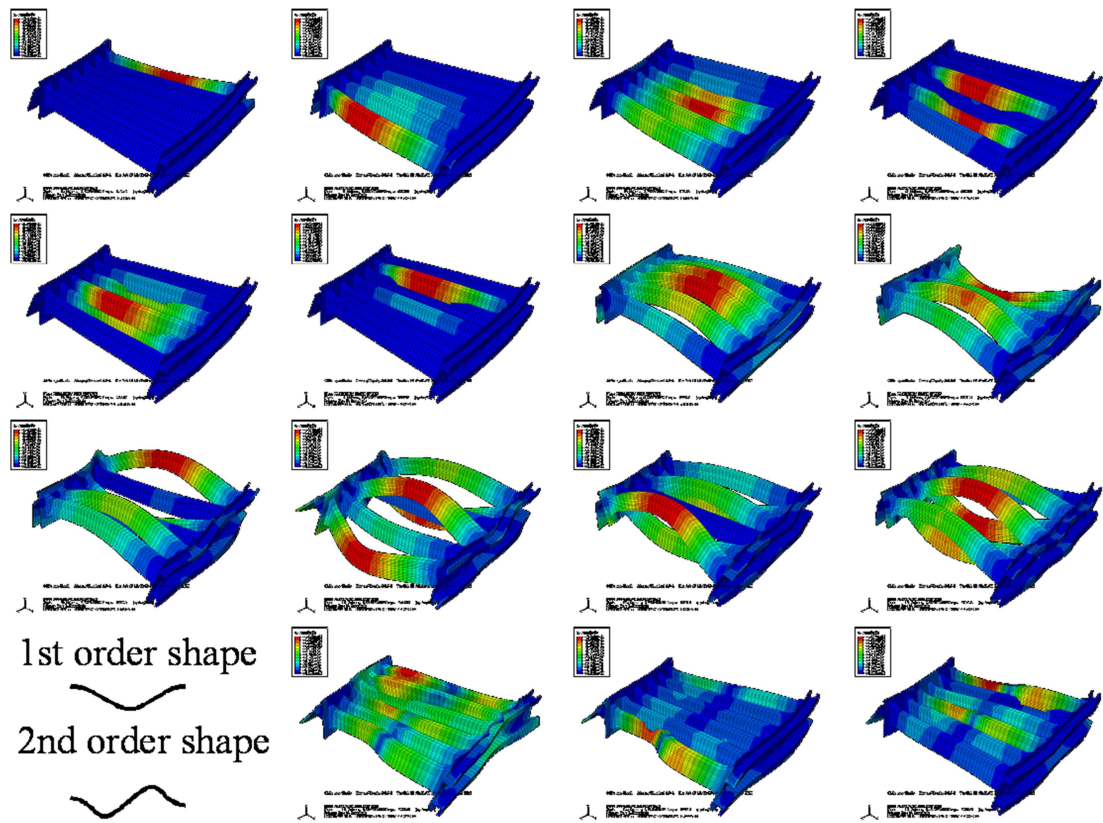
Figure B.1: The first 15 fixed interface modes (FIMs) of the NGV, the first FIM is at top left, mode number ascends in left to right direction; with bottom left, the definition of the first and the second order shape for wing displacement.

Useful Results from Thin Plate Theory

The thin plate theory [158] is founded on the Kirchhoff-Love assumptions, which are analogue to the assumptions used in the Bernoulli beam theory [159]. For the symmetrical bending of circular plates in cylindrical coordinate system they can be formulated as follows [158]:

- The effect/contribution of the transversal normal stresses σ_z is negligible for the relations between stresses and displacements.

- Material points that are on line which is perpendicular with respect to the undeformed midplane, will after deformation again be on one line which is perpendicular with respect to the deformed midplane. Furthermore the distance between the material points will not change.

Under these two assumptions only the normal stresses σ_r in radial direction and the stresses σ_θ in tangential direction play a role.

C.1 Obtaining the Deflection for a Circular Disc with a Hole in the Centre

Based on Timoshenko [158, Chapter 1 & 2] the spring stiffness for the disc springs can be derived analytically. Eq. (57) in [158] gives constitutive relation for a circular disc that is loaded out of plane:

$$\frac{d}{dr}\left[\frac{1}{r}\frac{d}{dr}\left(r\frac{dw}{dr}\right)\right] = \frac{Q}{D}, \tag{C.1.1}$$

Where stiffness coefficient D is defined as [158, Eq. (3)]:

$$D = \frac{Et^3}{12(1 - \nu^2)}.$$ (C.1.2)

Applying a point load P on the centre of the mass M in Figure 6.6 is equivalent to applying shearing forces Q_0 that are equally distributed over inner r_1: $P = 2\pi r_1 Q_0$. The shearing force per unit length of a circumference of radius r on a infinitesimal volume is then

$$Q = \frac{Q_0 r_1}{r} = \frac{P}{2\pi r}.$$ (C.1.3)

Substituting Eq. (C.1.3) into (C.1.1) and solving for deflection w gives [158, p. 59, (f)]:

$$w = \frac{Pr^2}{8\pi D}\left[\ln\left(\frac{r}{r_2}\right) - 1\right] - \frac{C_1 r^2}{4} - C_2 \ln\left(\frac{r}{r_2}\right) + C_3.$$ (C.1.4)

Integration constants C_1, C_2 and C_3 can be determined from the boundary conditions given by (6.3.5). They are respectively:

$$C_1 = P\frac{2r_1^2 \ln\left(\dfrac{r_1}{r_2}\right) - r_1^2 + r_2^2}{4\pi D(r_1^2 - r_2^2)},$$ (C.1.5a)

$$C_2 = P\frac{r_1^2 r_2^2 \ln\left(\dfrac{r_1}{r_2}\right)}{4\pi D(r_2^2 - r_1^2)},$$ (C.1.5b)

$$C_3 = Pr_2^2\frac{2r_1^2 \ln\left(\dfrac{r_1}{r_2}\right) + r_1^2 - r_2^2}{16\pi D(r_1^2 - r_2^2)}.$$ (C.1.5c)

C.2   Correction for Shear

Timonshenko [158] proposed for a correction for the shear stresses, analogue as the correction for shear stresses in the beam theory [159].

In order to fulfill the boundary conditions for plane stress the shear stress τ_{rz} is zero on outsides, $z = \pm\frac{1}{2}t$, parallel to the neutral plane of the plate and will vary across the thickness of the plate in a parabolic distribution [158, 159]. The maximum shearing stress at a distance r from the centre is [158, p. 74]:

$$\tau_{rz,\text{max}} = \frac{3}{2}\frac{P}{2\pi rt}.$$ (C.2.1)

The corresponding shear strain for a plate with a central hole is [158, p. 74, Eq. (i)]

$$\frac{dw_1}{dr} = -\frac{3}{2}\frac{P}{2\pi rtG},$$

(C.2.2)

where G is the shear modulus of elasticity defined by $G = \frac{E}{2(1+\nu)}$.

The deflection due to shear may be obtained by integrating the expression above [158, p. 74, Eq. (j)]

$$w_1 = \frac{Pt^2}{8\pi(1-\nu)D}\ln\left(\frac{r_2}{r}\right).$$

(C.2.3)

C.2.1 Application for the Simplified Model in Presented in Figure 6.6

In order to fulfill the clamped boundary conditions at r_1 and r_2, see Figure 6.6 and Eq. (6.3.5), another solution of (C.1.1) needs to be superimposed on w_1. In case when only uniformly distributed moments are applied at r_1 and r_2 of the disc. The deflection due to the applied moments is [158, p. 58 (b)]

$$w_2 = -\frac{C_4 r^2}{4} - C_5\ln\left(\frac{r}{r_2}\right) + C_6.$$

(C.2.4)

One can obtain the coefficients C_4, C_5 and C_6, by applying the boundary conditions such that superposing solutions w_1 and w_2 give zero displacement at r_2 and that there is a zero gradient in radial direction of the deflection. Not unsurprisingly the constants are found to be:

$$C_4 = C_6 = 0,$$

(C.2.5)

$$C_5 = -\frac{Pt^2}{8\pi(1-\nu)D}.$$

(C.2.6)

This gives that the shear stress does not contribute towards the deflection of the disc, hence there is no shear strain, and therefore there is no shear stress τ_{rz} in disc. Note that this does not imply that there is no shear stress present in reality, other models predict the presence of shear stress. It should be concluded that the solution (C.1.4) is exact.

C.3 Stresses in a Circular Plate

It has been established that in the thin plate model of the clamped-clamped disc with central hole no shear stress is present. The bending moments in M_r radial and M_θ

tangential direction are [158]

$$M_r = -D\left(\frac{d^2w}{dr^2} + \frac{\nu}{r}\frac{dw}{dr}\right), \qquad M_\theta - D\left(\frac{1}{r}\frac{dw}{dr} + \nu\frac{d^2w}{dr^2}\right).$$

The normal stresses radial direction σ_r and tangential direction σ_θ are [51, 158]

$$\sigma_r = \frac{12y}{t^3}M_r = -\frac{E}{1-\nu^2}\left(\frac{d^2w}{dr^2} + \frac{\nu}{r}\frac{dw}{dr}\right)y, \qquad \sigma_\theta = \frac{12y}{t^3}M_\theta = -\frac{E}{1-\nu^2}\left(\frac{1}{r}\frac{dw}{dr} + \nu\frac{d^2w}{dr^2}\right)y.$$

The Von Mises equivalent stresses for a circular thin plate with no shearing stresses present, are given by:

$$\sigma_{Mises} = \sqrt{\sigma_r^2 + \sigma_\theta^2 - \sigma_\theta\sigma_r}. \tag{C.3.1}$$

C.4 On the Force-Displacement Relationship of a Circular Disc with a Hole in the Centre

Substituting (C.1.2) (C.1.5a), (C.1.5b) and (C.1.5c) into (C.1.4) gives an expression for deflection w. The load P as function of the displacement w can be obtained by simple algebraic manipulation. The stiffness k of the disc springs is obtained by differentiating load P with respect to displacement w

$$k = \frac{dP}{dw}\bigg|_{r=r_1} = \frac{16\pi D(r_2^2 - r_1^2)}{(r_2^2 - r_1^2)^2 - 4r_1^2 r_2^2 \ln^2\left(\frac{r_1}{r_2}\right)}. \tag{C.4.1}$$

C.5 Limitations to the Thin Plate Theory

The thin plate theory is limited in several ways. Firstly, since the combination of shearing load $P = 2\pi r_1 Q_0$ applied on the inner edge of the annular flexure and its boundary conditions means shearing stresses τ_{rz} are present, hence the thin plate theory can not yield an exact solution. Secondly, whilst the first of the Kirchhoff-Love assumptions implies plane stress [158, 159] in order to reach the conditions for the second assumption would actually mean that large stresses in transversal direction can occur. Hence a probable inconsistency is introduced.

In order to make more reliable models for the bending of (especially) thicker plates, Reissner developed a model take accounts for the transverse shear stresses [149, 150].

In the mean time, Mindlin developed independently a more advanced model for plate bending [149, 150] and continued to direct his work on the vibrations of piezoelectric crystals. Mindlin's solution and the solutions that have been developed subsequently on basis of Mindlin's plate theory [149, 150] are also applicable for thicker plates as this theory presupposes the presence of transverse shear deformation. In this case the shear strain displacement relationship is [159]

$$\gamma_{rz} = \frac{dw}{dr}.$$

And the equations for the equilibrium of an element are as as follows:

$$\frac{\partial \sigma_r}{\partial r} + \frac{\partial \tau_{rz}}{\partial z} + \frac{\sigma_r - \sigma_\theta}{r} = 0,$$

$$\frac{\partial \tau_{rz}}{\partial r} + \frac{\tau_{rz}}{r} = 0.$$

Commercial FE software, such as ABAQUS, often solves a variant of the Mindlin plate theory, the Mindlin-Reissner plate theory [149, 150]. Thirdly, a linear analysis ignores the membrane stresses, as the strain in radial direction is ignored. Taking the membrane stresses into account in a nonlinear analysis actually makes the disc stiffer [158].

Bibliography

[1] 'IEEE Standard on Piezoelectricity', *ANSI/IEEE Std 176-1987*, Jan 1988.

[2] ABB Ltd (ABB Group), video clip of FlexaLean concept, accessed on 09-06-2010, URL: `http://www.youtube.com/watch?v=7JdUCrb1IFw`.

[3] E. Abele, H. Hanselka, F. Haase, D. Schlote and A. Schiffler, 'Development and Design of an Active Work Piece Holder Driven by Piezo Actuators', *Production Engineering: Research and Development*, **2** (4), pp. 437–442, 2008.

[4] H. J. M. T. A. Adriaens, W. L. de Koning and R. Banning, 'Modeling Piezoelectric Actuators', *IEEE/ASME Transactions on Mechatronics*, **5** (4), pp. 331–341, 2000.

[5] AFFIX, website, accessed on 09-07-2009, URL: `http://www.affix-ip.eu`.

[6] Anonymous, 'Intelligent Robots Take the Tooling out of Nissan's Sunderland Floor Pan Assembly Operation', *Industrial Robot: An International Journal*, **33** (5), 2006, mini feature.

[7] S. Arzanpour, J. Fung, J. K. Mills and W. L. Cleghorn, 'Flexible Fixture Design with Applications to Assembly of Sheet Metal Automotive Body Parts', *Assembly Automation*, **26** (2), pp. 143–153, 2006.

[8] J. C. Aurich, D. Biermann, H. Blum, C. Brecher, C. Carstensen, B. Denkena, F. Klocke, M. Kröger, P. Steinmann and K. Weinert, 'Modelling and Simulation of Process: Machine Interaction in Grinding', *Production Engineering: Research and Development*, **3** (1), pp. 111–120, 2009.

[9] J. C. Aurich, O. Braun and G. Wamecke, 'Development of a Superabrasive Grind-

ing Wheel with Defined Grain Structure Using Kinematic Simulation', *CIRP Annals – Manufacturing Technology*, **52** (1), pp. 275–280, 2003.

[10] O. J. Bakker, A. A. Popov and S. M. Ratchev, 'Investigation into Feedback Control of Part-Fixture Systems Undergoing Dynamic Machining Forces', in: P. Sas and B. Bergen (eds.), 'Proceedings of ISMA2008', pp. 131–140, ISMA2008 - International Conference on Noise and Vibration Engineering, Leuven (Heverlee): Katholieke Universiteit Leuven - Departement Werktuigkunde, 2008.

[11] O. J. Bakker, A. A. Popov and S. M. Ratchev, 'Fixture Control by Hydraulic Actuation Using a Reduced Workpiece Model', *Proceedings of the Institution of Mechanical Engineers Part B: Journal of Engineering Manufacture*, **223**, pp. 1553–1566, 2009.

[12] O. J. Bakker, A. A. Popov and S. M. Ratchev, 'Model-Based Control of an Advanced Actuated Part-Fixture System', in: 'Proceedings of 2009 ASME International Manufacturing Science and Engineering Conference', MSEC2009-84175, ASME, 2009.

[13] O. J. Bakker, A. A. Popov, E. Salvi, A. Merlo and S. M. Ratchev, 'Model-Based Control of an Active Fixture for Advanced Aerospace Components', *Proceedings of the Institution of Mechanical Engineers, Part B: Journal of Engineering Manufacture*, 2010, to appear in the special issue on Manufacturing Technology for Advanced Aerospace Components and Systems.

[14] K. J. Bathe, *Finite Element Procedures*, Englewood Cliffs, New Jersey: Prentice-Hall, 1996.

[15] A. van Beek, *Machine Lifetime Performance and Reliability*, Gouda: Tribos, 2004.

[16] B. Benhabib, K. C. Chan and M. Q. Dai, 'A Modular Programmable Fixturing System', *Transactions of the ASME – Journal of Engineering for Industry*, **113**, pp. 93–100, 1991.

[17] Z. M. Bi, S. Y. T. Lang, M. Verner and P. Orban, 'Development of Reconfigurable

Machines', *International Journal of Advanced Manufacturing Technology*, **39**, pp. 1227–1251, 2008.

[18] Z. M. Bi and W. J. Zhang, 'Flexible Fixture Design and Automation: Review, Issues and Future Directions', *International Journal of Production Research*, **39** (13), pp. 2867–2894, 2001.

[19] C. Brecher, M. M. Esser and S. Witt, 'Interaction of Manufacturing Process and Machine Tool', *CIRP Annals – Manufacturing Technology*, **58**, pp. 588–607, 2009.

[20] C. Brecher, D. Manoharan, U. Ladra and H.-G. Köpken, 'Chatter Suppression with an Active Workpiece Holder', *Production Engineering: Research and Development*, **4** (2-3), pp. 239–245, 2010.

[21] E. Brinksmeier, J. C. Aurich, E. Govekar, C. Heinzel, H.-W. Hoffmeister, F. Klocke, J. Peters, R. Rentsch, D. J. Stephenson, E. Uhlmannh, K. Weinert and M. Wittmann, 'Advances in Modeling and Simulation of Grinding Processes', *CIRP Annals – Manufacturing Technology*, **55** (2), pp. 667–696, 2006.

[22] A. Bukowski, W. Kwasny and J. Jedrzejewski, 'Mechatronic Approach to the Development of an Intelligent Fixturing Device Test-Bed', *Journal of Machine Engineering*, **8** (3), pp. 66–76, 2008.

[23] J. Cecil, 'Computer-Aided Fixture Design - A Review and Future Trends', *International Journal of Advanced Manufacturing Technology*, **18**, pp. 790–793, 2001.

[24] D. Ceglarek, H. F. Li and Y. Tang, 'Modeling and Optimization of End Effector Layout for Handling Compliant Sheet Metal Parts', *Transactions of the ASME – Journal of Manufacturing Science and Engineering*, **123**, pp. 473–480, 2001.

[25] K. C. Chan and C. S. Lin, 'Development of a Computer Numerical Control (CNC) Modular Fixture-Machine Design of a Standard Multifinger Module', *International Journal of Advanced Manufacturing Technology*, **11**, pp. 18–26, 1996.

[26] CINDAS, 'Aerospace Structural Metals Handbook', Purdue University, West Lafayette, Indiana.

[27] J. A. Couey, E. R. Marsh, B. R. Knapp and R. R. Vallance, 'Monitoring Force in Precision Cylindrical Grinding', *Precision Engineering*, **29**, pp. 307–314, 2005.

[28] R. R. Craig Jr. and M. C. C. Bampton, 'The Coupling of Substructures for Dynamic Analyses', *AAIA Journal*, **6** (7), pp. 1313–1319, 1968.

[29] R. R. Craig Jr. and A. J. Kurdila, *Fundamentals of Structural Dynamics*, 2nd edition, Hoboken, New Jersey: John Wiley & Sons, 2006.

[30] M. L. Culpepper, K. M. Varadarajan and C. DiBiasio, 'Design of Integrated Eccentric Mechanisms and Exact Constraint Fixtures for Micron-Level Repeatability and Accuracy', *Precision Engineering*, **29**, pp. 65–80, 2005.

[31] W. Cuypers, N. Van Gestel, A. Voet, J.-P. Kruth, J. Mingneau and P. Bleys, 'Optical Measurement Techniques for Mobile and Large-Scale Dimensional Metrology', *Optics and Lasers in Engineering*, **47**, pp. 292–300, 2009.

[32] M. Daimon, T. Yoshida, N. Kojima, H. Yamamoto and T. Hoshi, 'Study for Designing Fixtures Considering Dynamics of Thin-Walled Plate- and Box-Like Workpieces', *CIRP Annals – Manufacturing Technology*, **34** (1), pp. 319–322, 1985.

[33] Danaher Motion, Washington, D.C., *AKM Series Motors*, 2006.

[34] Danaher Motion, Washington, D.C., *AKM Synchronous Servo Motors: Product Manual*, 2009.

[35] A. I. Dashchenko, *Reconfigurable Manufacturing Systems and Transformable Factories*, Berlin Heidelberg: Springer-Verlag, 2006.

[36] E. C. De Meter, 'Light Activated Adhesive Gripper (LAAG) Workholding Technology and Process', *Journal of Manufacturing Processes*, **6** (2), pp. 201–214, 2004.

[37] I. M. Deiab, 'On the Effect of Fixture layout on Part Stability and Flatness During Machining: A Finite Element Analysis', *Proceedings of the Institution of Mechanical Engineers Part B: Journal of Engineering Manufacture*, **220**, pp. 1613–1620, 2006.

[38] DELFOi, website, accessed on 23-04-2010, URL: `http://www.delfoi.com`.

[39] H. Deng, *Analysis and Synthesis of Fixturing Dynamic Stability in Machining Accounting for Material Removal Effect*, Ph.D. thesis, Georgia Institute of Technology, Atlanta, Georgia, 2006.

[40] B. Denkena, H.-C. Möhring and K. M. Litwinski, 'Sensing Fixtures for Process Monitoring', in: D. T. Pham, E. E. Eldukhri and A. J. Soroka (eds.), 'Innovative Production Machines and Systems', Fourth I*PROMS Virtual International Conference, 6-17th July 2009, Manufacturing Engineering Centre, Cardiff University: Whittles Publishing, 2009.

[41] R. C. Dorf and R. H. Bishop, *Modern Control Systems*, 11th edition, Upper Saddle River, New Jersey: Prentice-Hall, 2008.

[42] H. Du and G. C. I. Lin, 'Development of an Automated Flexible Fixture for Planar Objects', *Robotics and Computer-Integrated Manufacturing*, **14**, pp. 173–183, 1998.

[43] H. Du, G. C. I. Lin, J. Zhao and O. Gol, 'An Approach to Enhancing the Intelligence of a Three-Fingered Automated Flexible Fixturing System by Using Adaptive Control Theory', *Robotics and Computer-Integrated Manufacturing*, **15**, pp. 101–110, 1999.

[44] A. T. Elfizy, G. M. Bone and M. A. Elbestawi, 'Design and Control of a Dual-Stage Feed Drive', *International Journal of Machine Tools & Manufacture*, **45**, pp. 153–165, 2005.

[45] Enerpac, website, accessed on 04-06-2010, URL: http://www.enerpac.com.

[46] L.-S. Fan, H. H. Ottesen, T. C. Reiley and R. W. Wood, 'Magnetic Recording Head Positioning at Very High Track Densities Using a Microactuator-Based, Two-Stage Servo System', *IEEE Transactions on Industrial Electronics*, **42** (3), pp. 222–233, 1995.

[47] J. Fleischer, B. Denkena, B. Winfough and M. Mori, 'Workpiece and Tool Handling in Metal Cutting Machines', *Annals of the ClRP*, **55** (2), pp. 817–839, 2006.

[48] G. F. Franklin, J. D. Powell and A. Emami-Naeini, *Feedback Control of Dynamic Systems*, 5th edition, Upper Saddle River, New Jersey: Prentice-Hall, 2006.

[49] T. Fujita, A. Matsubara, D. Kono and I. Yamaji, 'Dynamic Characteristics and Dual Control of a Ball Screw Drive with Integrated Piezoelectric Actuator', *Precision Engineering*, **34**, pp. 34–42, 2010.

[50] C. R. Fuller, S. J. Elliott and P. A. Nelson, *Active Control of Vibration*, London: Academic Press, 1996.

[51] Y. C. Fung, *Foundations of Solid Mechanics*, Englewood Cliffs, New Jersey: Prentice-Hall, 1965.

[52] R. H. Gallagher, *Finite Element Analysis: Fundamentals*, Prentice-Hall Civil Engineering and Engineering Mechanics Series, Englewood Cliffs, New Jersey: Prentice-Hall, 1975.

[53] Y. Gao, D. Zhang and C. W. Yu, 'Dynamic Modeling of a Novel Workpiece Table for Active Surface Grinding Control', *International Journal of Machine Tools & Manufacture*, **41**, pp. 609–624, 2001.

[54] V. Giurgiutiu and S. E. Lyshevski, *Micromechatronics: Modeling, Analysis, and Design with MATLAB®*, 2nd edition, Boca Raton, Florida: CRC Press, 2009.

[55] M. Goldfarb and N. Celanovic, 'Modeling Piezoelectric Stack Actuators for Control of Micromanipulation', *IEEE Control Systems*, **17** (3), pp. 69–79, 1997.

[56] G. H. Golub and C. F. Van Loan, *Matrix Computations*, Oxford: North Oxford Academic, 1983.

[57] GOM Gesellschaft für Optische Messtechnik, website, accessed on 01-05-2010, URL: `http://www.gom.com`.

[58] E. Govekar, A. Baus, J. Gradišek, F. Klocke and I. Grabec, 'A New Method for Chatter Detection in Grinding', *CIRP Annals – Manufacturing Technology*, **51** (1), pp. 267–270, 2002.

[59] E. Govender, *An Intelligent Deflection Prediction System for Machining of Flexible Components*, Ph.D. thesis, University of Nottingham, School of Mechanical, Materials and Manufacturing Engineering, Nottingham, 2001.

[60] M. Grochowski, A. Bukowski and J. Jedrzejewski, 'Modelling of Mechatronic Workpiece-Fixture System Focusing on Active Compensation of Displacements', in: 'Proceedings of the 21st International Computer-Aided Production Engineering Conference (CAPE 2010)', pp. 1–8, Edinburgh: The University of Edinburgh, 2010, on CD-ROM.

[61] A. Guran, H.-S. Tzou, G. L. Anderson, M. Natori, U. Gabbert, J. Tani and E. Breitbach, *Structronic Systems: Smart Structures, Devices and Systems*, *Series on Stability Vibration and Control of Systems, Series B*, volume 4, Singapore: World Scientific Publishing Company, 1998.

[62] R. J. Guyan, 'Reduction of Mass and Stiffness Matrices', *AAIA Journal*, **3** (2), p. 380, 1964.

[63] R. A. Hameed, M. A. Mannan and A. Y. C. Nee, 'The Cutting Force Measurement in a Fixturing Setup with Instrumented Locators', *International Journal of Advanced Manufacturing Technology*, **23**, pp. 783–793, 2004.

[64] S.-S. Han and S.-B. Choi, 'Position Control of a Dual-Servo Stage Featuring an Electrorheological Fluid Clutch and Piezostack Actuator', *Proceedings of the Institution of Mechanical Engineers Part C: Journal of Mechanical Engineering Science*, **218**, pp. 1435–1448, 2004.

[65] D. E. Hardt, 'Modeling and Control of Manufacturing Processes: Getting More Involved', *Journal of Dynamic Systems, Measurement, and Control – Transactions of the ASME*, **115**, pp. 291–300, 1993.

[66] S. K. Hargrove and A. Kusiak, 'Computer-Aided Fixture Design: A Review', *International Journal of Production Research*, **32** (4), pp. 733–753, 1994.

[67] J. F. Hurtado and S. N. Melkote, 'Modeling and Analysis of the Effect of Fixture-Workpiece Conformability on Static Stability', *Transactions of the ASME – Journal of Manufacturing Science and Engineering*, **124**, pp. 234–241, 2002.

[68] I. Inasaki, B. Karpuschewski and H.-S. Lee, 'Grinding Chatter - Origin and Suppression', *CIRP Annals – Manufacturing Technology*, **50** (2), pp. 515–534, 2001.

[69] D. J. Inman, *Vibration with Control*, Chichester, United Kingdom: John Wiley & Sons, 2006.

[70] H. Janocha, *Actuators: Basics and Applications*, Heidelberg: Springer-Verlag, 2004.

[71] H. Janocha, *Adaptronics And Smart Structures: Basics, Materials, Design, and Applications*, 2nd edition, Berlin: Springer-Verlag, 2007.

[72] K. L. Johnson, *Contact Mechanics*, Cambridge: Cambridge University Press, 1985.

[73] M. Jonsson, H. Kihlman and G. Ossbahr, 'Coordinate Controlled Fixturing for Affordable Reconfigurable Tooling', in: 'Proceedings of the 2nd CIRP Conference on Assembly Technologies and Systems', pp. 1–11, Toronto, 2008.

[74] H. J. J. Kals, C. A. van Luttervelt and K. Moulijn, *Industriële Productie, Het Voortbrengen van Mechanische Producten {∼Industrial Production, The Manufacturing of Mechanical Products}*, 2nd edition, Diemen: Wegener Tijdschriften Groep, 1998, in Dutch.

[75] X. Kang and Q. Peng, 'Recent Research on Computer-Aided Fixture Planning', *Recent Patents on Mechanical Engineering*, **2** (1), pp. 8–18, 2009.

[76] Y. Kang, Y. Rong and J. C. Yang, 'Computer-Aided Fixture Design Verification. Part 2. Tolerance Analysis', *International Journal of Advanced Manufacturing Technology*, **21**, pp. 836–841, 2003.

[77] D. C. Karnopp, D. L. Margolis and R. C. Rosenberg, *System Dynamics: Modeling and Simulation of Mechantronic Systems*, 4th edition, Hoboken, New Jersey: John Wiley & Sons, 2006.

[78] N. Kaya and F. Öztürk, 'The Application of Chip Removal and Frictional Contact Analysis for WorkpieceŬFixture Layout Verification', *International Journal of Advanced Manufacturing Technology*, **21**, pp. 411–419, 2003.

[79] A. R. Khattak, S. Garvey and A. Popov, 'Proper Orthogonal Decomposition of the Dynamics in Bolted Joints', *Journal of Sound and Vibration*, **329**, pp. 1480–1498, 2010.

[80] B.-S. Kim, J. Li and T.-C. Tsao, 'Two-Parameter Robust Repetitive Control with Application to a Novel Dual-Stage Actuator for Noncircular Machining', *IEEE/ASME Transactions on Mechatronics*, **9** (4), pp. 644–652, 2004.

[81] Kistler, website, accessed on 12-05-2010, URL: `http://www.kistler.com`.

[82] M. Klärner, *Modelling and Simulation of Nozzle Guide Vanes Considering Mechanic-Thermal Loads of Grinding*, Diploma Thesis, Technische Universität Chemnitz, Chemnitz, 2007.

[83] M. Klärner, J. Leopold and L. Kroll, 'Analysis of Clamping within a Fixing System', in: C. Xiong, H. Liu and Y. Huang, Y. Xiong (eds.), 'Intelligent Robotics and Applications', *Lecture Notes in Computer Science*, volume 5315/2008, pp. 356–367, ICIRA 2008, Wuhan, China, October 15-17, 2008 Proceedings, Part II, Berlin Heidelberg: Springer-Verlag, 2008.

[84] J. W. Kleinwinkel, W. Lenselink, R. van den Bosch, J. van de Put, R. Kousbroek, P. van Ackooy and P. Boers, *Toepassen van Slimme Opspanmiddelen {∼Application of Smart Fixturing}*, Tech-Info-Blad {∼Technical Information Publication} TI.06.30, FME-CMW {∼Dutch Trade Association for Manufacturing, Metal and Electronic Industry}, Zoetermeer, 2006, in Dutch.

[85] Z. Kong and D. Ceglarek, 'Fixture Workspace Synthesis for Reconfigurable Assembly Using Procrustes-Based Pairwise Configuration Optimization', *Journal of Manufacturing Systems*, **25** (1), pp. 25–38, 2006.

[86] H. Kruggel-Emden, S. Wirtz and V. Scherer, 'Applicable Contact Force Models for the Discrete Element Method: The Single Particle Perspective', *Transactions of the ASME – Journal of Pressure Vessel Technology*, **131**, pp. 024001–1–024001–11, 2009.

[87] K. Kulankara, S. Satyanarayana and S. N. Melkote, 'Iterative Fixture Layout and Clamping Force Optimization Using the Genetic Algorithm', *Transactions of the ASME – Journal of Manufacturing Science and Engineering*, **124**, pp. 119–125, 2002.

[88] K. Kurz, K. Craig, B. Wolf and F. Stolfi, 'Developing a Flexible Automated Fixturing Device', *Mechanical Engineering*, **116** (7), pp. 59–63, 1994.

[89] J. Leopold, 'Clamping Modeling – State-of-the-Art and Future Trends', in: C. Xiong, H. Liu and Y. Huang, Y. Xiong (eds.), 'Intelligent Robotics and Applications', *Lecture Notes in Computer Science*, volume 5315/2008, pp. 289–300, ICIRA 2008, Wuhan, China, October 15-17, 2008 Proceedings, Part II, Berlin Heidelberg: Springer-Verlag, 2008.

[90] J. Leopold, D. Clauß, M. Klärner, A. Poppitz, M. Baldoli, A. Merlo, M. Giménez and J. Larranaga, 'Investigations to New Fixturing Principles for Aerospace Structures', in: F. Vollertsen (ed.), 'Proceedings', pp. 173–189, APT 2007, International Conference on Applied Production Technology, Bremen: BIAS, 2007.

[91] J. Leopold, A. Poppitz, M. Klärner, A.-K. Schmidt and J. Berger, 'Interaction Between Machining and New Fixturing Principles for Aerospace Structures', *International Journal of Material Forming*, **1**, pp. 531–533, 2008, ESAFORM2008 Conference on Material Forming. Lyon, France, Symposium MS09: Machining and Cutting.

[92] Q. Li, *Virtual Reality for Fixture Design and Assembly*, Ph.D. thesis, University of Nottingham, School of Mechanical, Materials and Manufacturing Engineering, Nottingham, 2008.

[93] Y. G. Liao and S. J. Hu, 'Flexible Multibody Dynamics Based Fixture-Workpiece Analysis Model for Fixturing Stability', *International Journal of Machine Tools & Manufacture*, **40**, pp. 343–362, 2000.

[94] Y. G. Liao and S. J. Hu, 'An Integrated Model of a Fixture-Workpiece System for Surface Quality Prediction', *International Journal of Advanced Manufacturing Technology*, **17**, pp. 810–818, 2001.

[95] A. E. H. Love, *A Treatise on the Mathematical Theory of Elasticity*, 4th edition, London: Cambridge University Press, 1927, republished by Dover Publications, New York, 1944.

[96] J. J. Madden, *Welding Fixture with Active Position Adapting Functions*, Bachelor's thesis, Worchester Polytechnic Institute, Worchester, Massachusetts, 2007.

[97] M. A. Mannan and J. P. Sollie, 'A Force-Controlled Clamping Element for Intelligent Fixturing', *Annals of the ClRP*, **46** (1), pp. 265–268, 1997.

[98] R. A. Marin and P. M. Ferreira, 'Analysis of the Influence of Fixture Locator Errors on the Compliance of Work Part Features to Geometric Tolerance Specifications', *Transactions of the ASME – Journal of Manufacturing Science and Engineering*, **125**, pp. 606–616, 2003.

[99] I. D. Marinescu, M. Hitchiner, E. Uhlmann, W. B. Rowe and Inasaki, *Handbook of Machining with Grinding Wheels*, Manufacturing Engineering and Materials Processing, Boca Raton, Florida: CRC Press, 2007.

[100] The MathWorks Inc., Natick, Massachusetts, *MATLAB*® *Control System Toolbox*^{TM} *8: Getting Started Guide*, 2008.

[101] The MathWorks Inc., Natick, Massachusetts, *MATLAB*® *7 - Getting Started Guide*, 2009.

[102] L. Meirovitch, *Dynamics and Control of Structures*, New York: John Wiley & Sons, 1990.

[103] H. E. Merritt, *Hydraulic Control Systems*, New York: John Wiley & Sons, 1967.

[104] M. Meshreki, J. Kövecses, H. Attia and N. Tounsi, 'Dynamics Modeling and Analysis of Thin-Walled Aerospace Structures for Fixture Design in Multiaxis Milling', *Transactions of the ASME – Journal of Manufacturing Science and Engineering*, **130**, pp. 031011–1–031011–12, 2008.

[105] E. C. de Meter, 'Fast Support Layout Optimization', *International Journal of Machine Tools & Manufacture*, **38**, pp. 1221–1239, 1998.

[106] E. C. de Meter and M. J. Hockenberger, 'The Application of Tool Path Compensation for the Reduction of Clamping-Induced Geometric Errors', *International Journal of Production Research*, **35** (12), pp. 3415–3432, 1997.

[107] E. C. de Meter, W. Xie, S. Choudhuri, S. Vallapuzha and M. W. Trethewey, 'A model to Predict Minimum Required Clamp Pre-Loads in Light of Fixture-Workpiece Compliance', *International Journal of Machine Tools & Manufacture*, **41**, pp. 1031–1054, 2001.

[108] R. T. Meyer and F. W. Liou, 'Fixture analysis under dynamic machining', *International Journal of Production Research*, **35** (5), pp. 1471–1489, 1997.

[109] R. O. Mittal, P. H. Cohen and B. J. Gilmore, 'Dynamic Modeling of the Fixture-Workpiece System', *Robotics & Computer Integrated Manufacturing*, **8** (4), pp. 201–217, 1991.

[110] N. Mohan, *Electric Drives: An Integrative Approach*, Minneapolis, Minnesota: MNPERE, 2001.

[111] S. O. R. Moheimani and A. J. Fleming, *Piezoelectric Transducers for Vibration Control and Damping*, Advances in Industrial Control, London: Springer-Verlag, 2006.

[112] M. Molfino, R. Zoppi and D. Zlatanov, 'Reconfigurable Swarm Fixtures', in: J. S. Dai, M. Zoppi and X. Kong (eds.), 'Proceedings of the ASME/IFToMM International Conference on Reconfigurable Mechanisms and Robots', pp. 730–735, London: IEEE, 2009.

[113] C. Munro and D. F. Walczyk, 'Reconfigurable Pin-Type Tooling: A Survey of Prior Art and Reduction to Practice', *Transactions of the ASME – Journal of Manufacturing Science and Engineering*, **129**, pp. 551–565, 2007.

[114] A. Y. C. Nee, A. Senthil Kumar and Z. J. Tao, 'An Intelligent Fixture with a Dynamic Clamping Scheme', *Proceedings of the Institution of Mechanical Engineers Part B: Journal of Engineering Manufacture*, **214**, pp. 183–196, 2000.

[115] A. Y. C. Nee, Z. J. Tao and A. Senthil Kumar, *An Advanced Treatise on Fixture Design and Planning*, Series on Manufacturing Systems and Technology, Singapore: World Scientific Publishing Company, 2004.

[116] A. Y. C. Nee, K. Whybrew and A. Senthil Kumar, *Advanced Fixture Design for FMS*, London: Springer-Verlag, 1995.

[117] V. A. Neelakantan, G. N. Washington and N. K. Bucknor, 'Model Predictive Control of a Two Stage Actuation System Using Piezoelectric Actuators for Controllable Industrial and Automotive Brakes and Clutches', *Journal of Intelligent Material Systems and Structures*, **19**, pp. 845–857, 2008.

[118] T. T. Nikov, *Material Removal Simulation in Machining of Low Rigidity Parts*, Ph.D. thesis, University of Nottingham, School of Mechanical, Materials and Manufacturing Engineering, Nottingham, 2004.

[119] T. Papastathis, *PhD thesis in preparation*, Ph.D. thesis, University of Nottingham, School of Mechanical, Materials and Manufacturing Engineering, Nottingham, 2011.

[120] T. Papastathis, M. Ryll and S. Ratchev, 'Rapid Reconfiguration and Part Repositioning with an Intelligent Fixturing System', in: 'Proceedings of the 2007 International Manufacturing Science And Engineering Conference', MSEC2007-31036, ASME, 2007.

[121] E. J. Park and J. K. Mills, 'Static Shape and Vibration Control of Flexible Payloads With Applications to Robotic Assembly', *IEEE/ASME Transactions on Mechatronics*, **10** (6), pp. 675–687, 2005.

[122] H. L. Phuah, *Part-Fixture Behaviour Prediction Methodology for Fixture Design Verification*, Ph.D. thesis, University of Nottingham, School of Mechanical, Materials and Manufacturing Engineering, Nottingham, 2005.

[123] Physik Instrumente, website, accessed on 04-11-2008, URL: http://www.physikinstrumente.com.

[124] Piezomechanik GmbH, München, *Piezo-Mechanics: An Introduction*, 2009.

[125] P. Pillay and R. Krishnan, 'Modeling, Simulation, and Analysis of Permanent-Magnet Motor Drives, Part II: The Brushless DC Motor Drive', *IEEE Transactions on Industry Applications,*, **25** (2), pp. 274–279, 1989.

[126] R. Pomirleanu and V. Giurgiutiu, 'Full-Stroke Static and Dynamic Analysis of High-Power Piezoelectric Actuators', *Journal of Intelligent Material Systems and Structures*, **13**, pp. 275–289, 2002.

[127] J. L. Pons, *Emerging Actuator Technology: A Micromechatronic Approach*, Chichester: Wiley & Sons, 2005.

[128] A. Preumont, *Vibration Control of Active Structures: An Introduction*, *Solid Mechanics and its Applications*, volume 96, 2nd edition, Dordrecht: Kluwer Academic Publishers, 2002.

[129] A. Preumont, *Mechatronics: Dynamics of Electromechanical and Piezoelectric Systems*, *Solid Mechanics and its Applications*, volume 136, Dordrecht: Springer-Verlag, 2006.

[130] A. Preumont and K. Seto, *Active Control of Structures*, Chichester: John Wiley & Sons, 2008.

[131] G. Qin, W. Zhang, Z. Wu and M. Wan, 'Systematic Modeling of Workpiece-Fixture Geometric Default and Compliance for the Prediction of Workpiece Machining Error', *Transactions of the ASME – Journal of Manufacturing Science and Engineering*, **129**, pp. 789–801, 2007.

[132] Z. Q. Qu, *Model Order Reduction Techniques: with Applications in Finite Element Analysis*, London: Springer-Verlag, 2004.

[133] J. K. Rai and P. Xirouchakis, 'Finite Element Method Based Machining Simulation Environment for Analyzing Part Errors Induced During Milling of Thin-Walled Components', *International Journal of Machine Tools & Manufacture*, **48**, pp. 629–643, 2008.

[134] R. Ramesh, M. A. Mannan and A. N. Poo, 'Error Compensation in Machine Tools – A Review Part I: Geometric, Cutting-Force Induced and Fixture Dependent Errors', *International Journal of Machine Tools & Manufacture*, **40**, pp. 1235–1256, 2000.

[135] A. Rashid and C. M. Nicolescu, 'Active Vibration Control in Palletised Workholding System for Milling', *International Journal of Machine Tools & Manufacture*, **46**, pp. 1626–1636, 2006.

[136] A. Rashid and C. M. Nicolescu, 'Design and Implementation of Tuned Viscoelastic Dampers for Vibration Control in Milling', *International Journal of Machine Tools & Manufacture*, **48**, pp. 1036–1053, 2008.

[137] S. Ratchev, K. Phuah, G. Lämmel and W. Huang, 'An Experimental Investigation of Fixture-Workpiece Contact Behaviour for the Dynamic Simulation of Complex Fixture-Workpiece Systems', *Journal of Materials Processing Technology*, **164-165**, pp. 1597–1606, 2005.

[138] S. Ratchev, K. Phuah and S. Liu, 'FEA-Based Methodology for the Prediction of Part-Fixture Behaviour and its Applications', *Journal of Materials Processing Technology*, **191**, pp. 260–264, 2007.

[139] S. M. Ratchev, W. Huang, H. L. Phuah, S. Liu and A. A. Becker, 'FEA-Based Simulation for Dynamic Fixture-Workpiece Behaviour During Grinding Processes', *CIRP Journal of Manufacturing Systems*, **34**, 2005, on CD-ROM, also as conference paper: Proceedings of the 37th CIRP international seminar on manufacturing system, Budapest, Hungary, May 19-21, 2004, pp.141-147, ISBN 963 214 905X.

[140] Roemheld, website, accessed on 04-06-2010, URL: `http://www.roemheld.de`.

[141] Y. Rong, Y. Hu, W. Kang, Y. Zhang and D. W. Yen, 'Locating Error Analysis and Tolerance Assignment for Computer-Aided Fixture Design', *International Journal of Production Research*, **39** (15), pp. 3529–3545, 2001.

[142] Y. Rong, S. H. Huang and Z. Hou, *Advanced Computer-Aided Fixture Design*, Amsterdam: Elsevier Academic Press, 2005.

[143] M. Ryll, T. N. Papastathis and S. Ratchev, 'Towards an Intelligent Fixturing System with Rapid Reconfiguration and Part Positioning', *Journal of Materials Processing Technology*, **201**, pp. 198–203, 2008.

[144] W. H. A. Schilders, H. A. van der Vorst and J. Rommes, *Model Order Reduction: Theory, Research Aspects and Applications*, *Mathematics in Industry*, volume 13, Berlin: Springer-Verlag, 2008.

[145] G. S. A. Shawki and M. M. Abdel-Aal, 'Rigidity Considerations in Fixture Design – Contact Rigidity at Locating Elements', *International Journal of Machine Tool Design and Research*, **6**, pp. 31–43, 1966.

[146] G. S. A. Shawki and M. M. Abdel-Aal, 'Rigidity Considerations in Fixture Design – Rigidity of Clamping Elements', *International Journal of Machine Tool Design and Research*, **6**, pp. 207–209, 1966.

[147] B. Shirinzadeh, 'Flexible and Automated Workholding Systems', *Industrial Robot*, **22** (2), pp. 29–34, 1995.

[148] F. Sikström, M. Ericsson, A.-K. Christiansson and K. Niklasson, 'Tools for Simulation Based Fixture Design to Reduce Deformation in Advanced Fusion Welding', in: C. Xiong, H. Liu and Y. Huang, Y. Xiong (eds.), 'Intelligent Robotics and Applications', *Lecture Notes in Computer Science*, volume 5315/2008, pp. 398–407, ICIRA 2008, Wuhan, China, October 15-17, 2008 Proceedings, Part II, Berlin Heidelberg: Springer-Verlag, 2008.

[149] SIMULIA, Dassault Systèmes S.A., Providence, Rhode Island, *Abaqus Analysis User's Manual, Edition 6.7-1*, 2007.

[150] SIMULIA, Dassault Systèmes S.A., Providence, Rhode Island, *Abaqus Theory Manual, Edition 6.7-1*, 2007.

[151] S. Skogestad and I. Postlethwaite, *Multivariable Feedback Control: Analysis and Design*, 2nd edition, Chichester: John Wiley & Sons, 2005.

[152] A. Sudsang, J. Ponce and N. Srinivasa, 'Grasping and In-Hand Manipulation: Geometry and Algorithms', *Algorithmica*, **26**, pp. 466–493, 2000.

[153] E. Y. T. Tan, A. Shentil Kumar, J. Y. H. Fuh and A. Y. C. Nee, 'Modeling, Analysis, and Verification of Optimal Fixturing Design', *IEEE Transaction on Automation Science and Engineering*, **1** (2), pp. 121–132, 2004.

[154] I. Tansel, A. Nedbouyan and M. Trujillo, 'Design of a Smart Workpiece Holder (SWH) to Extend The Useful Life of Micro-Tools', in: 'Proceedings of the IEEE IECON 95, 21st International Conference on Industrial Electronics, Control and Instrumentation', volume 1, pp. 116–120, IEEE, 1995.

[155] Z. J. Tao, A. Senthil Kumar and A. Y. C. Nee, 'Automatic Generation of Dynamic Clamping Forces for Machining Fixtures', *International Journal of Production Research*, **37** (12), pp. 2755–2776, 1999.

[156] Z. J. Tao, A. Senthil Kumar and A. Y. C. Nee, 'A Computational Geometry Approach to Optimum Clamping Synthesis of Machining Fixtures', *International Journal of Production Research*, **37** (15), pp. 3495–3517, 1999.

[157] R. A. Thompson, 'The Dynamic Behavior of Surface Grinding Part 2 - Some Surface Grinding Tests', *Transactions of the ASME - Journal of Engineering for Industry*, **93**, pp. 492–497, 1971.

[158] S. Timoshenko and S. Woinowsky-Krieger, *Theory of Plates and Shells*, 2nd edition, Engineering Mechanics Series, Singapore: McGraw-Hill, 1959, International Edition.

[159] S. P. Timoshenko and J. N. Goodier, *Theory of Elasticity*, 3rd edition, Engineering Mechanics Series, Singapore: McGraw-Hill, 1970, International Edition.

[160] U. A. Tol, *Design of a Mechanically Adaptable Locating and Supporting System for an Intelligent Fixture*, Master's thesis, University of Florida, Gainesville, Florida, 2003.

[161] K. M. Varadarajan and M. L. Culpepper, 'A Dual-Purpose Positioner-Fixture for Precision Six-Axis Positioning and Precision Fixturing Part I. Modeling And Design', *Precision Engineering*, **31**, pp. 276–286, 2007.

[162] K. Velíšek, P. Košt'ál and R. Zvolenský, 'Clamping Fixtures for Intelligent Cell Manufacturing', in: C. Xiong, H. Liu and Y. Huang, Y. Xiong (eds.), 'Intelligent Robotics and Applications', *Lecture Notes in Computer Science*, volume

5315/2008, pp. 966–972, ICIRA 2008, Wuhan, China, October 15-17, 2008 Proceedings, Part II, Berlin Heidelberg: Springer-Verlag, 2008.

[163] T. J. Viersma, 'Analysis, Synthesis and Design of Hydraulic Servosystems and Pipelines', Lecture Notes WB2402, Technische Universiteit Delft (NL), 1990.

[164] R. Wagner, Y. Zhuang, and K. Goldberg, 'Fixturing Faceted Parts with Seven Modular Struts', in: '1995 IEEE International Symposium on Assembly and Task Planning', pp. 133–139, IEEE, 1995.

[165] D. F. Walczyk and R. S. Longtin, 'Fixturing of Compliant Parts Using a Matrix of Reconfigurable Pins', *Transactions of the ASME – Journal of Manufacturing Science and Engineering*, **122**, pp. 766–772, 2000.

[166] Y. Wang, *A Methodology of Fixture Evaluation, Analysis and Optimisation*, Ph.D. thesis, University of Nottingham, School of Mechanical, Materials and Manufacturing Engineering, Nottingham, 2004.

[167] Y. Wang, Z. Wang and N. Gindy, 'Collision-Free Machining Fixture Space Design Based on Parametric Tool Space for Five-Axis Grinding', *International Journal of Advanced Manufacturing Technology*, **45**, pp. 1–7, 2009.

[168] Y. F. Wang, J. Y. H. Fuh and Y. S. Wong, 'A Model-Based Online Control of Optimal Fixturing Process', in: 'Proceedings of the 1997 IEEE International Conference on Robotics and Automation', pp. 2019–2024, Albuquerque, New Mexico: IEEE, 1997.

[169] Y. F. Wang, Y. S. Wong and J. Y. H. Fuh, 'Off-Line Modelling and Planning of Optimal Clamping Forces for an Intelligent Fixturing System', *International Journal of Machine Tools & Manufacture*, **39**, pp. 253–271, 1999.

[170] D. E. Whitney, *Mechanical Assemeblies, Their Design, Manufacture, and Role in Product Development*, Oxford Series on Advanced Manufacturing, Oxford: Oxford University Press, 2004.

[171] G. J. Wiens, K. J. Rao and T. B. Rippere, 'Active Fixturing for Micro/Mesoscale Machine Tool Systems', WO 2010/042502 A2, April 2010, patent.

[172] C. Xiong, H. Ding and Y. Xiong, *Fundamentals of Robotic Grasping and Fixturing*, Series on Manufacturing Systems and Technology, Singapore: World Scientific Publishing Company, 2007.

[173] T. Yamaguchi, N. Furushiro and M. Higuchi, 'Application of the Active Flexible Fixture to a Peg-in-hole Task', in: K. Shirase and S. Aoyagi (eds.), 'Service Robotics and Mechatronics: Selected Papers of the International Conference on Machine Automation ICMA2008', chapter 3, pp. 49–54, London: Springer-Verlag, 2010.

[174] B. D. Yang, M. L. Chu and C. H. Menq, 'Stick-Slip-Separation Analysis and Non-Linear Stiffness and Damping Characterization of Friction Contacts Having Variable Normal Load', *Journal of Sound and Vibration*, **210** (4), pp. 350–370, 1998.

[175] J. H. Yeh and F. W. Liou, 'Contact Condition Modelling for Machining Fixture Setup Processes', *International Journal of Machine Tools & Manufacture*, **39**, pp. 787–803, 1999.

[176] D. Zhang, D. G. Chetwynd, X. Liu and Y. Y. Tian, 'Investigation of a 3-DOF Micro-Positioning Table for Surface Grinding', *International Journal of Mechanical Sciences*, **48**, pp. 1401–1408, 2006.

[177] J. Zhang, J. Yang and B. Li, 'Development of a Reconfigurable Welding Fixture System for Automotive Body', in: J. S. Dai, M. Zoppi and X. Kong (eds.), 'Proceedings of the ASME/IFToMM International Conference on Reconfigurable Mechanisms and Robots', pp. 736–742, London: IEEE, 2009.

[178] X.-M. Zhang, L.-M. Zhu and H. Ding, 'Matrix Perturbation Method for Predicting Dynamic Modal Shapes of the Workpiece in High-Speed Machining', *Proceedings of the Institution of Mechanical Engineers Part B: Journal of Engineering Manufacture*, **144**, pp. 177–183, 2009.

[179] Y. Zhang and N. D. Sims, 'Milling Workpiece Chatter Avoidance Using Piezoelectric Active Damping: A Feasibility Study', *Smart Materials and Structures*, **24**, pp. N65–N70, 2005.

[180] Y. Zheng, Y. Rong and Z. Hou, 'The Study of Fixture Stiffness Part I: A Finite Element Analysis for Stiffness of Fixture Units', *International Journal of Advanced Manufacturing Technology*, **36**, pp. 865–876, 2008.

[181] Z. W. Zhong and H. B. Yang, 'Development of a Vibration Device for Grinding with Microvibration', *Materials and Manufacturing Processes*, **19** (6), pp. 1121–1132, 2004.

[182] O. C. Zienkiewicz, R. L. Taylor and J. Z. Zhu, *The Finite Element Method: Its Basis and Fundamentals*, 6th edition, Oxford: Elsevier Butterworth-Heinemann, 2005.

List of Publications

- O.J. Bakker, A.A. Popov, and S.M. Ratchev, 'Investigation into Feedback Control of Part-Fixture Systems Undergoing Dynamic Machining Forces', in: 'Proceedings of the ISMA2008 Conference on Noise and Vibration Engineering, Leuven, Belgium, 2008 September 15-17', pp. 131–140.

- O.J. Bakker, A.A. Popov, and S.M. Ratchev, 'Active Control of a Workpiece Holder with Piezo-Electro-Mechanical Actuation', *Journal of Machine Engineering*, **8** (3), pp. 17–28, 2008.

- O.J. Bakker, A.A. Popov, and S.M. Ratchev, 'Model Based Control of an Advanced Actuated Part-Fixture System', in: 'Proceedings of the 2009 ASME International Manufacturing Science & Engineering Conference (MSEC2009)', paper MSEC2009-84175, 2009.

- O.J. Bakker, A.A. Popov, and S.M. Ratchev, 'Fixture Control by Hydraulic Actuation Using a Reduced Workpiece Model', *Proceedings of the Institution of Mechanical Engineers, Part B: Journal of Engineering Manufacture*, **223** (B12), pp. 1553–1566, 2009.

- O.J Bakker, A.A. Popov, E. Salvi, A. Merlo and S.M. Ratchev, 'Model-Based Control of an Active Fixture for Advanced Aerospace Components', to appear in: *Proceedings of the Institution of Mechanical Engineers, Part B: Journal of Engineering Manufacture*, special issue on Manufacturing Technology for Advanced Aerospace Components and Systems, 2010.